JOURNAL OF THE AERONAUTICAL SCIENCES

VOLUME 11 JULY, 1944 NUMBER 3

Directional Stability of Flying Boat Hulls During Taxiing

JOHN D. PIERSON*

The Glenn L. Martin Company

ABSTRACT

Increased loading of flying boats to the maximum operational limit has led to a renewed interest in the directional stability characteristics of hulls. Cases have arisen wherein yawing at speeds below the hump has prevented take-off. Also, cross-wind operation is often impossible below hump speed because of weathercocking. At these low speeds rudder effectiveness is slight and unbalanced power would reduce accelerating forces with the net result that inherent directional instability is uncontrollable.

Investigation of these characteristics was made on several flying boat models in the Experimental Towing Tank, Stevens Institute of Technology. Yawing moments versus yaw angle were determined at various model speeds and loadings. Assembling of these individual stability curves on a grid of loading versus speed formed the composite charts of directional stability which show the overall picture of the hull directional stability. The charts exposed regions of severe instability on the basic hull forms.

Tests of the forebody alone demonstrated its responsibility for the low speed, moderate instability and showed that the flow along the rounded afterbody lines caused the severe discontinuities near hump speed. Modifications to straighten or separate this flow on the afterbody were tested in a similar manner and included skegs along the keel and under the tail cone and chine strips and side steps near the second step. The side steps were most effective on the models and were applied full scale. Flight-test results, while qualitative in extent, indicated substantial improvement in the taxiing performance of the ship.

SYMBOLS

b = beam of hull at main step
w = density of water (lbs. per cu.ft.)
g = acceleration of gravity
ψ = angle of yaw
M_ψ = yawing moment
$C_{M\psi} = M_\psi/wb^4$
Δ = hydrodynamic lift of hull
$C_\Delta = \Delta/wb^3$
V = water speed
$C_V = V/\sqrt{bg}$
P = port, bow to port
S = starboard, bow to starboard

Because of the military situation, all data are given in non-dimensional form only.

Presented at the Airplane Design Session, Twelfth Annual Meeting, I.A.S., New York, January 25–27, 1944.

* Hydrodynamics Development Engineer.

INTRODUCTION

RECENTLY THERE HAS BEEN a strong tendency to increase the operating loads of flying boats to the maximum that can be taken off the water. This desire for increased pay load has resulted in the overloading of existing hull designs to a point where, in some cases, directional stability of the ship at prehump speeds is the limiting factor for take-off gross weight. Also, emergency operating conditions and restricted harbors have made the ability to taxi and take off cross-wind highly desirable, if not a necessity. This has not been possible in certain wind conditions for some modern flying boats.

Since present large flying boats are usually multi-engined, the discussion to follow will be based upon an assumed twin-engined installation with small excess thrust at the hump speed (which is the condition that exists under the overload conditions). The comments below are based upon flight-test data from large modern flying boats.

Directional Instability in Calm or Light Airs

Apparently, almost all boat and hull forms are directionally unstable at some speeds, and the pilot must make use of rudder and/or unbalanced power to maintain a proper heading. As the weight of a given flying boat is increased at the same power, the excess thrust (acceleration) is decreased. This causes the ship to remain in the unstable region for a longer time and reduces the amount of unbalanced power available (while still maintaining forward acceleration). When the instability of the ship gets beyond the control of the pilot, a rapid turning results. This is often quite severe,

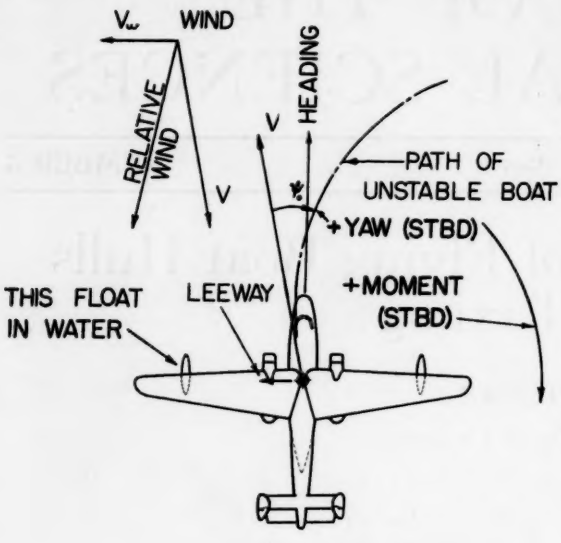

FIG. 1. Cross-wind taxiing condition.

necessitating complete reduction of power, and the take-off has to be started again. If the pilot is expert and attentive, he may guide an unstable boat through the critical region by rapid counteraction of incipient yaw. However, even this is not sufficient in some cases where the ship is heeled (because of normally insufficient aileron control at low speeds).

Cross-Wind Taxiing

The relative motions of wind, water, and flying boat (equal power) are shown by diagram in Fig. 1. This condition occurs at prehump speeds where the wind side force is sufficient to cause a measurable leeway (ψ) in the water. In general, there is insufficient aileron control to raise the leeward tip float from the water. When the hull is directionally unstable, the combination of heel angle and initial yaw results in a turning of the ship into the wind. Since the wind force induces an initial angle of yaw, the pilot's skill is of no avail. A straight cross-wind path is possible only with a stable hull or sufficient available unbalanced power to overcome the moment of an unstable hull. In moderate to strong winds even maximum power on the windward engine with the leeward engine idling has occasionally been found to give insufficient corrective moment to prevent a slow turn into the wind. At prehump speeds in moderate to heavy cross-wind conditions the effectiveness of the rudders in controlling yaw is ordinarily not much in excess of the moments required to counteract the aerodynamic forces alone.

MODEL TEST PROGRAM

Since the early design days of seaplanes and flying boats there has not been much active work on the matter of directional stability during taxiing. Qualitative comments on the directional behavior of models have accompanied many resistance test reports, but quantitative data have heretofore been lacking. In order to obtain a logical method for study of the directional characteristics of present designs and to provide a basis for the development of improvements, a program of model tests was carried out at the Experimental Towing Tank, Stevens Institute of Technology.[1]

Description of Models Tested

The two basic models tested in detail are designated 404 and 406 with dash numbers to identify the various modifications. The forebodies of the two hulls are similar and of conventional form with 20° deadrise at the main step.

Model 404 has by far the more powerful afterbody, having wide plan form and large chine flare near the second step. Model 406 has a sharply tapered afterbody with higher deadrise angle. The difference in power of the afterbodies makes about 2° difference in trim angle at the hump under similar loading conditions.

Typical total resistance and thrust curves versus speed for this general hull form are shown in Fig. 2 for the overload conditions with small excess thrust at the hump speed.

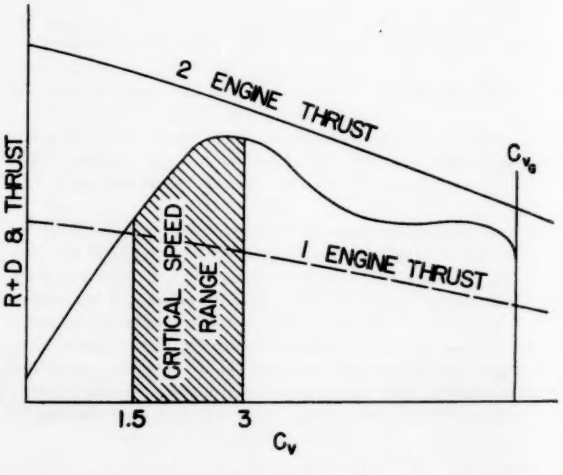

FIG. 2. Typical $R + D$ and thrust curves for a highly loaded twin-engined flying boat.

Description of Model Test Apparatus

For such an experimental investigation into a relatively new field, small-scale model-testing equipment was particularly well adapted. A diagrammatic sketch of the apparatus (especially designed by the tank staff for this study) is shown in Fig. 3. Complete freedom in vertical motion and pitch was allowed, while the motion in yaw was restrained by a calibrated spring. Various weight and moment combinations were obtained by counterweighting the model and towing gate. To simu-

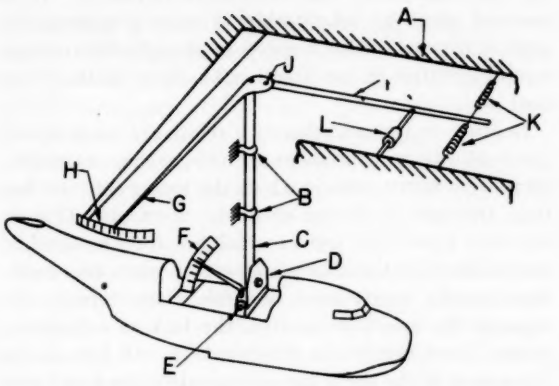

FIG. 3. Diagrammatic sketch of apparatus for yaw tests. A—Main towing gate (free vertically). B—Strut bearings attached to frame (A). C—Model support tube (free to rotate about vertical axis). D—Heel angle adjustment. E—Pivot points, model attachment (freedom in pitch). F—Trim scale on model. G—Yaw angle indicator fastened to tube (C). H—Yaw angle scale fastened to (A). I—Torque arm pivoted at axis of (C) clamped to (G). J—Yaw angle adjustment. K—Spring restraining yaw. L—Dashpot, yaw damper.

late cross-wind taxiing or any other condition wherein the ship would be heeled, provision was made for fixing the angle of heel (roll) at the required value. Damping was provided for both the pitching and yawing motions when required.

Test Procedure

A static angle of yaw was set before the model was run down the tank. The running yaw angle was obtained in the constant-speed portion of the run. The spring calibration applied to the difference between running and static yaw angles yielded the yawing moment. Several points were taken at each speed and load combination to determine a curve of moment versus angle such as Fig. 4. The curve shown is a typical unstable

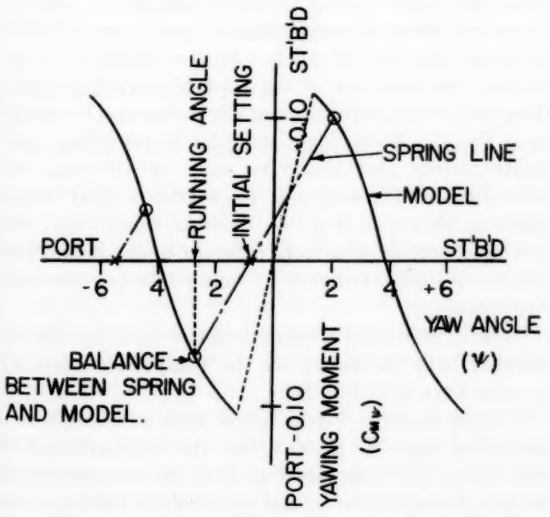

FIG. 4. Typical curves of moment versus angle of yaw.

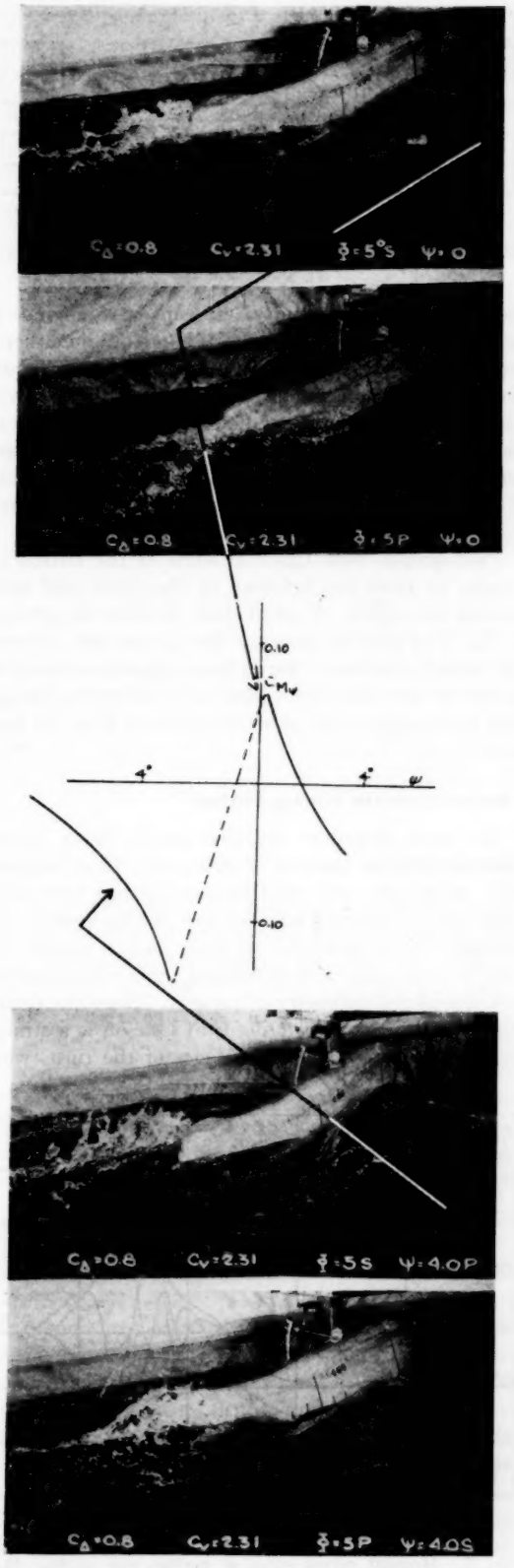

FIG. 5. Photograph of Model 406 during testing.

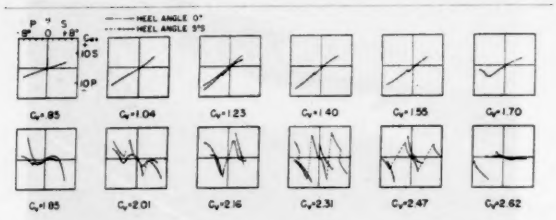

FIG. 6. Directional stability versus speed; Model 406, C_Δ = 0.80.

plot with a "discontinuity" at zero yaw angle. As shown in Fig. 4, it was often possible to obtain either of two running angles from one initial setting. This was accomplished by pushing the model toward one side or the other during the run. The "discontinuities" as indicated by dashed lines may not be such in the strict sense of the word, but only regions in which the rate of change of model moment was greater than the spring rate.

Photographs were taken at some of the critical attitudes to show the behavior of the water and spray around the model. Four of these pictures are grouped in Fig. 5 by pairs to show the flow at two test points in the heeled condition. Views from opposite sides of the model at each point were effected by reversing the heel and yaw angles while taking the pictures from the same side.

Limitations of the Testing Method

The test procedure outlined above yields yawing moment data for the case of pure yaw. In actual practice, except for cross-wind taxiing, turning follows the yaw and a combined rotation and yawing ensues. Although testing technique to study such a motion of a ship in a turn has been developed,[1] this refinement was not considered necessary at present. Since the desired result in the case of a flying boat take-off is a straight path, a study of the initial stages of the turn (where yaw predominates) was considered sufficient. It is assumed that the relationship of yawing moment to angle of yaw at constant speed in straight-line motion is representative of the directional stability of the flying boat.

Because of the selection of a relatively weak spring (to facilitate measurement of the yawing moment), there were many cases in which the spring rate was less than the rate of change of model moment. This resulted in gaps in the curves which are approximated by dashed lines on the charts. However, since this condition usually represented unstable characteristics far beyond the available control, the lack of actual test points is not much of a disadvantage. In fact, in the discussion of the data, the spring rate is used as a convenient dividing line between slightly unstable and extremely unstable attitudes.

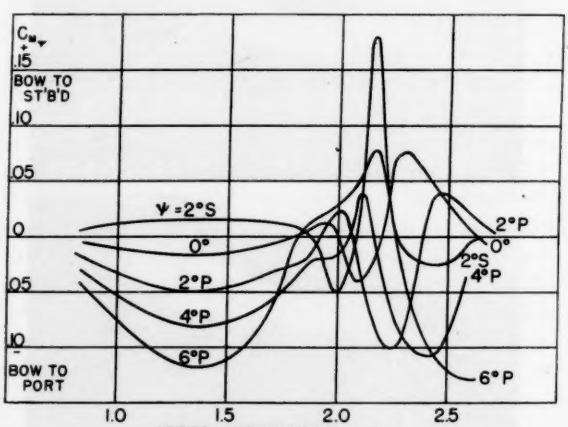

FIG. 7. Moment versus speed at various yaw angles; Model 406, C_Δ = 0.80. Heel angle 5° starboard.

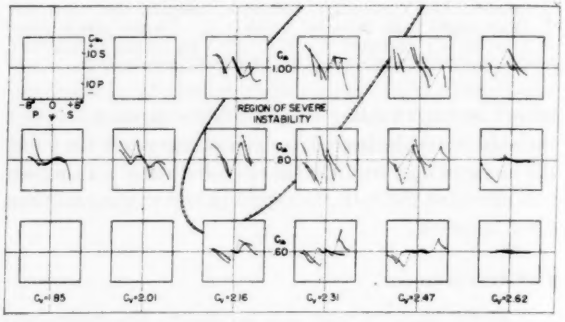

FIG. 8. Composite chart of directional stability; Model 406.

Method of Plotting Test Data

From preliminary studies and tests it appeared that trim angle (within the range of moderate trimming moments) was not a critical variable in the investigation. Thus, the variables to be considered were speed, load, heel angle, yawing moment, and angle. Curves of yawing moment versus angle of yaw were obtained at various speeds and loads. It was confusing to determine the behavior of the boat by trying to study these individual pictures, even when arranged by speeds as in Fig. 6. Accordingly, in order to provide a composite picture that would be more enlightening, the individual curves were put on a grid of load versus speed as shown on Fig. 8. In some cases where the yawing characteristics were different in the heeled and upright attitudes, both curves were plotted on the same coordinates.

General regions of various types of stability and instability may be shown on the composite charts by contour lines as in Fig. 8.

Yawing moment versus speed with yaw angle as a parameter may be plotted, but the interpretation of this type of plotting (see Fig. 7) is not so apparent as in that described above, and the effect of loading is not clearly shown in the latter type.

Discussion of Tests on Basic Models

From Figs. 6 and 7 it can be seen that there are two distinct critical speed ranges for directional instability. The unstable slope, $dC_M/d\psi$, increases with speed in the low speed range ($C_V = 0.85$ to 1) to a maximum and then decreases again. At slightly higher speeds the variation of $dC_M/d\psi$ is quite radical at zero yaw, and there is a region of severe instability. This region is evident in flight test, although apparently not so severe as indicated by the model.

This latter region is critical for take-off or cross-wind taxiing, since the speed is close to hump speed where the excess thrust is small. A more complete coverage of this region is shown in Fig. 8. Probably the most spectacular aspect of the tests was the rapid change of flow pattern for relatively small speed and yaw angle change in this region. Photographs (Fig. 5) of the model at 5° heel angle show the strong flow of water around the afterbody and under the tail cone. At some speeds the behavior of this water flow around the stern and along the tail indicated that it was the major cause of the instability. However, in most cases it was not possible to decide from the appearance of the water flow whether the model was experiencing stabilizing or destabilizing moments. Only the plots of moment versus angle of yaw were definite means of determining the yawing characteristics of the model.

Even though the flow of water along the sides of Model 404 was much less than that of 406, a comparison of the test data (Figs. 8 and 9) shows that the unstable region is even more extended in the former. This is probably due to the increased curvature of the water lines near the second step of 404.

Test curves for only one of the forebodies (404) are given in Fig. 10, since the two are nearly alike. For these tests the trim and draft were held at the values determined from the tests of the complete hull. The yawing characteristics of the 406 forebody were checked by several random tests and proved to be similar to those of 404. At speeds lower than those shown in Fig. 10, the yawing moments of complete model and forebody alone were quite similar.

Comparison of Full Model and Forebody Alone

After the forebody alone passes through the low speed maximum instability ($C_V = 1.4$), the unstable slope of the yawing moment curves steadily declines. Since the effect of the afterbody upon the flow on the forebody (at specified trim, draft, and speed) is small, the difference between the yawing moments of forebody and complete model must be due to the flow along the afterbody.

Essentially, a conventional forebody must be directionally unstable at low speeds because of the long wetted length ahead of the center of gravity. Therefore, it is the duty of the afterbody to supply a stabilizing moment in the critical speed range (Fig. 2). That the

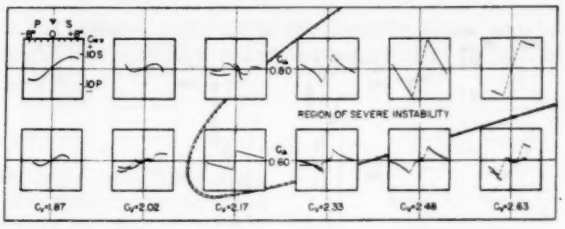

FIG. 9. Composite chart of directional stability; Model 404.

afterbody has done just the opposite to this in the case of the two models tested is obvious from a comparison of the tank test data in Figs. 8, 9, and 10. Since the destabilizing action of the afterbody appeared (from visual observations) to arise from the flow along the rounded stern lines, modifications were made to remedy this condition.

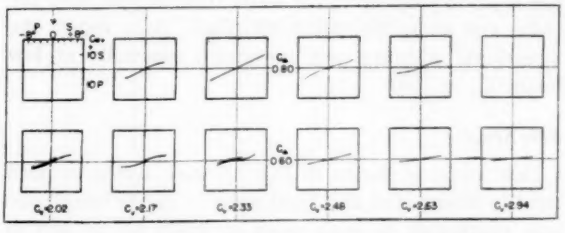

FIG. 10. Composite chart of directional stability; Model 404 (forebody).

MODIFICATIONS TO IMPROVE DIRECTIONAL STABILITY

In this investigation the goal was to improve the directional stability by simple alterations to existing hull forms (preferably by changes external and separate from the hull structure). Two general types of modifications were tried: first, to straighten the flow as it left the afterbody by a skeg; second, to break the flow of water from the sides of the stern by chine strips or side steps. Although these alterations were applied to a hull already designed and built, the principles behind their action may still be applied to the design of any similar flying boat hull.

Skegs

Model 406-1 and 404-1 had closely similar skegs as shown in Fig. 11 for 406. The fin, or skeg as it is termed, from second step to tail end of hull acts to straighten out the water flowing along the rounded water lines above the chine lines. Both models were tested in the region of greatest instability to determine the improvement in flow conditions. From a comparison of the partial tests of 406-1 (Fig. 11) with the basic model composite chart (Fig. 8) the action of the skeg is evident. The skeg was less effective on 404 than 406 since the amount of water flowing along the sides was quite small.

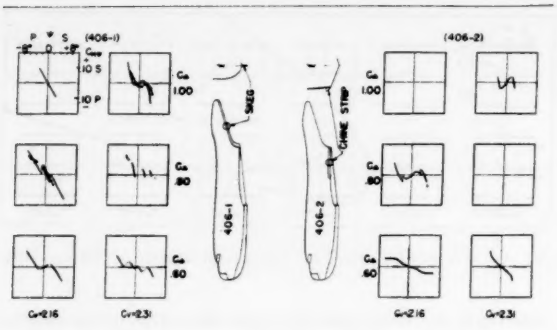

FIG. 11. Composite chart of directional stability; Model 406-1, 406-2.

Chine Strips

Chine strips were effective only on Model 406. This modification, designated 406-2, is shown with the test curves in Fig. 11. These strips were quite effective at low loads in preventing the water from flowing over the chine and along the afterbody sides. As a result, the directional stability was improved, especially at low loads ($C_\Delta = 0.60$).

Side Steps

Side steps as shown in Fig. 12 were added to both models (designated 404-3 and 406-3). Severe instability was eliminated in both cases at loads up to and in excess of $C_\Delta = 0.80$. The comparison of Figs. 13 and 14 with the basic models clearly indicates that substantial improvement was obtained at almost all speeds and loads by the breaking away of the water flow from the afterbody sides.

On 406-3 side steps it was necessary to have a cap strip (or lip) as shown to prevent the water from rising

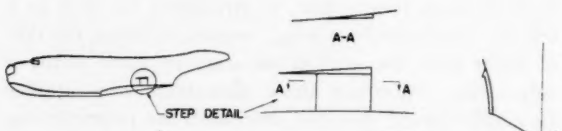

FIG. 12. Side step; Model 406-3.

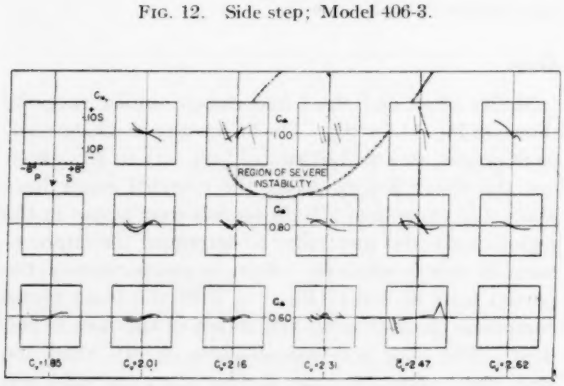

FIG. 13. Composite chart of directional stability; Model 406-3.

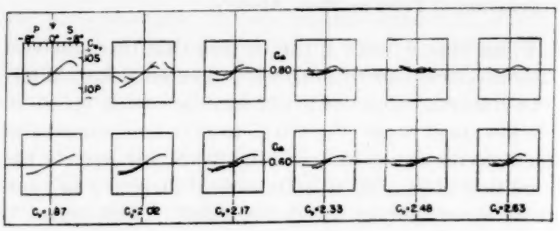

FIG. 14. Composite chart of directional stability; Model 404-3.

TABLE 1

Model Hull Proportions

	404	406
Forebody length/beam	3.44	3.35
Afterbody length/beam	2.74	2.74
Step depth at centerline/beam	0.050	0.049
Forebody-afterbody keel angle	7°	7½°
Deadrise angle at main step	20°	20°
C.G. above keel/beam	0.9	1.1
C.G. forward step/beam	0.43	0.37

over the top of the step. This was not included on 404-3, since the water in that case did not rise to the top of the step.

Flight Test

The side steps developed on both 404-3 and 406-3 were installed on the respective ships for flight-test correlation. The results from the former were inconclusive, but tests of the latter were carried far enough to determine their usefulness.

Whereas 406 had been directionally unstable cross-wind (even at $C_\Delta = 0.60$) and had exhibited severe directional instability at higher loads in calm weather ($C_\Delta = 0.80$); 406-3 was greatly improved. At high load ($C_\Delta = 0.80$) the ship with side steps installed could be taxied cross-wind up to hump speed in a fairly strong breeze. On a calm day it was possible to turn the ship in either direction by rudder control only at speeds and loads that before had caused uncontrollable swerving. In addition to the improvement in the directional stability, the resistance was lowered by the clearance of the water flow from the afterbody side and tail cone.

CONCLUSIONS

(1) Directional instability of a flying boat when taxiing in the water is a problem that has been brought about by the overloading of present hull designs rather than by a change in design methods.

(2) The problem on a particular ship can be investigated through the medium of small-model tests in a towing tank.

(3) In general, severe instability arises from unstable flow conditions around the afterbody sides and tail cone

(4) Simple devices to clear the water from the hull sides (side steps) or to straighten the flow (skegs) are effective in increasing the stability of the afterbody.

(5) Model test results are partially borne out by flight test, although the model results tend to be conservative.

REFERENCE

[1] Davidson, K. S. M., *The Growing Importance of Small Models for Studies in Naval Architecture*, Transactions of the Society of Naval Architects and Marine Engineers, Vol. 49, p. 91, 1941.

Letters to the Editor

Dear Sir:

Regarding the recent controversy in the wing theory with sweepback, (JOURNAL OF THE AERONAUTICAL SCIENCES, pp. 320, 321, October, 1943), the following points seem to deserve attention.

First, Cauchy's principal value of a *divergent* improper integral $\int_a^b f(y, c)dy$ is defined by

$$P\int_a^b f(y, c)dy = \lim_{\delta\to 0}\left\{\int_a^{c-\delta} f(y, c)dy + \int_{c+\delta}^b f(y, c)dy\right\} \tag{1}$$

if $f(y, c)$ becomes infinite at $y = c$. (See, e.g., Whittaker and Watson ,*Modern Analysis*, Cambridge, 1927, p. 75.) It is to be noted that we also have

$$2P\int_a^b f(y, c)dy = \lim_{\zeta_1\to 0}\int_a^b f(y, c+\zeta_1)dy + \lim_{\zeta_2\to 0}\int_a^b f(y, c+\zeta_2)dy \tag{2}$$

where $\zeta_1 = y_1 + iz_1$ and $\zeta_2 = y_2 + iz_2$ are two complex numbers such that $c + \zeta_1$ and $c + \zeta_2$ are on *opposite* sides of the real y-axis. This method of keeping the singular point *off* the path of integration can easily be seen to be equivalent to the usual method of "indenting" that path.

Let us now turn to the problem at hand—namely, the calculation of the down-wash velocity at the bound vortex in the lifting-line theory of a wing with a sweepback β. To avoid the difficulty of divergent integrals, calculate the down-wash at points *off* the vortex sheet, analogous to the mathematical procedure above. It can be easily verified that the down-wash w at a point which is at a distance z above (or below) the bound vortex is given by (see Fig. 1)

$$4\pi w = -\int_{-a}^{0}\frac{y}{y^2+z^2}\frac{d\Gamma}{dy}dy(1+\sin\beta') + \int_0^b\frac{y}{y^2+z^2}\frac{d\Gamma}{dy}dy(1-\sin\beta') = \int_0^a\frac{y\,dy}{y^2+z^2}\times\{\Gamma'(y)-\Gamma'(-y)\} - \int_0^a\frac{y\,dy}{y^2+z^2}\sin\beta'\times\{\Gamma'(y)+\Gamma'(-y)\} + \int_a^b\frac{y\,dy}{y^2+z^2}\frac{d\Gamma}{dy}(1-\sin\beta') \tag{3}$$

In the limit $z \to 0$, the first and the third integrals on the right-hand side becomes, respectively,

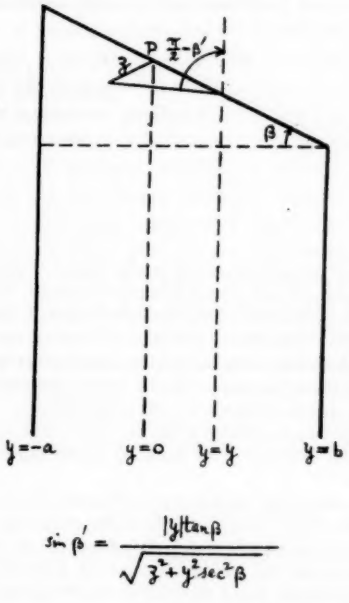

FIG. 1.

$$\int_0^a\frac{dy}{y}\{\Gamma'(y)-\Gamma'(-y)\} \quad\text{and}\quad \int_a^b\frac{dy}{y}\Gamma'(y)(1-\sin\beta)$$

which are both convergent. The second integral is, however, divergent for $z = 0$. This causes great difficulty unless $\sin\beta = 0$. In the case of zero sweepback, this difficulty disappears, and the down-wash at P is given by

$$4\pi w = \int_a^b\frac{dy}{y}\{\Gamma'(y)-\Gamma'(-y)\} + \int_a^b\frac{dy}{y}\Gamma'(y) \tag{4}$$

being in fact the values just above P and just below P (and, hence, also their average). This value agrees with that obtained from Cauchy's principal value of the integral $\int_{-a}^b (dy/y)\Gamma'(y)$. Hence, the usual application of Cauchy's principal value is justified. In fact, we have a direct application of Eq. (2) if we deal with the down-wash in the Trefftz plane (which is twice that in the plane at the load line in the case of zero sweepback) and use the method of complex variables for the two-dimensional motion in that plane.

Finally, it must be said that the use of any unconventional mathematical device must be justified by physical considerations. The above considerations indicate that the difficulty in the lift-line theory of a wing with sweepback is due to an over-simplification of the physical picture and can hardly be remedied by a mere mathematical artifice. It may also be noted that the disturbing term $(1 + u) \log \sin (\delta/2) - (1 - u) \log \sin (\epsilon/2)$ can be made equal to any real value if we suitably assign the manner in which $\epsilon, \delta \to 0$. In the case $u = 0$ (zero sweepback), the restriction $\epsilon = \delta$ is imposed, according to Cauchy's definition of principal value, because it can be justified as demonstrated above. In the case $u \neq 0$ (finite sweepback), the restriction imposed according to Mr. Theilheimer's definition of principal value can hardly be accepted, unless he can give a justification that also explains the difficulty associated with the second integral on the right-hand side of Eq. (3).

It appears that Professor Gail's objection, which expresses commonly accepted knowledge among aerodynamicists, is justified.

CHIA-CHIAO LIN
Guggenheim Laboratory
California Institute of Technology
Pasadena, California

Dear Sir:

Mr. Sandorff brings out in his recent paper, "Notes on Columns" (JOURNAL OF THE AERONAUTICAL SCIENCES, Vol. 11, p. 1, January, 1944), a host of points that are important and that are sometimes either overlooked or accepted more or less fatalistically. Even though nothing can be done about some of them, it is well to keep them in mind. About others something can be done. A few specific comments occur to the writer.

There appears to be a misprint in Eq. (11). The L in the first term should be deleted. This equation is the same as Eq. (8) in reference 3.

The usual concept of "end-fixity coefficient" is a carry-over of thinking in the Euler range. In the Euler range the concept is a perfectly natural one and is directly related to the critical load. In the plastic range the concept is artificial, however, and gives no direct information about the load or anything else. Thus, in the Euler range an "end-fixity coefficient" of 4 means that the column can carry four times the load it could carry if simply supported. In the plastic range an "end-fixity coefficient" of 4 means nothing of the kind. The coefficient 4 here tells nothing about the load. A much more preferable concept, it seems to the writer, is that of free length, applicable regardless of whether the elastic range or the plastic range is being considered. If one defines a "coefficient of length" (to avoid confusion with existing terminology) K as $K = L_0/L$, where L_0 is the free length or distance between successive points of inflection, then the specification of K immediately gives a direct picture of the given column in terms of a simply supported column of the same cross section; for $L_0 = KL$ is the length of the simply supported column that would fail at the same critical load as the given column of length L, *regardless of whether the average stress is in the elastic range or the plastic.* Here L_0 is the author's L_e, and $K = 1/\sqrt{c}$.

In the section on "End-Fixity of Column Test Specimens" the author gives an excellent summary of matters to be considered. The only valid argument for flat-end testing of columns is that tests with known end conditions are either impossible or highly impracticable. To justify flat-end tests on any other basis is to rationalize, as the author's discussion well brings out.

An additional reason may be cited why built-in support is not achieved. When the fluid in a hydraulic machine is confined by packing around the ram, rotation of the lower head of the testing machine about a horizontal axis is possible since the packing is relatively not very stiff and can give. A so-called lapped ram is preferable where compressive tests are to be made.

Under the subheading "Testing with Known End-Restraint" should the reference not be 3 rather than 5? In any event it is questionable whether tests with known elastic end restraints give any information that tests with simply supported ends do not give. If the loading is central, they certainly do not (in spite of reference 3!). If the loading consists of an axial load applied with a constant eccentricity combined with elastic end restraints, the problem, especially in the plastic range, becomes complicated, and it may be that the way to handle it is to test under these conditions and determine an equivalent constant eccentricity. Or it may be possible to determine an equivalent length corresponding to the given constant eccentricity, that is, to determine the length of a column that would fail at the same load applied with the same constant eccentricity as the test column but without the latter's end restraint.

WM. R. OSGOOD
Materials Engineer
National Bureau of Standards

Dear Sir:

I should like to call your attention to several errors I have noted in the article "Take-Off Distance of a Glider Train" by Wieslaw Z. Stepniewski which appeared in the January, 1944 issue of the JOURNAL.

The following errors are in the derivations of the equations:

(1) Eq. (4) is not dimensionally correct as it is written. The value $\rho/2$ was omitted as a multiplier of the quantities within the parentheses of the right side of the equation. Correctly written, the equation is:

$$T_s = T - \left[(B_a S_a + B_g S_g) \frac{\rho}{2} V^2 + W\mu \right]$$

(2) The notation given for aspect ratio is not the same as that used in presenting the equations.

(3) In Eq. (20a), the subscript on the velocity in the lower right-hand member of the equation should be a not g.

(4) In Eq. (21a), the bracketed expression "(nD)" in the lower right-hand member of the equation should be raised to the third power rather than have the subscript "3."

The "Numerical Example" at the end of the derivation of the equations contained these errors:

(1) The assumed take-off speed for the glider, V_g, is 59 m.p.h. This is not equal to 72 ft. per sec. as stated but equal to 86.5 ft. per sec. This error, of course, affects practically the whole problem.

(2) The given value of $W_g(C_{Dg}/C_{Lg})_b$ appears to be wrong even using the incorrect value of $V_g = 72$ ft. per sec. in the computation.

(3) The computed value of c_b seems high by about 5 per cent.

(4) The value of $W_a(C_{Da}/C_{La})_c$ given is about 13 per cent. low.

(5) The value of $s_c = 530$ ft. seems to be wrong even using the given erroneous values in its computation.

For the assumed characteristics, I find the following results:

	Exact Formula	Approximate Formula
s_g	908	878
s_a	740	680
s_c	570	...
$s_g + s_a + s_c$	2,218	2,128

RICHARD H. SAWYER
Aeronautical Engineer
N.A.C.A

Theory of the Centrifugally Tuned Vibration Absorber

RALPH J. HARKER*

United Aircraft Corporation

SUMMARY

This investigation is primarily concerned with the performance of an idealized centrifugally tuned pendulum at the condition of maximum response of the main system on which it operates. It is therefore possible to dispense with the consideration of the response curve as a whole by focusing attention on the peak, which is the singularly important point. Calculations are made which show the effect of tuning, damping, and mass ratio upon absorber characteristics at the peak frequency, providing a rational basis for design and the interpretation of test results.

The absorber is found to produce maximum reduction in vibratory amplitude when there is minimum absorber damping, minimum main system damping, optimum tuning, and maximum mass ratio. Optimum tuning is slightly less than exact and is a function only of mass ratio. Relative motion of the absorber is a minimum at optimum tuning, and at this condition the motion is practically independent of absorber damping. The frequency at which maximum motion occurs in the response curve of the main system is always decreased if the absorber is "overtuned" or if the tuning is optimum or exact; however, the peak frequency may be increased or decreased by an "undertuned" absorber, depending on the extent of off-tuning. A chart is presented by means of which the main system response peak frequency and amplitude can be determined for any combination of absorber tuning, damping, and mass ratio.

INTRODUCTION

THE CENTRIFUGALLY TUNED VIBRATION ABSORBER is a device for suppressing vibratory amplitudes in rotating systems. Regardless of the form in which it may appear, any centrifugal absorber is equivalent to a pendulum, depending upon the acceleration field produced by rotational velocity for the force tending to restore it to its equilibrium position. Because of this feature it can be shown that the natural frequency of the absorber is directly proportional to rotative speed and, hence, may be tuned to any order or multiple of the speed. Since most vibrations are caused by order excitations, this type of absorber is particularly useful in suppressing one undesirable order throughout the entire speed range.

Fundamentally, a centrifugal pendulum is a single degree of freedom system receiving its excitation from the vibratory amplitude of the main system upon which it is superimposed, and there are three variables defined by the absorber design which contribute to the behavior of the main and absorber systems during operation. These are the absorber mass, tuning, and damping; however, as the absorber participates in the vibration as a part of a complex system it cannot be isolated, but must be treated as an integral part of the entire system. In the rational analysis of a vibration absorber, therefore, the main system on which it is to operate must first be established.

If an absorber is installed on a rotating system, there is always a modification of the vibratory mode shape because the absorber applies a force at a single point on an elastic system; however, in many cases this change is negligible since the absorber force is inherently a damping component which, in effect, increases the damping of the main system. Since the damping forces are ordinarily small with respect to the mass and spring forces existing in a vibrating system, the absorber will often produce little change in mode shape. In the following analysis it is assumed that the mode shape is unchanged, and that therefore the main system may be reduced to an equivalent single degree of freedom system, consisting of a concentrated mass and single spring, having the same natural frequency and the same moment of inertia as the actual system.

ASSUMED CONDITIONS

In addition to the selection of the general type of main system to be analyzed, certain other assumptions must be made regarding the idealized system shown in Fig. 1. For simplicity small amplitudes are assumed, and the centers of gravity of both masses are taken at the same distance from the center of rotation. Viscous damping is assumed in both the main and auxiliary systems. As the entire system rotates at a constant angular velocity, an alternating force excites the main mass at a frequency that is a multiple of rotational velocity; that is, there is an order excitation. The magnitude of the excitation is assumed to be constant and independent of frequency. As shown in Fig. 2 the system under consideration is really a classic two degree of freedom system with minor modifications necessary to convert from a linear to a rotational case.

NOTATION

M	= equivalent mass of main system at radius $(R + r)$
m	= mass of absorber
R	= distance from center of rotation to pivot of pendulum
r	= length of absorber pendulum
K	= effective spring constant for main system
k	= equivalent spring constant of the absorber

Presented at the Power Plants and Propellers Session, Twelfth Annual Meeting, I.A.S., New York, January 25–27, 1944.

* Senior Analytical Engineer, Hamilton Standard Propellers Division.

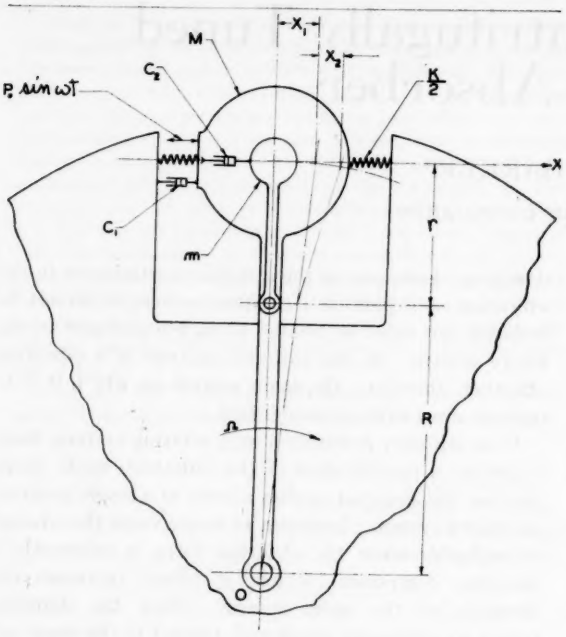

FIG. 1. Idealized centrifugal absorber and main system.

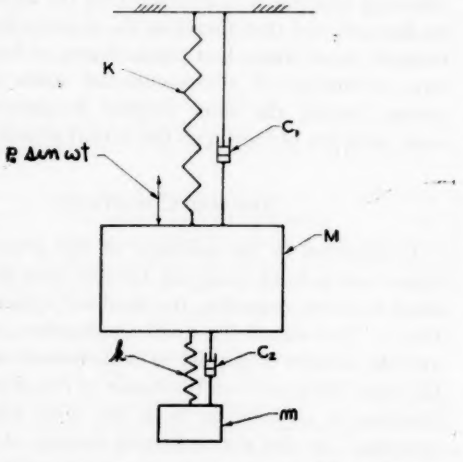

FIG. 2. Equivalent linear system with viscous damping in both the main and auxiliary systems.

Ω = angular velocity of rotation of the system
x_1 = displacement of the main mass
x_2 = relative displacement of the absorber mass
P_t = amplitude of the exciting force
ω = frequency of the exciting force
n = order of the excitation = ω/Ω
c_1 = damping coefficient of the main system
c_c' = critical damping coefficient of the main system
c_2 = damping coefficient of the absorber system
c_c'' = critical damping coefficient of the absorber system
ω_a = natural frequency of the absorber system
Ω_n = natural frequency of the system, absorber locked = $\sqrt{K/(M+m)}$
N = order to which absorber is tuned = ω_a/Ω
j = complex operator
μ = mass ratio, = $m/(M+m)$
f = ratio of absorber to main system natural frequency = ω_a/Ω_n
g = ratio of the exciting frequency to the natural frequency of the main system = ω/Ω_n
g_m = ratio of the frequency of maximum response with the absorber acting to the resonant frequency with the absorber locked
x_{st} = static deflection of the main system = P_0/K
x/x_{st} = magnification factor
c/c_c = ratio of actual to critical damping
A = ratio of absorber natural frequency to exciting frequency = $f/g = \omega_a/\omega = N/n$
α = tuning parameter = $(A^2 - 1)$ (α is positive for an overtuned and negative for an undertuned absorber)
γ_1 = main system damping parameter = $2(c_1/c_c')$
γ_2 = absorber system damping parameter = $2(c_2/c_c'')$
B = reduction factor or the ratio of magnification factor of the main system at maximum response without an absorber to the same factor with an absorber
a_1 = complex variable representing linear displacement of main mass
a_2 = complex variable representing relative linear displacement of absorber mass
F_{21} = the force exerted by the absorber on the main mass
φ = time phase angle between rotating vectors

EQUATIONS OF MOTION FOR THE MAIN MASS

Taking the summation of all forces on the total and on the absorber systems, respectively, Fig. 2, the following equations are obtained:

$$\Sigma F_x = -Kx_1 - M\ddot{x}_1 - m(\ddot{x}_1 + \ddot{x}_2) - c_1\dot{x}_1 + P_0 \sin \omega t = 0 \quad (1)$$

$$\Sigma F_x = -m(\ddot{x}_1 + \ddot{x}_2) - kx_2 - c_2\dot{x}_2 = 0 \quad (2)$$

These equations, representing the spring, inertia, damping, and exciting forces, may be solved by making the usual substitutions for displacement, velocity, and acceleration.

$$x = x_0 \sin \omega t = a$$
$$\dot{x} = x_0\, \omega \cos \omega t = ja\omega$$
$$\ddot{x} = -x_0\, \omega^2 \sin \omega t = -a\omega^2$$

Then

$$a_1[K - (M+m)\omega^2 + jc_1\omega] - a_2(m\omega^2) = P_0 \quad (3)$$

$$a_1(m\omega^2) - a_2(k - m\omega^2 + jc_2\omega) = 0 \quad (4)$$

These equations now represent the motion of a main system with a spring-coupled absorber. Equations for the motion of the rotational system under consideration, Fig. 1, differ in only one respect—in the absorber spring constant, k, which becomes, for a pendulum in a purely radial field,

$$k = (R/r)m\Omega^2$$

where the equivalent spring is located at the center of gravity of the pendulum. In other words, the change is from a spring-coupled to a mass-coupled absorber.

It can be seen that if $a_2 = 0$ in Eq. (3), which is the condition of a locked absorber, the resulting equation

is that of a single degree of freedom system with a mass equal to $(M + m)$. Also in Eq. (4) if $a_1 = 0$, the equation for the natural frequency of a damped pendulum results since the pendulum fulcrum becomes fixed; however, the effect of the damping term upon the natural frequency may be neglected for ordinary values of damping.

$$(\omega_a/\Omega)^2 = (R/r) = N^2 \tag{5}$$

Eqs. (3) and (4) can be made dimensionless by dividing Eq. (3) by K and Eq. (4) by $m\Omega_n^2$

$$a_1(1 - g^2 + j\gamma_1 g) - a_2(\mu g^2) = x_{st} \tag{6}$$

$$a_1(g^2) + a_2(g^2 - f^2 - j\gamma_2 g) = 0 \tag{7}$$

But f is functionally related to g because both variables are multiples of the rotational velocity, shown graphically in Fig. 3.

$$f/g = \omega_a/\omega = N/n = A$$

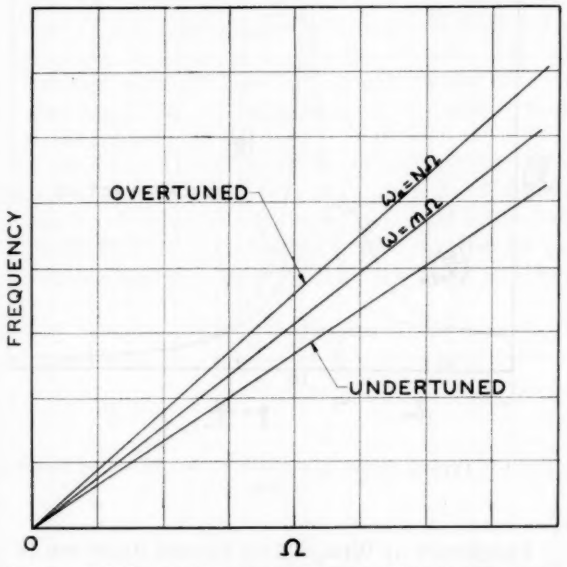

FIG. 3. Relation of the natural frequency of the absorber system to the external exciting frequency.

Then Eq. (7) reduces to

$$a_1(g^2) + a_2[g^2(1 - A^2) - j\gamma_2 g] = 0 \tag{8}$$

When Eqs. (6) and (8) for a_1 are solved, an expression is obtained for the magnification factor of the main mass amplitude; that is, the ratio of the actual amplitude to the static deflection.

$$\frac{a_1}{x_{st}} = \frac{\alpha g + j\gamma_2}{[-g^3(\mu + \alpha) + g(\alpha - \gamma_1\gamma_2)] + j[g^2(\alpha\gamma_1 - \gamma_2) + \gamma_2]} \tag{9}$$

Thus, the main mass amplitude is proportional to the quotient of two complex terms and may be represented by a vector of constant length rotating in a complex plane at a constant angular velocity. Eq. (9) may be simplified by neglecting damping in the main system so that all terms involving γ_1 vanish.

$$\frac{a_1}{x_{st}} = \frac{\alpha g + j\gamma_2}{[\alpha g(1 - g^2) - \mu g^3] + j[\gamma_2(1 - g^2)]} \tag{10}$$

Although the frequency at which the main mass motion is maximum is not necessarily the frequency at which response is maximum with the absorber acting, it is often a good approximation. Letting $g = 1$

$$a_1/x_{st} = (\alpha + j\gamma_2)/-\mu \tag{11}$$

Also, for exact tuning, $\alpha = 0$, and the magnitude becomes

$$a_1/x_{st} = -j(\gamma_2/\mu) \tag{12}$$

The $-j$ operator simply means that the main mass amplitude lags the exciting force by a time phase angle of 90° under these conditions and has a magnitude of (γ_2/μ). This is an important relation. It indicates that for an exactly tuned absorber with operation at the frequency of the locked absorber resonance and with zero damping in the main system the magnification factor is directly proportional to the damping in the absorber and inversely proportional to the mass ratio. Thus it is desirable to make the absorber mass as large as practical and the absorber damping as low as possible.

By applying the foregoing assumptions but retaining damping in the main system, Eq. (9) becomes, considering amplitude only,

$$a_1/x_{st} = 1/[\gamma_1 + (\mu/\gamma_2)] \tag{13}$$

A large main system damping factor is seen to correspond to a low magnification factor; however, from the standpoint of absorber effectiveness, large main system damping tends to minimize the reduction factor that can be obtained with a given absorber. The reduction factor is approximately

$$B = \frac{(1/\gamma_1)}{\left(\dfrac{1}{\gamma_1 + (\mu/\gamma_2)}\right)} = 1 + \frac{\mu}{\gamma_1\gamma_2} \tag{14}$$

RELATIVE MOTION

Motion of the absorber mass with respect to the main mass can be obtained by solving Eqs. (6) and (8).

$$\frac{a_2}{x_{st}} = \frac{g}{[-g^3(\mu + \alpha) + g(\alpha - \gamma_1\gamma_2)] + j[g^2(\alpha\gamma_1 - \gamma_2) + \gamma_2]} \tag{15}$$

It must be remembered, however, that Eq. (15) does not represent the magnification factor of the auxiliary sys-

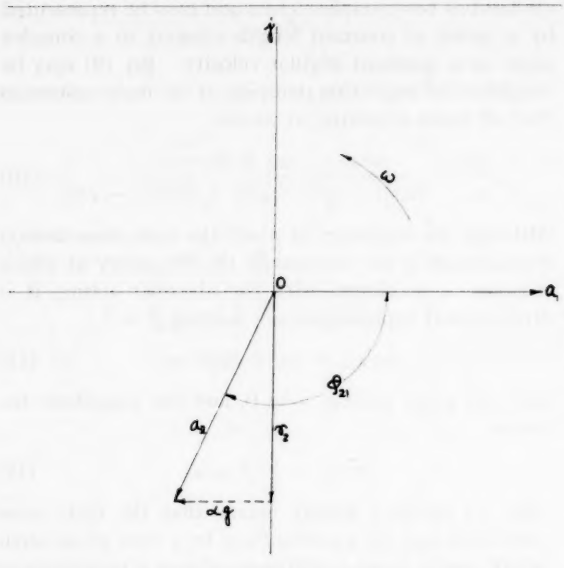

FIG. 4. Phase relationship between the main mass and the absorber mass for an undertuned absorber ($N < n$).

tem, since it involves the ratio of the absorber amplitude to the static deflection of the main system, P_0/K. The true magnification factor of the auxiliary system is the ratio of the absorber amplitude to the motion of the main mass, or

$$a_2/a_1 = g/(\alpha g + j\gamma_2) \tag{16}$$

For exact tuning, $\alpha = 0$, and at $g = 1$, the ratio of the two amplitudes becomes

$$a_2/a_1 = g/\gamma_2 = 1/\gamma_2 \tag{17}$$

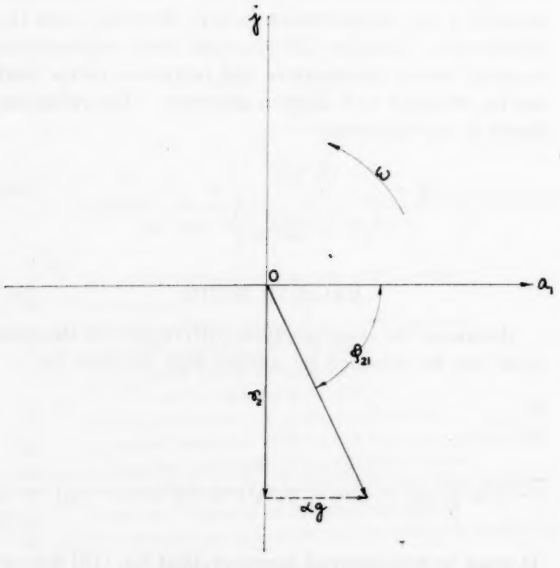

FIG. 5. Phase relationship between the main mass and the absorber mass for an overtuned absorber ($N > n$).

Thus, at resonance, the absorber acts as a single degree of freedom system with a magnification factor $a_2/a_1 = 1/2(c/c_c)$.

Vectorially, the phase relationship of a_2 to a_1 may be seen in Figs. 4 and 5, which illustrate the cases of undertuning and overtuning, respectively. The absorber motion lags the main mass motion by an angle φ_{21}:

$$\tan \varphi_{21} = \gamma_2/\alpha g \tag{18}$$

where the angle is measured in a negative or counterclockwise direction. If the relative motion vector lies in the fourth quadrant, the absorber is overtuned; that is, it is tuned to a somewhat higher order than that of the exciting frequency. In the third quadrant it is undertuned and, if φ_{21} is 90°, the tuning is exact.

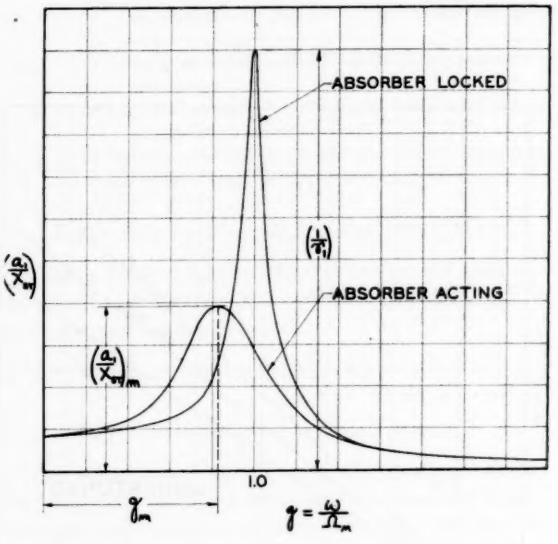

FIG. 6. Typical change in response curve effected by absorber action.

FREQUENCY AT WHICH MAIN SYSTEM RESPONSE IS MAXIMUM

Eqs. (12), (13), and (14) are not true indications of absorber performance because the assumption is made that the maximum main system response occurs at $g = 1$ or that the original peak is not shifted by the absorber. Also, the absorber has been assumed to be exactly tuned, $\alpha = 0$. It will now be shown that, except under certain conditions of damping, tuning, and mass ratio, the frequency at which the main system motion becomes maximum is changed by the action of the absorber. Fig. 6 illustrates a typical alteration effected in the shape of the response curve. The point on the response curve which has a horizontal tangent may be obtained by differentiating Eq. (9) with respect to g^2, after first having divided the numerator and denominator by μ and then squared the real and imaginary components to obtain an expression for the magnitude of the magnifica-

tion factor. Setting this derivative equal to zero, the equation is

$$A'g^6 + B'g^4 + C'g^2 + D' = 0 \qquad (19)$$

where

$$A' = 2(\alpha/\mu)^2[(\alpha/\mu) + 1]^2$$

$$B' = \left(\frac{\alpha}{\mu}\right)^2\left[\left(\frac{\gamma_2}{\mu}\right)^2 - 2\left(\frac{\alpha}{\mu}\right)^2 - 2\left(\frac{\alpha}{\mu}\right)\right] + 3\left(\frac{\gamma_2}{\mu}\right)^2\left(\frac{\alpha}{\mu} + 1\right)^2 + \gamma_1\left(\frac{\alpha}{\mu}\right)^2\left(2\frac{\gamma_2}{\mu} + \gamma_1\right)$$

$$C' = 2\left(\frac{\gamma_2}{\mu}\right)^2\left[\left(\frac{\gamma_2}{\mu}\right)^2 - 2\left(\frac{\alpha}{\mu}\right)^2 - 2\left(\frac{\alpha}{\mu}\right)\right] + 2\,\gamma_1\left(\frac{\gamma_2}{\mu}\right)^2\left[2\left(\frac{\gamma_2}{\mu}\right) + \gamma_1\left(\frac{\alpha}{\mu}\right)^2\right]$$

$$D' = (\gamma_2/\mu)^4(\gamma_1^2 - 2)$$

It can be shown that for zero main system damping, $\gamma_1 = 0$, there will be only one real, positive root of Eq. (19) and, hence, only one maximum in the response curve. The same appears to be true with main system damping, although the proof is not obvious. This is in contrast with the constant or spring-tuned absorber that has, under certain conditions, two definite peaks in the response curve.

Since g_m is a function of three variables (α/μ), (γ_2/μ), and γ_1, the peak shift resulting from a given absorber can be calculated directly from Eq. (19) by determining the coefficients and solving the cubic equation for g_m^2. This has been done for the case of $\gamma_1 = 0$ and $\gamma_1 = 0.04$.

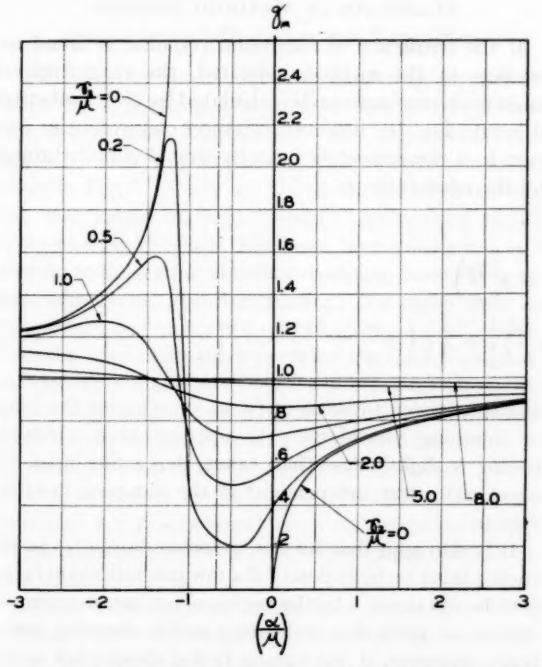

FIG. 7. Shift in peak frequency resulting from the absorber for a main system damping of $\gamma_1 = 0.04$. If $g_m > 1$, the peak shifts up; if $g_m < 1$, the peak shifts down.

As there is practically no difference between the results obtained for each condition, only the damped condition is plotted, Fig. 7. The parameters are (α/μ) and (γ_2/μ); that is, the effect of absorber damping and tuning can be observed for a constant absorber mass. Negative values of (α/μ) correspond to undertuning; positive values, to overtuning. Apparently, an overtuned absorber always shifts the peak to a lower frequency than it was originally; however, an undertuned absorber can shift the peak up or down, depending upon the extent of off-tuning as indicated by the curves.

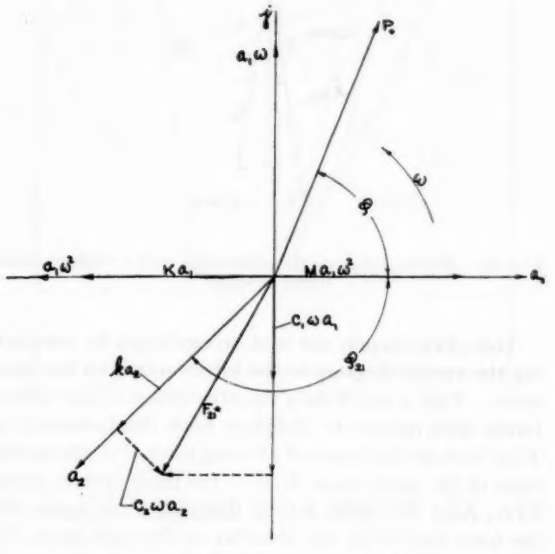

FIG. 8. Forces acting on the main mass with an undertuned absorber.

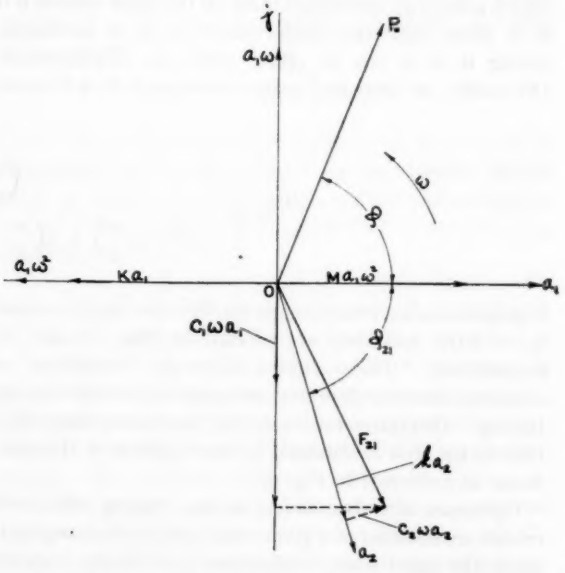

FIG. 9. Forces acting on the main mass with an overtuned absorber.

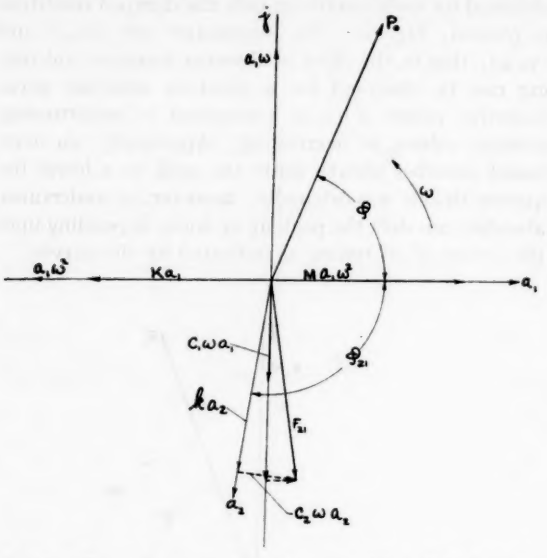

FIG. 10. Forces acting on the main mass with a slightly undertuned absorber.

This phenomenon can best be explained by considering the vector diagram of the forces acting on the main mass. Figs. 8 and 9 show the orientation of the various forces with respect to the main mass displacement, a_1. They include the external exciting force, P_0; the inertia force of the main mass, $Ma_1\omega^2$; the main system spring force, Ka_1; the main system damping force, $c_1a_1\omega$; and the force exerted by the absorber on the main mass, F_{21}. This latter force may be resolved into two components—one in phase with the main system damping force, and one in or out of phase with the main mass displacement, which acts as an additional mass on the main system if it is in phase with the displacement or as an additional spring if it is out of phase with the displacement. Obviously, an increased mass corresponds to a lowered resonant frequency, and an increased spring corresponds to an increased resonant frequency, so, in general, an overtuned absorber shifts the peak down and an undertuned absorber shifts the peak up. As shown in Fig. 10, however, a slightly undertuned absorber actually adds a mass component to the main system because the absorber damping force, $c_2a_2\omega$, shifts the force vector, F_{21}, from the third quadrant to the fourth. In these vector diagrams only general relations are represented, and the magnitudes and phase angles shown do not represent any exact set of conditions.

In Fig. 7 it is also of interest to note the large shift in peak which usually occurs if the ratio of absorber damping to mass ratio is a small quantity and the extreme sensitivity of the system to slight changes in tuning in the vicinity of $(\alpha/\mu) = -1$. On the other hand, for high values of (γ_2/μ) there will be practically no shift in peak regardless of tuning. For zero absorber damping the peak frequency approaches zero if the tuning is decreased to approach exact tuning, but, if the tuning is increased to approach exact tuning, the peak frequency approaches infinity. In the tuning range between these conditions no maximum exists in the response curve since there is no horizontal tangent to the curve at any frequency. All curves are seen to approach $g_m = 1$ if the tuning is sufficiently away from exact. This means that there will be little peak shift affected by an untuned absorber because an absorber cannot have an important effect on the main system unless it is in a resonant or nearly resonant condition.

MAGNITUDE OF MAXIMUM RESPONSE

If the frequency of maximum response is found according to the method indicated, the magnitude of main mass response can be calculated by direct substitution into Eq. (9); however, it is more convenient to convert to a dimensionless form by first dividing through by the mass ratio, μ.

$$\frac{a_1}{x_{s1}} = \frac{\left(\frac{\alpha}{\mu}\right)g + j\left(\frac{\gamma_2}{\mu}\right)}{\left[-g^3\left(1+\frac{\alpha}{\mu}\right) + g\left(\frac{\alpha}{\mu} - \gamma_1\frac{\gamma_2}{\mu}\right)\right] + j\left[g^2\left(\gamma_1\frac{\alpha}{\mu} - \frac{\gamma_2}{\mu}\right) + \frac{\gamma_2}{\mu}\right]} \tag{20}$$

Calculations have been made for the case of $\gamma_1 = 0$ and $\gamma_1 = 0.04$, and they are plotted in Figs. 11 and 12, respectively. These curves represent conditions of constant absorber damping and mass ratio with varying tuning. Ordinates represent the maximum magnification factor that is obtained in the response of the main mass, as indicated in Fig. 6.

Optimum absorber tuning is that tuning which will enable an absorber of a given mass and given damping to allow the main mass a minimum peak in its response curve. In Figs. 11 and 12, therefore, optimum tuning corresponds to the lowest point on each of the curves, and this is seen to occur at $(\alpha/\mu) = -2/3$ for the range of damping considered. It appears that optimum tuning is slightly less than exact, depending upon the mass ratio, but independent of the damping in either system.

It is also seen that for low absorber damping, γ_2, the tuning must be held closely if a low magnification factor is to be obtained. In the region of optimum tuning all curves are quite flat, indicating stable absorber operation; however, if the tuning factor should fall at the steep portion of the curve the absorber would be extremely sensitive to tuning changes.

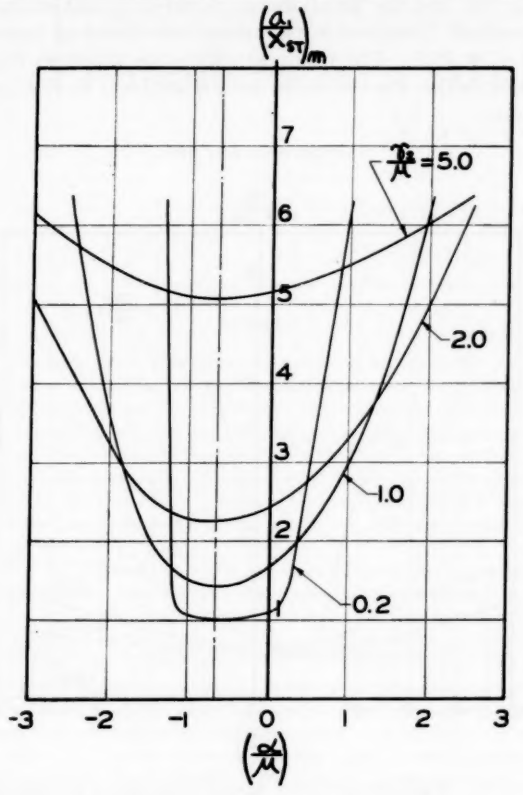

FIG. 11. Reduction in main system magnification factor for zero main system damping ($\gamma_1 = 0$).

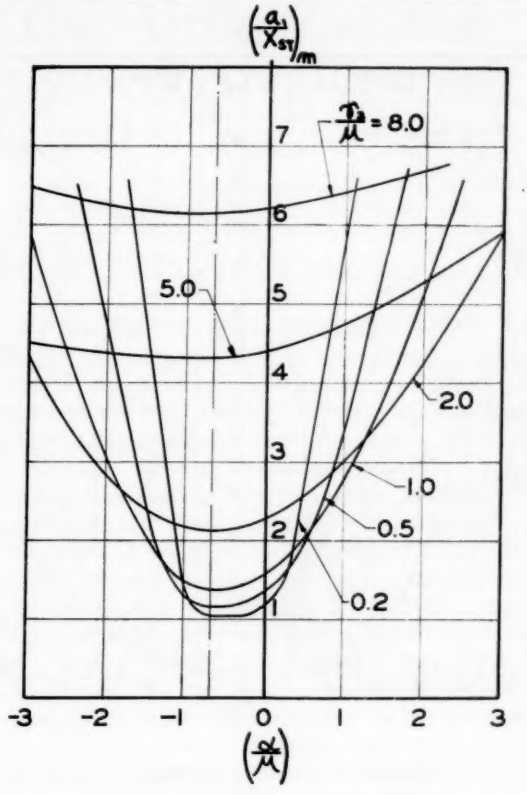

FIG. 12. Reduction in main system magnification factor for a main system damping of $c/c_c = 0.02$ ($\gamma_1 = 0.04$).

SIMULTANEOUS SOLUTION FOR VARIABLES

If a frequency versus vibratory amplitude curve is obtained on a rotating system and then the system is equipped with an absorber and a new response curve is obtained, two important factors are determined, as shown in Fig. 6. They are the shift in peak frequency and the change in main system magnification factor. By employing the data that have been calculated, it is possible to determine absorber damping, mass ratio, or, more important, absorber tuning. To make such an interpretation requires the superposition of two families of curves—one made up of curves of constant peak shift, and the other made up of curves of constant maximum main system magnification factor, Fig. 13. The former set of curves emanates from a single point at $(\alpha/\mu) = -1$, while the latter set is a series of somewhat circular curves converging at $(\alpha/\mu) = -1$ and $(\alpha/\mu) = 0$. Ordinates are proportional to absorber damping and abscissas are proportional to absorber tuning for a given mass ratio.

Suppose that response curves have been obtained on a system with the absorber locked and then with it acting, with the result that the peak is shifted down to $g_m = 0.95$ and the peak magnitude is reduced to one-quarter of its original value or $B = 4$. Also suppose that the main system damping factor γ_1 is 0.04, so that Fig. 13 applies, and that the mass ratio is 0.01. Now the magnification factor of the main system at resonance without an absorber is a function only of the damping in the system:

$$a_1/x_{st} = 1/\gamma_1 = 1/2(c/c_c)$$

Therefore, if the magnitude of the peak is reduced to one-quarter of its original value by the absorber action and if the exciting force remains constant, the maximum magnification factor with the absorber acting must be (25)(0.25) or 6.25.

The point P as located on Fig. 13 represents conditions outlined; that is, it is on the curve $g_m = 0.95$ and one-quarter of the distance from the curve $(a_1/_s x_t) = 6$ to $(a_1/x_{st}) = 7$. The corresponding ordinate is $(\gamma_2/\mu) = 5.15$, and the corresponding abscissa is $(\alpha/\mu) = 3.30$. Since $\mu = 0.01$, the absorber system damping factor $\gamma_2 = 0.0515$ or the damping is 2.575 per cent of critical. The absorber tuning is seen to be $(N/n)^2 = 1.033$ with respect to exact tuning; however, optimum tuning for this mass ratio is $\alpha = -(^2/_3)\mu$ or -0.0067, $(N/n)^2 = 0.9933$. To change the absorber tuning from its actual value to the optimum value therefore requires a reduction of (1.033 − 0.9933) or 0.0397 in the order

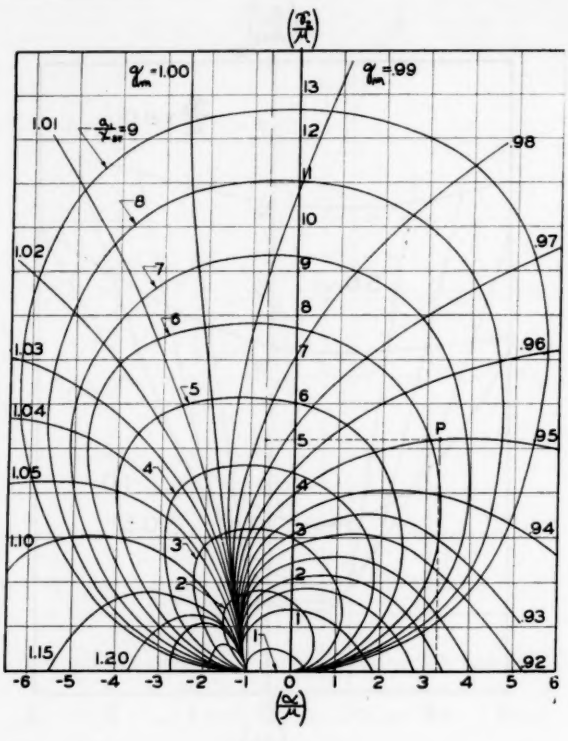

FIG. 13. Characteristic absorber performance curves (γ_1 = 0.04).

squared. If the tuning is so corrected, the optimum maximum magnification factor can be found by shifting horizontally from the point P to the dashed line that indicates optimum tuning, and it is seen to be (a_1/x_{st}) = 4.40 instead of the previous 6.25. The new g_m will be 0.977 instead of 0.950.

Fig. 13 is especially useful in indicating general absorber characteristics. For instance, if an absorber does not produce an appreciable peak shift, there is little to be gained by adjusting the tuning because the curve of $g_m = 1$ is close to the dashed line representing optimum tuning. Also, large shifts in peak frequency are not to be expected except when the absorber damping is a small quantity. When this is the case careful adjustment of the tuning can make a tremendous difference in both the peak shift and the peak reduction effected.

VARIATION IN RELATIVE MOTION

Motion of the absorber mass with respect to the main mass can also be expressed in dimensionless form by manipulating Eq. (16) as follows:

$$a_2\left(\frac{\mu}{x_{st}}\right) = \left(\frac{a_1}{x_{st}}\right)\left[\frac{g}{(\alpha/\mu)g + j(\gamma_2/\mu)}\right] \qquad (21)$$

Since the amplitude of relative motion is usually of primary importance at the peak frequency of the main system, values of $a_2(\mu/x_{st})$ have been calculated using Eq. (21) and the simultaneous values of g_m and (a_1/x_{st}) previously computed for a main system damping factor of $\gamma_1 = 0.04$. The resultant curves are shown in Fig. 14, in which the ordinates are proportional to relative motion.

(*Continued on page 246*)

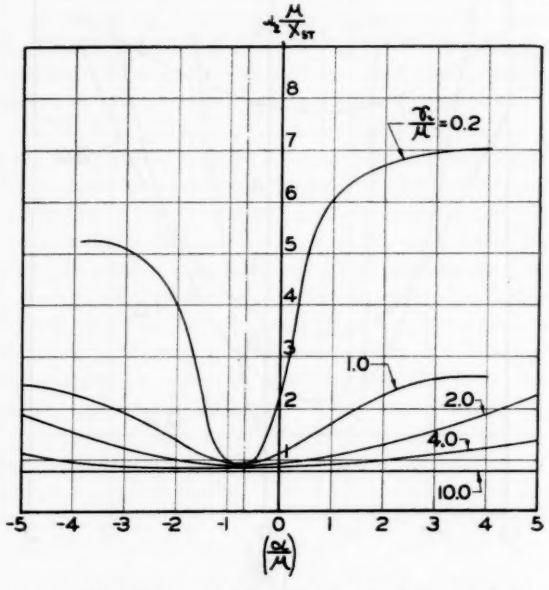

FIG. 14. Variation in relative motion amplitude of the absorber mass with tuning (γ_1 = 0.04).

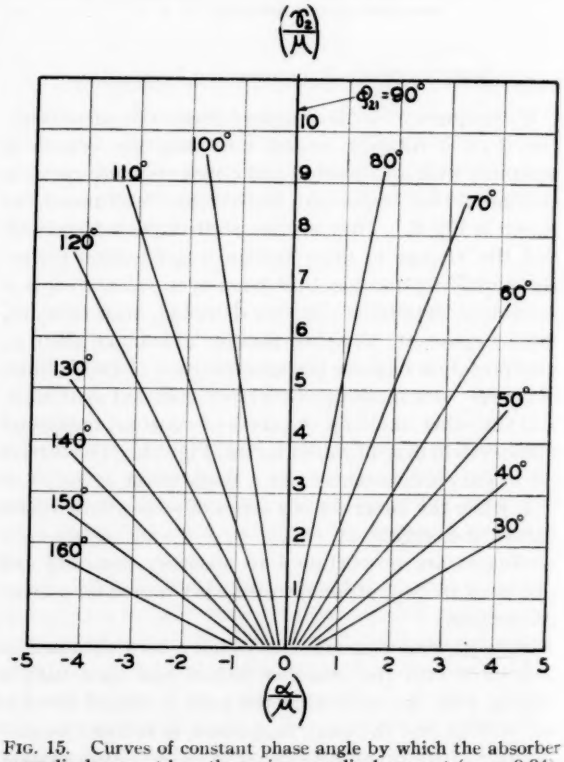

FIG. 15. Curves of constant phase angle by which the absorber mass displacement lags the main mass displacement (γ_1 = 0.04).

Fuselage Influence on the Airflow at the Propellers of a Multiengined Airplane in Yawed Flight

R. P. HARRINGTON* AND VICTOR ZADIKOV†

Polytechnic Institute of Brooklyn

SUMMARY

The paper develops expressions for the aerodynamic interference of the fuselage of multiengined airplanes on the propellers for the general case of yawed flight. Such effects of the fuselage are considered as increased or decreased velocity components—one of which is parallel to the axis of rotation of the propeller; and the other, along a radius of the fuselage cross section in the plane of the propeller. The latter velocity component is later expressed as a tangential increment at any radius and position of the blade.

The fore part of the fuselage is approximated by an ellipsoid of revolution. The disturbances attributed to the fuselage are considered as those due to an additional potential that satisfies the equation of continuity and the boundary conditions at the surface of the ellipsoid—i.e., that the normal velocity components at the surface vanish. The development is facilitated by the application of ellipsoidal harmonics. The coordinate system consists of confocal ellipsoids of revolution and hyperboloids of two sheets. The third coordinate is the angle of rotation about the major axis of the ellipsoid. The velocity components desired are found by differentiating the additional potential partially with respect to the line element in the desired direction.

Values of the disturbing velocities expressed in terms of W_0, the resultant velocity of the airplane, are worked out for a special case of propeller location. The effect of these velocities on the angle of attack of a blade element at 75 per cent radius is depicted by curves for yawing angles between $\pm 90°$. When the propeller diameter is assumed to be $3b$, where b is the maximum radius of the fuselage, and is located in a plane at $1.2b$ from the nose with its axis located $2.75b$ from the centerline of the fuselage, the angle-of-attack increments of the element amount to 2.6° at certain blade positions for a typical installation at zero yaw.

INTRODUCTION

CERTAIN AERODYNAMIC DISTURBANCES of the flow through the propellers of multiengined airplanes may be attributed to the presence of the fuselage. Such disturbances, sometimes referred to as interference, appear as additional velocities superimposed on the resultant velocity of the airplane and, of course, vary in magnitude and direction at various points throughout the disc of propeller-blade travel. These variations in velocity change the angle of attack of the blade elements and, because of the resulting variations of lift, drag, and center of pressure location, may be a source of torsional and bending vibrations.

Presented at the Aerodynamics Session, Twelfth Annual Meeting, I.A.S., New York, January 25–27, 1944.

* Head of the Department of Aeronautical Engineering.

† Student Assistant. Now Research Engineer, Republic Aviation Corporation.

This problem was first investigated by Gail and Lu,[1] who superimposed a point source on a uniform flow as a representation of the fuselage. Effects of changes in the velocity, only in the axial direction, through the propeller disc were considered. Since it was felt that velocity components induced by the fuselage in the plane of the propeller might have considerable effect, it was suggested by the senior author to Harry M. Goldberg in 1942 to carry out a similar investigation considering the fore part of the fuselage as an ellipsoid of revolution. The velocity components and their effects on the propeller were investigated in this manner for the case of axial flow, and the results showed that the radial component had about the same effect as the axial component on the angle of attack of a blade element in certain blade positions.

The present paper expands the work of Goldberg by investigating the interference of the fuselage on the propeller for the general case—namely, yawed flight. Although in practice yawed flight up to an angle of 25° may exist, this investigation was carried out for all angles between $\pm 90°$ because of purely theoretical interest. Angles of yaw from 60° to 90°, however, may exist in taxiing cross wind, when warming up the engines, or at the beginning of take-off in cross wind. No effects of the engine nacelles and the wings have been taken into account, nor has any direct consideration been given to the separation of the flow from the leeward side of the fuselage at large angles of yaw. It is assumed that influences due to geometric differences between the rear part of a fuselage and that of an ellipsoid will be negligible at the propeller location.

The present paper deals specifically with the case where the axes of rotation of the propellers lie in a plane containing the fuselage axis and are parallel to it. The pitch angle of the fuselage is assumed to be zero. The method, however, may be applied to cases where the propeller axes are not in the same plane as the axis of the fuselage, which would occur in the case of airplanes of other than midwing designs. It may also be applied in the case of pitched flight.

The paper will first deal briefly with the development of the coordinate system and with the expressions for the Legendre polynomials. It will then outline the development of the velocity potential necessary for representation of the fuselage in a free stream and will

show the method used in obtaining the velocity components at the propeller disc. The application of these components in determining changes in angle of attack and resultant velocity of blade elements will be complemented by their use in a practical example in order to gain some idea of their relative magnitude and effects.

The Coordinate System

The fore part of the fuselage will be approximated by a prolate ellipsoid of revolution. The origin of the three mutually perpendicular axes is located at the centroid of the ellipsoid. The x axis coincides with the longitudinal axis of the ellipsoid and is positive forward. The y axis coincides with the horizontal minor axis and is positive to the left when viewed from the cockpit. The z axis is mutually perpendicular to these two and is positive upward. In addition, the distance in any direction perpendicular to the x axis making an angle ω with the y axis will be denoted by r.

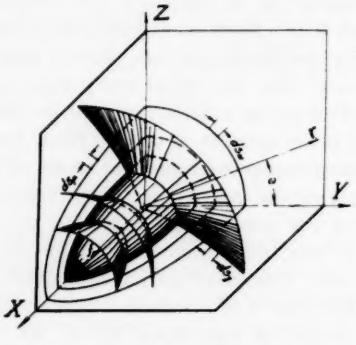

Fig. 1. Ellipsoidal coordinate system.

However, a new system of orthogonal coordinates, consisting of a series of confocal ellipsoids of revolution and hyperboloids of revolution of two sheets will be found much more convenient to use in connection with ellipsoidal harmonics. Fig. 1 represents a combination of a confocal coordinate system and the regular rectangular coordinate system. The distance between the foci is denoted by $2k$.

Considering one meridianal section, one obtains for the equation of the ellipses

$$(x^2/k^2\zeta^2) + [r^2/k^2(\zeta^2 - 1)] = 1 \qquad (1)$$

where ζ is a parameter that is constant upon the surface of a particular ellipsoid of revolution. For the hyperbolas one finds

$$(x^2/k^2\mu^2) - [r^2/k^2(1 - \mu^2)] = 1 \qquad (2)$$

where μ is a parameter that is constant on the surface of any hyperboloid of revolution. ζ is constructed from the fineness ratio of the fore part of the fuselage so that

$$\zeta^2 = 1/[1 - (b^2/a^2)] \qquad (3)$$

where a and b are one-half the major and minor axes, respectively. ζ must always have such a value that

$$1 \leq \zeta \leq \infty \qquad (4)$$

while μ must vary according to

$$-1 \leq \mu \leq 1 \qquad (5)$$

Positive values of μ pertain to hyperboloids along the positive x axis.

The angle of revolution, ω, about the x axis shall be measured from the y axis in a clockwise direction when viewed from the cockpit and must always have the value

$$0 \leq \omega \leq 2\pi \qquad (6)$$

It can be shown that the following relationships exist between the various variables and parameters:

$$x = k\mu\zeta \qquad (7)$$

$$r = k(1 - \mu^2)^{1/2}(\zeta^2 - 1)^{1/2} \qquad (8)$$

$$y = r\cos\omega \qquad (9)$$

from which one arrives at the following values for

$$\zeta = \frac{[r^2 + (k + x)^2]^{1/2} + [r^2 + (k - x)^2]^{1/2}}{2k} \qquad (10)$$

$$\mu = \frac{[r^2 + (k + x)^2]^{1/2} - [r^2 + (k - x)^2]^{+1/2}}{2k} \qquad (11)$$

The linear elements corresponding to the new orthogonal coordinates ζ, μ, and ω may be called ds_ζ, ds_μ, and ds_ω. In such a case ds_μ is the linear element in a meridianal plane (ω = constant) of an ellipsoid (ζ = constant) and is tangential to the latter; ds_ζ is also in a meridianal plane but is tangential to a hyperboloid (μ = constant)—i.e., ds_μ and ds_ζ are mutually perpendicular; finally, ds_ω is the linear element of a circle lying in a plane perpendicular to the x axis and having its center on it.

Applying Eqs. (7), (8), and (9) to the expression for ds_ζ in terms of x, y, and z,

$$ds_\zeta = \left[\left(\frac{\partial x}{\partial \zeta}\right)^2 + \left(\frac{\partial y}{\partial \zeta}\right)^2 + \left(\frac{\partial z}{\partial \zeta}\right)^2\right]^{1/2} d\zeta \qquad (12)$$

one obtains

$$ds_\zeta = k(\zeta^2 - \mu^2)^{1/2}(\zeta^2 - 1)^{-1/2}d\zeta \qquad (13)$$

In a similar manner, applying the same equations to the expressions for ds_μ and ds_ω in terms of x and y,

$$ds_\mu = k(\zeta^2 - \mu^2)^{1/2}(1 - \mu^2)^{-1/2}d\mu \qquad (14)$$

and

$$ds_\omega = k(1 - \mu^2)^{1/2}(\zeta^2 - 1)^{1/2}d\omega \qquad (15)$$

Now, given a velocity potential, ϕ, the velocity component in any direction may be determined, as for example, in the direction along a hyperboloid—i.e., increasing ζ—by

$$v_\zeta = \partial\phi/\partial s_\zeta \tag{16}$$

and similarly for all other components.

Ellipsoidal Harmonics

Since this work deals mainly with velocity components, as will be seen later, the need will arise to express the velocity potential as a series, each term of which will have to be expressed as a product of a function of μ alone, a function of ω alone, and a function of ζ alone. The terms must satisfy Laplace's equation of continuity expressed in ellipsoidal coordinates as

$$\frac{\partial}{\partial\zeta}\left(\frac{\partial\phi}{\partial s_\zeta}\, ds_\mu ds_\omega\right)d\zeta + \frac{\partial}{\partial\mu}\left(\frac{\partial\phi}{\partial s_\mu}\, ds_\zeta ds_\omega\right)d\mu + \frac{\partial}{\partial\omega}\left(\frac{\partial\phi}{\partial s_\omega}\, ds_\zeta ds_\mu\right)d\omega = 0 \tag{17}$$

This will make it possible and easy to obtain velocity components in any direction of the ellipsoidal coordinates and also to satisfy the boundary condition at the surface of the fuselage.

Upon substitution of Eqs. (13), (14), and (15), Eq. (17) becomes:

$$\frac{\partial}{\partial\mu}\left[(1-\mu^2)\frac{\partial\phi}{\partial\mu}\right] + \frac{1}{1-\mu^2}\frac{\partial^2\phi}{\partial\omega^2} = \frac{\partial}{\partial\zeta}\left[(1-\zeta^2)\frac{\partial\phi}{\partial\zeta}\right] + \frac{1}{1-\zeta^2}\frac{\partial^2\phi}{\partial\omega^2} \tag{18}$$

The so-called "ellipsoidal harmonics" are such functions that will comprise the terms of the series that will be required. The ellipsoidal harmonics have the following form:

$$\left.\begin{aligned} \Phi_n &= P_n(\mu)Q_n(\zeta) \\ \Phi_n^m &= P_n^m(\mu)Q_n^m(\zeta)\cos m\omega \\ \text{or } \Phi_n^m &= P_n^m(\mu)Q_n^m(\zeta)\sin m\omega \end{aligned}\right\} \tag{19}$$

where m is an index assuming the values of integers 1, 2, 3, 4 and so on and where n assumes the values of the same integers including zero. $P_n(\mu)$ are the Legendre functions of degree n of the first kind, and $Q_n(\zeta)$ are the Legendre functions of degree n of the second kind.

The functions $P_n^m(\mu)$ are called the associated Legendre functions of degree n and order m of the first kind; $Q_n^m(\zeta)$, the associated Legendre functions of degree n and order m of the second kind, which were introduced by Ferrers.[2] Both are expressed in terms of the Legendre functions as

$$\begin{aligned} P_n^m(\mu) &= (1-\mu^2)^{m/2}(d^m P_n(\mu)/d\mu^m) \\ Q_n^m(\zeta) &= (\zeta^2-1)^{m/2}(d^m Q_n(\zeta)/d\zeta^m) \end{aligned} \tag{20}$$

The first of Eqs. (19) represents the special case when $m = 0$ and applies in the symmetrical case only—i.e., zero yaw. The first derivatives of Eq. (19) vanish for $\zeta = \infty$—i.e., at infinity—but give infinite velocity components for $\zeta = 1$. However, this latter peculiarity will not cause trouble if the potential refers to a flow outside a given ellipsoid upon which ζ has a constant value, say ζ_0.

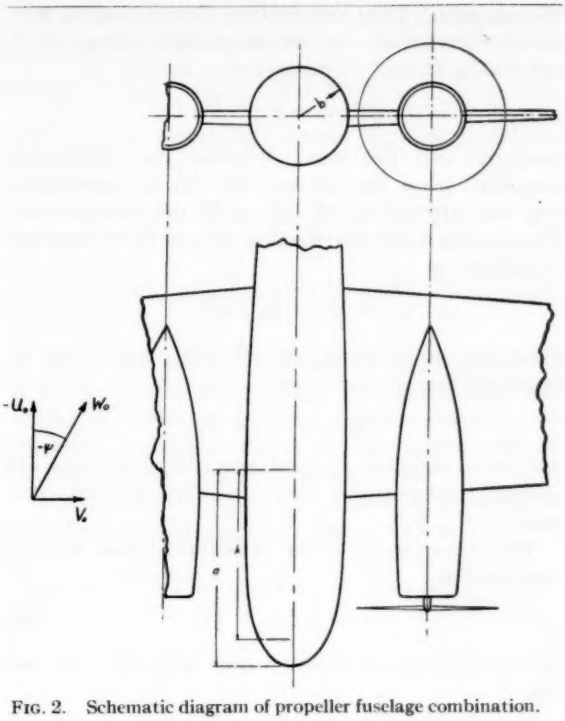

Fig. 2. Schematic diagram of propeller fuselage combination.

The expressions for the lowest degrees of the Legendre polynomials follow

$$\left.\begin{aligned} &P_0(\mu) = 1;\ P_1(\mu) = \mu;\ P_2(\mu) = {}^3/_2\mu^2 - {}^1/_2 \\ &Q_0(\zeta) = {}^1/_2\log\frac{\zeta+1}{\zeta-1};\ Q_1(\zeta) = {}^1/_2\zeta\log\frac{\zeta+1}{\zeta-1} - 1 \\ &Q_2(\zeta) = {}^1/_4(3\zeta^2-1)\log\frac{\zeta+1}{\zeta-1} - {}^3/_2\zeta \end{aligned}\right\} \tag{21}$$

A discussion of these functions and their development may be found in references 2 to 5.

The Velocity Potential

The paper will deal with the case where the fuselage-propeller combination is situated in a uniform but nonsymmetrical flow in the xy plane. The fuselage nose will be assumed to be an ellipsoid of revolution so that the aforementioned ellipsoidal harmonics are conveniently applied.

Let it be assumed that the fuselage is moving at 0° angle of pitch and let the different cases of yaw be referred only to the left-hand propeller of the airplane, looking from the pilot's cockpit, as seen in Fig. 2. Then for simplicity's sake, call this same propeller the "leeward propeller" when a uniform flow W_0 is approaching from the right side at an angle $-\psi$ to the

fuselage axis. Then this uniform flow W_0 can be represented vectorially by its components along the x and y axes, U_0 and V_0, respectively, as

$$\overline{W}_0 = -\overline{U}_0 + \overline{V}_0$$

Similarly, call the same propeller the "windward propeller" when the uniform flow W_0 is approaching from the left side at an angle ψ to the fuselage axis. Then in this latter case the flow W_0 can be represented vectorially as

$$\overline{W}_0 = -\overline{U}_0 - \overline{V}_0$$

From here on let those two different cases of yaw be expressed simultaneously as

$$\overline{W}_0 = -\overline{U}_0 \pm \overline{V}_0$$

and let it be borne in mind that the upper sign will always represent the case of the leeward propeller.

The potential, ϕ, of the undisturbed flow may be expressed as

$$\phi = -U_0 x \pm V_0 y \tag{22}$$

or, substituting for x and y from Eqs. (7), (8), and (9),

$$\phi = -U_0 k\mu\zeta \pm V_0 k(1-\mu^2)^{1/2}(\zeta^2-1)^{1/2}\cos\omega \tag{23}$$

The total potential flow, representing a fuselage in the uniform flow W_0, expressed by the potential ϕ, must be such that at the boundary of the fuselage the velocity component normal to the surface vanishes. If the velocity normal to that surface due to ϕ is denoted by v_n, then

$$v_n = (\partial\phi/\partial s_\zeta)_{\zeta=\zeta_0} \tag{24}$$

To satisfy the boundary condition mentioned, an additional potential Φ will be constructed which will compensate the normal velocity given in Eq. (24)—i.e., it must be such that

$$(\partial\Phi/\partial\zeta)_{\zeta=\zeta_0} = -(\partial\phi/\partial\zeta)_{\zeta=\zeta_0} \tag{25}$$

But Φ must also be such that its derivative vanishes at infinity so that the original flow may remain undisturbed there.

Thus Φ is expressed in a series of ellipsoidal harmonics which satisfy these conditions, since their first derivatives vanish at infinity as mentioned before. Thus

$$\Phi = \sum_m\sum_n A_n^m P_n^m(\mu)Q_n^m(\zeta)\cos m\omega + \sum_m\sum_n B_n^m P_n^m(\mu)Q_n^m(\zeta)\sin m\omega \tag{26}$$

$$\left(\frac{\partial\Phi}{\partial\zeta}\right)_0 = \sum_m\sum_n A_n^m P_n^m(\mu)\left[\frac{\partial Q_n^m(\zeta)}{\partial\zeta}\right]\cos m\omega + \sum_m\sum_n B_n^m P_n^m(\mu)\left[\frac{\partial Q_n^m(\zeta)}{\partial\zeta}\right]\sin m\omega \tag{27}$$

From Eq. (23)

$$\left(\frac{\partial\Phi}{\partial\zeta}\right)_{\zeta=\zeta_0} = -\left(\frac{\partial\phi}{\partial\zeta}\right)_{\zeta=\zeta_0} = U_0 k\mu \mp V_0 k\zeta_0(1-\mu^2)^{1/2}(\zeta_0^2-1)^{-1/2}\cos\omega \tag{28}$$

Comparing Eq. (28) with Eq. (27), it is seen first of all that there will be no term such as the one containing $\sin m\omega$. Furthermore, comparing them with respect to m, it is seen that for the first right-hand term of Eq. (28) $m = 0$, while for the second $m = 1$. Finally, comparing them with respect to μ, it is seen that in both terms of Eq. (28) μ appears in the first order; hence, $n = 1$. Thus Eq. (26) may be expressed by

$$\Phi = A_1 P_1(\mu)Q_1(\zeta) + A_1^1 P_1^1(\mu)Q_1^1(\zeta)\cos\omega = \Phi_1 + \Phi_2 \tag{29}$$

Substituting the proper values for the Legendre polynomials from Eq. (20),

$$\Phi_1 = A_1\mu\left(\tfrac{1}{2}\zeta\log\frac{\zeta+1}{\zeta-1} - 1\right) \tag{30}$$

$$\frac{\partial\Phi_1}{\partial\zeta} = A_1\mu\left(\tfrac{1}{2}\log\frac{\zeta+1}{\zeta-1} - \frac{\zeta}{\zeta^2-1}\right) \tag{31}$$

where A_1 is a constant that can be determined from the boundary conditions—namely,

$$\left(\frac{\partial\Phi_1}{\partial\zeta}\right)_{\zeta=\zeta_0} = A_1\mu\left[\tfrac{1}{2}\log\frac{\zeta_0+1}{\zeta_0-1} - \frac{\zeta_0}{\zeta_0^2-1}\right] = U_0 k\mu \tag{32}$$

This leads to the value of A_1 and the expression for the first term of the additional potential

$$\Phi_1 = -U_0 k\mu\left[\frac{\tfrac{1}{2}\zeta\log\dfrac{\zeta+1}{\zeta-1} - 1}{\dfrac{\zeta_0}{\zeta_0^2-1} - \tfrac{1}{2}\log\dfrac{\zeta_0+1}{\zeta_0-1}}\right] \tag{33}$$

Similarly

$$\Phi_2 = A_1^1(1-\mu^2)^{1/2}(\zeta^2-1)^{1/2}\times\left(\tfrac{1}{2}\log\frac{\zeta+1}{\zeta-1} - \frac{\zeta}{\zeta^2-1}\right)\cos\omega \tag{34}$$

$$\left(\frac{\partial\Phi_2}{\partial\zeta}\right)_{\zeta=\zeta_0} = A_1^1(1-\mu^2)^{1/2}(\zeta^2-1)^{-1/2}\times\left[\zeta_0\left(\tfrac{1}{2}\log\frac{\zeta_0+1}{\zeta_0-1} - \frac{\zeta_0}{\zeta_0^2-1}\right) + \frac{2}{\zeta_0^2-1}\right]\cos\omega = \mp V_0 k\zeta_0(1-\mu^2)^{1/2}(\zeta_0^2-1)^{-1/2}\cos\omega \tag{35}$$

and the second term of the additional potential Φ_2 is obtained in the form:

$$\Phi_2 = \pm \frac{V_0 k(1-\mu^2)^{1/2}(\zeta^2-1)^{1/2}\left(\frac{1}{2}\log\frac{\zeta+1}{\zeta-1} - \frac{\zeta}{\zeta^2-1}\right)\cos\omega}{\frac{1}{2}\log\frac{\zeta_0+1}{\zeta_0-1} - \frac{\zeta_0^2-2}{\zeta_0(\zeta_0-1)}} \quad (36)$$

The total additional potential from which the velocity disturbances at the propeller may be obtained is the sum of Φ_1 and Φ_2. Substituting for U_0 and V_0 in terms of W_0 the total potential for the disturbing velocities becomes

$$\Phi = \frac{-W_0 k\mu\cos\psi}{C_1}\left(\frac{1}{2}\zeta\log\frac{\zeta+1}{\zeta-1} - 1\right) \mp \frac{W_0 k\sin\psi}{C_2}(1-\mu^2)^{1/2}(\zeta^2-1)^{1/2} \times \left(\frac{1}{2}\log\frac{\zeta+1}{\zeta-1} - \frac{\zeta}{\zeta^2-1}\right)\cos\omega \quad (37)$$

where C_1 and C_2 are, respectively, the constant denominators in Eqs. (33) and (36).

The Velocity Components

Of primary concern in this investigation are the velocity disturbances Δu and Δv_θ due to the presence of the fuselage. The former is parallel to the x axis, and the latter is in the plane of the propeller and normal to the longitudinal axis of the blade elements at any position during rotation. This latter component Δv_θ is not obtainable directly but may be obtained as a function of Δv_n, the velocity component in the r direction.

Fig. 3 represents a general fuselage-propeller combination as viewed from the front.

The angle of rotation, θ, of the blade is measured from the y axis counterclockwise when viewed from the front.

L is the distance between the fuselage and propeller axis.

R is the tip radius of the blade.

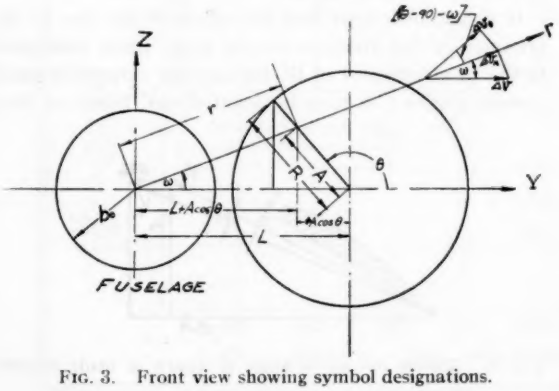

Fig. 3. Front view showing symbol designations.

A is the radius of any element along the blade.

It may be shown that

$$\Delta v_\theta = (\Delta v_n L \sin\theta)/r$$

The velocity components Δu and Δv_n may be obtained as follows:

$$\Delta u = \frac{\partial\Phi}{\partial x} = \frac{\partial\Phi}{\partial\zeta}\frac{\partial\zeta}{\partial x} + \frac{\partial\Phi}{\partial\mu}\frac{\partial\mu}{\partial x} \quad (38)$$

$$\Delta V_n = \frac{\partial\Phi}{\partial r} = \frac{\partial\Phi}{\partial\zeta}\frac{\partial\zeta}{\partial r} + \frac{\partial\Phi}{\partial\mu}\frac{\partial\mu}{\partial r} \quad (39)$$

It can be seen that the expression for the total potential Φ in the present form cannot be differentiated with respect to either of the two directions directly. It therefore seemed desirable to use the method indicated by the right-hand side of these equations.

The expressions for the partial derivatives obtained from Eqs. (10), (11), and (37) are as follows:

$$\frac{\partial\Phi}{\partial\zeta} = -\frac{k\mu W_0\cos\psi}{C_1}\left(\frac{1}{2}\log\frac{\zeta+1}{\zeta-1} - \frac{\zeta}{\zeta^2-1}\right) \mp \frac{kW_0\sin\psi}{C_2}(1-\mu^2)^{1/2}(\zeta^2-1)^{-1/2} \times \left[\zeta\left(\frac{1}{2}\log\frac{\zeta+1}{\zeta-1} - \frac{\zeta}{\zeta^2-1}\right) + \frac{2}{\zeta^2-1}\right]\cos\omega \quad (40)$$

$$\frac{\partial\Phi}{\partial\mu} = -\frac{kW_0\cos\psi}{C_1}\left(\frac{1}{2}\zeta\log\frac{\zeta+1}{\zeta-1} - 1\right) \mp \frac{kW_0\sin\psi}{C_2}(1-\mu^2)^{-1/2}(\zeta^2-1)^{1/2} \times \mu\left(\frac{1}{2}\log\frac{\zeta+1}{\zeta-1} - \frac{\zeta}{\zeta^2-1}\right)\cos\omega \quad (41)$$

$$\frac{\partial\zeta}{\partial x} = \frac{[r^2+(k+x)^2]^{-1/2}(k+x) - [r^2+(k-x)^2]^{-1/2}(k-x)}{2k} \quad (42)$$

$$\frac{\partial\mu}{\partial x} = \frac{[r^2+(k+x)^2]^{-1/2}(k+x) + [r^2+(k-x)^2]^{-1/2}(k-x)}{2k} \quad (43)$$

$$\frac{\partial\zeta}{\partial r} = \frac{[r^2+(k+x)^2]^{-1/2}r + [r^2+(k-x)^2]^{-1/2}r}{2k} \quad (44)$$

$$\frac{\partial\mu}{\partial r} = \frac{[r^2+(k+x)^2]^{-1/2}r - [r^2+(k-x)^2]^{-1/2}r}{2k} \quad (45)$$

By substituting the appropriate equations from Eqs. (40) to (45) in Eqs. (38) and (39), the velocity components in the required directions may be obtained.

Effect on Angle of Attack and Resultant Velocity of the Blade Element

Since the torque and thrust of the blade element is a function of α, the blade angle of attack, the velocity component obtained above will now be used to investigate such changes in angle of attack due to the presence of the fuselage. In addition, the torque and thrust are functions of the square of the resultant velocity of the propeller-blade element. Some consideration will also be given to this aspect of the problem.

Let $\Delta\alpha_1$ and $\Delta\alpha_2$ be the change of angle of attack due to Δu and Δv_θ, respectively, and let β be the angular velocity of the propeller blade. A is the radius of the element in question, as mentioned previously. Then, the resultant velocity, V_R', when the presence of the fuselage has been taken into account, becomes

$$V_R' = [(U_0 + \Delta u)^2 + (\beta A + \Delta v_\theta)^2] \qquad (46)$$

Fig. 4 shows how Δu changes both the angle of attack and the resultant velocity.

It should be noted that the component Δu may be either additive or subtractive, depending on whether the windward or the leeward propeller is considered, and upon the angle of yaw, as will be seen later.

Hence, if Δu is additive, it tends to decrease the angle of attack α by an amount $\Delta\alpha_1$ and vice versa.

Considering Δu as small in comparison with U_0 and βA, it may be shown that $\Delta\alpha_1$ has the following form:

$$\Delta\alpha_1 = \Delta u\beta A/(U_0^2 + \beta^2 A^2) \qquad (47)$$

Fig. 5 shows how the Δv_θ component changes the angle of attack. Its effect on $\Delta\alpha_2$ is shown by the following expression:

$$\Delta\alpha_2 = -\Delta v_\theta U_0/(U_0^2 + \beta^2 A^2)$$

It also may be additive or subtractive to the vector βA, depending on which propeller is considered and the magnitude of ψ, the angle of yaw. If it is additive, it increases the angle of attack by amount $\Delta\alpha_2$ and vice versa.

It should be understood that the changes due to Δu and Δv_θ must be treated simultaneously. Because of the fact that the increments Δu and Δv_θ are at right angles, they cannot be treated algebraically but must be treated vectorially. However; since both $\Delta\alpha_1$ and $\Delta\alpha_2$ are small, they can be added directly.

Thus, the resultant change of angle of attack is

$$\Delta\alpha = \Delta\alpha_1 + \Delta\alpha_2$$

where both $\Delta\alpha_1$ and $\Delta\alpha_2$ are taken with their appropriate signs.

Discussion

In order to determine the order of magnitude of the velocity components due to the presence of the fuselage, a typical example has been investigated. In this case

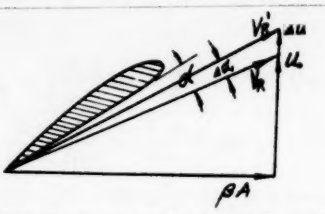

Fig. 4. Effects of Δu on angle of attack of blade element.

it is assumed that the propeller plane is located at $0.4a$ in front of the centroid of an ellipsoid of fineness ratio, $a/b = 2$. This would correspond to a location of $1.2b$ from the nose, where b is the maximum radius of the fuselage. The curves shown in Figs. 6 and 7 give the values of $\Delta u/W_0$ and $\Delta v_\theta/W_0$ plotted against the angle of rotation θ of the propeller. The propeller diameter is assumed to be $3b$, and its axis is located $2.75b$ from the centerline of the fuselage.

It may be seen from the curves that for the case of no yaw there is an appreciable effect of the presence of the fuselage on both $\Delta u/W_0$ and $\Delta v_\theta/W_0$. The maximum values of these ratios are approximately 0.065 and 0.04, respectively. These maximum values, however, do not occur at the same blade location. However, their effects on $\Delta\alpha$ are additive in the third quadrant of the propeller. It should be remembered that the effective angle of attack of the blade element is decreased with an increase in Δu and increased with an increase in Δv_θ. As the yawing angle increases and with the propeller on the windward side of the fuselage, the values of Δu are decreased, becoming negative when ψ is about 45° for all angular positions of the blade. For the same conditions, increasing yaw increases Δv_θ in the first two quadrants and decreases its value in the third and fourth quadrants. At the angular positions of 150° and 210° of this typical propeller installation on the windward side with the propeller rotating 2,000 r.p.m. on a plane traveling at 400 m.p.h. with zero yaw, the values of $\Delta\alpha$ are 0.25° and 2.6°, respectively, for an element at 75 per cent of the propeller radius. Thus, a change in angle of attack of 2.35° is experienced through an angular rotation of 60°. Under the same conditions at 10° yaw the corresponding values of $\Delta\alpha$ are −0.5° and 3.5°.

It is acknowledged that the effect of Δv_θ due to the presence of the fuselage is not large when compared to the V_0 component of W_0 for any but extremely small yawing angles. It may be pointed out, however, that

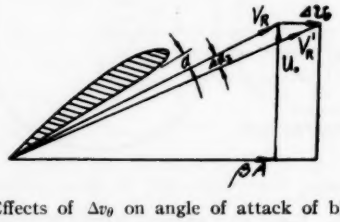

Fig. 5. Effects of Δv_θ on angle of attack of blade element.

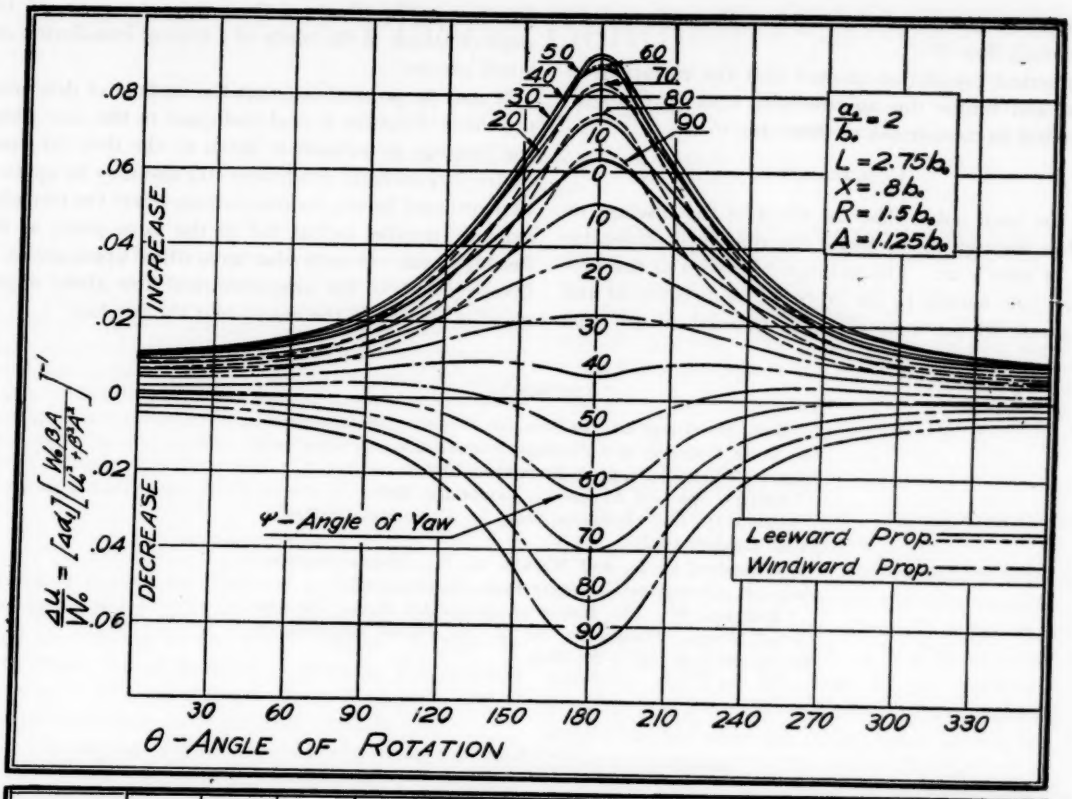

FIG. 6. $\Delta u/W_0$ for a typical example.

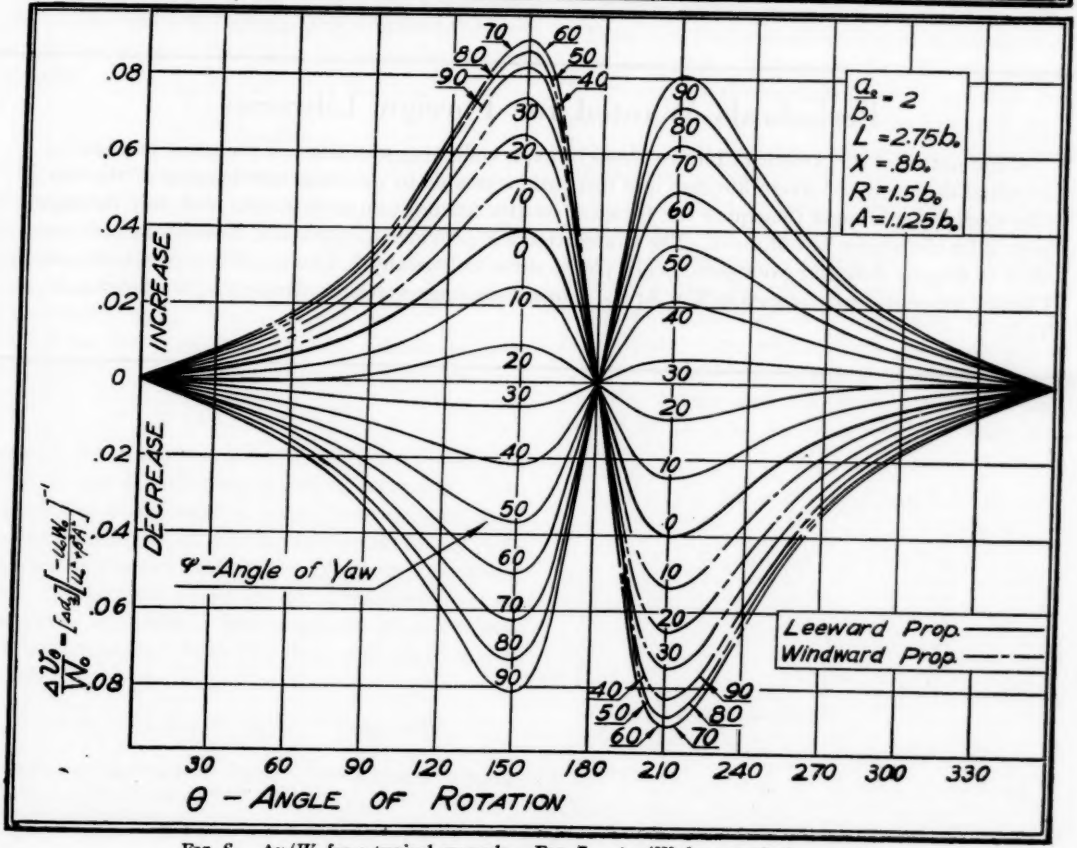

FIG. 7. $\Delta v_0/W_0$ for a typical example.

Δv_θ opposes the action of the sideward component V_0 of the main flow W_0.

Numerical calculation showed that the variations of thrust and torque due to resultant velocity changes were small in comparison to those due to $\Delta\alpha$.

Conclusion

It has been noted that the effect of the fuselage on the flow through the propeller disc may be considerable even at zero yaw. The induced velocities in the propeller plane normal to the propeller blade centroid axis are about 60 per cent of those induced in an axial direction. The effects of the former, however, on the angle of attack of the blade of a typical installation are much greater.

It may be pointed out that the method of determining these velocities is easily adapted to the case where the fuselage is inclined in pitch to the flow direction under various flight conditions and also may be applied, as mentioned before, to installations where the propeller axes are parallel to but not in the same plane as the fuselage axis. It may also have other applications in investigations of the unsymmetrical flow about engine nacelles located in the wings near the fuselage.

References

[1] Gail, Albert and Lu, Ho-Shen, *On Propeller-Tip Interference Due to the Proximity of a Fuselage*, Journal of the Aeronautical Sciences, Vol. 9, No. 1, p. 11, November, 1941.

[2] Ferrers, *Spherical Harmonics*, Cambridge, 1881.

[3] Lamb, H., *Hydrodynamics*, chap. 5; Cambridge University Press, London, 1932.

[4] Whittaker, E. T., and Watson, G. N., *Modern Analysis*, chap. 15; Cambridge University Press, London, 1927.

[5] Tollmien, W., *The Motion of Ellipsoidal Bodies Through Curved Streams*, Publication No. 2, The Daniel Guggenheim Airship Institute, pp. 5–20, 1935.

Periodicals Wanted for Foreign Libraries

A committee of the American Library Association is collecting scientific and technical journals for eventual shipment to foreign libraries and institutions unable to get them now because of the war. The Committee is eager to acquire the JOURNAL OF THE AERONAUTICAL SCIENCES, and only through your gifts can copies be obtained. The Committee will provide storage space if necessary. If you wish to help by donating your periodicals, please write to Dorothy J. Comins, Executive Assistant, Committee on Aid to Libraries in War Areas, Library of Congress Annex, Study 251, Washington 25, D.C.

Plastic Bending

WILLIAM R. OSGOOD*

National Bureau of Standards

ABSTRACT

The relation between bending moment and curvature in a beam is worked out on the assumption that the stress-strain relations are the same in bending as in pure tension and pure compression. The general equations are applied to an I-section with thin flanges, and a numerical case is worked out for the rectangular section, the idealized I-section (negligible web), and a T-section for three widely different stress-strain diagrams. Deflections of beams stressed in the plastic range are considered.

It is hoped to present later the solution for a beam the two sides of which are parabolas with the vertices out—that is, a beam with material concentrated toward the middle.

INTRODUCTION

RECENT PAPERS by Cozzone[1] and Wolford[2] present approximate methods for designing beams subjected to bending in the plastic range. It may be worth while and of interest to examine the problem somewhat more accurately, if only to evaluate approximate methods by a more accurate analysis.

For the purpose of checking theory by tests, the logical dimensional variables to consider are the bending moment and the curvature, and it is proposed to obtain the relation between them here for three hypothetical materials.

THEORY

The basic assumptions are made that "plane sections remain plane" and that the stress-strain relations are the same in bending as in pure tension and pure compression. There is evidence in the literature[3, 4] and strong unpublished evidence that these assumptions are reasonably valid.

It will be further assumed that the relation between stress and strain can be given by an equation of the form

$$e = (s/E) + K(s/E)^n \qquad (1)$$

where e is the strain, s is the stress, E is the modulus of elasticity, and K and n are empirical constants. This equation has been found to apply accurately to many structural materials, at least up to a strain of 0.01. If, when s/E is plotted against $e - (s/E)$ on logarithmic paper, the plotted points lie on a straight line, the equation is applicable. The constants K and n may then be determined from the slope and intercepts of this line, for

$$\log [e - (s/E)] = \log K + n \log (s/E)$$

A stress-strain curve that may be considered to consist of two straight lines—a modulus line and a constant-stress line—can theoretically be represented by the limit of Eq. (1) as K and n become infinite in a suitable manner. Practically, however, it is expedient in such cases to replace the equation by

$$e = \frac{s}{E}, \; e \leqq \frac{S}{E}; \; s = S, e \geqq \frac{S}{E} \qquad (2)$$

where S is a constant stress.

The following three possible combinations of stress-strain curves will be considered:

The general case: Case I, when equations of the form of Eq. (1) apply in both tension and compression.

The two limiting cases: Case II, when equations of the form of Eqs. (2) apply in both tension and compression; and Case III, when Eq. (1) applies in compression and Eqs. (2) in tension. The arguments are exactly similar when Eq. (1) applies in tension and Eqs. (2) in compression.

In order to find the relation between the curvature of a beam and the applied bending moment, one may proceed as follows. The curvature is directly proportional to the sum of the extreme fiber strains, and these are related to the extreme fiber stresses through Eq. (1) or Eqs. (2). Let Fig. 1(a) represent any distribution of stress over the cross section shown in Fig. 1(c) of a beam subjected to a bending moment M. Denote the maximum tensile stress on the cross section by s_1; the maximum compressive stress, by s_2; the stress at any distance y from the neutral axis, by s; the tensile and compressive extreme fiber distances, by c_1 and c_2, respectively; the width of the cross section at the distance y, by b; the depth of the cross section, by h; and the tensile and compressive areas of the cross section by A_t and A_c, respectively. Then for equilibrium

$$\int_A s dA = 0 \text{ and } \int_A sy dA = M$$

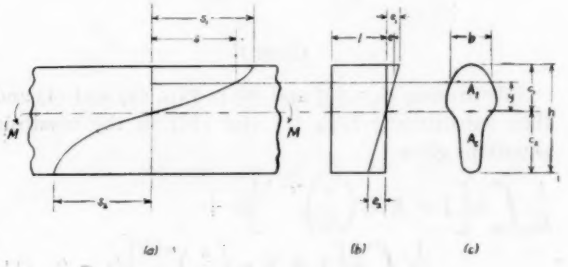

FIG. 1.

Presented at the Structures Session, Twelfth Annual Meeting, I.A.S., New York, January 25–27, 1944.

* Materials Engineer.

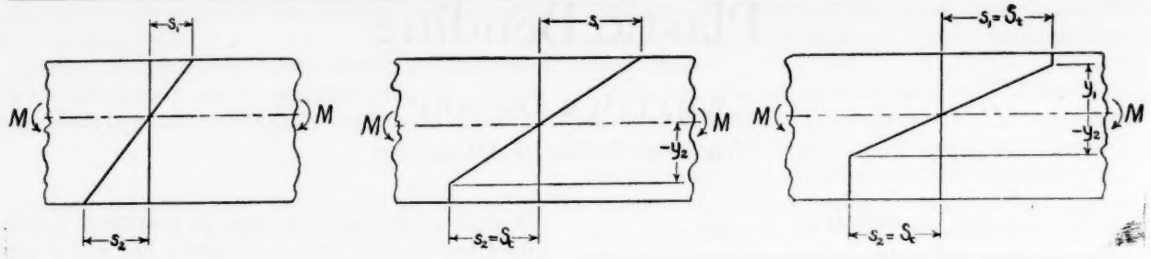

FIG. 2.

or

$$-\int_{A_2} sdA + \int_{A_1} sdA = 0$$

and

$$-\int_{A_2} sydA + \int_{A_1} sydA = M$$

or

$$-\int_{-c_2}^{0} sbdy + \int_{0}^{c_1} sbdy = 0 \qquad (3)$$

and

$$-\int_{-c_2}^{0} sbydy + \int_{0}^{c_1} sbydy = M \qquad (4)$$

Fig. 1(b) shows the strains in the longitudinal elements of the beam. The maximum tensile strain is e_1, the maximum compressive strain is e_2, and the strain at any distance y from the neutral axis is e. From the trigonometry of the figure

$$y = \pm he/(e_1 + e_2) = \pm e/k \qquad (5)$$

where

$$k = (e_1 + e_2)/h \qquad (6)$$

is the curvature, and the positive sign in Eq. (5) applies when y is positive and the negative sign applies when y is negative, all other quantities occurring in this paper always being considered positive. The extreme fiber distances are

$$c_1 = e_1/k,\ c_2 = e_2/k \qquad (7)$$

and

$$c_1 + c_2 = h \qquad (8)$$

Differentiation of Eq. (5) gives

$$dy = \pm(1/k)de \qquad (9)$$

From Eq. (1) by differentiation,

$$de = \frac{1}{E}\left[1 + nK\left(\frac{s}{E}\right)^{n-1}\right]ds \qquad (10)$$

CASE I

Substituting Eqs. (5) and (9) in Eqs. (3) and (4) and then substituting Eqs. (1) and (10) in the resulting equations gives

$$\frac{1}{E_c}\int_{s_1}^{0} bs\left[1 + K_c n_c\left(\frac{s}{E_c}\right)^{n_c-1}\right]ds + \frac{1}{E_t}\int_{0}^{s_1} bs\left[1 + K_t n_t\left(\frac{s}{E_t}\right)^{n_t-1}\right]ds = 0 \qquad (11)$$

$$-\frac{1}{E_c^2}\int_{s_2}^{0} bs^2\left[1 + K_c\left(\frac{s}{E_c}\right)^{n_c-1}\right]\left[1 + K_c n_c\left(\frac{s}{E_c}\right)^{n_c-1}\right]\times ds + \frac{1}{E_t^2}\int_{0}^{s_1} bs^2\left[1 + K_t\left(\frac{s}{E_t}\right)^{n_t-1}\right]\times \left[1 + K_t n_t\left(\frac{s}{E_t}\right)^{n_t-1}\right]ds = Mk^2 \qquad (12)$$

E, K, and n have been indicated as having different values in tension and compression. If E_t and E_c are not equal, in any case they will be so close that they may be taken equal. The values of K and n, however, will, in general, be different for tension and compression.

From Eqs. (11) and (12) two unknowns may be determined when the other quantities are given. In particular, for a given cross section, Eq. (11) may be solved for s_1 for an assumed value of s_2. k can then be determined from Eqs. (6) and (1) and M from Eq. (12). In order to evaluate the integrals in Eqs. (11) and (12),

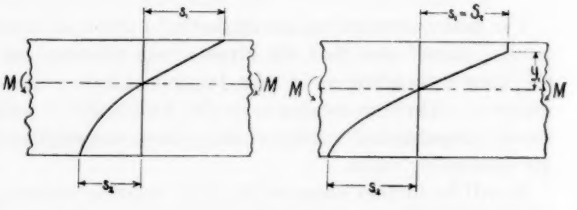

FIG. 3.

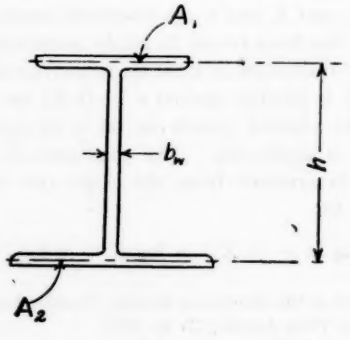

FIG. 4.

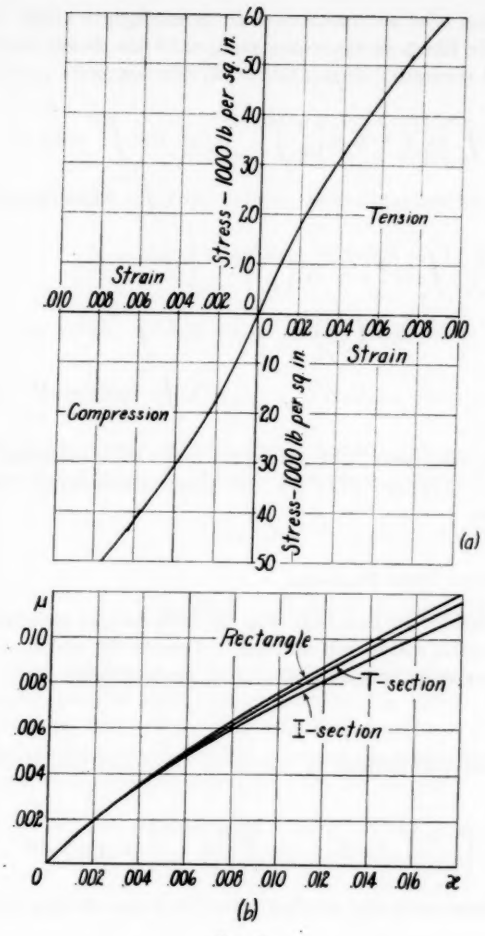

FIG. 5.

b, which will ordinarily be given as a function of y, must be expressed in terms of s by means of Eqs. (5) and (1).

CASE II

This case is represented in Fig. 2, all three parts of which correspond to Fig. 1(a). Fig. 1(b) and (c) may be considered still to apply to the case of Fig. 2. In Fig. 2(a) the moment is sufficiently small so that the action over the entire cross section is elastic:

$$s = Ee = \pm Eky \tag{13}$$

Substituting Eq. (13) in Eqs. (3) and (4) gives

$$E_c \int_{-c_2}^{0} bydy + E_t \int_{0}^{c_1} bydy = 0 \tag{14}$$

$$E_c \int_{-c_2}^{0} by^2dy + E_t \int_{0}^{c_1} by^2dy = M/k \tag{15}$$

In Fig. 2(b) the moment is sufficiently larger than in Fig. 2(a) so that $s_2 = S_c$, the compressive yield strength, but not large enough for s_1 to have reached the tensile yield strength S_t. If under increasing moment the tensile yield strength were reached before the compressive, the development that follows would be similar. Eq. (13) applies for $y \geqq y_2$, and Eqs. (3) and (4) now become

$$-S_c \int_{-c_2}^{y_2} bdy + E_c k \int_{y_2}^{0} bydy + E_t k \int_{0}^{c_1} bydy = 0 \tag{16}$$

$$-S_c \int_{-c_2}^{y_2} bydy + E_c k \int_{y_2}^{0} by^2dy + E_t k \int^{c_1} by^2dy = M \tag{17}$$

In Fig. 2(c) the moment is large enough so that both the compressive and the tensile yield strengths have been reached in the outer portions of the beam. Eq. (13) applies for $y_2 \leqq y \leqq y_1$, and Eqs. (3) and (4) become

$$-S_c \int_{-c_2}^{y_2} bdy + E_c k \int_{y_2}^{0} bydy + E_t k \int_{0}^{y_1} bydy + S_t \int_{y_1}^{c_1} bdy = 0 \tag{18}$$

$$-S_c \int_{-c_2}^{y_2} bydy + E_c k \int_{y_2}^{0} by^2dy + E_t k \int_{0}^{y_1} by^2dy + S_t \int_{y_1}^{c_1} bydy = M \tag{19}$$

Eqs. (14) and (15), (16) and (17), and (18) and (19) correspond to Eqs. (11) and (12) for the cases under discussion.

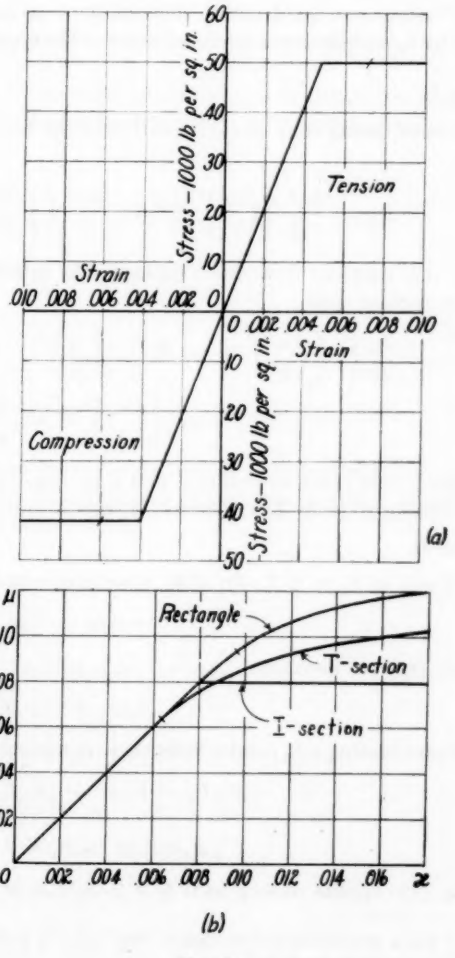

FIG. 6.

Case III

This case is represented in Fig. 3, where Eq. (1) applies on the compressive side and Eqs. (2) on the tensile side. Both parts of Fig. 3 correspond to Fig. 1(a). Fig. 1(b) and 1(c) may be considered as applying to the case of Fig. 3. In Fig 3(a) the moment is still sufficiently small so that the action over the part of the cross section in tension is elastic. For this condition Eqs. (3) and (4) become, by substitution from Eqs. (5), (9), (1), (10), (13), and (2),

$$\frac{1}{E_c k}\int_{s_2}^{0} bs\left[1 + K_c n_c\left(\frac{s}{E_c}\right)^{n_c-1}\right]ds + E_t k\int_{0}^{c_1} bydy = 0 \tag{20}$$

$$-\frac{1}{E_c{}^2k^2}\int_{s_2}^{0} bs^2\left[1 + K_c\left(\frac{s}{E_c}\right)^{n_c-1}\right]\times \left[1 + K_c n_c\left(\frac{s}{E_c}\right)^{n_c-1}\right]ds + E_t k\int_{0}^{c_1} by^2dy = M \tag{21}$$

In Fig. 3(b) the moment is large enough to stress the tensile fibers in the outer portion of the beam to the yield strength. Eqs. (3) and (4) now become

$$\frac{1}{E_c k}\int_{s_2}^{0} bs\left[1 + K_c n_c\left(\frac{s}{E_c}\right)^{n_c-1}\right]ds + E_t k\int_{y_1}^{c_1} bydy + S_t\int_{y_1}^{c_1} bdy = 0 \tag{22}$$

$$-\frac{1}{E_c{}^2k^2}\int_{s_2}^{0} bs^2\left[1 + K_c\left(\frac{s}{E_c}\right)^{n_c-1}\right]\times \left[1 + K_c n_c\left(\frac{s}{E_c}\right)^{n_c-1}\right]ds + E_t k\int_{0}^{y_1} by^2dy + S_t\int_{y_1}^{c_1} bydy = M \tag{23}$$

Eqs. (20) and (21), and (22) and (23) correspond to Eqs. (11) and (12) for the given stress-strain relations.

Application to I-Section with Thin Flanges

To illustrate the application of the preceding equations, consider an I-section (Fig. 4) with flanges sufficiently thin* relative to the depth so that the stress in each flange may be considered uniform. Denote the width of the web by b_w and the cross-sectional areas of the tensile and compressive flanges by A_1 and A_2, respectively.

Case I

Remembering that Eq. (11) (derived from Eq. (3)) expresses equilibrium of forces in the longitudinal direction,

$$-A_2s_2 - \frac{b_wE_c}{2k}\left[\left(\frac{s_2}{E_c}\right)^2 + 2K_c\frac{n_c}{n_c+1}\left(\frac{s_2}{E_c}\right)^{n_c+1}\right] + \frac{b_wE_t}{2k}\left[\left(\frac{s_1}{E_t}\right)^2 + 2K_t\frac{n_t}{n_t+1}\left(\frac{s_1}{E_t}\right)^{n_t+1}\right] + A_1s_1 = 0 \tag{24}$$

Eq. (12) (derived from Eq. (4)) expresses equilibrium of moments of the applied forces and the stresses on the cross section, and

$$A_2s_2c_2 + \frac{b_w}{3k^2}\left\{E_c\left[\left(\frac{s_2}{E_c}\right)^3 + 3K_c\frac{n_c+1}{n_c+2}\left(\frac{s_2}{E_c}\right)^{n_c+2} + 3K_c{}^2\frac{n_c}{2n_c+1}\left(\frac{s_2}{E_c}\right)^{2n_c+1}\right] + E_t\left[\left(\frac{s_1}{E_t}\right)^3 + 3K_t\frac{n_t+1}{n_t+2}\left(\frac{s_1}{E_t}\right)^{n_t+2} + 3K_t{}^2\frac{n_t}{2n_t+1}\left(\frac{s_1}{E_t}\right)^{2n_t-1}\right]\right\} + A_1s_1c_1 = M \tag{25}$$

where c_1 and c_2 are related to s_1 and s_2 by Eqs. (7) and (1). Eq. (24) may be solved for s_1 for an assumed value of s_2, k being given by Eqs. (6) and (1), and M may then be determined from Eq. (25).

Case II

For $s_1 < S_t$, $s_2 < S_c$, Eq. (14), when multiplied by k, becomes

$$-A_2s_2 - {}^1/_2b_wE_ckc_2{}^2 + {}^1/_2b_wE_tkc_1{}^2 + A_1s_1 = 0 \tag{26}$$

and Eq. (15) becomes

$$A_2s_2c_2 + {}^1/_3b_wE_ckc_2{}^3 + {}^1/_3b_wE_tkc_1{}^3 + A_1s_1c_1 = M \tag{27}$$

By eliminating s_1, s_2, and c_1 from these equations by means of Eqs. (2), (7), and (8), they become

$${}^1/_2b_w(E_t - E_c)c_2{}^2 - [E_cA_2 + E_t(b_wh + A_1)]c_2 + E_th({}^1/_2b_wh + A_1) = 0 \tag{28}$$

$${}^1/_3b_wk[E_cc_2{}^3 + E_t(h - c_2)^3] + k[E_cA_2c_2{}^2 + E_tA_1(h - c_2)^2] = M \tag{29}$$

Eq. (29) applies so long as $0 \leqq k \leqq S_c/E_cc_2$ or $S_t/E_t(h - c_2)$, whichever is the smaller, where c_2 is determined by

* For a stress-strain curve that is "flat" (nearly horizontal) in the yield range, the flanges need not be particularly thin when the stresses in them are in this range.

Eq. (28). Eq. (28) may be solved for c_2 and the value of c_2 substituted in Eq. (29), resulting in a relation between M and k in terms of the properties of the material and the dimensions of the cross section.

For $s_1 < S_t$, $s_2 = S_c$, Eqs. (16) and (17) become

$$-A_2S_c - b_w(y_2 + c_2)S_c - {}^1/_2b_wE_cky_2^2 + {}^1/_2b_wE_tkc_1^2 + A_1s_1 = 0$$
$$A_2S_cc_2 - {}^1/_2b_w(y_2^2 - c_2^2)S_c - {}^1/_3b_wE_cky_2^3 + {}^1/_3b_wE_tkc_1^3 + A_1s_1c_1 = M$$

By eliminating s_1, y_2, and c_1 from these equations by means of Eqs. (2), (7), (8), and (13), they become

$${}^1/_2b_wE_tkc_2^2 - [b_wS_c + E_tk(b_wh + A_1)]c_2 + E_tkh({}^1/_2b_wh + A_1) + {}^1/_2b_w\frac{S_c^2}{E_ck} - A_2S_c = 0 \tag{30}$$

$${}^1/_3b_wE_tk(h - c_2)^3 + {}^1/_2b_wS_cc_2^2 + E_tkA_1(h - c_2)^2 + A_2S_cc_2 - {}^1/_6b_w\frac{S_c^3}{E_c^2k^2} = M \tag{31}$$

Eq. (31) applies for $S_c/E_cc_2 \leqq k \leqq S_t/E_tc_1$, where c_2 is determined by Eq. (28) and $c_1 = h - c_2$ is determined by Eq. (30).

If the properties of the material and the dimensions of the cross section are such that under increasing moment S_t is reached before S_c—that is, $s_1 = S_t$, $s_2 < S_c$—the equations corresponding to Eqs. (30) and (31) become

$${}^1/_2b_wE_ckc_2^2 + (b_wS_t + A_2E_ck)c_2 - b_whS_t + {}^1/_2b_w\frac{S_t^2}{E_tk} - A_1S_t = 0 \tag{30a}$$

$${}^1/_3b_wE_ckc_2^3 + A_2E_ckc_2^2 + {}^1/_2b_wS_t(h - c_2)^2 + A_1S_t(h - c_2) - {}^1/_6b_w\frac{S_t^3}{E_t^2k^2} = M \tag{31a}$$

Eq. (31a) applies for $S_t/E_tc_1 \leqq k \leqq S_c/E_cc_2$, where $c_1 = h - c_2$ on the left of the inequality is determined by Eq. (28) and c_2 on the right is determined by Eq. (30a).

As before, Eqs. (30) or (30a) may be solved for c_2 and the value of c_2 substituted in Eq. (31) or (31a), resulting in a relation between M and k in terms of the properties of the material and the dimensions of the cross section.

For $s_1 = S_t$, $s_2 = S_c$, Eqs. (18) and (19) become

$$-A_2S_c - b_w(y_2 + c_2)S_c - {}^1/_2b_wE_cky_2^2 + {}^1/_2b_wE_tky_1^2 + b_w(c_1 - y_1)S_t + A_1S_t = 0$$
$$A_2S_cc_2 - {}^1/_2b_w(y_2^2 - c_2^2)S_c - {}^1/_3b_wE_cky_2^3 + {}^1/_3b_wE_tky_1^3 + {}^1/_2b_w(c_1^2 - y_1^2)S_t + A_1S_tc_1 = M$$

By eliminating y_1, y_2, and c_1 from these equations by means of Eqs. (13) and (8), they become

$$c_2 = \frac{1}{S_t + S_c}\left[\left(\frac{A_1}{b_w} + h\right)S_t - \frac{A_2}{b_w}S_c - \frac{1}{2}\frac{S_t^2}{E_tk} + \frac{1}{2}\frac{S_c^2}{E_ck}\right] \tag{32}$$

$${}^1/_2b_w(S_t + S_c)c_2^2 + [A_2S_c - (b_wh + A_1)S_t]c_2 + h({}^1/_2b_wh + A_1)S_t - {}^1/_6b_w\frac{S_c^3}{E_c^2k^2} - {}^1/_6b_w\frac{S_t^2}{E_t^2k^2} = M \tag{33}$$

Eq. (33) applies so long as $k \geqq S_t/E_t(h - c_2)$ or S_c/E_cc_2, whichever is the larger, where c_2 is determined by Eq. (32). Again, the value of c_2 may be substituted from Eq. (32) in Eq. (33), resulting in a relation between M and k in terms of the properties of the material and the dimensions of the cross section.

Case III

For $s_1 \leqq S_t$ Eqs. (20) and (21) become

$$-A_2s_2 - \frac{b_wE_c}{2k}\left[\left(\frac{s_2}{E_c}\right)^2 + 2K_c\frac{n_c}{n_c + 1}\left(\frac{s_2}{E_c}\right)^{n_c+1}\right] + {}^1/_2b_wE_tkc_1^2 + A_1s_1 = 0 \tag{33a}$$

$$A_2s_2c_2 + \frac{b_wE_c}{3k^2}\left[\left(\frac{s_2}{E_c}\right)^3 + 3K_c\frac{n_c + 1}{n_c + 2}\left(\frac{s_2}{E_c}\right)^{n_c+2} + 3K_c^2\frac{n_c}{2n_c + 1}\left(\frac{s_2}{E_c}\right)^{2n_c+1}\right] + {}^1/_3b_wE_tkc_1^3 + A_1s_1c_1 = M \tag{33b}$$

By eliminating s_1, c_2, and c_1 from these equations by means of Eqs. (2), (7), (8), and (1), they become

$$E_th({}^1/_2b_wh + A_1)k^2 - \left\{A_2s_2 + E_t(b_wh + A_1)\left[\frac{s_2}{E_c} + K_c\left(\frac{s_2}{E_c}\right)^{n_c}\right]\right\}k -$$
$${}^1/_2b_w\left\{E_c\left[\left(\frac{s_2}{E_c}\right)^2 + 2K_c\frac{n_c}{n_c + 1}\left(\frac{s_2}{E_c}\right)^{n_c+1}\right] - E_t\left[\frac{s_2}{E_c} + K_c\left(\frac{s_2}{E_c}\right)^{n_c}\right]^2\right\} = 0 \tag{34}$$

$$\frac{A_2 s_2}{k}\left[\frac{s_2}{E_c}+K_c\left(\frac{s_2}{E_c}\right)^{nc}\right]+\frac{b_w E_c}{3k^2}\left[\left(\frac{s_2}{E_c}\right)^3+3K_c\frac{n_c+1}{n_c+2}\left(\frac{s_2}{E_c}\right)^{nc+2}+3K_c^2\frac{n_c}{2n_c+1}\left(\frac{s_2}{E_c}\right)^{2nc+1}\right]+$$
$$\frac{1}{3}\frac{b_w E_t}{k^2}\left[kh-\frac{s_2}{E_c}-K_c\left(\frac{s_2}{E_c}\right)^{nc}\right]^3+\frac{A_1 E_t}{k}\left[kh-\frac{s_2}{E_c}-K_c\left(\frac{s_2}{E_c}\right)^{nc}\right]^2=M \quad (35)$$

Eq. (35) applies so long as

$$0 \leqq k \leqq (S_t/E_t h)+(1/h)[(s_2/E_c)+K_c(s_2/E_c)^{nc}]$$

For a given value of s_2 Eq. (34) may be solved for k, and Eq. (35) then gives M for this value of k.

For $s_1 = S_t$ Eqs. (22) and (23) become

$$-A_2 s_2-\frac{b_w E_c}{2k}\left[\left(\frac{s_2}{E_c}\right)^2+2K_c\frac{n_c}{n_c+1}\left(\frac{s_2}{E_c}\right)^{nc+1}\right]+{}^1/_2 b_w E_t k y_1^2+b_w(c_1-y_1)S_t+A_1 S_t=0$$

$$A_2 s_2 c_2+\frac{b_w E_c}{3k}\left[\left(\frac{s_2}{E_c}\right)^3+3K_c\frac{n_c+1}{n_c+2}\left(\frac{s_2}{E_c}\right)^{nc+2}+3K_c^2\frac{n_c}{2n_c+1}\left(\frac{s_2}{E_c}\right)^{2nc+1}\right]+$$
$${}^1/_3 b_w E_t k y_1^3+{}^1/_2 b_w(c_1^2-y_1^2)S_t+A_1 S_t c_1=M$$

By eliminating y_1, c_2, and c_1 from these equations by means of Eqs. (13), (7), (1), and (8), they become

$$[(b_w h+A_1)S_t-A_2 s_2]k={}^1/_2 b_w\left\{E_c\left[\left(\frac{s_2}{E_c}\right)^2+2K_c\frac{n_c}{n_c+1}\left(\frac{s_2}{E_c}\right)^{nc+1}\right]+\frac{S_t^2}{E_t}+2S_t\left[\frac{s_2}{E_c}+K_c\left(\frac{s_2}{E_c}\right)^{nc}\right]\right\} \quad (36)$$

$$\frac{A_2 s_2}{k}\left[\frac{s_2}{E_c}+K_c\left(\frac{s_2}{E_c}\right)^{nc}\right]+\frac{b_w E_c}{3k^2}\left[\left(\frac{s_2}{E_c}\right)^3+3K_c\frac{n_c+1}{n_c+2}\left(\frac{s_2}{E_c}\right)^{nc+2}+3K_c^2\frac{n_c}{2n_c+1}\left(\frac{s_2}{E_c}\right)^{2nc+1}\right]-$$
$$\frac{1}{6}b_w\frac{S_t^3}{E_t^2 k^2}+\frac{1}{2}\frac{b_w S_t}{k^2}\left[kh-\frac{s_2}{E_c}-K_c\left(\frac{s_2}{E_c}\right)^{nc}\right]^2+\frac{A_1 S_t}{k}\left[kh-\frac{s_2}{E_c}-K_c\left(\frac{s_2}{E_c}\right)^{nc}\right]=M \quad (37)$$

Equation (37) applies for

$$k \geqq (S_t/E_t h)+(1/h)[s_2/E_c+K_c(s_2/E_c)^{nc}]$$

For a given value of s_2 Eq. (36) may be solved for k, and Eq. (37) then gives M for this value of k.

Equations for the I-Section in Nondimensional Form

When it is permissible to set $E_t = E_c = E$, as will usually be the case, the preceding equations for the I-section with thin flanges become somewhat simpler. It is then also particularly advantageous, in order to study the effect of different cross sections on the relation between bending moment and curvature, to introduce the nondimensional quantities

$$\kappa = kh(=e_1+e_2);\ \mu = Mh/EI;\ \rho_1 = A_1/b_w h;\ \rho_2 = A_2/b_w h \quad (38)$$

where I is the moment of inertia of the cross-sectional area with respect to a centroidal axis normal to the plane of bending and is given by

$$I = {}^1/_{12} b_w h^3\left\{4-3[(1-4\rho_1\rho_2)/(1+\rho_1+\rho_2)]\right\} = {}^1/_{12} b_w h^3/R \quad (39)$$

Here

$$R = (1+\rho_1+\rho_2)/(1+4\rho_1+4\rho_2+12\rho_1\rho_2) \quad (39a)$$

If the web is considered negligible, $b_w = 0$ and $\rho_1 = \rho_2 = \infty$. In this case of an idealized I-section

$$I = h^2[A_1 A_2/(A_1+A_2)] \quad (39b)$$

The ratio of the tensile-flange area to the compressive-flange area will be denoted by α:

$$\alpha = A_1/A_2 \quad (39c)$$

In terms of the quantities defined by Eqs. (38) to (39c) the equations that have been developed for the I-section become as follows:

Case I

Eqs. (24) and (25) become, with the aid of Eqs. (1), (6), and (7),

$$(1+2\rho_1)\left(\frac{s_1}{E}\right)^2+2K_t\left(\rho_1+\frac{n_t}{n_t+1}\right)\left(\frac{s_1}{E}\right)^{nt+1}+2\rho_1\frac{s_1}{E}\frac{s_2}{E}+2\rho_1K_c\frac{s_1}{E}\left(\frac{s_2}{E}\right)^{nc}=$$
$$(1+2\rho_2)\left(\frac{s_2}{E}\right)^2+2K_c\left(\rho_2+\frac{n_c}{n_c+1}\right)\left(\frac{s_2}{E}\right)^{nc+1}+2\rho_2\frac{s_1}{E}\frac{s_2}{E}+2\rho_2K_t\frac{s_2}{E}\left(\frac{s_1}{E}\right)^{nt} \quad (40)$$

$$\mu=12R\left\{\frac{\rho_1}{\kappa}\frac{s_1}{E}\left[\frac{s_1}{E}+K_t\left(\frac{s_1}{E}\right)^{nt}\right]+\frac{1}{3\kappa^2}\left[\left(\frac{s_1}{E}\right)^3+3K_t\frac{n_t+1}{n_t+2}\left(\frac{s_1}{E}\right)^{nt+2}+3K_t^2\frac{n_t}{2n_t+1}\left(\frac{s_1}{E}\right)^{2nt+1}+\right.\right.$$
$$\left.\left.\left(\frac{s_2}{E}\right)^3+3K_c\frac{n_c+1}{n_c+2}\left(\frac{s_2}{E}\right)^{nc+2}+3K_c^2\frac{n_c}{2n_c+1}\left(\frac{s_2}{E}\right)^{2nc+1}\right]+\frac{\rho_2}{\kappa}\frac{s_2}{E}\left[\frac{s_2}{E}+K_c\left(\frac{s_2}{E}\right)^{nc}\right]\right\} \quad (41)$$

For the idealized I-section Eqs. (24) and (25) reduce to

$$A_1s_1=A_2s_2;\ A_1s_1c_1+A_2s_2c_2=M$$

From these equations one obtains, by means of Eqs. (1), (7), and (8),

$$K_t[\mu/(1+\alpha)]^{n_t}+K_c[\alpha\mu/(1+\alpha)]^{n_c}+\mu=\kappa \quad (41a)$$

Case II

Eq. (28) gives

$$c_2=(h/2)[(1+2\rho_1)/(1+\rho_1+\rho_2)] \quad (42)$$

When this value of c_2 is substituted in Eq. (29),

$$\mu=\kappa;\ 0\leqq\kappa\leqq(2S_c/E)[(1+\rho_1+\rho_2)/(1+2\rho_1)]\text{ or }(2S_t/E)[(1+\rho_1+\rho_2)/(1+2\rho_2)] \quad (43)$$

If the first of the upper limits in Eq. (43) is smaller than the second, Eqs. (30) and (31) apply for κ greater than the first limit. Eq. (30) becomes

$$\kappa^2\frac{c_2^2}{h^2}-2\left[\frac{S_c}{E}+\kappa(1+\rho_1)\right]\kappa\frac{c_2}{h}+\kappa^2(1+2\rho_1)+\frac{S_c}{E}\left(\frac{S_c}{E}-2\rho_2\kappa\right)=0 \quad (44)$$

When this equation is solved for c_2 and the value of c_2 substituted in Eq. (31),

$$\left.\begin{aligned}\mu=2R\left\{4\rho_1^3\kappa+3[1+\rho_1+\rho_2+(1+2\rho_1)(\rho_1+\rho_2)]\frac{S_c}{E}-\right.\\ \left.2\left[(1+\rho_1+\rho_2)\frac{S_c}{E}+2\rho_1^2\kappa\right]\sqrt{2(1+\rho_1+\rho_2)\frac{S_c}{\kappa E}+\rho_1^2}\right\}\\ (2S_c/E)[(1+\rho_1+\rho_2)/(1+2\rho_1)]\leqq\kappa\leqq(S_t+S_c)^2/2E[(1+\rho_2)S_c-\rho_1S_t]\end{aligned}\right\} \quad (45)$$

If the second of the upper limits in Eq. (43) is smaller than the first, Eqs. (30a) and (31a) apply for κ greater than the second limit. If Eq. (30a) is solved for c_2 and the value of c_2 substituted in Eq. (31a), an equation for μ will result which is the same as Eq. (45) when S_c is replaced by S_t and ρ_1 and ρ_2 are interchanged:

$$\left.\begin{aligned}\mu=2R\left\{4\rho_2^3\kappa+3[1+\rho_1+\rho_2+(1+2\rho_2)(\rho_1+\rho_2)]\times\right.\\ \left.\frac{S_t}{E}-2\left[(1+\rho_1+\rho_2)\frac{S_t}{E}+2\rho_2^2\kappa\right]\sqrt{2(1+\rho_1+\rho_2)\frac{S_t}{\kappa E}+\rho_2^2}\right\}\\ (2S_t/E)[(1+\rho_1+\rho_2)/(1+2\rho_2)]\leqq\kappa\leqq(S_t+S_c)^2/2E[(1+\rho_1)S_t-\rho_2S_c]\end{aligned}\right\} \quad (45a)$$

Eq. (32) becomes

$$c_2=h(\{[(1+\rho_1)S_t-\rho_2S_c]/(S_t+S_c)\}-[(S_t-S_c)/2\kappa E])$$

When this value of c_2 is substituted in Eq. (33),

$$\left.\begin{aligned}\mu=R\left\{\frac{6}{E(S_t+S_c)}[-\rho_1^2S_t^2+(1+2\rho_1+2\rho_2+2\rho_1\rho_2)S_tS_c-\rho_2^2S_c^2]-\frac{(S_t+S_c)^3}{2\kappa^2E^3}\right\}\\ \kappa\geqq(S_t+S_c)^2/2E[(1+\rho_2)S_c-\rho_1S_t]\text{ or }(S_t+S_c)^2/2E[(1+\rho_1)S_t-\rho_2S_c]\end{aligned}\right\} \quad (46)$$

The lower limit of κ that applies depends on whether Eq. (45) or Eq. (45a) governs.

For the idealized I-section Eq. (28) reduces to $c_2 = \alpha h/(1+\alpha)$. When this value of c_2 is substituted in Eq. (29),

$$\mu = \kappa,\ 0 \leqq \kappa \leqq (S_c/E)[(1+\alpha)/\alpha] \text{ or } (S_t/E)(1+\alpha) \tag{43a}$$

As soon as the stress in either flange reaches its limiting value S_c or S_t, the stress in neither flange can increase. Therefore

$$\mu = \frac{S_c}{E}\frac{1+\alpha}{\alpha},\quad \kappa \geqq \frac{S_c}{E}\frac{1+\alpha}{\alpha},\quad \text{or}\quad \mu = \frac{S_t}{E}(1+\alpha),\quad \kappa \geqq \frac{S_t}{E}(1+\alpha) \tag{46a}$$

whichever is lower.

Case III

Eqs. (34) and (35) become

$$(1+2\rho_1)\kappa^2 - 2\left\{\rho_2\frac{s_2}{E} + (1+\rho_1)\left[\frac{s_2}{E} + K_c\left(\frac{s_2}{E}\right)_{nc}\right]\right\}\kappa + K_c\left[\frac{2}{n_c+1}\left(\frac{s_2}{E}\right)^{n_c+1} + K_c\left(\frac{s_2}{E}\right)^{2n_c}\right] = 0 \tag{47}$$

$$\left.\begin{aligned}\mu = 12R\Bigg\{&\frac{\rho_1}{\kappa}\left[\kappa - \frac{s_2}{E} - K_c\left(\frac{s_2}{E}\right)^{n_c}\right]^2 + \frac{1}{3\kappa^2}\left[\left(\frac{s_2}{E}\right)^3 + 3K_c\frac{n_c+1}{n_c+2}\left(\frac{s_2}{E}\right)^{n_c+2} + \right.\\ &\left.3K_c^2\frac{n_c}{2n_c+1}\left(\frac{s_2}{E}\right)^{2n_c+1}\right] + \frac{1}{3\kappa^2}\left[\kappa - \frac{s_2}{E} - K_c\left(\frac{s_2}{E}\right)^{n_c}\right]^3 + \frac{\rho_2}{\kappa}\frac{s_2}{E}\left[\frac{s_2}{E} + K_c\left(\frac{s_2}{E}\right)^{n_c}\right]\Bigg\}\\ &0 \leqq \kappa \leqq (S_t/E) + (s_2/E) + K_c(s_2/E)^{n_c}\end{aligned}\right. \tag{48}$$

Eqs. (36) and (37) become

$$\left[(1+\rho_1)\frac{S_t}{E} - \rho_2\frac{s_2}{E}\right]\kappa = \frac{1}{2}\left(\frac{S_t}{E} + \frac{s_2}{E}\right)^2 + K_c\left[\frac{S_t}{E}\left(\frac{s_2}{E}\right)^{n_c} + \frac{n_c}{n_c+1}\left(\frac{s_2}{E}\right)^{n_c+1}\right] \tag{49}$$

$$\left.\begin{aligned}\mu = 12R\Bigg\{&\frac{\rho_1}{\kappa}\frac{S_t}{E}\left[\kappa - \frac{s_2}{E} - K_c\left(\frac{s_2}{E}\right)^{n_c}\right] + \frac{1}{2\kappa^2}\frac{S_t}{E}\left[\kappa - \frac{s_2}{E} - K_c\left(\frac{s_2}{E}\right)^{n_c}\right]^2 - \frac{1}{6\kappa^2}\left(\frac{S_t}{E}\right)^3 + \\ &\frac{1}{3\kappa^2}\left[\left(\frac{s_2}{E}\right)^3 + 3K_c\frac{n_c+1}{n_c+2}\left(\frac{s_2}{E}\right)^{n_c+2} + 3K_c^2\frac{n_c}{2n_c+1}\left(\frac{s_2}{E}\right)^{2n_c+1}\right] + \frac{\rho_2}{\kappa}\frac{s_2}{E}\left[\frac{s_2}{E} + K_c\left(\frac{s_2}{E}\right)^{n_c}\right]\Bigg\}\\ &\kappa \geqq (S_t/E) + (s_2/E) + K_c(s_2/E)^{n_c}\end{aligned}\right. \tag{50}$$

For the idealized I-section Eqs. (33a) and (33b) reduce to

$$A_1s_1 = A_2s_2;\quad A_1s_1c_1 + A_2s_2c_2 = M$$

From these equations one obtains, by means of Eqs. (1), (2), (7), and (8),

$$K_c\left(\frac{\alpha\mu}{1+\alpha}\right)^{n_c} + \mu = \kappa;\quad 0 \leqq \kappa \leqq (1+\alpha)\frac{S_t}{E} + K_c\left(\frac{\alpha S_t}{E}\right)^{n_c} \tag{48a}$$

As soon as the stress in the tensile flange reaches S_t, the stress in neither flange can increase and, therefore, as in Case II.

$$\mu = (1+\alpha)\frac{S_t}{E};\quad \kappa \geqq (1+\alpha)\frac{S_t}{E} + K_c\left(\frac{\alpha S_t}{E}\right)^{n_c} \tag{50a}$$

Numerical Solutions with Different Stress-Strain Diagrams

In order to make more graphic the preceding relations and to show the effect of different stress-strain curves and different cross sections, numerical solutions with three different stress-strain diagrams will be considered for the rectangular section, the symmetrical idealized I-section ($A_1 = A_2$, $b_w = 0$), and a T-section with the flange in compression. The rectangular section represents a fairly compact section, and the idealized I-section represents an extreme condition for a symmetrical section with all the material carrying the same stress in tension and compression. The stress-strain curves assumed are shown in Figs. 5(a), 6(a), and 7(a). The yield strengths are indicated by short crosslines. The curves of Figs. 5(a) and 6(a) are extreme curves, those of the former figure having extremely blunt knees and those of the latter figure the limiting sharp knees. The curves of Fig. 7(a) are made up of the compressive curve of Fig. 5(a) and the tensile curve of Fig. 6(a), thus representing a material with markedly

different characteristics in tension and compression. The modulus of elasticity in each case is taken the same in tension as in compression and the same for all the curves—namely, 10,500,000 lbs. per sq.in. The $^2/_3E$ secant yield strength* in each case is 50,000 lbs. per sq.in. in tension and 42,000 lbs. per sq.in. in compression.

The equations of the curves of Fig. 5(a) are: for tension (Case I)—$e = (s/E) + 105(s/E)^2$; for compression (Case I)—$e = (s/E) + 125(s/E)^2$.

The equations of the curves of Fig. 6(a) are: for tension (Case II)—$e = s/E$, $e \leqq 1/210$; $s = 50{,}000$, $e \geqq 1/210$; for compression (Case II)—$e = s/E$, $e \leqq 1/250$; $s = 42{,}000$, $e \geqq 1/250$.

The equations of the curves of Fig. 7(a) are: for tension (Case III)—$e = s/E$, $e \leqq 1/210$; $s = 50{,}000$, $e \geqq 1/210$; for compression (Case III)—$e = (s/E) + 125(s/E)^2$.

The ratios S_t/E and S_c/E, which occur repeatedly, are

$$S_t/E = 1/210;\ S_c/E = 1/250 \tag{51}$$

The Rectangular Section

For the rectangular section $\rho_1 = \rho_2 = 0$, and $R = 1$.

Case I

Eqs. (40) and (41) reduce to

$$(s_1/E)^2 + 140(s_1/E)^3 = (s_2/E)^2 + (500/3)(s_2/E)^3 \tag{52}$$

$$\mu = \frac{4}{\kappa^2}\left[\left(\frac{s_1}{E}\right)^3 + \frac{945}{4}\left(\frac{s_1}{E}\right)^4 + 13{,}230\left(\frac{s_1}{E}\right)^5 + \left(\frac{s_2}{E}\right)^3 + \frac{1{,}125}{4}\left(\frac{s_2}{E}\right)^4 + 18{,}750\left(\frac{s_2}{E}\right)^5\right] \tag{53}$$

where $\kappa = e_1 + e_2$, $e_1 = (s_1/E) + 105(s_1/E)^2$, and $e_2 = (s_2/E) + 125(s_2/E)^2$. By assuming values of s_2/E, solving Eq. (52) for s_1/E, and substituting these values of s_2/E and s_1/E in Eq. (53), the relation between μ and κ can be found. This has been done, and the result is shown in Fig. 5(b).

Case II

Eqs. (43), (45), and (46) become

$$\left.\begin{aligned} \mu &= \kappa,\ 0 \leqq \kappa \leqq 1/125 \\ \mu &= (3/125)[1 - {}^2/_3\sqrt{(1/125\kappa)}],\ 1/125 \leqq \kappa \leqq 529/55{,}125 \\ \mu &= {}^1/_2[(3/115) - (23/2{,}625)^3(1/\kappa^2)],\ \kappa \geqq 529/55{,}125 \end{aligned}\right\} \tag{54}$$

These relations are shown in Fig. 6(b). The point corresponding to $\kappa = 529/55{,}125$ is indicated by a short crossline.

Case III

Eqs. (47) and (48) may be written

$$\kappa = (s_2/E)[1 + 125(s_2/E) + \sqrt{1 + (500/3)(s_2/E)}] \tag{55}$$

$$\left.\begin{aligned} \mu = \frac{4}{\kappa^2}\left\{\left(\frac{s_2}{E}\right)^3 + \frac{1{,}125}{4}\left(\frac{s_2}{E}\right)^4 + 18{,}750\left(\frac{s_2}{E}\right)^5 + \left[\kappa - \frac{s_2}{E} - 125\left(\frac{s_2}{E}\right)^2\right]^3\right\} \\ 0 \leqq \kappa \leqq (1/210) + (s_2/E) + 125(s_2/E)^2 \end{aligned}\right. \tag{56}$$

Eqs. (49) and (50) become

$$\kappa = (1/420) + (s_2/E) + 230(s_2/E)^2 + 17{,}500(s_2/E)^3 \tag{57}$$

$$\left.\begin{aligned} \mu = \frac{4}{\kappa^2}\left\{\left(\frac{s_2}{E}\right)^3 + \frac{1{,}125}{4}\left(\frac{s_2}{E}\right)^4 + 18{,}750\left(\frac{s_2}{E}\right)^5 + \frac{1}{140}\left[\kappa - \frac{s_2}{E} - 125\left(\frac{s_2}{E}\right)^2\right]^2 - \frac{1}{18{,}522{,}000}\right\} \\ \kappa \geqq (1/210) + (s_2/E) + 125(s_2/E)^2 \end{aligned}\right. \tag{58}$$

By assuming values of s_2/E, solving Eqs. (55) and (57) for κ and substituting these values in Eqs. (56) and (58), respectively, the relation between μ and κ can be found. This has been done, and the result is shown in Fig. 7(b). The point corresponding to the limiting value of κ is indicated by a short crossline.

* Stress at the intersection of the stress-strain curve of a line through the origin having a slope $^2/_3E$.

The Idealized I-Section

For the symmetrical idealized I-section, $\alpha = 1$.

Case I

Eq. (41a), solved for μ, becomes

$$\mu = -(1/115)(1 - \sqrt{1 + 230\kappa}) \tag{59}$$

This relation is shown in Fig. 5(b).

Case II

Eqs. (43a) and (46a) become

$$\mu = \kappa,\ 0 \leqq \kappa \leqq 1/125;\quad \mu = 1/125,\ \kappa \geqq 1/125 \tag{60}$$

These relations are shown in Fig. 6(b).

Case III

When Eq. (48a) is solved for μ,

$$\mu = -(2/125)(1 - \sqrt{1 + 125\kappa}),\ 0 \leqq \kappa \leqq 109/8{,}820 \tag{61}$$

Eq. (50a) becomes

$$\mu = 1/105,\ \kappa \leqq 109/8{,}820 \tag{62}$$

Eqs. (61) and (62) are shown in Fig. 7(b).

The T-Section

For the T-section with the flange in compression, $\rho_1 = 0$. In the numerical solution that follows $\rho_2 = 1$—that is, a T-section with flange area equal to web area is considered. Then $R = {}^2/_5$ (Eq. (39a)).

Case I

Eqs. (40) and (41) reduce to

$$\left(\frac{s_1}{E}\right)^2 + 140\left(\frac{s_1}{E}\right)^3 = 3\left(\frac{s_2}{E}\right)^2 + \frac{1{,}250}{3}\left(\frac{s_2}{E}\right)^3 + 2\,\frac{s_1}{E}\frac{s_2}{E} + 210\,\frac{s_2}{E}\left(\frac{s_1}{E}\right)^2 \tag{63}$$

$$\mu = \frac{8}{5\kappa^2}\left[\left(\frac{s_1}{E}\right)^3 + \frac{945}{4}\left(\frac{s_1}{E}\right)^4 + 13{,}230\left(\frac{s_1}{E}\right)^5 + 3\kappa\left(\frac{s_2}{E}\right)^2 + (1 + 375\kappa)\left(\frac{s_2}{E}\right)^3 + \frac{1{,}125}{4}\left(\frac{s_2}{E}\right)^4 + 18{,}750\left(\frac{s_2}{E}\right)^5\right] \tag{64}$$

where $\kappa = e_1 + e_2$, $e_1 = (s_1/E) + 105(s_1/E)^2$, and $e_2 = (s_2/E) + 125(s_2/E)^2$. As for the rectangular section, by assuming values of s_2/E, solving Eq. (63) for s_1/E, and substituting these values of s_2/E and s_1/E in Eq. (64), the relation between μ and κ can be found. This has been done, and the result is shown in Fig. 5(b).

Case II

Eqs. (43), (45a), and (46) become

$$\left.\begin{aligned} \mu &= \kappa,\ 0 \leqq \kappa \leqq 2/315 \\ \mu &= \frac{16}{5}\left[\frac{1}{56} + \kappa - \left(\frac{1}{210} + \kappa\right)\sqrt{1 + \frac{2}{105\kappa}}\right],\ \frac{2}{315} \leqq \kappa \leqq \frac{529}{10{,}500} \\ \mu &= {}^1/_5[(162/2{,}875) - (23/2{,}625)^3/\kappa^2],\ \kappa \geqq 529/10{,}500 \end{aligned}\right\} \tag{65}$$

These relations are shown in Fig. 6(b). The point corresponding to $\kappa = 2/315$ is indicated by a short crossline.

Case III

Eqs. (47) and (48) may be written

$$\kappa = 2(s_2/E)[1 + (125/2)(s_2/E) + \sqrt{1 + (625/6)(s_2/E)}] \tag{66}$$

$$\mu = \frac{8}{5\kappa^2}\left\{\left(\frac{s_2}{E}\right)^3 + \frac{1{,}125}{4}\left(\frac{s_2}{E}\right)^4 + 18{,}750\left(\frac{s_2}{E}\right)^5 + \left[\kappa - \frac{s_2}{E} - 125\left(\frac{s_2}{E}\right)^2\right]^3 + 3\kappa\frac{s_2}{E}\left[\frac{s_2}{E} + 125\left(\frac{s_2}{E}\right)^2\right]\right\} \tag{67}$$
$$0 \leqq \kappa \leqq (1/210) + (s_2/E) + 125(s_2/E)^2$$

Eqs. (49) and (50) become

$$\left(\frac{1}{210} - \frac{s_2}{E}\right)\kappa = \frac{1}{88{,}200} + \frac{1}{210}\left(\frac{s_2}{E}\right) + \frac{23}{21}\left(\frac{s_2}{E}\right)^2 + \frac{250}{3}\left(\frac{s_2}{E}\right)^3 \tag{68}$$

$$\mu = \frac{2}{175\kappa^2}\left[\kappa^2 - \frac{1}{132{,}300} - 2\kappa\left(\frac{s_2}{E}\right) + (1 + 170\kappa)\left(\frac{s_2}{E}\right)^2 + (390 + 52{,}500\kappa)\left(\frac{s_2}{E}\right)^3 + 55{,}000\left(\frac{s_2}{E}\right)^4 + 2{,}625{,}000\left(\frac{s_2}{E}\right)^5\right] \tag{69}$$
$$\kappa \geqq (1/210) + (s_2/E) + 125(s_2/E)^2$$

As for the rectangular section, by assuming values of s_2/E, solving Eqs. (66) and (68) for κ, and substituting these values in Eqs. (67) and (69), respectively, the relation between μ and κ can be found. This has been done, and the result is shown in Fig. 7(b). The point corresponding to the limiting value of κ is indicated by a short cross-line.

Discussion

In discussing the effects of the different cross sections and the different stress-strain relations that have been considered, it may be noted that only the ratios of the mechanical properties (Eq. (51)), not the absolute values, are determinative. This fact adds something to the generality of any conclusions that may be drawn.

For a stress-strain diagram like Fig. 5(a) with blunt knees (hardly knees at all), Case I, Fig. 5(b) shows a relatively small percentage difference in μ for the widely different sections, the rectangle and the idealized I. The T-section lies between the other two. At $\kappa = 0.018$ the difference in μ and thus in M for the same EI/h is about 8 per cent for the rectangle and the idealized I. For a sharp-kneed stress-strain diagram, Fig. 6, Case II, there is no difference in the elastic range, and then the difference increases rapidly, the moments becoming, for $\kappa = 0.018$, over 50 per cent higher for the rectangle than for the I-section. As $\kappa = \infty$, this difference approaches 61.3 per cent. On the other hand, the values of μ for the rectangle in Fig. 6 are higher than for both the rectangle and the I-section in Fig. 5 up to about $\kappa = 0.018$. Up to about $\kappa = 0.0105$ the values of μ for the I-section are higher in Fig. 6 than for both the rectangle and the I-section in Fig. 5. It may be noted that the curve for the T-section crosses the one for the I-section. Fig. 7, Case III, shows a difference in μ for the rectangle and the I-section of about 5.5 per cent at $\kappa = 0.0123$, and then the difference increases, the value for the rectangle becoming 200 per cent greater than for the I-section as $\kappa = \infty$. The curve for the T-section crosses the one for the rectangle once and the one for the I-section twice.

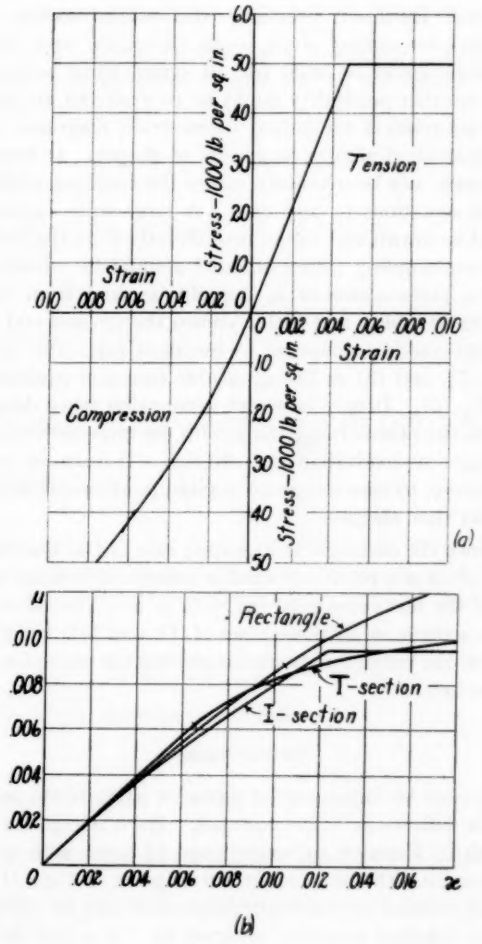

Fig. 7.

Figs. 8(a)–8(d) are Figs. 5, 6, and 7 redrawn to show the effect of the stress-strain diagram on the κ,μ-relation for the rectangle (Fig. 8(b)), for the I-section (Fig. 8(c)), and for the T-section (Fig. 8(d)). The curves marked I, II, and III correspond to Cases I, II, and III. These figures show roughly the same maximum spread for values of κ from 0 to 0.018 for widely different stress-strain diagrams.

A significant thing indicated by Figs. 5 to 8 is that widely different moment-curvature relations are obtained for a given stress-strain diagram and different cross sections and also for a given cross section and different stress-strain diagrams. Consequently, any approximate solution to be both safe and economical must take these differences into account.

Figs. 5 and 6 suggest that an average κ,μ-relation might be worked out for actual stress-strain diagrams (those assumed were extreme) that would be suitable for all symmetrical cross sections up to values of κ which would be considered allowable in practice. This relation could be approximated to by a simpler equation than those presented here. Or, to be on the safe side, the exact κ,μ-relations could be worked out for the symmetrical idealized I-section (the easiest section to handle) for actual stress-strain diagrams, and these relations could be used for all symmetrical sections. Still another possibility might be to work out an accurate κ,μ-relation for actual stress-strain diagrams and for individual shapes or groups of shapes. It would, of course, not be necessary to use the resulting complicated equations in any case. A large-scale κ,μ-curve could be drawn and values read directly from the curve, or corresponding values of κ and μ could be tabulated. For a given value of μ, κ could be read from such curves or tables, and with κ known the stresses and the strains could be computed by means of Eqs. (38), (1) or (2), (7), and (3) or the applicable equation equivalent to Eq. (3). It may be worth noting that when designing in the plastic range the strains are more sensitive to changes in load than the stresses. It may be well, therefore, to base design on maximum allowable strains rather than stresses.

Since the rectangle is a limiting case of the T-section, the effect of a relatively smaller compressive flange area than the one considered ($\rho_1 = 0$, $\rho_2 = 1$) would be to give a curve in all three cases (I, II, and III) lying between the curve for the rectangle and the curve for the T-section.

Deflections

It may be important at times to estimate the maximum deflections to be expected. Here, except for the idealized I-section and certain special cases, such as the rectangle with the stress-strain diagram of Case II, an exact solution is practically impossible and an approximate solution must be resorted to. If κ can be expressed approximately as a sufficiently simple function

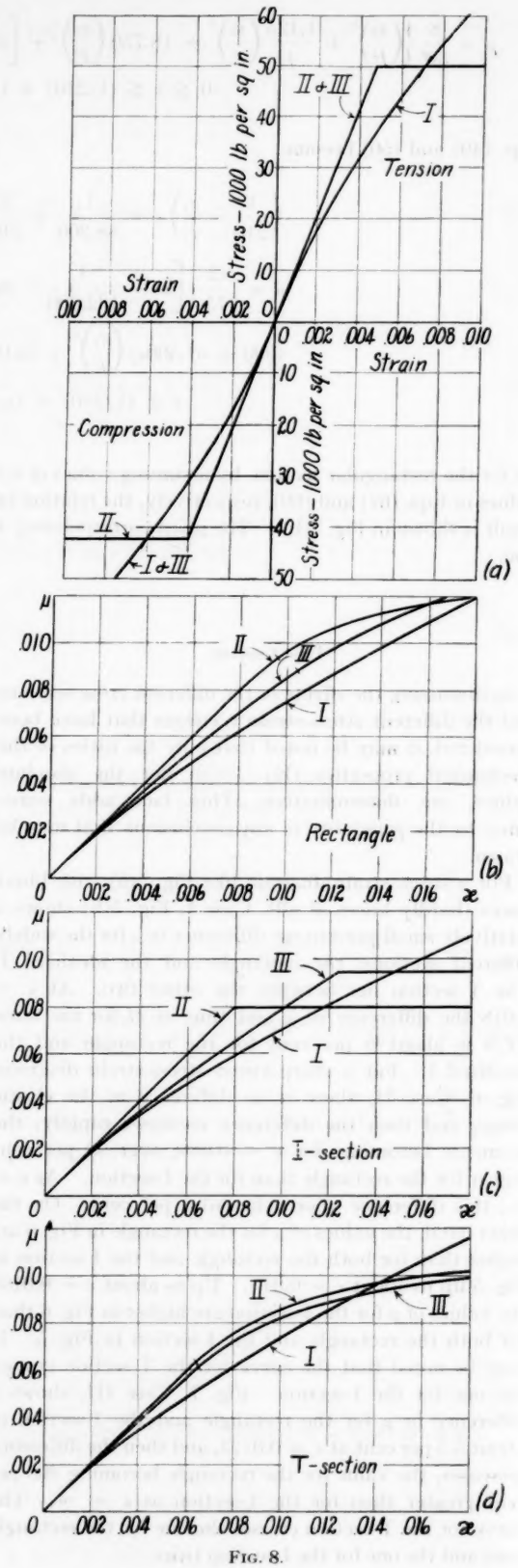

Fig. 8.

of μ for the given cross section, the deflections can be computed without too much difficulty. The general procedure will be outlined, the differential equations will be written for the idealized I-section, and they will be applied to the numerical case considered in the paper and integrated for three beams.

If the curvatures remain sufficiently small,

$$d^2v/dx^2 = k \tag{70}$$

where x is measured along the length of the beam and v is the deflection. In any practical case the curvatures will remain sufficiently small to justify Eq. (70). In order to integrate Eq. (70) without too much trouble, k should be expressible explicitly as a function of x. In most cases, as the equations of the paper show, k is a complicated function of M, which will ordinarily be expressible as a function of x. It is practically necessary, therefore, to approximate to the exact k,M-relation (or κ,μ-relation) by a simpler relation in the interval within which k lies. If this can be done successfully, as it often no doubt can, Eq. (70) may be integrated by standard methods.

The idealized I-section can be handled exactly and will now be considered. For comparative purposes it is convenient to introduce the nondimensional variables

$$\xi = x/l, \ \phi = hv/l^2 \tag{71}$$

where l is the length of the beam. Then Eq. (70) becomes

$$d^2\phi/d\xi^2 = \kappa \tag{70a}$$

and it takes the following forms for Cases I, II, and III.

Case I

From Eq. (41a)

$$\frac{d^2\phi}{d\xi^2} = K_t\left(\frac{\mu}{1+\alpha}\right)_{n_t} + K_c\left(\frac{\alpha\mu}{1+\alpha}\right)^{n_c} + \mu \tag{72}$$

Case II

From Eq. (43a)

$$\left.\begin{aligned} d^2\phi/d\xi^2 &= \mu \\ 0 \leqq \kappa \leqq \frac{S_c}{E}\frac{1+\alpha}{\alpha} &\text{ or } \frac{S_t}{E}(1+\alpha) \end{aligned}\right\} \tag{73}$$

The lower of the upper limiting values of κ is the greatest value μ can have. When μ reaches this value, the curvature increases indefinitely (Fig. 6(b)).

Case III

From Eq. (48a)

$$\left.\begin{aligned} d^2\phi/d\xi^2 &= K_c[\alpha\mu/(1+\alpha)]^{n_c} + \mu \\ 0 \leqq \kappa \leqq (1+\alpha)\frac{S_t}{E} &+ K_c\left(\frac{\alpha S_t}{E}\right)^{n_c} \end{aligned}\right\} \tag{74}$$

When κ reaches the upper limiting value, μ has the greatest value it can have and the curvature increases indefinitely (Fig. 7(b)).

If n_t and n_c are integers, Eqs. (72) and (74) can usually be integrated, although difficulty may be experienced when n_t or n_c, or both, are large.

To continue the study of the idealized I-section, the same stress-strain diagrams will be assumed as before, and the cross-sectional areas of the two flanges will be taken equal, $\alpha = 1$. Then Eqs. (72), (73), and (74) become

$$\textit{Case I:} \qquad \frac{d^2\phi}{d\xi^2} = \frac{115}{2}\mu^2 + \mu \tag{75}$$

$$\textit{Case II:} \qquad \frac{d^2\phi}{d\xi^2} = \mu, \quad 0 \leqq \kappa \leqq \frac{1}{125} \tag{76}$$

$$\textit{Case III:} \qquad \frac{d^2\phi}{d\xi^2} = \frac{125}{4}\mu^2 + \mu, \ 0 \leqq \kappa \leqq \frac{109}{8{,}820} \tag{77}$$

It will be useful to examine the maximum deflections of a few beams for the three cases treated (I, II, and III).

Beam Loaded at the Ends By Couples

In this simplest possible case μ is constant. Take the origin of coordinates at one end of the beam. The integration of Eq. (75) gives

$$\textit{Case I:} \qquad \phi = \frac{1}{2}\mu\left(\frac{115}{2}\mu + 1\right)(\xi - 1)\xi$$

The maximum deflection, at the middle ($\xi = {}^1/_2$), is given by

$$|\phi_{max.}| = {}^1/_8\mu[1 + (115/2)\mu] \tag{78}$$

Integration of Eq. (76) gives

$$\textit{Case II:} \qquad \phi = {}^1/_2\mu(\xi - 1)\xi \tag{79}$$

with $|\phi_{max.}| = {}^1/_8\mu$. Integration of Eq. (77) gives

$$\textit{Case III:} \qquad \phi = \frac{1}{2}\mu\left(\frac{125}{4}\mu + 1\right)(\xi - 1)\xi \tag{80}$$

with $|\phi_{max.}| = {}^1/_8\mu[1 + (125/4)\mu]$. If the extreme fibers are stressed to 42,000 lbs. per sq.in., $\mu = {}^1/_{125}$, and the ratios of the maximum deflections for the three cases are

$$\phi_{\mathrm{I}} : \phi_{\mathrm{II}} : \phi_{\mathrm{III}} = 146 : 100 : 125 \tag{81}$$

In the two subsequent examples

$$\omega = Whl/EI \tag{82}$$

where W is the total load on the beam.

Simply Supported Beam, Centrally Loaded

With the origin of coordinates taken at one end, for $0 \leqq \xi \leqq {}^1/_2$,

$$\mu = {}^1/_2\omega\xi \tag{83}$$

Integration of Eq. (75) gives

$$\textit{Case I:}\quad \phi = \frac{115}{192}\omega^2(2\xi^3 - 1)\xi + \frac{1}{48}\omega(4\xi^2 - 3)\xi$$

The maximum deflection, at the middle ($\xi = {}^1/_2$), is given by

$$|\phi_{max.}| = (1/48)\omega[1 + (345/32)\omega] \qquad (84)$$

Integration of Eq. (76) gives

$$\textit{Case II:}\qquad \phi = \frac{1}{48}\omega(4\xi^2 - 3)\xi \qquad (85)$$

with $|\phi_{max.}| = (1/48)\omega$. Integration of Eq. (77) gives

$$\textit{Case III:}\quad \phi = \frac{125}{384}\omega^2(2\xi^3 - 1)\xi + \frac{1}{48}\omega(4\xi^2 - 3)\xi \qquad (86)$$

with $|\phi_{max.}| = (1/48)\omega[1 + (375/64)\omega]$. If the extreme fibers are stressed to 42,000 lbs. per sq.in., $\omega = {}^4/_{125}$, and the ratios of the maximum deflections for the three cases are

$$\phi_I : \phi_{II} : \phi_{III} = 538 : 400 : 475 \qquad (87)$$

Simply Supported Beam, Uniformly Loaded

With the origin of coordinates taken at one end

$$\mu = {}^1/_2\omega\xi - {}^1/_2\omega\xi^2 \qquad (88)$$

Integration of Eq. (75) gives

Case I:

$$\phi = \frac{23}{96}\omega^2(2\xi^5 - 6\xi^4 + 5\xi^3 - 1)\xi - \frac{1}{24}\omega(\xi^3 - 2\xi^2 + 1)\xi$$

The maximum deflection, at the middle ($\xi = {}^1/_2$), is given by

$$|\phi_{max.}| = (5/384)\omega\,[1 + (253/40)\omega] \qquad (89)$$

Integration of Eq. (76) gives

$$\textit{Case II:}\qquad \phi = -(1/24)\omega(\xi^3 - 2\xi^2 + 1)\xi \qquad (90)$$

with $|\phi_{max.}| = (5/384)\omega$. Integration of Eq. (77) gives

Case III:

$$\phi = \frac{25}{192}\omega^2(2\xi^5 - 6\xi^4 + 5\xi^3 - 1)\xi - \frac{1}{24}\omega(\xi^5 - 2\xi^2 + 1)\xi \qquad (91)$$

with $|\phi_{max.}| = (5/384)\omega[1 + (55/16)\omega]$. If the extreme fibers are stressed to 42,000 lbs. per sq.in., $\omega = {}^8/_{125}$, and the ratios of the maximum deflections for the three cases are

$$\phi_I : \phi_{II} : \phi_{III} = 1756 : 1250 : 1525 \qquad (92)$$

It happens in the three examples just presented that μ was naturally positive. In using Eqs. (75) and (77), μ must be taken positive because in deducing Eqs. (41a) and (48a), which entered in deriving Eqs. (75) and (77), μ was assumed positive, since s_1 and s_2 are always considered positive. The point really is that k and κ have always been considered positive, and thus v in Eq. (70) must be taken in the direction to make d^2v/dx^2 positive.

References

[1] Cozzone, Frank P., *Bending Strength in the Plastic Range*, Journal of the Aeronautical Sciences, Vol. 10, No. 5, p. 137, May, 1943.

[2] Wolford, Don. S., *Significance of the Secant and Tangent Moduli of Elasticity in Structural Design*, Journal of the Aeronautical Sciences, Vol. 10, No. 6, p. 169, June, 1943.

[3] Mayer, Eugen, *Die Berechnung der Durchbiegung von Stäben, deren Material dem Hookeschen Gesetze nicht folgt*, Zeitschrift des Vereines deutscher Ingenieure, Vol. 52, p. 167, February 1, 1908.

[4] Bach, C., and Baumann, R., *Elastizität und Festigkeit*, 9th Ed., p. 289, footnote 2; Julius Springer, Berlin, 1924.

The Thermodynamics of Air at High Velocities

NEIL P. BAILEY*

General Electric Company

SUMMARY

The flow of air at velocities near and above sound velocity is involved in an ever-increasing number of cases, and a satisfactory solution often requires the use of the highly specialized tools of modern fluid mechanics. However, there are many engineering problems that may be solved with sufficient accuracy in terms of average velocities without following through the paths of individual particles.

When these thermodynamic equations of high velocity gas flow are solved in terms of such variables as velocity and density, they are not simple or easy to handle. If Mach number is used as a primary variable, all of these equations become quite simple and usable.

This is illustrated by the solution of the cases of flow with friction and with heat transfer and for nozzles and diffusers with and without friction. Diffusers are discussed in more detail and measures of diffuser performance are suggested because, in proportion to their importance, they have received far less attention than nozzles.

In conclusion, the case of flow through plane shock waves is solved in terms of Mach number and the theoretical correction for impact tubes in superacoustic flow is worked out.

SYMBOLS

A or a	=	flow area, sq.ft.
C_v	=	specific heat at constant volume, B.t.u. per lb. per °F.
C_p	=	specific heat of constant pressure, B.t.u. per lb. per °F.
f	=	flow friction factor
g	=	acceleration of gravity = 32.2 ft. per sec. per sec.
J	=	778.26 ft.lbs. per B.t.u.
L	=	mechanical work
m	=	hydraulic radius, ft.
M	=	Mach number
P	=	absolute pressure, lbs. per sq.ft.
γ	=	adiabatic gas constant, 1.395 for dry air at 80°F.† Evaluated from *The New Specific Heats*, by Dr. R. C. H. Heck, Mechanical Engineering, January, 1940, and February, 1941.
Q	=	heat added or removed, B.t.u.
R	=	gas constant for air, 53.3 in.lbs., ft., °R. (deg. Rankine) units
S	=	entropy, B.t.u. per lb. per °R.
T	=	static temperature, °R.
T_0	=	total temperature, °R.
v	=	velocity, ft. per sec.
V	=	specific volume, cu.ft. per lb.
W	=	flow, lbs. per sec.
x	=	distance, ft.
ρ	=	mass density, slugs per cu.ft.
ϵ	=	base of natural logarithms

Presented at the Aerodynamics Session, Twelfth Annual Meeting, I.A.S., New York, January 25–27, 1944.

* Research Engineer, Research Laboratory.

† NOTE: For other initial temperatures, the following are average values.

Initial Temperature, °F.	γ
80	1.395
240	1.385
490	1.370
740	1.350

Since $[(\gamma - 1)/\gamma]$ enters as an exponent, the use of $\gamma = 1.4$ instead of 1.395 changes the exponent 1.2 per cent, which becomes important at high pressure ratios.

MACH NUMBER AS A PHYSICAL CONCEPT

THE BASIC EQUATIONS for the flow of gases at high velocities are simple individually, but, when they are solved simultaneously, the resulting relationships are often complicated and tedious to use. This is because the state of a moving gas cannot be defined with fewer than three of the variables commonly used. A further complication is the fact that the general gas equation, $PV = RT$, was devised for the case of a gas at rest. When it is used to define the condition of a moving gas, both the temperature (T) and the pressure (P) must be *static* values measured relative to the stream; that is, they must be the values that would be observed by an instrument moving with the stream.

Much of this complication can be avoided by replacing the velocity (v) and the static temperature (T) by the Mach number (M) of the gas. The simplest definition is that the Mach number is the ratio of the flow velocity to the local velocity of sound in the gas at that point. However, such a definition fails to bring out the significance of Mach number or to explain why it is a single variable in terms of which all the others may be readily expressed. The velocity of sound or the acoustic velocity is $\sqrt{\gamma g R T}$, and the Mach number is

$$M = v/\sqrt{\gamma g R T} \tag{1}$$

or

$$M^2 = v^2/\gamma g R T \tag{2}$$

It is in the form given by Eq. (2) that the physical significance of Mach number is revealed. From the kinetic theory of gases it is known that the absolute temperature (T) measures the kinetic energy of random translation and rotation of the molecules and, of course, v^2 measures the controlled or directed kinetic energy of flow. This means that M^2 reflects any

change in the ratio of the controlled or directed kinetic energy to the random kinetic energy of the individual molecules, regardless of what causes the change. The total internal molecular energy of a gas changes as the translational and rotational parts change, and, since the equations of gas flow involve both the thermal energy and the directed kinetic energy, it is not surprising that Mach number proves to be a useful fundamental variable and that it almost always occurs in equations as M^2 and rarely as M.

To define the state of a moving fluid it is necessary to specify the type of fluid flowing and the kind of flow involved. These things are accomplished by so-called basic equations of flow.

Gas Equation

$$PV = RT \text{ or } \rho = \frac{1}{Vg} = \frac{P}{gRT} \tag{3}$$

Energy Equation

If as a pound of gas flows a distance (dx) an amount of mechanical work (dL) is done on it and an amount of heat (dQ) is added to it, the sum must appear as increased kinetic energy $[(1/Jg)vdv]$, as flow work, or as an internal or thermal energy change. The forcing of a volume of gas (V) into a region of higher pressure involves an amount of work $(1/J)Vdp$. If after it is in this higher pressure region its volume changes dV, $(1/J)PdV$ of work is required. Since the internal energy of a gas depends only on temperature, the energy equation is

$$dL + dQ = C_v dT + \frac{1}{J} Vdp + \frac{1}{J} PdV + \frac{1}{Jg} vdv \tag{4}$$

Since

$$C_v dT + (1/J)d(PV) = [C_v + (R/J)]dT = C_p dT$$

$$dL + dQ = C_p dT + \frac{1}{Jg} vdv \tag{5}$$

or using

$$C_p = [\gamma/(\gamma - 1)](R/J)$$

$$dL + dQ = \frac{\gamma}{(\gamma - 1)} \frac{R}{J} dT + \frac{1}{Jg} vdv \tag{6}$$

For the special case of no mechanical work done or heat transferred, it is

$$\gamma gRdT + (\gamma - 1)vdv = 0 \tag{7}$$

Continuous Flow

If the velocity is uniform across the channel area (A), the statement that the flow is steady is

$$\rho vA = \text{Constant} \tag{8}$$

or in differential form, when combined with the gas equation, it is

$$(dP/P) + (dA/A) + (dv/v) - (dT/T) = 0 \tag{9}$$

Mach Number

From Eq. (2)

$$M^2 = v^2/\gamma gRT \tag{10}$$

or

$$(dM/M) = (dv/v) - {}^1/_2(dT/T) \tag{11}$$

Flow Conditions

The case of reversible flow with no heat transfer is defined by noting that the change in internal energy ($C_v dT$) is caused entirely by the expansion or compression work $[(1/J)PdV]$ or

$$JC_v dT + PdV = 0 \tag{12}$$

If the gas equation $PV = RT$ is differentiated,

$$PdV = RdT - RT(dP/P) \tag{13}$$

From Eqs. (12) and (13)

$$J\left(C_v + \frac{R}{J}\right) dT = RT \frac{dP}{P} \text{ or } \frac{dT}{T} = \frac{(\gamma - 1)}{\gamma} \frac{dP}{P} \tag{14}$$

If friction is involved, the total pressure change is the result of friction and acceleration, or

$$dP = -(\rho f dx\, v^2/2m) - \rho v dv \tag{15}$$

The practical solution of high velocity airflow problems for the various types of flow is greatly aided by expressing each of the variables involved in terms of the Mach number as a primary concept.

The general relationship between the static temperature (T), when the air is moving at a Mach number (M), and the impact or total temperature (T_0), indicated by an ideal stationary thermometer that brings the air to rest without heat transfer, may be had by integrating Eq. (7),

$$\int_T^{T_0} \gamma gRdT + (\gamma - 1) \int_v^0 vdv = 0 \tag{16}$$

$$\frac{T_0}{T} - 1 = \frac{(\gamma - 1)}{2} \frac{v^2}{\gamma gRT} = \frac{\gamma - 1}{2} M^2 \tag{17}$$

$$\frac{T_0}{T} = \frac{\text{total temperature}}{\text{static temperature}} = 1 + \frac{(\gamma - 1)}{2} M^2 \tag{18}$$

If this value of static temperature (T) is used in Eq. (10), the result is

$$\frac{v}{\sqrt{\gamma gRT_0}} = \frac{M}{\sqrt{1 + [(\gamma - 1)/2]\, M^2}} \tag{19}$$

This relates Mach number and total temperature with velocity as shown by Fig. 1. The fact that Mach number is not affected by the difference between total and static temperature explains why thermodynamic equations are simplified when it is used as a primary variable.

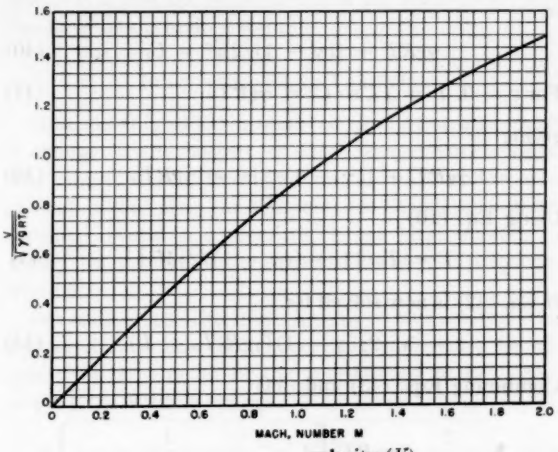

FIG. 1. Mach number versus $\frac{\text{velocity } (V)}{\sqrt{\gamma g R T_0}}$ (Eq. (19)).

REVERSIBLE OR FRICTIONLESS FLOW

The relationship between pressure and Mach number for a reversible acceleration or deceleration is found by eliminating dv/v and dT/T from Eqs. (7), (11), and (14). From Eqs. (7) and (11)

$$\frac{dv}{v} = -\frac{\gamma g R dT}{(\gamma-1)v^2} = \frac{dM}{M} + \frac{1}{2}\frac{dT}{T} \tag{20}$$

Using Eqs. (10), (14), and (20)

$$\frac{dT}{T} = \frac{(\gamma-1)}{\gamma}\frac{dP}{P} = -\frac{dM}{M}\left\{\frac{1}{[1/(\gamma-1)M^2]+{}^1/_2}\right\} \tag{21}$$

Eq. (21) may be written

$$\frac{(\gamma-1)}{\gamma}\frac{dP}{P} = -\frac{2MdM}{M^2+[2/(\gamma-1)]} \tag{22}$$

The ideal pressure change required to accelerate air from rest to a Mach number (M) or the pressure rise as it is brought to rest in an ideal diffuser may be found by integrating Eq. (22).

$$-\frac{\gamma-1}{\gamma}\int_{P_0}^{P}\frac{dP}{P} = \int_0^M \frac{2MdM}{M^2+[2/(\gamma-1)]} \tag{23}$$

$$\left(\frac{P_0}{P}\right)^{(\gamma-1)/\gamma} = \frac{\gamma-1}{2}\left[M^2+\frac{2}{\gamma-1}\right] \tag{24}$$

or

$$M = \sqrt{\frac{2}{\gamma-1}\left[\left(\frac{P_0}{P}\right)^{(\gamma-1)/\gamma}-1\right]} \tag{25}$$

Fig. 2 from Eq. (25) may also be used to find the pressure ratio required to go from any Mach number to any other merely by taking the proper ratio of the pressure ratios shown. For example, if air is decelerated from $M = 0.907$ to $M = 0.406$, in an ideal diffuser the pressure rise ratio is $1.70/1.12 = 1.52$.

The variation of flow area required to produce a Mach number change with reversible flow may be expressed by eliminating P, T, and v from the energy Eq. (7), the flow Eq. (9), the Mach number Eq. (11), and the reversibility Eq. (14).

From Eq. (7)

$$\frac{dT}{T} + \frac{(\gamma-1)v^2}{\gamma g R T}\frac{dv}{v} = \frac{dT}{T} + (\gamma-1)M^2\frac{dv}{v} = 0 \tag{26}$$

Using Eqs. (26) and (11)

$$\frac{dT}{T} = -(\gamma-1)M^2\frac{dv}{v} = 2\frac{dv}{v} - 2\frac{dM}{M} \tag{27}$$

This gives

$$\frac{dv}{v} = \frac{dM/M}{[(\gamma-1)/2]M^2+1} \tag{28}$$

and

$$\frac{dT}{T} = -\frac{(\gamma-1)MdM}{[(\gamma-1)/2]M^2+1} \tag{29}$$

From Eqs. (29) and (14)

$$\frac{dP}{P} = \frac{\gamma}{\gamma-1}\frac{dT}{T} = -\frac{\gamma MdM}{[(\gamma-1)/2]M^2+1} \tag{30}$$

Using Eqs. (28), (29), and (30) in (9),

$$-\frac{\gamma MdM}{[(\gamma-1)/2]M^2+1} + \frac{dA}{A} + \frac{dM/M}{[(\gamma-1)/2]M^2+1} + \frac{(\gamma-1)MdM}{[(\gamma-1)/2]M^2+1} = 0 \tag{31}$$

or

$$\frac{dA}{A} = -\frac{(1-M^2)dM}{M\{[(\gamma-1)/2]M^2+1\}} \tag{32}$$

Integrating Eq. (32)

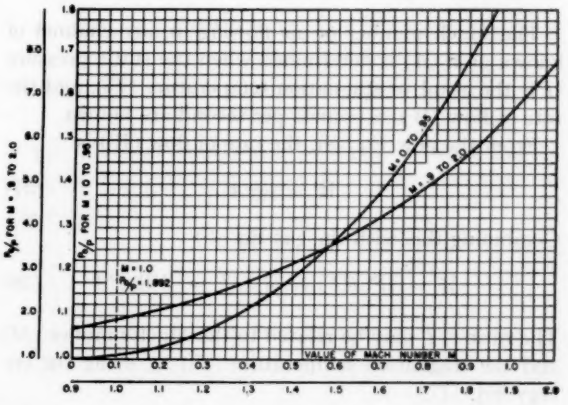

FIG. 2. Pressure ratio versus Mach number for a reversible change. (From Eq. (25).)

$$\log_e A = \log_e \left\{ \frac{\left[1 + \frac{(\gamma - 1)}{2} M^2\right]^{(\gamma+1)/2(\gamma-1)}}{M} \right\} + \log_e C_1 \quad (33)$$

$$A = \frac{C_1\{1 + [(\gamma - 1)/2]M^2\}^{(\gamma+1)/2(\gamma-1)}}{M} \quad (34)$$

If at $A = A_0$, $M = M_0$, then

$$C_1 = \frac{A_0 M_0}{\{1 + [(\gamma - 1)/2]M_0^2\}^{(\gamma+1)/2(\gamma-1)}} \quad (35)$$

Giving

$$\frac{A}{A_0} = \frac{M_0}{M}\left\{\frac{1 + [(\gamma - 1)/2]M^2}{1 + [(\gamma-1)/2]M_0^2}\right\}^{(\gamma+1)/2(\gamma-1)} \quad (36)$$

Fig. 3 shows this relationship using the area A_0 as unity at the acoustic velocity where $M_0 = 1$. This curve may be used to find the area change required for any reversible Mach number change. For example, to diffuse from $M = 0.8$ to $M = 0.3$ would require a diffuser with an area ratio of $2.07/1.04 = 1.99$.

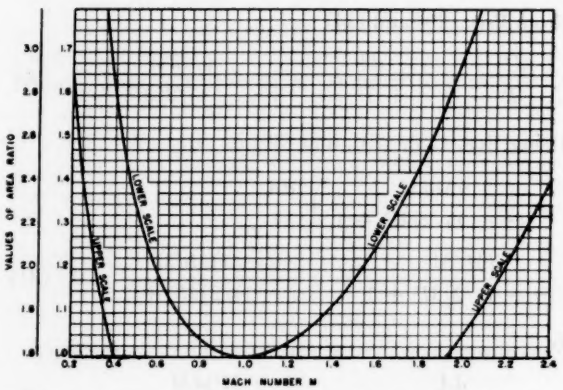

FIG. 3. Area ratio versus Mach number for reversible flow. Area at $M = 1.0$ used as unity. (From Eq. (36).)

THE DETERMINATION OF MACH NUMBER

The Mach number of air flowing in any channel of known area (A) is determined when the static pressure (P), the total or stagnation temperature (T_0), and the rate of flow (W) in pounds per second are known.

From the flow Eq. (8), the rate of flow (W) is

$$W = \rho g v A \quad (37)$$

Combining this with the gas Eq. (3)

$$W = (P/RT)Av \text{ or } v/T = WR/PA \quad (38)$$

The ratio v/T may be related to the Mach number (M) and the stagnation temperature (T_0) by using the energy Eq. (7).

$$\gamma g R dT + (\gamma - 1)v dv = 0 \quad (39)$$

or

$$\gamma g R T + [(\gamma - 1)/2]v^2 = C_1 \quad (40)$$

For $v = 0$, $T = T_0$, so $C_1 = \gamma g R T_0$ (41)

giving

$$\gamma g R T + [(\gamma - 1)/2]v^2 = \gamma g R T_0 \quad (42)$$

Using Eq. (10)

$$T = T_0/\{1 + [(\gamma - 1)/2]M^2\} \quad (43)$$

If Eq. (42) is now solved for v

$$v = \sqrt{[2/(\gamma - 1)]\gamma g R(T_0 - T)} \quad (44)$$

Combining Eqs. (43) and (44)

$$v = \sqrt{\frac{2}{(\gamma - 1)}\gamma g R T_0 \left[1 - \frac{1}{1 + [(\gamma - 1)/2]M^2}\right]} = \sqrt{\frac{\gamma g R T_0 M^2}{1 + [(\gamma - 1)/2]M^2}} \quad (45)$$

From Eqs. (38), (43), and (45)

$$\frac{v}{T} = \frac{WR}{PA} = \sqrt{\frac{\gamma g R M^2\{1 + [(\gamma - 1)/2]M^2\}}{T_0}} \quad (46)$$

or

$$\frac{W\sqrt{T_0}}{PA} = M\sqrt{\frac{\gamma g}{R}\left[1 + \frac{(\gamma - 1)}{2}M^2\right]} \quad (47)$$

Fig. 4 gives values of M for various values of $W\sqrt{T_0}/PA$, and from it the Mach number for any set of data may be found.

From Eq. (47) it may be seen that when air flows in a constant area channel with no heat transfer, with or without friction,

$$PM\sqrt{1 + [(\gamma - 1)/2]M^2} = \text{Constant} \quad (48)$$

This is the equation of a Fanno line, and it holds for all cases of constant area, constant total temperature

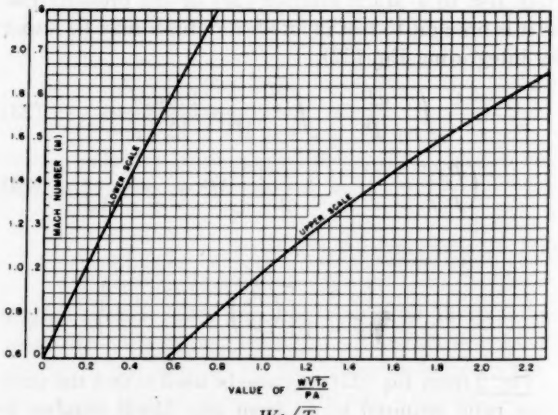

FIG. 4. Mach number versus $\frac{W\sqrt{T_0}}{PA}$. Units: PA = lb., W = lbs. per sec., T_0 = total temperature degrees R. (From Eq. (47).)

flow. It is just the statement that the total energy and the flow area remain constant.

Flow with Heat Transfer

When heat is added or removed from a flowing stream a change in the impact or total temperature results. The simplest case is that of heating at constant flow area at such a rate that the temperature change in a short distance results in a pressure change large enough to justify the neglect of the pressure losses resulting from friction.

For such a case the friction term of Eq. (15) may be neglected, and the total pressure change may be assumed to be a result of the acceleration made necessary by the volume change. This gives

$$dP = -\rho v dv \tag{49}$$

Since, for constant area flow,

$$\rho v = \rho_1 v_1 = \rho_2 v_2 = \text{Constant} \tag{50}$$

$$\int_{P_1}^{P_2} dP = -\rho v \int_{v_1}^{v_2} dv \tag{51}$$

$$P_2 - P_1 = -\rho v(v_2 - v_1) = -\rho_2 v_2^2 + \rho_1 v_1^2 \tag{52}$$

Using the general gas Eq. (3)

$$P_2 - P_1 = (P_2 V_2^2/gRT_2) + (P_1 V_1^2/gRT_1) \tag{53}$$

Combining Eq. (53) with the Mach number Eq. (10),

$$P_2 - P_1 = -\gamma P_2 M_2^2 + \gamma P_1 M_1^2 \tag{54}$$

or

$$P_1/P_2 = (1 + \gamma M_2^2)/(1 + \gamma M_1^2) \tag{55}$$

Eq. (55), which defines any pressure change that occurs at constant area with no friction, is known as the equation of a Rayleigh line.

Using Eq. (46) for flow at constant area,

$$P\sqrt{\frac{\gamma g R M^2\{1 + [(\gamma - 1)/2]M^2\}}{T_0}} = \frac{WR}{A} = \text{Constant} \tag{56}$$

or

$$P_1\sqrt{\frac{\gamma g R M_1^2\{1 + [(\gamma - 1)/2]M_1^2\}}{T_{0_1}}} = P_2\sqrt{\frac{\gamma g R M_2^2\{1 + [(\gamma - 1)/2]M_2^2\}}{T_{0_2}}} \tag{57}$$

where T_{0_1} is the stagnation or total temperature before the constant area heating and T_{0_2} is the final value, both in degrees Rankine.

Combining Eqs. (55) and (57),

$$\frac{M_2\sqrt{1 + [(\gamma - 1)/2]M_2^2}}{(1 + \gamma M_2^2)} = \sqrt{\frac{T_{0_2}}{T_{0_1}}}\,\frac{M_1\sqrt{1 + [(\gamma - 1)/2]M_1^2}}{(1 + \gamma M_1^2)} \tag{58}$$

Fig. 5 of $M\sqrt{1 + [(\gamma - 1)/2]M^2}/(1 + \gamma M^2)$ plotted versus M is useful in solving problems involving constant area heating or cooling with no friction. If the initial value of this function is multiplied by $\sqrt{T_{0_2}/T_{0_1}}$ the final M_2 may be found. The resulting pressure ratio may then be calculated from Eq. (55). As an example for $M_1 = 0.5$,

$$M_1\sqrt{1 + [(\gamma - 1)/2]M_1^2}/(1 + \gamma M_1^2) = 0.3795$$

For an initial total temperature of 540°R. and a 100° rise, $\sqrt{T_{0_2}/T_{0_1}} = 1.09$, the new

$$M_2\sqrt{1 + [(\gamma - 1)/2]M_2^2}/(1 + \gamma M_2^2) = 0.414$$

and from Fig. 4, $M_2 = 0.60$.

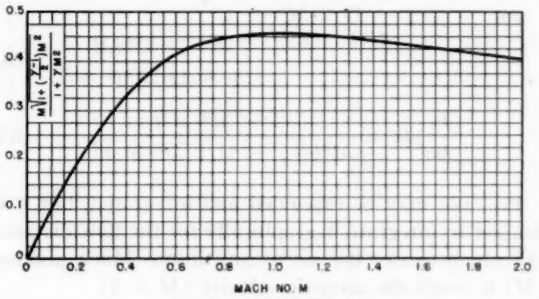

Fig. 5. Values of $\dfrac{M\sqrt{1 + [(\gamma - 1)/2]M^2}}{1 + \gamma M^2}$ versus M for constant area heating and cooling (Eq. (58)). Use: Find value of function for M_1. Multiply this by $\sqrt{T_{0_2}/T_{0_1}}$. Find M_2 for this value of function. Calculate P_1/P_2 from Eq. (55). $P_1/P_2 = (1 + \gamma M_2^2)/(1 + \gamma M_1^2)$.

It is of interest to note that heating means acceleration and cooling deceleration below the acoustic velocity, but in the superacoustic region heating produces a deceleration and a small amount produces a large change in Mach number. For example, it is only necessary to heat through a ratio of $T_{2_0}/T_{1_0} = (0.4566/0.4415)^2 = 1.07$ to reduce the Mach number from 1.4 to 1.0. For an initial temperature of 540°R. this would mean only a 37.8°F. rise. It would result in a pressure change from Eq. (55) of

$$\frac{P_1}{P_2} = \frac{1 + \gamma M_2^2}{1 + \gamma M_1^2} = \frac{1 + 1.395}{1 + 1.395(1.4)^2} = 0.64$$

Flow with Friction

The pressure change when friction is present is defined by Eq. (16) and, when it is combined with the gas equation

$$dP = -\frac{P}{gRT}\frac{fdx}{m}\frac{v^2}{2} - \frac{P}{gRT}vdv \tag{59}$$

For a constant area channel Eq. (9) becomes

$$(dP/P) + (dv/v) - (dT/T) = 0 \tag{60}$$

dP/P may be eliminated from Eqs. (59) and (60), or

$$\frac{dP}{P} = -\frac{fdx}{2m}\frac{\gamma v^2}{\gamma gRT} - \frac{\gamma v^2}{\gamma gRT}\frac{dv}{v} = \frac{dT}{T} - \frac{dv}{v} \quad (61)$$

This becomes

$$-\frac{f\gamma M^2}{2m}\,dx - \gamma M^2\frac{dv}{v} = \frac{dT}{T} - \frac{dv}{v} \quad (62)$$

If there is no change in total energy, dv/v and dT/T may be evaluated from Eqs. (28) and (29).

$$\frac{f\gamma M^2 dx}{2m} = \frac{dv}{v}(1 - \gamma M^2) - \frac{dT}{T} \quad (63)$$

This becomes

$$\frac{f\gamma M^2 dx}{2m} = \frac{(1 - \gamma M^2)(dM/M)}{[(\gamma - 1)/2]M^2 + 1} + \frac{(\gamma - 1)MdM}{[(\gamma - 1)/2]M^2 + 1} \quad (64)$$

$$\frac{f\gamma}{2m}\,dx = \frac{(1 - M^2)\,dM}{M^3\{[(\gamma - 1)/2]M^2 + 1\}} \quad (65)$$

Eq. (65) may be expanded and integrated, but it is simpler to integrate it graphically for the flow distance (x) which causes the air at any initial Mach number (M) to reach the acoustic velocity ($M = 1$).

The values for the integration of

$$\int_0^x \frac{\gamma f dx}{m} = \int_M^1 \frac{(1 - M^2)dM}{M^3\{1 + [(\gamma - 1)/2]M^2\}} \quad (66)$$

are shown on Fig. 6 and given in Table 1.

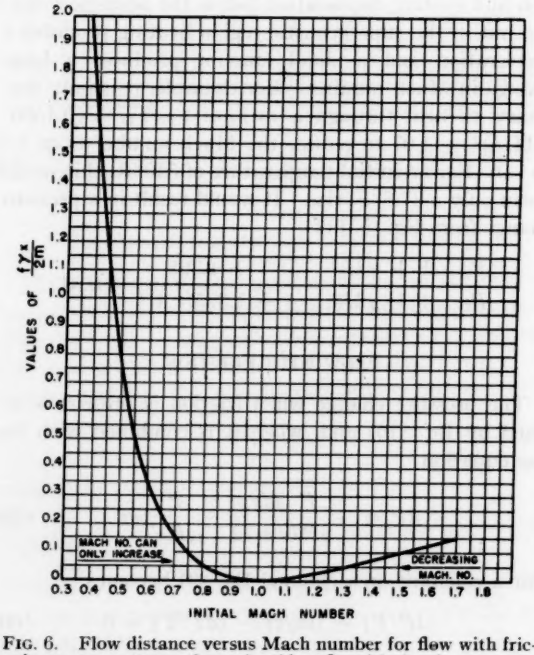

FIG. 6. Flow distance versus Mach number for flow with friction in a constant area channel. (f = flow friction factor, m = hydraulic radius, x = flow distance.)

TABLE 1

Values of the Integral

$$\frac{f\gamma x}{2m} = \int_M^1 \frac{(1 - M^2)dM}{M^3\{1 + [(\gamma - 1)/2]M^2\}}$$

M	$\frac{f\gamma x}{2m}$	M	$\frac{f\gamma x}{2m}$	M	$\frac{f\gamma x}{2m}$
0.350	2.4310	0.625	0.2804	1.15	0.0137
0.375	1.9861	0.650	0.2276	1.20	0.0228
0.400	1.6298	0.675	0.1831	1.25	0.0333
0.425	1.3433	0.700	0.1456	1.30	0.0447
0.450	1.1096	0.750	0.0891	1.35	0.0566
0.475	0.9186	0.800	0.0507	1.40	0.0691
0.500	0.7508	0.850	0.0254	1.45	0.0819
0.525	0.6204	0.90	0.01014	1.50	0.0946
0.550	0.5116	0.95	0.0023	1.55	0.1074
0.575	0.4204	1.0	0.0	1.60	0.1202
0.600	0.3441	1.05	0.0019	1.65	0.1330
		1.10	0.0066	1.70	0.1453

At $M_1 = 0.7$, $f\gamma x_1/2m = 0.1456$, and at $M_2 = 0.9$, $f\gamma x_2/2m = 0.01014$. Thus for friction to raise the Mach number from 0.7 to 0.9 would require a distance.

$$x_1 - x_2 = (2m/f\gamma)(0.1456 - 0.01014)$$

The units of x will be the units used for hydraulic radius (m).

The friction factor (f) is a function of Reynolds number and values are given up to extremely high Reynolds and Mach numbers in *N.A.C.A. T.M. No. 844*. Most of the cases of interest here are at Reynolds number between 250,000 and 600,000 where (f) does not vary much from 0.005.

Test of a $^1/_2$ in. by $^5/_{16}$ in. channel check calculations based on $f = 0.005$ to the effect that a 3.5-in. length raises the Mach number from 0.725 to unity and that only a 0.25-in. length is required to raise the Mach number from 0.92 to the acoustic.

Friction raises the Mach number with falling pressure below the acoustic but lowers the Mach number with rising pressure for a superacoustic stream. The pressure change is found from the Fanno Eq. (48) as,

$$P_1M_1\sqrt{1 + \frac{(\gamma - 1)}{2}M_1^2} = P_2M_2\sqrt{1 + \frac{(\gamma - 1)}{2}M_2^2} \quad (67)$$

Since the pressure loss due to friction is

$$dP = (\rho f dx/m)(v^2/2) \quad (68)$$

the friction work in B.t.u. per lb. is VdP/J.

This much energy goes from controlled to random molecular energy and causes an entropy change given by

$$dS = (VdP/TJ) = (\rho f dx/m)(v^2/2)(V/TJ) \quad (69)$$

but $\rho V = 1/g$; so, using Eq. (10)

$$dS = \frac{R\gamma f dx}{J2m}\frac{v^2}{\gamma gRT} = \frac{R}{J}M^2\frac{fdx\gamma}{2m} \quad (70)$$

Using Eq. (65),

$$dS = \frac{R}{J} M^2 \frac{(1 - M^2)dM}{M^2\{[(\gamma - 1)/2]M^2 + 1\}} \quad (71)$$

or

$$\frac{dS}{dM} = \frac{R}{J} \frac{(1 - M^2)}{M\{[(\gamma - 1)/2]M^2 + 1\}} \quad (72)$$

The entropy (S) is a maximum when

$$dS/dM = 0 \text{ or } M = 1 \quad (73)$$

This shows why a pure friction process will always cause the airflow to approach the acoustic, since that is the condition of maximum entropy.

Friction in Diffusers and Nozzles

For the case of friction in diffusers or nozzles that diverge or converge, (dA/A) of Eq. (9) is present and Eq. (61) becomes

$$\frac{dP}{P} = -\frac{f\gamma M^2}{2m} dx - \gamma M^2 \frac{dv}{v} = \frac{dT}{T} - \frac{dv}{v} - \frac{dA}{A} \quad (74)$$

from Eq. (28)

$$dv/v = (dM/M)/\{[(\gamma - 1)/2]M^2 + 1\} \quad (75)$$

and from Eq. (29)

$$dT/T = -(\gamma - 1)MdM/\{[(\gamma - 1)/2]M^2 + 1\} \quad (76)$$

and from Eq. (7)

$$dT/T = -(\gamma - 1)M^2(dv/v) \quad (77)$$

Combining Eqs. (74) and (77)

$$\frac{f\gamma M^2}{2m} dx = -\gamma M^2 \frac{dv}{v} + (\gamma - 1) M^2 \frac{dv}{v} + \frac{dv}{v} + \frac{dA}{A} \quad (78)$$

$$f\gamma M^2/2m = (1 - M^2)(1/v)(dv/dx) + (1/A)(dA/dx) \quad (79)$$

or

$$\frac{dv}{dx} = v\left[\frac{(f\gamma M^2/2m) - (1/A)(dA/dx)}{1 - M^2}\right] \quad (80)$$

In Eq. (80) the velocity gradient (dv/dx) is expressed in terms of the rate of divergence [$(1/A)(dA/dx)$], the friction ($f\gamma M^2/2m$), and the Mach number (M). For the parallel wall or constant area case previously considered, dA is zero, and the velocity gradient is positive for $M < 1$ and negative for $M > 1$.

For the ideal diffuser or nozzle ($f = 0$) and below the acoustic, a positive (dA/dx) or divergence gives a negative (dv/dx) or a diffusion. A convergence or ($-dA/dx$) represents an acceleration. Above the acoustic ($M > 1$), a plus (dA/dx) or divergence gives an acceleration and a minus (dA/dx) represents deceleration.

When both friction and area change are present, there are four possible cases.

Subacoustic Nozzles

For this case dA/dx is negative, and both friction and convergence act together to produce a positive velocity gradient that gets extremely large when (v) is large, A is small, and M is near unity.

Subacoustic Diffusers

A divergence or positive (dA/dx) tends to produce a minus (dv/dx) or a deceleration, but the effect of friction is contrary to this, tending to accelerate. Diffusion would cease when

$$f\gamma M^2/2m = (1/A)(dA/dx) \quad (81)$$

for a conical diffuser $A = \pi r^2$.

$$m = \frac{\pi r^2}{2\pi r} \text{ and } \frac{dA}{dx} = \frac{dA}{dr}\frac{dr}{dx} = 2\pi r \frac{dr}{dx}$$

This gives

$$\frac{dr}{dx} = \text{tangent of the wall angle} = \frac{f\gamma M^2}{2} \quad (82)$$

Superacoustic Nozzles

A divergence when $M > 1$ produces acceleration, while friction tends to decelerate, so such a nozzle would be subject to the limitations of Eq. (82).

Superacoustic Diffusers

For this case a minus (dA/dx) and friction both produce deceleration when $M > 1.0$. In fact, friction alone is an efficient superacoustic diffuser at velocities less than $M = 1.3$.

Diffuser Efficiency

The purpose of a nozzle is to change thermal energy into directed kinetic energy and its efficiency is usually defined as the kinetic energy change produced divided by the kinetic energy increase available with a reversible expansion between the same pressures.

Since the purpose of a diffuser is to produce a pressure rise starting with a given initial kinetic energy, it is apparent that the efficiency concepts used for nozzles cannot be applied without modification. Eq. (24) shows that the ideal pressure ratio available may be completely defined by stating the Mach number, and this Mach number can be readily found from Eq. (47) and Fig. 4.

If a diffuser is charged with the complete diffusion pressure ratio of Eq. (24), the air would have to be brought completely to rest to realize this, even with reversible flow, so this is not a logical basis. It seems better to charge the diffuser with the ideal pressure

rise and energy conversion of a reversible diffusion between the initial and final Mach numbers of the actual diffuser. This would lead to the definition of the *pressure rise ratio* as the ratio of the actual pressure rise divided by the reversible pressure rise available between the same Mach numbers.

This results in a useful concept for reporting test results and working out new designs. Suppose, for example, it is necessary to design a diffuser to reduce air from 0.88 Mach number to 0.30 Mach number and the diffuser is of a type for which a pressure rise ratio of 0.70 could be expected. From Fig. 2 the ideal pressure ratio is 1.652/1.065 = 1.55. The actual pressure rise would be (0.70)(0.55) = 0.385 and the actual pressure ratio would be 1.385 instead of the ideal 1.55.

From Fig. 3 the ideal area ratio is 2.05/1.013 = 2.02. Since the ideal and actual diffusers will have the same discharge Mach number, their discharge velocities and static temperatures must be the same. From the flow Eq. (8) and the gas Eq. (3), PvA/gRT = Constant. This means that the discharge areas must vary inversely as the pressure ratios, so the actual diffuser must have an area ratio of (2.02)(1.55/1.385) = 2.26.

The *energy efficiency* of a diffuser should measure the effects of friction and turbulence directly, and this may be done by finding the entropy increase caused by friction.

From Eqs. (75), (76), and (78)

$$\frac{f\gamma M^2 dx}{2m} = \frac{(1-\gamma M^2)(dM/M)}{[(\gamma-1)/2]M^2+1} + \frac{(\gamma-1)MdM}{[(\gamma-1)/2]M^2+1} + \frac{dA}{A} \quad (84)$$

or

$$\frac{f\gamma dx}{2m} = \frac{(1-M^2)dM}{M^3\{[(\gamma-1)/2]M^2+1\}} + \frac{1}{M^2}\frac{dA}{A} \quad (85)$$

From Eqs. (85) and (70)

$$dS = \frac{R}{J}M^2\frac{f dx\gamma}{2m} = \frac{R}{J}\frac{(1-M^2)dM}{M\{[(\gamma-1)/2]M^2+1\}} + \frac{R}{J}\frac{dA}{A} \quad (86)$$

Eq. (32) expresses

$$\frac{R}{J}\frac{(1-M^2)dM}{M\{[(\gamma-1)/2]M^2+1\}}$$

in terms of the ideal area ratio to produce a Mach number change, so using (a) for the area of the ideal diffuser and (A) for the actual one, the entropy increase caused by friction may be expressed as

$$dS = -(R/J)(da/a) + (R/J)(dA/A) \quad (87)$$

or

$$\int_{S_0}^{S} dS = -(R/J)\int_{a_0}^{a}(da/a) + (R/J)\int_{A_0}^{A}(dA/A) \quad (88)$$

or

$$S - S_0 = (R/J)\log_e[(A/A_0)/(a/a_0)] \quad (89)$$

where (A/A_0) is the actual area ratio required to produce a given Mach number change and (a/a_0) is the area ratio required for the same change in a reversible diffuser.

The kinetic energy per pound of air at any Mach number from Eq. (19) is

$$\frac{v^2}{2Jg} = \frac{M^2\gamma gRT_0}{2Jg\{1+[(\gamma-1)/2]M^2\}} \quad (90)$$

The change in kinetic energy between M_0 and M is

$$\frac{v_0^2}{2Jg} - \frac{v^2}{2Jg} = \frac{M_0^2\gamma gRT_0}{2Jg\{1+[(\gamma-1)/2]M_0^2\}} - \frac{M^2\gamma gRT_0}{2Jg\{1+[(\gamma-1)/2]M^2\}} \quad (91)$$

The increase in unavailable energy caused by friction and turbulence measured at the total temperature of the air when it is brought to rest is

$$T_0(S-S_0) = \frac{T_0R}{J}\log_e\left[\frac{(A/A_0)}{a/a_0}\right] \quad (92)$$

The energy efficiency is: efficiency = change in kinetic

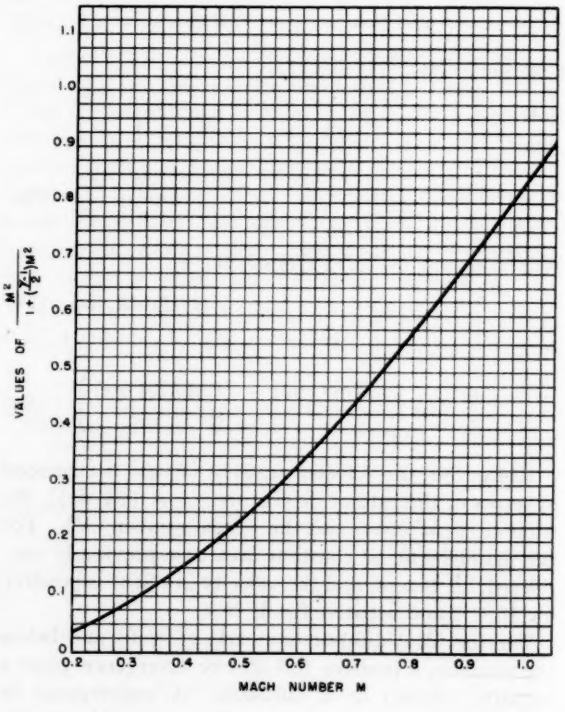

FIG. 7. Values of $\frac{M^2}{1+[(\gamma-1)/2]M^2}$ versus M for Eq. (94)

energy − increase in unavailable energy ÷ change in kinetic energy.

$$\text{efficiency} = 1 - \frac{(T_0R/J)\log_e[(A/A_0)/(a/a_0)]}{\frac{\gamma RT_0}{2J}\left\{\frac{M_0^2}{1+[(\gamma-1)/2]M_0^2} - \frac{M^2}{1+[(\gamma-1)/2]M^2}\right\}} \tag{93}$$

$$\text{efficiency} = 1 - \frac{(2/\gamma)\log_e[(A/A_0)/(a/a_0)]}{\frac{M_0^2}{1+[(\gamma-1)/2]M_0^2} - \frac{M^2}{1+[(\gamma-1)/2]M^2}} \tag{94}$$

Fig. 7 of $M^2/\{1-[(\gamma-1)/2]M^2\}$ plotted versus M is convenient for solving Eq. (94).

The calculations for diffuser efficiency may be illustrated by a test point for a small diffuser with an entrance area $A_0 = 0.1841$ sq.in. and a discharge area $A = 0.2752$ or an $A/A_0 = 1.49$. When tested with a flow, $W = 0.0763$ lb. per sec., the initial static pressure was 20.43 in. of mercury absolute, and the discharge pressure was 29.27 in., with a total air temperature $T_0 = 540°$R.

$$\frac{W\sqrt{T_0}}{P_0A_0} = \frac{0.0763\sqrt{540}}{(20.43/29.92)\ (14.7)\ (0.1841)} =$$

$$0.957 \text{ and } \frac{W\sqrt{T_0}}{PA} = 0.447$$

From Fig. 4, $M_0 = 0.960$ and $M = 0.472$. From Fig. 2 the ideal pressure ratio for this Mach number change is: ideal $P/P_0 = 1.81/1.164 = 1.555$; test $P/P_0 = 29.27/20.43 = 1.43$. This gives a pressure rise ratio of $0.43/0.555 = 0.785$.

Using Fig. 3, the ideal area ratio is

$$a/a_0 = 1.39/1.002 = 1.389$$

Using Fig. 7 and Eq. (94),

$$\text{energy efficiency} = 1 - \frac{(2/1.395)\log_e(1.49/1.389)}{0.785 - 0.213} = 0.821$$

Fig. 8 and Table 2 show typical test results for small diffusers, and it may be seen that the energy efficiency is consistently higher than the pressure rise ratio.

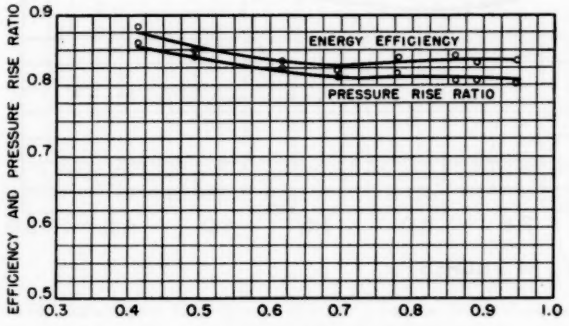

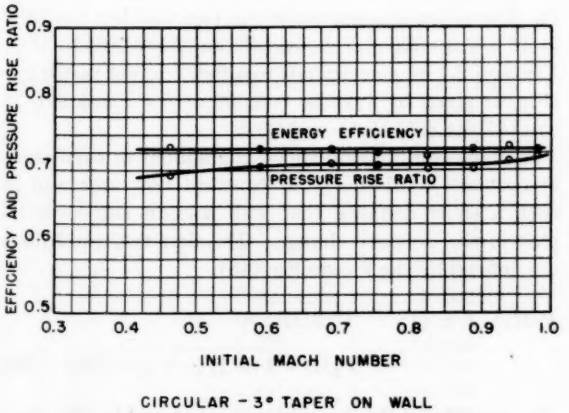

FIG. 8. Diffuser test data.

FLOW THROUGH PLANE COMPRESSION SHOCKS

When air is flowing at a velocity below the acoustic ($M < 1$), a pressure wave that moves at the acoustic velocity can travel upstream. In this way any ob-

TABLE 2

M_0	M	P/P_0 Test	P/P_0 Ideal	Pressure Rise Ratio	Ideal a/a_0	Efficiency
Rectangular Diffuser Test Data—1½° Taper on Each Wall: Throat, 0.50" by 0.376"; Discharge, 0.625" by 0.505", 2.40" Long; Area Ratio, 1.712						
0.413	0.222	1.074	1.086	0.86	1.695	0.882
0.492	0.263	1.105	1.124	0.840	1.681	0.855
0.619	0.321	1.170	1.205	0.829	1.660	0.83
0.695	0.342	1.221	1.276	0.81	1.640	0.82
0.78	0.367	1.293	1.360	0.814	1.630	0.837
0.859	0.386	1.373	1.460	0.811	1.612	0.840
0.888	0.392	1.405	1.501	0.806	1.602	0.833
0.946	0.401	1.476	1.591	0.805	1.585	0.832
Circular Diffuser Test Data—3° Taper on Each Wall; Throat, 0.1841 Sq.In.; Discharge, 0.2752 Sq.In. 1" Long; Area Ratio, 1.495						
0.464	0.299	1.0627	1.094	0.693	1.46	0.73
0.59	0.359	1.1115	1.1581	0.705	1.44	0.73
0.69	0.410	1.1635	1.230	0.710	1.42	0.727
0.755	0.438	1.197	1.279	0.706	1.40	0.727
0.825	0.463	1.245	1.349	0.702	1.38	0.720
0.89	0.483	1.301	1.427	0.706	1.365	0.73
0.94	0.492	1.353	1.496	0.712	1.351	0.730
0.98	0.50	1.402	1.560	0.718	1.340	0.726

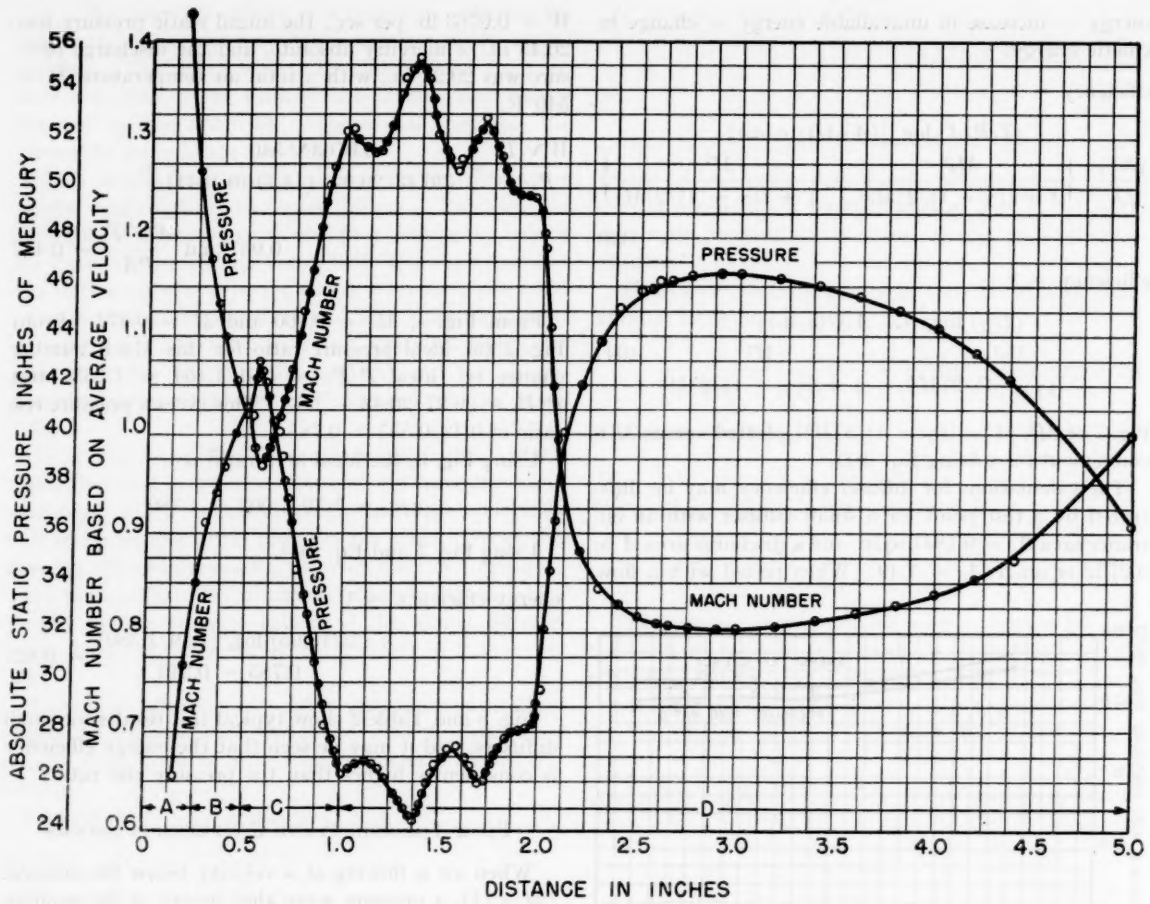

FIG. 9. Plane compression shock in a tube. Flow, 0.1832 lb. per sec.; initial pressure, 84.31 in. Abs.; total temperature, 80.5° F. Static pressures from 0.11-in. diameter traversing tube moved along center were checked by wall taps. *A*, rounded approach; *B*, parallel 0.525-in. diameter; *C*, divergence to 0.565-in. diameter; *D*, parallel 0.565-in. diameter.

struction or restriction in a passage can cause the entering flow to adjust to fit it. However, when the airflow is superacoustic ($M > 1$), a pressure wave cannot travel against the flow and the air upstream cannot be warned of trouble ahead. Each particle of air must discover the obstruction for itself.

Such a situation is illustrated by the data plotted in Fig. 9. The air left the parallel portion of the nozzle throat at a distance of 0.50 in., with a velocity slightly above the acoustic. For the next 0.05 in. it attempted to diffuse but later used the divergence to accelerate to 1.31 Mach number at 1.0 in. In the next inch, under the influence of friction and angle shocks from the walls, the Mach number dropped to 1.245, and at that point it still had 3 in. to flow to the end of the tube.

From Fig. 5 the value of $f\gamma x/2m$ for $M = 1.245$ air to reach the acoustic by friction is 0.0323. For $m = 0.565/4 = 0.1415$ in. and $f = 0.005$, only 1.31 in. of pipe is required to bring the flow to $M = 1$, below which it cannot drop by pure friction.

This situation brought about the *plane compression shock* at the 2-in. point at which the Mach number was reduced to 0.805 at 2.9 in. For the remaining 2.1 in. the flow again accelerated by friction and left the tube at $M = 1.0$. This acceleration from $M = 0.805$ to $M = 1$ in $x = 2.1$ in. corresponds to a flow friction factor (f) (Fig. 6) given by $f\gamma x/2m = 0.050$ or $f = (2)(0.050) \times (0.1415)/(1.395)\ (2.1) = 0.0048$.

A plane compression shock is assumed to take place at constant total energy at constant flow area and in such a short distance that wall friction can have no part in the pressure change. The first two conditions are defined by the Fanno Eq. (48),

$$P_1M_1\sqrt{1 + [(\gamma - 1)/2]M_1^2} = P_2M_2\sqrt{1 + [(\gamma - 1)/2]M_2^2} \quad (95)$$

The second and third conditions are stated by the Rayleigh Eq. (55),

$$P_1/P_2 = (1 + \gamma M_2^2)/(1 + \gamma M_1^2) \quad (96)$$

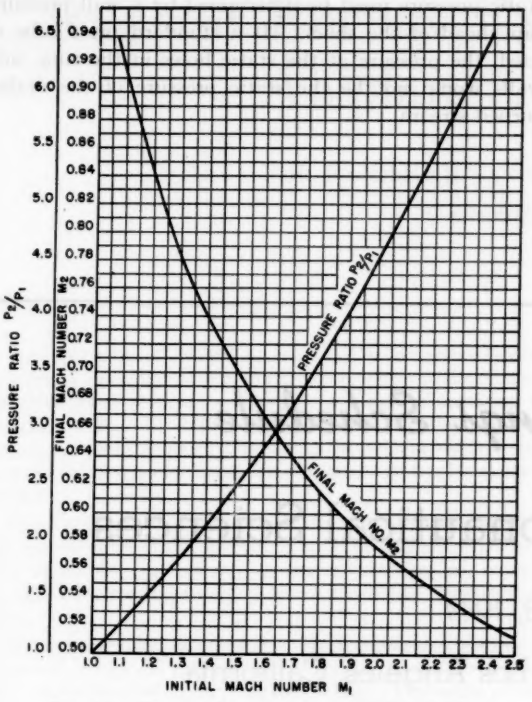

FIG. 10. Changes in a plane compression shock.

If Eqs. (95) and (96) are solved for the relationship between M_1 ahead of the shock and M_2 after the shock, the result is

$$\frac{1 + \gamma M_1^2}{M_1\sqrt{M_1^2 + [2/(\gamma - 1)]}} = \frac{1 + \gamma M_2^2}{M_2\sqrt{M_2^2 + [2/(\gamma - 1)]}} \tag{97}$$

Table 3 and Fig. 10 show the solution of Eqs. (96) and (97) for the theoretical plane shock. The shock of Fig. 9 started at $M_1 = 1.245$ and $P_1 = 28.0$ in. of mercury and terminated at $M_2 = 0.805$ and $P_2 = 46.5$, giving a pressure ratio of $P_2/P_1 = 1.66$. Using Fig. 10, such a shock should terminate at $M_2 = 0.81$ and yield a pressure ratio $P_2/P_1 = 1.65$. This is typical of the check between theory and test for plane compression shocks.

TABLE 3

Plane Compression Shocks—Eqs. (96) and (97)

Initial Mach No. M_1	Final Mach No. M_2	Pressure Ratio P_2/P_1
1.0	1.00	1.000
1.1	0.912	1.246
1.2	0.842	1.520
1.3	0.779	1.824
1.4	0.739	2.120
1.5	0.701	2.455
1.6	0.668	2.820
1.7	0.640	3.200
1.8	0.616	3.604
1.9	0.595	4.043
2.0	0.577	4.500
2.1	0.561	4.970
2.2	0.546	5.480
2.3	0.534	6.000
2.4	0.522	6.550
2.5	0.512	7.400

The location of a compression shock in a passage and the Mach number at which it is initiated in any case depend on the initial Mach number, the pipe length, and the back pressure, but for a given set of conditions it will always occur in the same way.

If an impact tube is placed in an air stream flowing below sound velocity, the ratio of total or impact absolute pressure to the static pressure at that point is given by the reversible compression of Eq. (25) and Fig. 2. However, when the flow is superacoustic, a plane shock bow forms ahead of the impact tube, and in that shock the pressure rise and Mach number change of Fig. 10 occur.

When the air is then brought to rest reversibly at the stagnation point at the impact tube nose, the total pressure rise realized is not the reversible value from Fig. 2. It would be, instead, the product of the shock pressure ratio and the reversible pressure ratio to bring air at the resulting Mach number to rest.

For example, for an initial Mach number of 2.0, the shock would produce a pressure ratio of 4.50 and reduce the Mach number to 0.577. When air at this Mach number (0.577) is brought to rest reversibly, the additional pressure ratio would be 1.252, giving a total

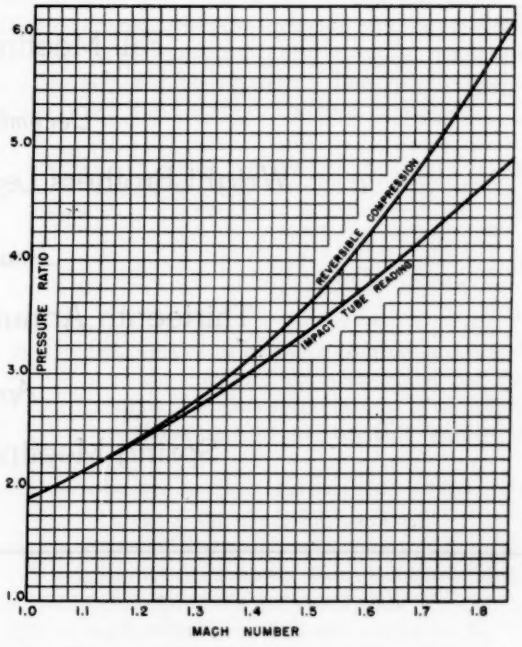

FIG. 11. Theoretical effect of compression shock on impact tube readings.

pressure ratio of (1.252)(4.50) or 5.65 instead of the ratio of 7.90 that would result from a reversible compression.

Fig. 11 shows this impact tube correction for various Mach numbers, and it should be remembered that the static pressure must be determined by a wall pressure tap ahead of the shock. If a standard pitot tube is used, the pressure at the static holes in the tube side walls would not be the static pressure of the undisturbed stream.

National Meetings Schedule

Institute of the Aeronautical Sciences

July 27–28, 1944

Summer Annual Meeting, Los Angeles, California

September 22, 1944

Air Transport Meeting, Washington, D.C.

November 9–10, 1944

Fall Meeting, Dayton, Ohio

December 17, 1944

Wright Brothers Lecture, Washington, D.C.

January, 1945

Thirteenth Annual Meeting, New York

April, 1945

Spring Meeting, Detroit, Michigan

Radiant Energy Exchange as a Factor in Airplane Cabin Heating

B. F. RABER* AND F. W. HUTCHINSON†
University of California

ABSTRACT

Accepted ideas of comfort, as evidenced in convective heating systems of conventional design, are not applicable to the problem of establishing occupant comfort in an airplane operating at great elevation. By setting up a heat balance on the occupant, an approximate "comfort equation" is established which is suggested as a criterion for the design of heating systems for airplane cabins.

Panel heating is discussed as an alternative method of meeting the special problems of aircraft heating design, and equations are developed for calculating the interception of radiant energy, by an occupant, from panels located in various positions.

Solution of the fundamental radiant exchange equation is discussed in terms of uniformity of heating effect and compensation for extremes of "spot" surface cooling. The intent of the paper is analytical rather than descriptive, but sufficient equations and references are given to permit the designer to apply the radiant exchange method to practical aircraft heating problems.

INTRODUCTION

THE PROBLEM OF ESTABLISHING a cabin environment conducive to effective operation by the personnel is unusually difficult in military aircraft. Weight and space limitations, plus the need of maintaining a high degree of accessibility, restrict the use of insulating materials, while the high altitudes at which the planes operate result both in a large heating load and in extraordinarily great temperature drops from the inside air to the uninsulated and exposed interior surfaces. This condition is intensified because of the large external film coefficient of heat transfer and also because of the necessary use of metallic walls having low thermal resistance.

For the above reasons the cabin of a military airplane requires provisions for either offsetting or preventing the large radiant energy loss that would normally occur from the occupants to the cold walls. In the sections that follow, three methods of attacking this problem will be considered, and the fundamental criteria of effective heating design will be re-examined in terms of the special conditions that exist in the cabin of an airplane.

Presented at the Airplane Design Session, Twelfth Annual, Meeting, I.A.S., New York, January 25–27, 1944.

* Professor of Mechanical Engineering and Chairman of the Department of Mechanical Engineering.

† Assistant Professor of Mechanical Engineering.

EQUATIONS FOR RADIANT ENERGY EXCHANGE

In any environment for which continued healthy existence is possible, a state of equilibrium is reached whereby the occupant achieves a fixed and constant loss of energy by radiation to the enclosing surfaces. Corresponding to any particular value of this radiant loss there is—for a given state of physical activity—only a narrow range of air temperatures in which the realization of comfort is possible. Thus, as the net radiant loss increases, the design value of the inside air temperature must likewise increase; the popular concept of comfort as being associated with an air temperature of 70°F. breaks down entirely when the heated space is one—as an airplane cabin—where the air and surface temperatures have widely different values. The importance of this fact cannot be overemphasized, since failure to establish a design air temperature in terms of the existing radiant exchange conditions may result in an inadequate or wholly unacceptable heating system.

The first step necessary in the consideration of the radiant exchange factor is to establish means for precisely evaluating the exchange rate and for calculating the effect on net radiant loss of a change in temperature of a surface of limited extent. This can be done by means of the fundamental radiation equation:

$$q_R = \sum_{n=1}^{n=n} (F_{e_n} \sigma A_n) \left[\frac{1}{A_n} \int_{A_n} \int_{A_0} \frac{\cos \phi_n \cos \phi_0 \, dA_n dA_0}{\pi r_n^2} \right] \times \left[\left(\frac{T_0}{100} \right)^4 - \left(\frac{T_n}{100} \right)^4 \right] \quad (1)$$

where

q_R = net energy loss by radiation from an occupant to the enclosing surfaces, B.t.u. per hour, when the enclosure consists of n different surfaces each of area A_n and temperature T_n

A_0 = effective area of the occupant (different for each of the enclosing surfaces)

σ = Stefan-Boltzman constant = 0.172

r_n = distance from center of area A_n to midpoint of occupant's projected area

ϕ_n = angle between r_n and the normal to A_n

ϕ_0 = angle between r_n and the normal to A_0

F_{e_n} = emissivity factor of surfaces A_n and A_0

Evaluation of the exchange rate by direct use of the above equation would be tedious and impractical. Further, the nonmathematical shape of the human body introduces a complication into the double integral which makes an analytical solution practically impossible. Fortunately, however, the equation can be greatly simplified and nonanalytical means can be used for evaluation of the double integral.

The first bracketted term on the right side of the equation is defined as the shape factor, F_{0n}, of the occupant with respect to radiation from surface A_n and is numerically equal to the fraction of total energy emitted by A_n which strikes the occupant (neglecting gaseous absorption). Experimental determinations of F_{0n} for many shapes and positions of ceiling and wall surfaces have been made in the laboratory and the data are available in the literature.[1] Except in unusual cases, all values of F_{0n} needed for any practical problem can be taken directly from the published values and computed from them or can be obtained by interpolation or extrapolation. For this reason, the F_{0n} term will not be further considered in this paper, assumption being that the designer will evaluate it numerically from the published curves and tables.

A further simplification of Eq. (1) is possible by defining an equivalent first power radiant transfer factor, h_R, by

$$h_R = \sigma[(T_0/100)^4 - (T_n/100)^4]/(t_0 - t_n) \qquad (2)$$

and noting that, over the temperature range likely to be of importance in comfort heating installations, the value of h_R does not greatly vary and can, with ±5 per cent accuracy, be taken as a constant at 1.03. Eq. (1) now reduces to the more acceptable form,

$$q_R = \sum_{n=1}^{n=n} 1.03\, F_{e_n} A_n F_{0_n}(t_0 - t_n) \qquad (3)$$

where t_0 and t_n are expressed in °F., t_0 being the average temperature of exposed surfaces (skin or clothing) of the occupant.

Exchange with a Homogeneous Receiver

A greatly simplified form of Eq. (3), which has two extensive fields of usefulness, is that in which the net exchange is to be evaluated only with respect to a single receiver. The entire problem of local cooling or local heating can frequently be treated as an application of the "single receiver" equation, while the problem of exchange in a uniform environment can be similarly treated. Consider, for example, an insulated airplane cabin in which an adequate convective heating system has been installed. If, now, the insulation is removed from one section of the cabin, the heat loss by radiation from the occupants will increase and, for equal comfort, a compensating rise in the air temperature is required. Neglecting the effect of the cold panel on the other surfaces of the enclosure, the change in radiant loss experienced by the occupant can be calculated by

$$\Delta q_R = 1.03 F_{e_u} A_u F_{0u}(t_{u1} - t_{u2}) \qquad (4)$$

where the subscript u denotes the uninsulated section of the cabin and subscripts 1 and 2 are for the temperatures of this section before and after removal of the insulation.

Having determined the increase in radiant loss, Δq_R, it is now necessary to calculate the change in air temperature needed to reduce the convective heat loss, Δq_c, by a like amount. To do this, Newton's Law of Cooling can be used:

$$\Delta q_c = h_c A_0(t_{a2} - t_{a1}) \qquad (5)$$

where subscript a denotes cabin air temperature and subscripts 1 and 2 indicate initial and final values of the air temperature. The surface of the average occupant, A_0, which is effective for convective heat transfer, is approximately 19.5 sq.ft. There remains then only the film transfer coefficient, h_c, as an unknown. To evaluate h_c it is sufficient to note that an average person, in a room with air and walls at a uniform 70°F., has been found to lose approximately 180 B.t.u. per hour by radiation and 120 B.t.u. per hour by convection; the equivalent transfer area of the average human body for radiation is approximately 15.5 sq.ft. in contrast to the 19.5 for convection.

For completely enclosing uniformly heated walls of fixed emissivity, the emissivity factor F_e is equal to unity and the average surface temperature of the occupant (exposed skin or clothing) can be calculated,

$$q_R = 180 = 1.03 \times 1 \times 15.5 \times 1\ (t_0 - 70)$$

giving $t_0 = 81.2$°F. The average convective film coefficient of heat transfer from occupant to room air is then obtained from

$$q_c = 120 = h_c \times 19.5\ (81.2 - 70)$$

giving $h_c = 0.55$. Thus, an increase in the air temperature of 1°F. is needed for each $0.55 \times 19.5 = 10.7$ B.t.u. increase in radiant loss, and the required temperature change needed to compensate for local cooling from a single receiver is (from Eq. (4)),

$$\Delta t_a = 0.096\, F_{e_u} A_u F_{0u}(t_{u1} - t_{u2}) \qquad (6)$$

The accuracy of Eq. (6) is, of course, limited by the experimental data and by the approximations involved in the determination of h_c.

An alternative method of compensating for local cooling is to provide a source of radiation sufficient to offset the effect of the receiver. For a source of known area and position Eq. (4) can be used to determine the necessary surface temperature. The effectiveness of a source depends largely on its position (which determines the shape factor). Improvement in this respect can sometimes be attained by using a small

inverted diffusing source backed by a parabolic spectral reflector; such a combination can increase the shape factor—and, hence, the effectiveness—by significant amounts.

Exchange with a Homogeneous Surround

A special and important case of the single receiver problem occurs in a cabin having uniform conductance. Complete realization of such a condition in practice is unlikely (because of windows, flooring, etc.), but this case does represent a limit that is frequently approached closely. Further, as will be seen, it is a starting point for analysis of the more common heterogeneous exchange problem.

The emissivity factor for a small body (the occupant) completely enclosed by a large body (the cabin) becomes equal to the emissivity of the occupant and, for practical computations, can be taken as unity. Since all radiant energy leaving the occupant is intercepted by the surround, the shape factor of the surround with respect to the occupant is also unity. Eq. (3) then reduces to

$$q_R = 1.03A_0(t_0 - t_s) = 1.03 \times 15.5(81.2 - t_s) = 16(81.2 - t_s) \quad (7)$$

where t_s is the surface temperature, °F., of the surround. Thus a 1°F. change in the temperature of the surround is responsible for a change of 16 B.t.u. in the net radiant energy loss from the occupant. Recalling that a 1°F. air temperature change alters the convective transfer by 10.7 B.t.u., it appears that each 1°F. variation in the temperature of the surround is equivalent to an opposite air temperature change of 1.5°F. This value is an approximation based on the assumptions already discussed plus the further implicit assumptions that the body (or clothing) surface temperature is constant (but not necessarily uniform) and that, for comfort, the sum of convective and radiant losses is constant. The latter assumption requires that the evaporative loss of about 100 B.t.u. per hour (for a sedentary adult) remain constant in the comfort region; experiment has shown that this is reasonably true.

The above relationship between Δt_a and Δt_s permits writing a "comfort equation," which must be satisfied if comfortable conditions are to be realized in a convective heated cabin. This equation is

$$t_a + 1.5t_s = 175 \quad (8)$$

and it can be used to establish a fundamental design equation from which the required air temperature in an enclosure with homogeneous surround can be readily calculated. By the resistance concept,

$$(t_a - t_s)/(t_a - t_d) = r_i/R = r_iU \quad (9)$$

where

t_d = design temperature of outside air
r_i = resistance of inside air film
R and U = overall resistance and overall coefficient, respectively, from inside to outside air

Then $t_s = t_a - r_iU(t_a - t_d) = (175 - t_a)/1.5$, giving $t_a(1 - r_iU + 0.67) = 116.5 - r_iUt_d$ or

$$t_a = (116.5 - r_iUt_d)/(1.67 - r_iU) \quad (10)$$

Example: Consider a cabin having an overall coefficient of 0.3 and an inside film coefficient of 1.5. Design outside temperature is 0°F. Calculate the value at which the inside air temperature must be maintained if comfort conditions equivalent to those in a cabin with air and walls at 70°F. are to exist.

$$t_a = \frac{116.5 - 0}{1.67 - (0.3/1.5)} = \frac{116.5}{1.47} = 79.5°\text{F.}$$

The Mean Radiant Temperature

As a desirable preliminary to the transition from homogeneous to heterogeneous systems, the concept of an equivalent homogeneous surround must be considered. For any complex surround the net rate of radiant exchange between occupant and surround can be calculated from Eq. (3), and this value then substituted into Eq. (7) permits determination of the temperature of a homogeneous surround for which the same exchange rate would occur. This *equivalent* surround temperature is defined as the mean radiant temperature, m.r.t.

As indicated by the definition and from a consideration of the terms of Eq. (3), the m.r.t. is a function not only of the temperature and area of each elementary homogeneous surface making up the heterogeneous surround but also both of the emissivity and the geometric position of each such surface. When correctly evaluated, the m.r.t. can be substituted for t_s in Eq. (8), and this equation can then be applied to any type of heating system. Frequently, however, there is need for an approximate method of calculating the m.r.t. without resort to the complexities of shape factor analysis. For this purpose the equation frequently used is,

$$\text{m.r.t.} = \sum A_n t_n / \sum A_n \quad (11)$$

Eq. (11) gives a result that may differ widely from the correct value and must, therefore, always be used with the greatest care. As an example of the possible discrepancy, consider a man standing in the center of a room in which the floor is uniformly heated and all wall and ceiling surfaces are at some other, but likewise uniform, temperature. In such a case all radiation that leaves the man but does not strike the floor must be received by the walls and ceiling. If all surfaces are considered to have unit emissivity, it is evident that the net radiant loss experienced by the man must be completely independent of the ceiling height. In consequence, the true m.r.t. of this system is also

independent of the ceiling height. But the value that would be obtained if Eq. (11) were used would obviously vary greatly, going from an amount approaching halfway between the wall and floor temperatures (for low ceiling) to a value equal to the wall temperature (for an infinite ceiling).

The above example becomes even more striking if the occupant is considered as standing in a fixed position with respect to a heated panel which is part of, but does not occupy, the entire floor. The same reasoning again applies, and the conclusion is that the true m.r.t. for this system is independent of both the size and shape of the room. Use of Eq. (11) could therefore lead to erroneous results.

For the reasons discussed above, the m.r.t. should always be calculated from the correct equation or, if conditions permit, determined experimentally. If it is to be determined by experiment, care must be exercised to assure that the recording element receives and integrates irradiation in the same way as would an occupant.

When the conditions of a design problem are such that the true m.r.t. cannot be used and some approximate method, as Eq. (11), is resorted to, the comfort equation can no longer be written as in Eq. (8) but must be expressed in the empirical form,

$$t_a + x(\text{m.r.t.}) = y \qquad (12)$$

where x and y are constants that fix both the slope of the comfort curve and the relationship between t_a and m.r.t. for standard conditions.

Returning to the example considered above and assuming that comfort was attained with an air temperature of 70°F. and a wall temperature of 50°F.: In order for this to be possible the heated panel would have to be at a temperature such that the true m.r.t. of the room would be 70°F. But the previous discussion established that the value of m.r.t. that would be obtained from Eq. (11) could be as low as the wall temperature; thus use of this equation might lead to the erroneous conclusion that comfort could be attained in a room with air at 70°F. and the surround at 50°F. Obviously, if the result obtained from Eq. (11) is to have any significance, it must be used in the comfort equation, Eq. (12), with values of x and y which compensate for the erroneous m.r.t.

The above condition is responsible, at least in part, for the diversity of opinion as to the relationship between a rise in m.r.t. and the associated change in t_a. When Eq. (11) is used, the number of degrees change in t_a needed to compensate for a 1°F. change in m.r.t. is by no means a constant but varies with the size and shape of the room and with the area, position, and temperature of the heating panel. Various investigators have found values of the air temperature change between 0.2° and 1.2°F. corresponding to a 1°F. m.r.t. change.

With respect to the above condition, the selection of wall, floor, or ceiling as a location for the heated surfaces will greatly alter the slope of the comfort curve. In an average size cabin, wall panels provide the steepest slope and ceiling panels the flattest. Experiences with actual installations soon provide the designer with a background of representative types that will permit him to estimate readily both the slope and the base point of a particular comfort curve corresponding to a given room shape and size and panel location. Thus, the alternatives are to calculate the true m.r.t. and use it in the general comfort equation or to calculate an approximate m.r.t. and use it in an empirical comfort equation the constants of which must be evaluated, from the designer's experience, for each different installation. The latter method is less difficult in airplane cabins than in other types of heating installations because of the greater degree of geometric similarity.

Exchange with a Heterogeneous Surround—Method

Panel Heating Systems

The general problem of setting up equations for evaluation of equilibrium conditions in an enclosure bounded by a heterogeneous surround is one that rarely occurs in practice except in the design of panel heating systems. Before proceeding with the analytic treatment of this case it is well to consider briefly the practical reasons that lead to the adoption of a panel-type heating installation and to investigate the special factors that make this type of system appear to be particularly attractive for use in some types of aircraft.

Basically, panel and convective heating systems differ more widely with respect to intention than they do with respect to result. The usual convective installation is designed to control the air temperature; such effect as it has on the m.r.t. is purely secondary and indirect. In such a system the m.r.t. must always be less than the air temperature and the value of the latter must therefore always be, for comfort, in excess of the 70° base value. In the limiting case, with perfectly insulating walls, a convective heating system would establish comfort with an air temperature equal to 70°F.

The objective of a panel, or radiant, heating system is to provide primary control of the m.r.t., raising it to a value such that comfort will be realized with an enclosure air temperature substantially less than 70°F. In the ideal case a panel that did not lose energy by convection could establish comfort in an enclosure with air at the outside temperature; this case would, however, be subject to the additional condition that the outside air temperature could not be so low as to have undesirable respiratory effects or an undue influence on the evaporative fraction of normal body heat loss.

In practice all heating panels dissipate a substantial fraction of their total energy loss by convection to the room air; further, a large portion of the energy initially emitted by the panel is later dissipated by convection from the nonheated interior surfaces of the enclosure. In consequence, all heating panels act as secondary convectors and have a definite effect on the air temperature. This fact limits the extent to which a depression of t_a below m.r.t. can be attained, but it is noteworthy that in any well-designed panel installation some depression can be realized. Thus, while all panel systems do provide a fairly large fraction of convective heating, they also permit maintaining comfort in an enclosure with the air temperature lower than would otherwise be necessary. The magnitude of the air temperature depression reflects the skill and ability of the designer to a great extent.

The advantages of lowered air temperature are both physiologic and economic. A greater feeling of "freshness" is universally associated with air at 65°F. than at 75°F. When radiant exchange is controlled so that such air can enter the respiratory tract, yet without the chilling effect associated with a 65°F. convective system, there is evidence that both psychologic and physiologic advantages may result. Similarly, breathing cooler air reduces the shock effect associated with entering or leaving a heated space.

Economically, reduced air temperature means a smaller ventilation heating cost and may permit reduction in the volume of outside air introduced and in the volume of recirculated air needed for the system. These latter items can be particularly significant in aircraft installations where the weight- and space-saving are so much to be desired. Furthermore, as already discussed, aircraft construction is frequently such that if radiant sources are not provided the cold panel effect of uninsulated sections will result in either discomfort or in an objectionably high air temperature.

An even more significant advantage of panels for aircraft cabins is in the excellent opportunity for use of local heating elements. Depending on the functions of the crew, heat can be provided from auxiliary radiant units at necessary stations but not elsewhere. As an extreme example of such "spot" heating, directed emitters can be used to supply energy to exposed armament and other mechanical parts which—while located in an ambient atmosphere of low temperature—must be prevented from freezing.

Autoradiant Panels

One method of reducing radiant energy loss from the occupants without provision of an emitting source is to provide an enclosure the inside surface of which has a low emissivity. This method is usually impractical in room heating because interreflections and reflections absorb the flux so that irradiation of the occupant is not much greater than it would be if the surfaces were perfect emitters.[2] In an airplane cabin, however, the greater relative size of the occupant with respect to the enclosure greatly increases the effectiveness of reflecting surfaces and may permit a substantial amount of autoradiation.

To consider the ideal case, an occupant of a cabin with perfectly reflecting walls would be unable to lose any energy by radiation as the flux would build up to a value such that he would be irradiated (with energy originally emitted by himself) at a rate equal to that at which he is emitting energy. Thus, conditions within the cabin would be the same as though the surround were a perfect emitter operating at a temperature equal to that of the occupant's clothing surface. Taking this surface temperature as 81.2°F. and making use of the comfort relationship previously established, it would appear that comfort could be attained in such a cabin with an air temperature of 53.2°F. and with walls at any temperature whatsoever. Laboratory tests[2] in a cabin 5 by 5 by 5 ft. with an interior surface emissivity of approximately 0.025 established comfort with air at 60°F. and walls at 57°F.

Aside from the possibility of developing effective autoirradiation, reflective surfaces of commercial emissivity are useful as covering for local cold spots and can also be used in developing reflectors for high emissivity heating sources.

Panel Performance

Since the objective of a panel system is to provide the largest practicable fraction of energy transfer by radiation, the panel should be located in a position for which the film transfer factor is a minimum. This condition dictates use of ceiling panels, as the convective fraction for horizontal, flush-mounted, ceiling units is 28 per cent as against 41 per cent for wall panels and 48 per cent for floor panels. However, the required area of heating surface is likely to be somewhat greater for ceiling panels because of their lesser shape factor with respect to the occupant, and this fact will in some cases control the selection and dictate the use of wall or floor elements.

The surface temperature is a design constant and can be varied over a wide range, but calculations[3] show that it does not materially affect the depression that is obtained from a given installation. This factor is, however, a vital one in terms of adequate distribution; surface temperatures of primary panels can rarely exceed 120°F.—except in extremely large enclosures—without constituting local heating sources for some positions of the occupants. When auxiliary spot-heating panels are used, the situation is reversed and it then becomes desirable to raise the surface temperature as a means of reducing panel area and thereby localizing, as much as possible, the zone of spot heating.

A semiradiant system, which is a compromise between radiant and convective systems, has been used in many forms in house heating and has also been used as the basis of a number of aircraft heating designs. By this method heated air is caused to flow through the annular space between the skin and the inside finishing material of the plane. After passing through this space the air is introduced directly into the cabin and allowed to escape through exit passages of the usual type. Calculation of the t_a depression for such a system is difficult, since the surface temperature varies along the path of airflow. Usually, however, such systems need not be precisely designed, since the panel effect is secondary and does not lead to a wide departure from the performance of a conventional hot air system.

When a full low temperature type of heating system is used, particular care is needed in distributing the heated surface so as to achieve reasonable uniformity of radiant exchange irrespective of the position of the occupant. Distribution analysis is fundamentally a problem in comparative shape factors and can in many cases be greatly simplified by interpolating between the standard cases that have been treated in the literature.

Exchange with a Heterogeneous Surround—Analysis

Rational Solution

Consider an airplane cabin that is to be heated by a panel of area A_p. All remaining surfaces of the cabin are unheated but come to equilibrium temperatures that are dependent on many factors. For a given ventilation rate of W lbs. per hour of outside air and for unheated inside surfaces of known areas A_1, A_2, $\ldots A_n$ at unknown equilibrium temperatures t_1, t_2, $\ldots t_n$, the equilibrium inside air and panel temperatures will be at unknown values t_a and t_p for any particular outside design air temperature, t_0. Thus, when equilibrium is reached, there will be $n + 2$ unknown temperatures in the cabin and a complete solution of the problem obviously will require $n + 2$ independent equations. But the comfort equation, Eq. (8), relates all $n + 2$ variables (since all n unheated surface temperatures and the panel temperature are implicitly included in the term t_s, which is the true mean radiant temperature). Thus, the comfort equation is itself one of the required $n + 2$ equations. The remaining $n + 1$ equations can be written as heat balances on the ventilation air and on each of the unheated enclosure surfaces.

Letting C_1, C_2, C_3, $\ldots C_n$ represent the conductances from each unheated inside surface to the outside air and, assuming that all unheated surfaces are at a lower temperature than the room air (an assumption which does not limit the validity of the result as it disproves itself, if incorrect, in the work), a heat balance can be written on area A_1 as follows:

$$\sum_{n=2}^{n=n} 1.03F_{e_n}A_1F_{n1}(t_n - t_1) + 1.03F_{e_p}A_1F_{p1}(t_p - t_1) + h_{c_1}A_1(t_a - t_1) = C_1A_1(t_1 - t_0)$$

or

$$\sum_{n=2}^{n=n} 1.03F_{e_n}F_{n_1}(t_n - t_1) + 1.03F_{e_p}F_{p1}(t_p - t_1) + h_{c_1}(t_a - t_1) = C_1(t_1 - t_0) \quad (13)$$

A similar equation can be established for any other unheated surface, A_m, where $1 < m < n$,

$$\sum_{n=1}^{n=(m-1)} 1.03F_{e_n}F_{nm}(t_n - t_m) + \sum_{n=(m+1)}^{n=n} 1.03F_{e_n}F_{n_m}(t_n - t_m) + 1.03F_{e_p}F_{pm}(t_p - t_m) + h_{c_m}(t_a - t_m) = C_m(t_m - t_0) \quad (14)$$

Thus, Eq. (14) provides the form for $n - 1$ heat balance equations.

The remaining equation needed for solution of the problem is the heat balance on ventilation air as it enters the cabin at t_0, gains heat from the panel, loses heat to the other surfaces, and leaves at t_a. This equation takes the form

$$h_{c_p}(t_p - t_a)A_p = \sum_{n=1}^{n=n} h_{c_n}(t_a - t_n)A_n + 0.24W(t_a - t_0) \quad (15)$$

By simultaneously solving the $n + 2$ equations, a complete determination is possible of temperature and energy distribution conditions throughout the enclosure. The adequacy of the solution depends primarily on the validity of the empirical comfort equation, while the accuracy of the solution is limited by failure to take into account reflections by probable error in some of the empirical constants which must be used, by departure of the unheated surfaces from the assumed condition of uniform surface temperature, and by difficulty in evaluating the shape factors for complex cases. Because of these many assumptions and inaccuracies of basic data and the time required for its application, the rational method finds only limited use in the solution of practical cabin-heating problems. Less accurate, but more rapid, methods are in greater favor.

As a precise design procedure, however, the rational method of analysis is invaluable because it gives results equal in accuracy to the available basic data and the necessary assumptions. When more accurate basic data are available and fewer assumptions need be made, the rational procedure will remain of value while many of the approximate methods may be abandoned. Even at present the extra time and effort required for a rational design is more than justified when—as in the case of an airplane cabin heating system—one design is to be applied to hundreds or thousands of standard installations.

Equivalent Conductance Solution

One approximation that avoids the use of shape factors and reduces the number of equations to be

solved is based on the concept of an ideal homogeneous surround (exclusive of the panel) having the same heat transfer characteristics as the actual heterogeneous enclosure. The equivalent conductance of the unheated surround is calculated from the equation

$$C_e = \sum_{n=1}^{n=n}(C_n A_n)/\sum A_n \qquad (16)$$

and the equivalent convective film transfer coefficient, h_{c_e} can likewise be calculated as a weighted average of coefficients for vertical and horizontal surfaces or—more commonly—can be assumed equal to 0.8 B.t.u. per hour sq.ft. °F. A complete solution of the problem is now possible in terms of these equations of which the empirical comfort Eq. (12) is the first. A second independent equation is obtained by setting up a heat balance on the equivalent unheated surround

$$h_R A_p\,(t_p - t_e) + hc_e A_e(t_a - t_e) = C_e A_e(t_e - t_0)$$

or

$$t_e = \frac{h_R A_p t_p + hc_e A_e t_a + C_e A_e t_0}{h_R A_p + hc_e A_e + C_e A_e} \qquad (17)$$

The third independent equation can be established by writing a heat balance on the ventilation air,

$$hc_p(t_p - t_a)A_p = hc_e(t_a - t_e)A_e + 0.24W(t_a - t_0)$$

or

$$t_e = \frac{hc_e A_e t_a + 0.24W(t_a - t_0) - hc_e A_p(t_p - t_a)}{hc_e A_e} \qquad (18)$$

Now, substituting in Eq. (12), the approximate m.r.t. defined by Eq. (11) gives the empirical comfort equation

$$t_a + \left(\frac{xA_p}{A_p + A_e}\right)t_p + \left(\frac{xA_e}{A_p + A_e}\right)t_e = y$$

or

$$t_e = \left[y - t_a - \left(\frac{xA_p}{A_p + A_e}\right)\right] \Big/ \frac{xA_e}{A_p + A_e} \qquad (19)$$

Equating the two heat balance equations, Eqs. (17) and (18), eliminates t_e and gives an equation in terms of the two unknowns t_a and t_p which reflects the heat transfer characteristics of the room

$$\frac{h_R A_p t_p + hc_p A_e t_a + C_e A_e t_0}{h_R A_p + hc_e A_e + C_e A_e} = \frac{hc_e A_e t_a + 0.24W(t_a - t_0) - hc_p A_p(t_p - t_a)}{hc_e A_e} \qquad (20)$$

Eliminating t_e between Eqs. (18) and (19) gives another equation relating the two unknowns t_a and t_p, but this time one that implicitly takes account of the relationship needed for physiologic comfort,

$$\frac{xA_e}{A_p + A_e}\left[hc_e A_e t_a + 0.24W(t_a - t_0) - hc_p A_p(t_p - t_a)\right] = hc_e A_e\left[y - t_a - \left(\frac{xA_p}{A_p + A_e}\right)\right] \qquad (21)$$

For any given design problem Eq. (20) simplifies to the form

$$at_p + bt_a + c = 0 \qquad (20a)$$

and Eq. (21) reduces to

$$dt_p + et_a + f = 0 \qquad (21a)$$

Eqs. (20a) and (21a) can be solved simultaneously or graphically. The graphic solution is particularly effective because it clearly shows the limitations introduced into the design because of the necessity of satisfying the comfort equation. In such a graphic solution the curve of Eq. (20a) shows the relationship between t_a and t_p which must exist because of the physical characteristics of the enclosure, while the curve of Eq. (21a) illustrates the necessary t_a vs. t_p relationship that is obligatory if the occupant is to experience a satisfactory degree of comfort. Since the point of intersection of the two curves will be different for every value of the outside air temperature, the conclusion is evident that the air temperature in a panel heated space cannot be held at a constant value but *must*—for optimum comfort—be allowed to vary as a function of the heating load.

The principal limitation of the equivalent conductance method arises from the use of the fallacious m.r.t. of Eq. (11). If sufficient data from comparable installations are available, this difficulty can be corrected for in the evaluation of constants x and y of the comfort equation; lacking such data, assumed values of x and y are necessary and the error introduced into the results may be important. The equivalent conductance method likewise does not admit of determination of surface temperatures of the individual areas making up the unheated surround; in this respect it must also be used with checks and reservations, since undetected regions of severe local cooling may appear in the final design. For all such difficulties the only adequate procedure is to analyze the design in terms of shape factors by the more complex rational method.

Conclusion

When subject to the low temperatures associated with high level operation, uninsulated—or poorly insulated—airplane cabins constitute an unusual type of comfort heating problem because of the greatly increased loss of energy from the occupants by radiation to the cold inside walls. This condition requires adjustment in the value of the inside design air temperature or provision of auxiliary local radiant heating units to compensate for the excess radiant loss.

Equations have been developed for estimating the rise in design air temperature for convective heating systems and for calculating the size or surface temperature of radiant spot heaters for use as local auxiliaries in a hot air system. Two methods of analysis have been developed for designing a heated panel-type radiant cabin heating system for use in place of the standard convective heating system; the rational method is the more accurate but is relatively complex and time-consuming, while the approximate method requires a more extensive background of experience on the part of the designer.

In many respects panel heating offers attractive advantages as a method of cabin heating, but, even if it is not used as such, the aeronautical heating engineer is required—by the conditions of his problem—to make use of the basic equations for exchange of radiant energy.

References

[1] Raber, B. F., and Hutchinson, F. W., *Optimum Surface Distribution in Panel Heating and Cooling Systems*, Transactions, A.S.H.V.E., Vol. 50, 1944.

[2] Raber, B. F., and Hutchinson, F. W., *Panel Heating and Cooling Performance Studies*, Transactions, A.S.H.V.E., Vol. 48, 1942.

[3] Raber, B. F., and Hutchinson, F. W., *Trend Curves for Estimating Performance of Panel Heating Systems*, Transactions, A.S.H.V.E., Vol. 48, 1942.

(*Continued from page 204*)

Perhaps the most interesting feature of the curves is the fact that for all values of absorber damping there is minimum relative motion at optimum tuning and that at optimum tuning there is practically no difference in the magnitude of relative motion, regardless of absorber damping. The former conclusion is reasonable because the excitation of the absorber system is the main mass amplitude and, by definition, this is a minimum at optimum tuning. The latter conclusion follows because as the absorber damping is increased, the magnification factor of the absorber system decreases in direct proportion. But since the absorber becomes less effective the main mass motion must increase correspondingly, with the result that the absorber amplitude at optimum tuning is practically independent of absorber damping. Also, at optimum tuning, the absorber motion is directly proportional to the external exciting force, P_0, and inversely proportional to the main system spring, K, and to the mass ratio, μ. Another characteristic shown by the curves is the tendency of an absorber with low damping to have large relative motion if it is not properly tuned.

Phase Angle Relationship

The expression for the phase angle between main mass displacement and absorber mass displacement is given by Eq. (18). In dimensionless form it becomes

$$\tan \varphi_{21} = (\gamma_2/\mu)/(\alpha/\mu)g \qquad (22)$$

To calculate the phase angle at the peak frequency, g_m, requires only the substitution of the previously obtained values for (γ_2/μ) and (α/μ), which correspond to a given peak frequency. As shown in Fig. 15, the curves of constant phase angle are straight lines that could be superimposed on Fig. 13. For zero absorber damping ($\gamma_2 = 0$), the phase angle is either 0° or 180°.

References

[1] Den Hartog, J. P., *Mechanical Vibrations*, 2nd Edition, pp. 261–265; McGraw-Hill Book Company, Inc., New York, 1940.

[2] Den Hartog, J. P., *Tuned Pendulums as Torsional Vibration Eliminators*, Publications from the Graduate School of Engineering, No. 243, Harvard University, 1938–1939.

[3] Gerstenberger, Walter, *Notes on Vibration Absorber Theory*, unpublished, Hamilton Standard Propellers technical data.

[4] Moore, Vincent, *The Control of Torsional Vibration in Radial Aircraft Engines by Means of Tuned Pendulums*, Journal of the Aeronautical Sciences, Vol. 9, No. 7, p. 229, May, 1942.

[5] Shieh, A. H., *Optimum Performance of Pendulum-Type Torsional Vibration Absorber*, Journal of the Aeronautical Sciences, Vol. 9, No. 9, p. 337, July, 1942.

[6] Stieglitz, Albert, *Control of Torsional Vibrations by Pendulum Masses*, N.A.C.A. T.M. No. 1035, November, 1942.

[7] Taylor, E. S., *Eliminating Crankshaft Torsional Vibration in Radial Aircraft Engines*, SAE Journal, March, 1936.

Effects of Material Distribution on Strength of Panels

ADAM ZAHORSKI*

Lockheed Aircraft Corporation

SUMMARY

This article discusses the effect of material distribution between skin and longitudinal stiffeners on the strength of flat panels subjected to the action of compressive forces only. The idealized panel forms—such as square, triangular, or circular corrugations; various shapes of hat sections, double skin constructions; and variation in skin thicknesses—are analyzed. A structural parameter P/L, which determines the optimum design stress for a given panel form, is also introduced.

SYMBOLS

σ_a	= average stress on the panel, lbs. per sq.in. (Eq. 1)
σ_e	= Euler stress on the panel, lbs. per sq.in. (Eq. 2)
σ_c	= crippling stress on the panel, lbs. per sq.in. (Eq. 3)
σ_0	= stiffener stress, lbs. per sq.in.
σ_s	= skin stiffener stress, lbs. per sq.in.
σ_{op}	= optimum panel stress, lbs. per sq.in. (Eq. 21)
E	= modulus of elasticity, lbs. per sq.in.
η	= coefficient of effective modulus of elasticity
τ	= coefficient of tangent modulus of elasticity
t_0	= thickness of the stiffener, in.
t_s	= thickness of the skin, in.
t_{0_w}	= area of the stiffeners per inch of panel, sq.in. per in.
t_s	= area of the panel per inch of panel, sq.in. per in.
b_0	= unsupported width at an element of the stiffener, in.
b_s	= unsupported width of the skin, in.
β	= t_s/t_0
β_1	= $t_s/t_0 = b_s/b_0$ (special case where $t_0/b_0 = t_s/b_s$)
α	= b_s/b_0
P	= total load per inch of panel, lbs. per in.
P_0	= load carried by stiffener per inch of panel, lbs. per in.
P_s	= load carried by skin per inch of panel, lbs. per in.
L	= length of the panel, in.
x_0	= distance from skin to center of gravity at stiffener alone, in.
ρ_0	= radius of gyration of stiffener alone, in.
ρ	= radius of gyration of panel, in.
C_1	= coefficient of radius of gyration (Eq. 15)
C_2	= coefficient of area (Eq. 17)
C_0	= C_1/C_2
I	= moment of inertia of panel per inch, cu.in.
I_0	= moment of inertia of stiffeners alone per in., cu.in.
R_s	= stiffness ratio (Eq. 4)
K	= crippling constant (Eq. 3)
P/L	= structural index for panels, lbs. per sq.in.

INTRODUCTION

THE SELECTION of the form of a compression panel, particularly the form of its longitudinal stiffeners, can be made only after thorough examination of such items as service and maintenance, cost of fabrication, structural limitations, etc. This discussion deals primarily with the strength/weight ratio of flat panels subjected to compressive forces. Generally, the higher the working stresses, the lighter the structure. This paper analyzes the manner in which the working stresses are affected by the material distribution between the skin and stiffeners. Only flat, rectangular panels with longitudinal stiffeners are considered; the panels are subjected only to longitudinal compressive loads uniformly distributed along the width; and all discussions and charts are of qualitative character, not quantitative.

In the design of panels the equation

$$\sigma_a = P/t_e \tag{1}$$

gives an actual average stress on the panel by introducing the actual design load P. The usual restrictions on the value of σ_a are, first, that it should not exceed the yield stress of materials and, second, that it should not exceed the value at which the structure as the whole or any of its elements may become unstable.

The stability of the panel as the whole is usually determined by an allowable stress given by various forms of Euler's equations, such as

$$\sigma_e = \pi^2 E\eta/(L/\rho)^2 \tag{2}$$

If an element of the panel becomes unstable it may produce large deformations that destroy the form of the cross section and induce stresses that may exceed the elasticity of the material and cause destruction of the panel. These crippling stresses are usually determined for straight-line elements of the panel by "plate" allowable stress given in the form

$$\sigma_c = KE\eta(t/b)^2 \tag{3}$$

STIFFNESS RATIO

The stability of the panel, the critical compressive stress given by Eq. (2), in general depends on the value of the radius of gyration of the section, the modulus of elasticity, and the length of the panel. The weight of the panel depends on the area of the section per inch of the panel and the density of the material. For the present it will be assumed that the modulus of elasticity, the length of the panel, and the density are the same for all panels. It seems to be reasonable under the above assumption to measure the economy of the

Received December 13, 1943.

* Structures Research Engineer.

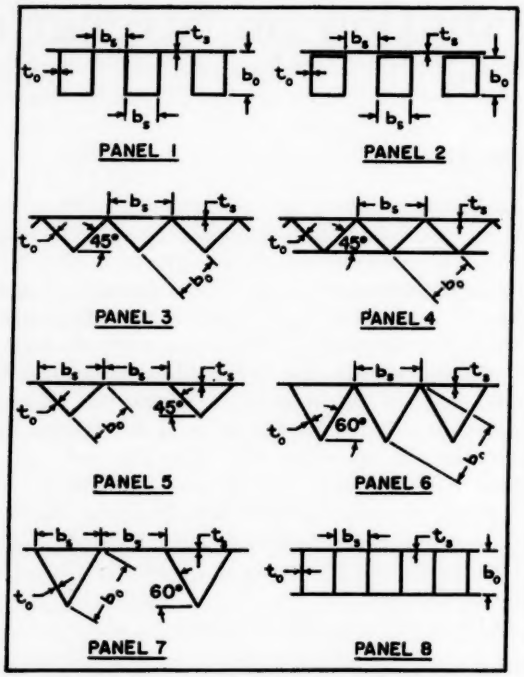

FIG. 1. Fundamental panel types having straight-line elements.

design by some number that is proportional to the ratio of ρ/t_e.

The stiffness ratio of the panel is defined as the ratio of the moment of inertia of a section of the panel per inch of width to the moment of inertia of a rectangle 1 in. wide and area the same as that of the panel. Thus, the definition of R_s is

$$R_s = 12I/t_e^3 = 12(\rho/t_e)^2 \tag{4}$$

Fourteen fundamental panel types were examined for stiffness ratio (Figs. 1 and 2). These were idealized panel forms—such as square, triangular, or circular corrugations; various shapes of hat sections; double

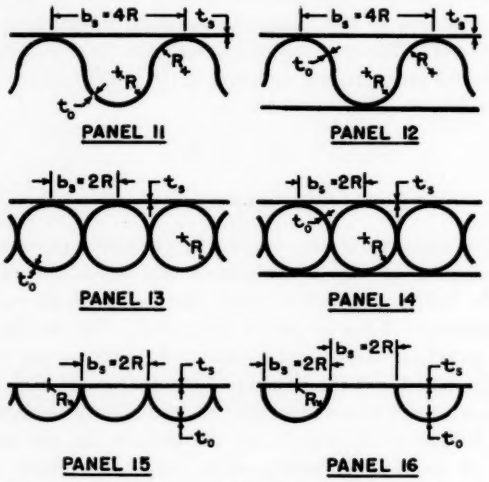

FIG. 2. Fundamental panel types having circular elements.

skin constructions, etc.—which are adaptable to simple analysis.

The term "form similarity" shall be used in a different sense from that of the more common term "geometric similarity." All panels of the same form are not necessarily geometrically similar—that is, in speaking of corrugation or "hat" stiffened panels, reference is made to two different forms of panels. However, the thickness of the hat section may be varied without varying its other dimensions, or the skin thickness may be varied without corresponding variations in the thickness of the hat. Variations in the thickness of the skin or stiffener shall not constitute a variation in the form of the panel.

All panels are subdivided into two groups: those having straight-line elements (Fig. 1) and those having circular elements (Fig. 2). In all cases the stiffness ratio can be expressed by either

$$R_s = 12(\rho/t_e)^2 = 12C_0^2(b_0/t_0)^2 \tag{5}$$

for the group of straight-line elements, or

$$R_s = 12(\rho/t_e)^2 = 12C_0^2(R/t_0)^2 \tag{6}$$

for the group of circular elements. In the analysis the variation in the thickness of the stiffener is carried as the variable (b_0/t_0) or (R/t_0), and the variation in the thickness of the skin is carried as the variable $\beta = t_s/t_0$, which is usually incorporated in the coefficient $12C_0^2$.

As an example, detailed calculations for panel No. 1 follow:

Area of stiffener per inch of panel:

$$t_{0_e} = 3bt_0/2b = {}^3/_2t_0 \tag{7}$$

Total area per inch of panel:

$$t_e = t_s + t_{0_e} = \beta t_0 + {}^3/_2t_0 = {}^1/_2(3 + 2\beta)t_0 \tag{8}$$

Distance to the skin from c.g. of the stiffener alone:

$$x_0 = (1/3bt_0)(2^1/_2b^2t_0 + b^2t_0) = {}^2/_3b \tag{9}$$

Moment of inertia of stiffener alone per inch of panel:

$$I_0 = \frac{b^2t_0}{12} + \frac{b^2t_0}{36} + \frac{b^2t_0}{18} = {}^1/_6b^2t_0 \tag{10}$$

Using simplified formulas for the moment of inertia and radius of gyration of stiffener-skin combination:

$$\begin{aligned} I/I_0 &= 1 + (x_0/\rho_0)^2(t_s/t_e) \\ I &= I_0 + x_0^2(t_s/t_e)t_{0_e} \\ \rho^2 &= \rho_0^2(t_{0_e}/t_e) + x_0^2\beta(t_0t_{0_e}/t_e^2) \end{aligned} \tag{11}$$

Substituting the proper values from Eqs. (7), (8), (9), and (10) into Eq. (11):

$$\rho^2 = {}^1/_3[(3 + 10\beta)/(3 + 2\beta)^2]b^2 \tag{12}$$

Substituting Eqs. (8) and (12) in Eq. (4):

$$R_s = [16(3 + 10\beta)/(3 + 2\beta)^4](b_0/t_0)^2 = f(\beta)(b_0/t_0)^2 \tag{13}$$

TABLE 1

PANEL NO.	R_s	PANEL NO.	R_s
STRAIGHT LINE ELEMENTS			
1	$\frac{16(3+10\beta)}{(3+2\beta)^4}\left(\frac{b_0}{t_0}\right)^2$	5	$\frac{4(1+4\sqrt{2}\beta)}{(\sqrt{2}+2\beta)^4}\left(\frac{b_0}{t_0}\right)^2$
2	$\frac{2(4+5\beta)}{(2+\beta)^4}\left(\frac{b_0}{t_0}\right)^2$	6	$\frac{3(1+2\beta)}{(2+\beta)^4}\left(\frac{b_0}{t_0}\right)^2$
3	$\frac{(1+2\sqrt{2}\beta)}{(\sqrt{2}+\beta)^4}\left(\frac{b_0}{t_0}\right)^2$	7	$\frac{3(1+4\beta)}{4(1+\beta)^4}\left(\frac{b_0}{t_0}\right)^2$
4	$\frac{(\sqrt{2}+6\beta)}{2(\sqrt{2}+2\beta)^3}\left(\frac{b_0}{t_0}\right)^2$	8	$\frac{\beta^2(6\beta^2+1)}{(2\beta^2+1)^3}\left(\frac{b_0}{t_0}\right)^2$
CIRCULAR ELEMENTS			
11	$\frac{24\pi(\pi+6\beta)}{(\pi+2\beta)^4}\left(\frac{R}{t_0}\right)^2$	14	$\frac{6(\pi+4\beta)}{(\pi+2\beta)^3}\left(\frac{R}{t_0}\right)^2$
12	$\frac{24(\pi+8\beta)}{(\pi+4\beta)^3}\left(\frac{R}{t_0}\right)^2$	15	$\frac{24(\pi^2-8+2\beta\pi)}{(\pi+2\beta)^4}\left(\frac{R}{t_0}\right)^2$
13	$\frac{6\pi(\pi+3\beta)}{(\pi+\beta)^4}\left(\frac{R}{t_0}\right)^2$	16	$\frac{96(\pi^2-8+4\beta\pi)}{(\pi+4\beta)^4}\left(\frac{R}{t_0}\right)^2$

It can be seen from Eq. (13) that, if the thickness of the skin equals the thickness of the stiffener ($\beta = 1$), $R_s = 0.3328(b_0/t_0)^2$ and if $t_s = 0$—i.e., $\beta = 0$—$R_s = 0.5926(b_0/t_0)^2$. Using, for example, the value of $(b_0/t_0) = 35$, which corresponds to about 30,000 lbs. per sq.in. on 24S-RT plate, $R_s = 407$ for $\beta = 1$ and $R_s = 726$ for $\beta = 0$. This means that if the material is put into panel form No. 1 instead of putting the same amount of material into plate the resulting structure in the former case is 407 times stiffer and in the latter case 726 times stiffer.

The stiffness ratios for various panel forms and skin thicknesses are tabulated in Table 1 and plotted on

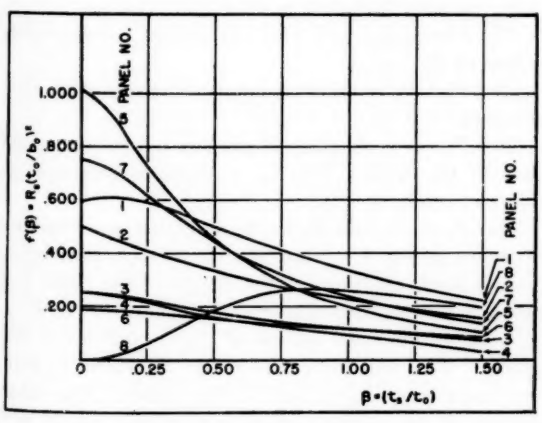

FIG. 3. Stiffness ratio vs. t_s/t_0 ratio for panel on Fig. 1 (see Table 1).

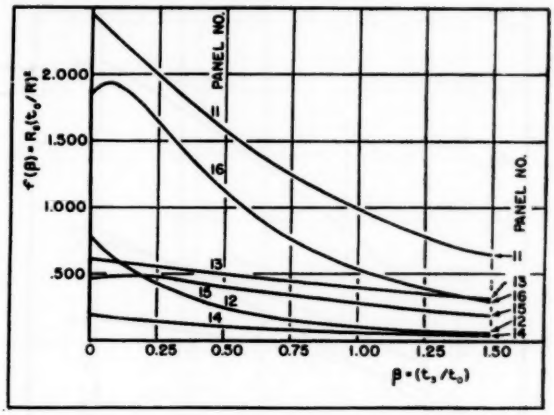

FIG. 4. Stiffness ratio vs. t_s/t_0 ratio for panel on Fig. 2 (see Table 1).

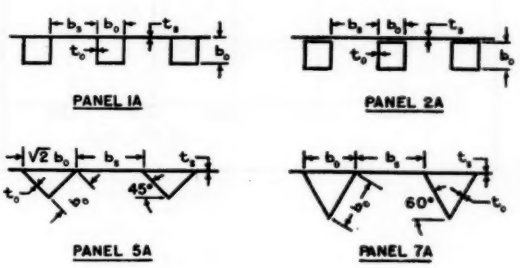

FIG. 5. Modified panel forms of Fig. 1.

Figs. 3 and 4. It can be concluded that, in general, an increase in skin thickness decreases the stiffness ratio; however, in some cases (panels 1, 13, and 15) there is a definite maximum of R_s at a particular value of β. As far as the stiffness ratio is concerned, single skin construction shows a definite advantage over double ("sandwich"-type) skin construction. Compare panels 3 and 4, 11 and 12, and 13 and 14.

In several panels (Fig. 5) it was assumed that β = constant = 1.0 (skin thickness = stiffener thickness), and the spacing of the stiffeners has been varied—that is, the ratio $\alpha = b_s/b_0$ was introduced as a new variable. The effect of this variable on the stiffness ratio is shown in Fig. 6. It can be said, in general, that the greater the distance between the stiffeners, the stiffer is the panel.

The spacing of the stiffeners has also been investigated under different conditions. The thicknesses of both skin and stiffener, as well as the spacing, have been varied under the condition of $t_s/b_s = t_0/b_0$ or $\beta_1 = t_s/t_0 = b_s/b_0$.

The results of calculations shown in Fig. 7 indicate an influence on the stiffness ratio different from that of Fig. 6.

Of all forms investigated it appears that hat stiffeners are most promising for economical designs.

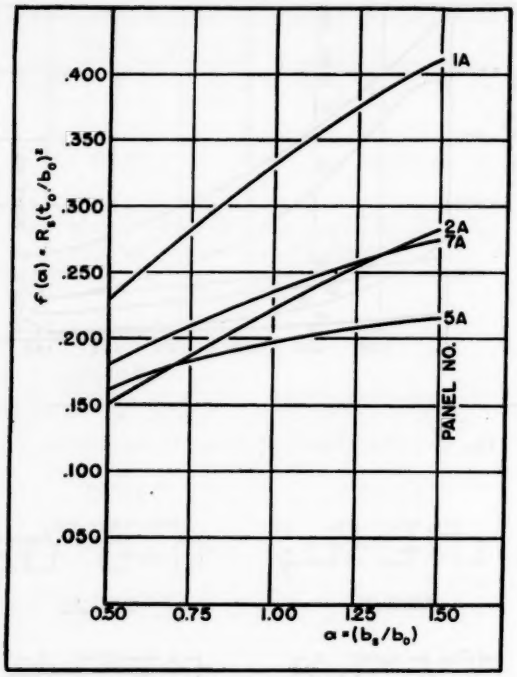

FIG. 6. Stiffness ratio vs. b_s/b_0 ratio for panel on Fig. 5.

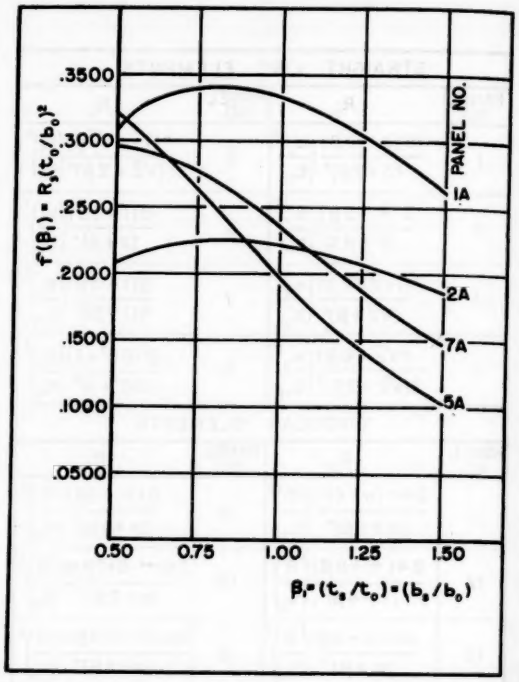

FIG. 7. Stiffness ratio vs. $b_s/b_0 = t_s/t_0$ ratio for panel on Fig. 5.

SKIN EFFICIENCY

It is more economical from the standpoint of weight to increase the stability of a compression panel by increasing the size of the stiffener instead of the thickness of the skin, provided the skin and the stiffener carry the same stress. In practice it is seldom possible to stress both the skin and the panel to the same degree. In many existing designs the skin is thin and is allowed to buckle at a fraction of the total load, thus decreasing the average stress of the whole panel.

The skin efficiency shall be defined as the ratio of the average stress on the panel to the stiffener stress—i.e.,

$$\text{skin efficiency} = \sigma_a/\sigma_0$$

The panel form No. 1 (Fig. 1) will be analyzed here in detail as an example of the method that can be applied to many forms of panels. It is assumed that the buckling of an element of the stiffener or skin can be predicted by Eq. (3), in which the constant K, independent of the size of the stiffener, can be determined experimentally or otherwise for any form of the panel under consideration.

The problem is to design the skin stiffener combination and find the stresses for a given load per inch of panel, given material properties ($E\eta$), and a given form of panel. This can be accomplished by solving the following seven equations:

$$\left.\begin{aligned} \sigma_s &= K_s E\eta(t_s/b_s)^2;\ \sigma_0 = K_0 E\eta(t_0/b_0)^2 \\ P_s &= \sigma_s t_s;\ P_0 = \sigma_0 t_{0_e};\ P = \sigma_a t_e \\ P &= P_0 + P_s;\ t_e = t_{0_e} + t_s \end{aligned}\right\} \qquad (14)$$

In general, the values of K_s and K_0 and the relations between b_s and b_0 and t_{0_e} and t_0 are given from the geometry of the panel. For panel form No. 1, it can be assumed that $K_s = K_0 = 3.62$, $b_s = b_0$, and $t_{0_e} = 1.5t_0$.

In order to facilitate the solution of Eqs. (14) and therefore the design of the panels, two diagrams are developed as follows:

(1) Solve for t_s/b_s in the equation $\sigma_s = 3.62E\eta \times (t_s/b_s)^2$ by using a number of values of σ_s. This can be tabulated easily if the relation between σ_s and $E\eta$ is given graphically. (In this example it was assumed that 24S-T aluminum alloy is used.)

(2) For the same values of σ_s and a number of values of P_s, tabulate t_s from $t_s = P_s/\sigma_s$.

(3) From Eqs. (1) and (2) obtain corresponding values of b_s.

(4) Plot P_s vs. b_s for a family of curves with σ_s = constant.

The P_0 vs. b_0 diagram is prepared similarly except that in the second step $t_{0_e} = P_0/\sigma_0$ is obtained; it follows from $t_{0_e} = 1.5t_0$.

The P_s vs. b_s and P_0 vs. b_0 diagrams are combined as shown in Fig. 8. Note that the P_s scale is inverted. To use these diagrams in the design of the panel it is necessary to measure the ordinate equal to $P = P_0 + P_s$ between any two σ-lines of upper and lower diagrams. This will determine σ_s and σ_0 which, in turn, determine the (t_s/b_s) and (t_0/b_0) ratios. The intersection of the vertical ordinate with the line $P = 0$ gives the necessary values of b_s and b_0. Thus, the sizes of the panels are completely determined. For

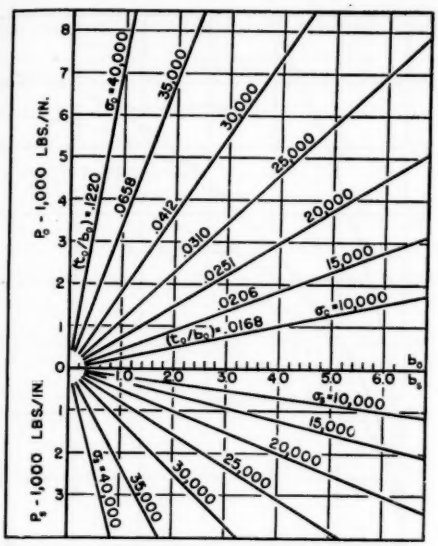

FIG. 8. Design diagram for panel No. 1 and 24S-T aluminum alloy.

ideal panel No. 1 shown in Fig. 1, $b_s = b_0$; in practice, however, they are seldom equal, but the relationship between them usually can be established and the scales of b_s and b_0 can be adjusted accordingly.

In Fig. 9 variations of stress are plotted for the function of β for three different stiffener stresses, σ_0, for panel form No. 1 with load P = 7,000 lbs. per in. of width of panel. For any desired stress the size of the elements of the panel can easily be obtained. Some of the numerical values are given in Table 2 for the purpose of comparison. The letters refer to the points in Fig. 9.

TABLE 2

Point	σ	t_s/t_0	b	t_0	t_s
A	35,000	0	3.64	0.1324	0
B	35,000	1	2.19	0.0798	0.0798
C	30,000	0	5.28	0.1553	0
D	30,000	1	3.17	0.0933	0.0933
E	25,000	0	7.06	0.1858	0
F	25,000	1	4.24	0.1115	0.1115

In the conditions in Table 2 the skin efficiency is 100 per cent; for any other condition it is the ratio of the σ_a and σ_0 ordinates.

OPTIMUM STRESS

The independent Eqs. (1), (2), and (3) represent three different ways in which the panel may fail. The stresses at any time must be below the yield point, and it is obvious that σ_a cannot be greater than either σ_e or σ_s. However, the economy of the design will be improved consistently as σ_a approaches the same value as σ_e or σ_c. It can be shown that the most economical design, the optimum, is obtained when all three stresses, given by Eqs. (1), (2), and (3), are equal.

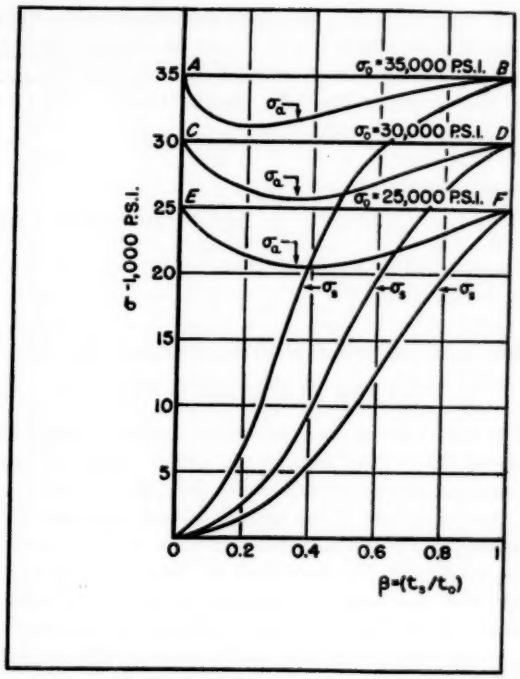

FIG. 9. Stress relations for load 7,000 lbs. per in. of panel obtained from diagram of Fig. 8 (see Table 2).

Consider the design in which load P, length L, and area t_e are constant; then from Eq. (1) the average stress σ_a is also constant. Any increase in the value of σ_e, Eq. (2), implies an increase in ρ, which calls for an increase in b or decrease in the ratio of (t/b). But a decrease in the ratio of (t/b) decreases the crippling stress σ_c, Eq. (3). In other words, any attempt to increase the value of σ_e by readjusting the material in the cross section will result in a decrease in the value of σ_c. It can be shown in a similar manner that any attempt to increase the value of σ_c will result in a simultaneous decrease in the value of σ_e. Since it is the lowest value of the two values, σ_c and σ_e, which decides the allowable stress, the highest allowable can be obtained when σ_c equals σ_e.

The radius of gyration of the section, ρ, can be defined for a given form in terms of a constant coefficient and a linear panel dimension, so that

$$\rho = C_1 b \tag{15}$$

Substituting the above into Eq. (2),

$$\sigma_e = (\pi^2 E\eta/L^2)\, C_1^2 b^2 \tag{16}$$

The area per inch of panel, t_e, also can be expressed for a given form of panel by a coefficient and the wall thickness—i.e.,

$$t_e = C_2 t \tag{17}$$

Substituting this formula in Eq. (1),

$$\sigma_a = P/C_2 t \tag{18}$$

Since Eqs. (3), (16), and (18) are independent equations, the variables t and b can be eliminated from them by finding the product of Eq. (3) and Eq. (16) and the square of Eq. (18), thus getting

$$\sigma_c\sigma_e\sigma_a^2 = (E\eta)^2\pi^2KC_0^2(P/L)^2 \tag{19}$$

where

$$C_0 = C_1/C_2 \text{ or } \rho/t_e = C_0(b/t) \tag{20}$$

Imposing the condition that

$$\sigma_c = \sigma_e = \sigma_a \equiv \sigma_{op}$$

where σ_{op} is the optimum stress, then from Eq. (19):

$$\sigma_{op} = \sqrt[4]{KC_0^2}\ \sqrt{\pi E\eta}\ \sqrt{P/L} \tag{21}$$

The first radical contains dimensionless terms that depend only on the form of the panel. The coefficient K determines the allowable crippling stress of elements of the panel, and it can be determined experimentally without much difficulty for any form of cross section. The coefficient C_0, as defined by Eqs. (15), (17), and (20), also can easily be obtained for any given form of panel. Note that this same coefficient C_0 appeared in Eqs. (5) and (6) as the coefficient of stiffness ratio R_s; thus, it shows a definite relation between optimum stress and stiffness ratio. The second radical includes the properties of the material, assuming that the effective modulus of elasticity $E\eta$ is a function only of the stress-strain relation and not of the form. The last radical includes only the length of the panel and the design load.

The selection of the proper coefficient η rests with the designer. If he chooses to use τ in Eq. (2), instead of η, or even incorporates the column fixity coefficient, the form of Eq. (21) will not be changed, nor, therefore, the existence of optimum stress as the function of P/L parameter. As a matter of fact, even if two different values of τ and η are used in Eqs. (2) and (3), respectively, they will appear in Eq. (21) as $\sqrt[4]{\tau\eta}$.

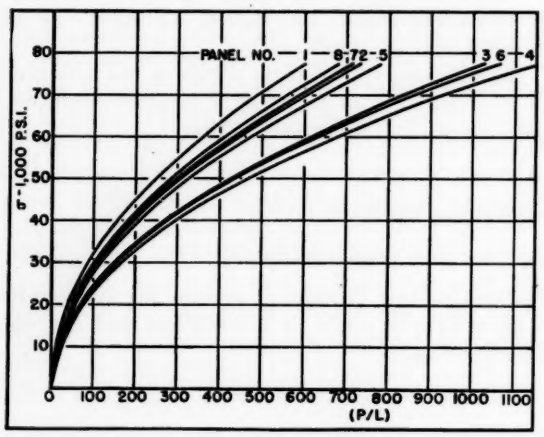

FIG. 10. P/L curves for panels of Fig. 1. $\beta = 1$; $E = 10^7$ lbs. per sq.in.

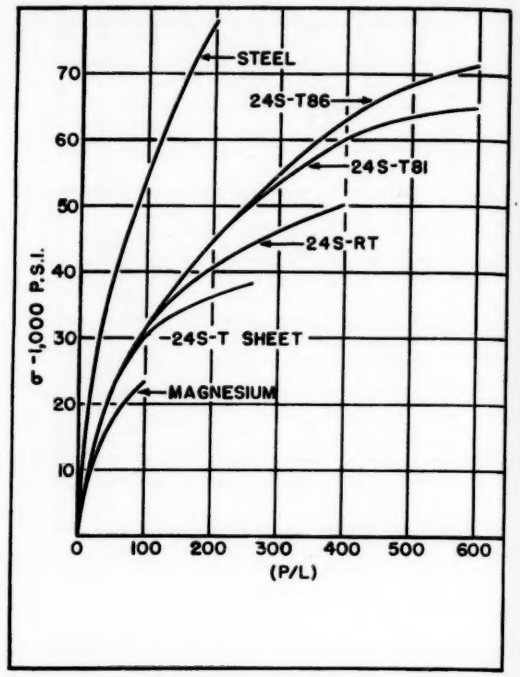

FIG. 11. P/L curves for panel No. 1, $\beta = 1$.

Since in most of the practical cases the values of τ and η are not far apart, the fourth root of the error will not be of great significance.

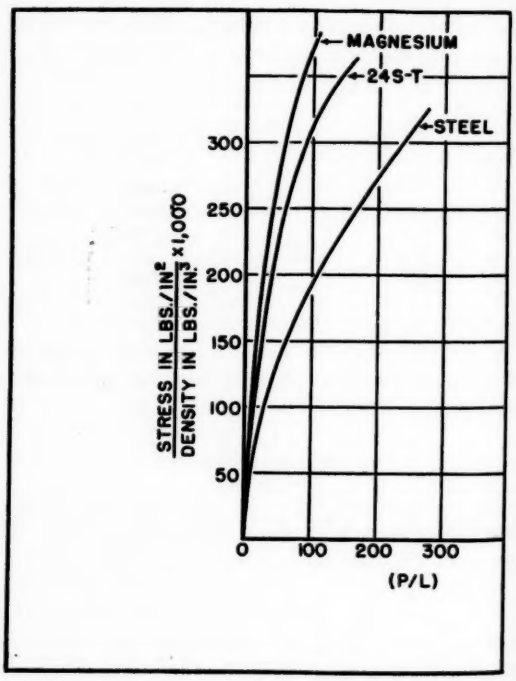

FIG. 12. P/L curves vs. stress/density ratio for panel No. 1; $\beta = 1$.

Given material properties—i.e., effective modulus—and having selected a stiffener form for which the constants K and C_0 can be determined, the working stress σ and dimensions t and b of the stiffener can be determined for the design conditions, expressed as the ratio (P/L). Conversely, if the loading P and working stress are known, the effective panel length can be determined. Using Eq. (21) an optimum stress σ_{op} is obtained which is, by definition, the actual stress as well as the allowable stress, thus giving a margin of safety equal to zero. Then the wall thickness t can be obtained from Eqs. (1) and (17) and the depth b of the panel from Eq. (3). The solution is direct without successive approximations.

In Fig. 10, σ vs. P/L ratios are plotted for various forms of panels as shown in Fig. 1. The curves are plotted under the assumption that $K = 3.62$, $\beta = 1$, and $\eta = 1$—that is, for materials that have a constant modulus of elasticity.

Fig. 11 gives curves for using different materials in panel form No. 1, $\beta = 1$. It has been assumed that the effective coefficient of elasticity η is related to the coefficient of the tangent modulus of elasticity by $\eta = {}^1/_4(\tau + 3\sqrt{\tau})$. This is arbitrary and similar curves can be constructed for any other relation.

For comparison purposes, the curves for steel ($E = 30 \times 10^6$) and magnesium ($E = 6.5 \times 10^6$) are also included. The same curves plotted on the basis of the stress/density ratio are shown in Fig. 12. The densities of steel, aluminum, and magnesium are taken as: 0.2829, 0.0975, and 0.0629 lbs. per cu.in., respectively. The curves show that there is a definite advantage in using light metals for higher values of the P/L ratio.

Letter to the Editor

Dear Sir:

The writer has read Mr. duPlantier's excellent paper[1] with much interest and wishes to call attention to an expeditious graphic method for analyzing elastic frames or rings, either symmetrical or unsymmetrical. A complete description of this method is easily available.[2, 3]

It is based on the elastic theory just as Mr. duPlantier's method is, but the integrations are performed graphically instead of numerically.

For those engineers who have a facility with graphic methods or are interested in acquiring one, this method should be a time-saver in solving such structures as fuselage rings.

CHARLES S. WHITNEY
Consulting Engineer

[1] duPlantier, Donald A., *Analysis of Fuselage Rings by the Column Analogy*, Journal of the Aeronautical Sciences, Vol. 11, No. 2, p. 137, April, 1944.

[2] Whitney, Charles S., *Reinforced-Concrete Conduit Analysis Simplified by Theory of Displacements*, Engineering Record, Vol. 72, page 486, October 16, 1915.

[3] Whitney, Charles S., *Graphical Analysis of Arches with Fixed Ends Greatly Simplified*, Engineering Record, Vol. 72, page 324, September 11, 1915.

Effect of Dive Brakes on Airfoil and Airplane Characteristics

PHILIP G. BLENKUSH,* RAYMOND F. HERMES,† AND MERLE A. LANDIS‡

University of Detroit, Aeronca Aircraft Corporation, and Curtiss-Wright Corporation

ABSTRACT

Tests have recently been completed at the University of Detroit 7- by 10-ft. wind tunnel to determine the effects of double split flap dive brakes on the lift, drag, and pitching moment characteristics of an airfoil and an airplane model. An NACA 0015 rectangular airfoil of 6-ft. span and 1-ft. chord was used for the airfoil tests. This was equipped with both perforated and nonperforated dive brakes that measured 25 per cent of the chord and 60 per cent of the span. These were mounted at the trailing edge at a deflection of 60° with respect to the chord line. A low-wing airplane model of 6.67-ft. span was also used for the tests. This model was equipped with perforated double split flaps measuring 25 per cent of the wing span and 15 per cent of the mean aerodynamic chord. Tests were made with variations in both chordwise and spanwise position of the dive brakes.

The information obtained from these tests shows that trailing-edge dive brakes tend to decrease lift curve slope at low angles of attack but increase it at higher angles of attack. Maximum lift, as well as the angle of attack at which it occurs, is increased in all cases. Moving the dive brakes forward on the chord results in a lift curve having a reduced maximum lift, as well as a reduced and varying slope.

Substantial drag increases are experienced with all dive-brake installations on both airfoil and airplane. In this case the advantage falls to the forward dive-brake location with about twice the drag being produced. Slight variation is shown between the perforated and nonperforated types.

In the case of airfoil pitching moments it was found that dive brakes at the trailing edge tend to shift the moments in the positive direction. For the airplane tests fore-and-aft location, as well as spanwise position, indicates considerable variations in pitching moments and stability. Likewise, tail position relative to the wake produced was found to have definite significance.

INTRODUCTION

WITH THE UNPRECEDENTED DEVELOPMENT of high performance military airplanes it has become necessary, both from a tactical standpoint and from the physiologic effects on the crew, to provide a positive means of controlling the speed of aircraft. This is particularly true in considering dive-bombing operations where high speeds are readily attainable in the dive on the target. In this instance speed control is desirable for two primary reasons.

(1) High diving speeds followed by rapid pull-out impose severe strain on both the airplane and its flight crew.

(2) Pull-out at dive speed must commence at higher altitude because of the greater radius of curvature of the flight path. This demands an earlier bomb release at the expense of accuracy.

Data are given on the effects of double split flap dive brakes on both airfoil and airplane characteristics. Some data of this general type have been published, the most notable sources are based on German tests.[1,2] The additional information presented here should serve to augment existing knowledge and to point out both desirable and undesirable practices to be followed in the design of dive-bombing aircraft.

All the data were obtained from tests conducted in the University of Detroit 7- by 10-ft. wind tunnel. The results of the airfoil tests were taken directly from reference 3. Additional investigation on the airplane model was carried out at a later date in order to determine more definitely the effects on its characteristics.

EQUIPMENT

The airfoil tests were conducted on the NACA 0015 airfoil. A rectangular section of 6-ft. span and 1-ft. chord was used. The model was built of $^3/_4$-in. laminated Honduras mahogany waxed and polished to a high finish. Three types of double split flaps were used in the tests. One of these was a solid flat plate type, while the remaining two were reduced in area 16.5 per cent by perforations of $^3/_4$- and $^3/_8$-in. diameter. In every case the flap chord was $0.25c$ and the span was $0.60b$. A typical flap mounted on the airfoil as tested is shown in Fig. 1.

Fig. 2 shows the airplane model used for the tests. Although the model does not measure up to present-

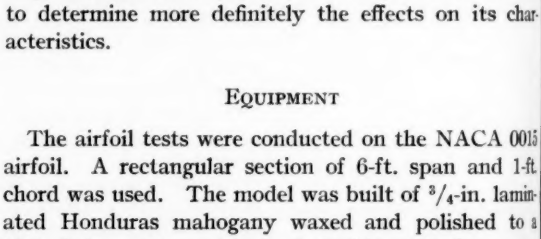

FIG. 1. Dive brakes with large perforations mounted on NACA 0015 airfoil as tested—perforations $^3/_4$ in.

Presented at the Aerodynamics Session, Twelfth Annual Meeting, I.A.S., New York, January 25–27, 1944.

* Instructor, Department of Aeronautics.

† Assistant Chief Engineer.

‡ Aerodynamicist, Airplane Division.

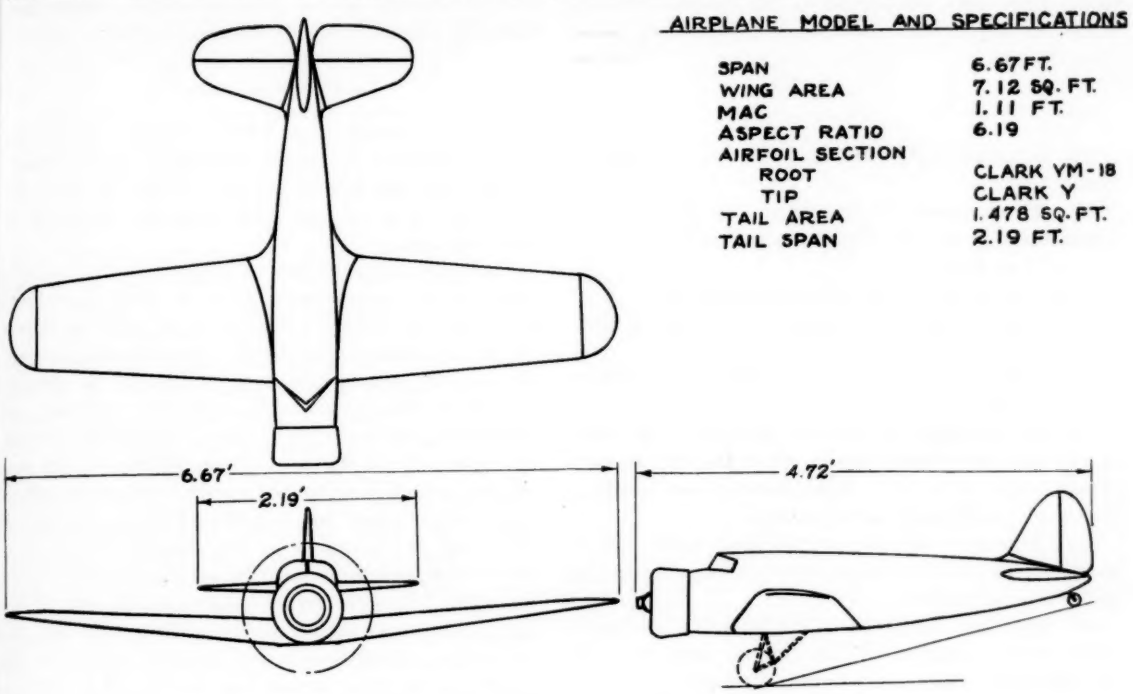

FIG. 2. Three views of airplane model.

day standards of aerodynamic refinement, it adequately serves to demonstrate the significant effects of a dive-brake installation. The principal model dimensions are as follows:

Span	6.67 ft.
Wing area	7.12 sq.ft.
Mean aerodynamic chord	1.11 ft.
Wing aspect ratio	6.19
Airfoil section	
Root	Clark YM-18
Tip	Clark Y
Horizontal tail area	1.478 sq.ft.
Tail aspect ratio	3.56
Center of gravity	30 per cent M.A.C.

Double split flap dive brakes with $^3/_8$-in. perforations were used on this airplane. These flaps each measured 25 per cent of the wing semispan and 15 per cent of the mean aerodynamic chord.

The University of Detroit 7- by 10-ft. wind tunnel is a single-return closed-throat type tunnel equipped with a 14-ft. four-blade fixed-pitch wood propeller located in the exit cone. Power is supplied by a 225-hp. d.c. motor operating on the Ward-Leonard system of control. This arrangement makes it possible to hold speeds accurately from 10 to over 100 m.p.h. Dynamic pressure in the test section is measured through a calibrated service pitot static tube connected to an alcohol manometer.

The control room is located directly above the test section and houses all balances, as well as operating controls. Balances are the beam type, electrically operated either manually or automatically. A typical test setup is shown in Fig. 3. Also shown is a schematic arrangement of the balance system. The entrance and exit cones and the test section have recently been modified into an octagonal section, but preserving maximum cross-sectional dimensions. All airplane

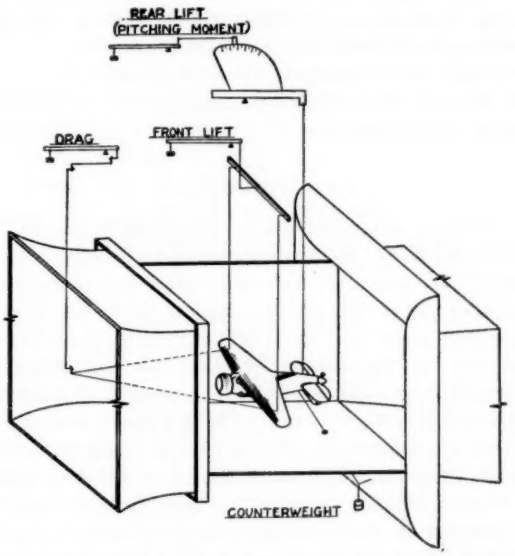

FIG. 3. Test setup showing schematic arrangement of balance system.

model tests were conducted in the modified tunnel, while the airfoil tests were made in the rectangular throat tunnel.

Tests

The following tests were made on the symmetrical airfoil:

(1) Measurement of lift, drag, and pitching moments through the full angle-of-attack range.
- (a) Airfoil alone.
- (b) Airfoil with nonperforated dive brakes.
- (c) Airfoil using dive brakes with small perforations.
- (d) Airfoil using dive brakes with large perforations.

(2) Measurement of dynamic pressure in the wake at two and three chord lengths aft of the trailing edge at zero angle of attack. These surveys were made at mid-span for all brake arrangements.

(3) Tuft flow surveys on the wing upper surface at 0°, 5°, 10°, and 14° angle of attack using the brakes with large perforations.

All tests were made at an air speed of 43 m.p.h. with brakes mounted at the trailing edge at a deflection of 60° with respect to the chord line.

In the case of the airplane model it was deemed desirable that both chordwise and spanwise dive-brake position would warrant investigation. Consistent with this, the following test program was carried out to determine lift, drag, and pitching moment characteristics over the flight range.

(1) Complete model without dive brakes.

(2) Dive brakes mounted at the wing trailing edge on upper and lower surface as close to the fuselage as the fillet would permit.

(3) Same as No. 2 but with dive brakes at 0.30c.

(4) Dive brakes at 0.30c but moved out on the wing a distance equivalent to a flap half-span.

These tests were made at an air speed of 61 m.p.h. In all cases the brakes were deflected 60° with respect to the wing chord line.

Results

All force measurements are presented in the form of standard N.A.C.A. nondimensional coefficients. These have been corrected for tunnel-wall interference and support drag. Measured moments about the mounting-stud point have been transferred to the center of gravity for the airplane model. For the airfoil the moments are measured about a point 1.58 in. below the quarter chord point. The lift and pitching moment variations are plotted against angle of attack, while drag variations are indicated by lift-drag polars.

The results of the wake surveys for the airfoil are presented in terms of the ratio q/q_0, where q is the measured dynamic pressure in the wake and q_0 represents the free-stream value. The variation of this ratio is plotted against vertical position above and below the extension of the airfoil chord line.

Lift Characteristics

Fig. 4 indicates some radical changes in the lift characteristics of the airfoil equipped with dive brakes. Of primary significance are the change in slope, the abnormal shape of the peak, and the variations in maximum lift.

The slope of the lift curve is considered first and it is found, from measurement, that the slope is reduced from 0.078 per degree (wing alone) to 0.059 per degree for the dive-brake installation. The variation between the various installations is insignificant. Of primary interest is the reduction between the no-brake and brake-extended condition. This characteristic is readily explainable in the light of flap theory. In the zero angle-of-attack position both upper and lower surface flaps exhibit equal but opposite effect on circulation; the result is no change in the original symmetry of the section and, consequently, no displacement of the lift curve. At some higher angle of attack, say 6°, the flap on the upper surface serves to disrupt the flow and to produce circulation in the negative sense. In the meantime the lower surface flap assumes its function as a high lift device. Thus, two counteracting effects are being produced, one tending to increase and the other tending to reduce the lift. The upper surface flap

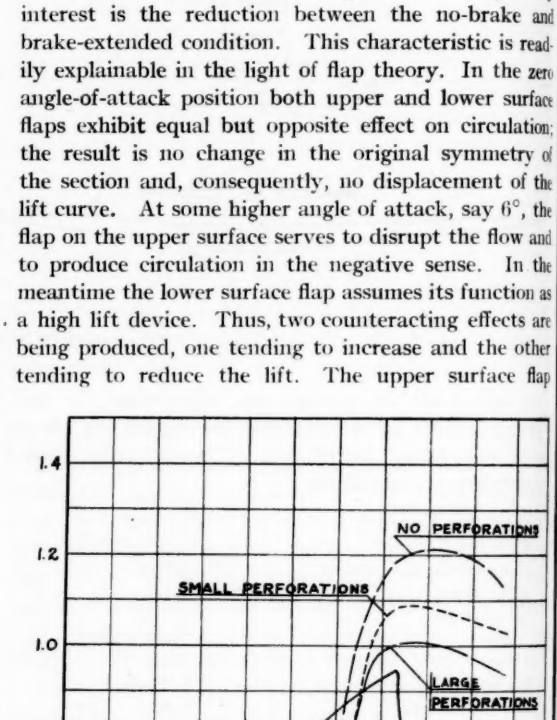

Fig. 4. Variation of lift coefficient with angle of attack for the airfoil with various dive-brake arrangements.

predominates in its effect, for it not only nullifies the circulation produced by the lower surface flap but also counteracts part of that lift which is due to the wing alone.

Insofar as the lift-curve peak is concerned, the abnormality borders on a discontinuity occurring just prior to maximum lift—a phenomenon rarely observed except in airfoils of extremely high camber. From the tuft survey tests it was observed that separation begins at some point forward of the flap when a 10° angle of attack is reached. This is also substantiated by the change in slope which occurs in this range as shown on wing-alone curve. Thus, it may be concluded that the upper surface flap begins to operate partially in the wing wake once separation has occurred forward. As the angle of attack is further increased, the upper flap progressively moves into the wing wake. Its effectiveness as a flap is destroyed; meanwhile, the lower surface flap exhibits its effect as a conventional split flap. The upper surface flap still serves to modify flow and pressure distribution, but it is no longer efficacious as an antilift device.

Considerable variation in the maximum lift is indicated between the various dive-brake installations. In every case an increase over wing-alone maximum lift is shown. The nonperforated brake shows the highest increase. This is followed by the brake with small perforations and then the brake with large perforations. Apparently, perforation size is of significance here in spite of the fact that equivalent area was removed in each case. The flap with larger perforations facilitates flow of air into the wake with resultant loss of pressure differential between points fore and aft of the flap. Also of interest is the fact that the peak of the lift curve for all dive-brake installations occurs at a higher angle of attack than for the wing alone. This is contrary to flap theory; it serves to indicate that the upper surface flap has not resigned itself wholly as a modifier of lift characteristics. Tests with upper surface flap removed would probably indicate a higher maximum lift than is shown by the dive brake. Also, the maximum lift would occur at a lower angle of attack.

Fig. 5 shows the effect of the various dive-brake installations on airplane lift. All lift values shown here are uncorrected for trim.

With dive brakes at the trailing edge the previously mentioned changes to lift characteristics have been modified in several ways. There is a shift in zero lift equal to 0.8° in a positive direction; also, the lift curve slope remains unchanged at zero lift. These modifications may be attributed partly to the decreased dive-brake dimensions as compared to those used in airfoil tests, but primarily they are due to the camber of the airfoil section used on the airplane model. Insofar as other lift characteristics are concerned, agreement with the airfoil tests is shown. There is an increase in lift-curve slope at some higher angle of attack;

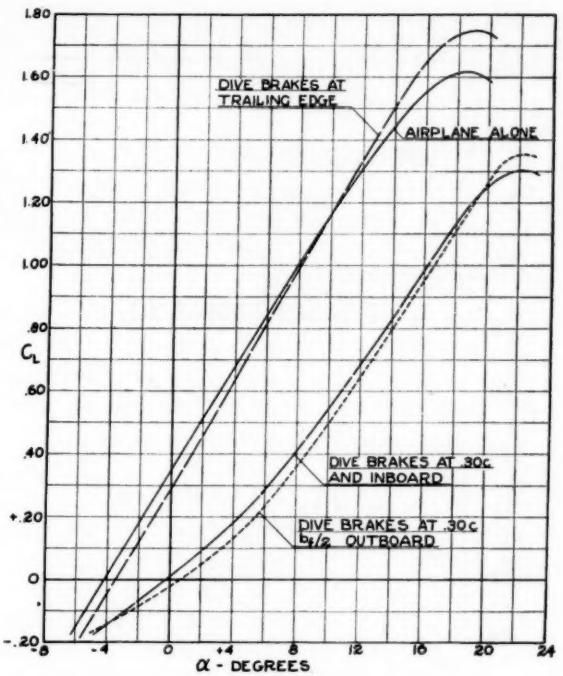

FIG. 5. Variation of lift coefficient with angle of attack for the airplane model with various dive-brake arrangements.

in this case it begins at zero degrees and is not so pronounced as in the airfoil tests. The maximum lift, as well as the angle of attack at which it occurs, is again increased.

Placing the dive brakes forward at 0.30c brings about changes in the lift curve quite different from those shown with dive brakes at the trailing edge. The order of these changes on lift indicates that the usual flap characteristics no longer exist. This is to be expected in view of the predominance of the leading edge in producing lift. The upper surface brake is now forward of the separation point for maximum lift and assumes the role of a spoiler. The result is a reduction in maximum lift and a decreased but variable lift-curve slope.

Spanwise position appears to have little effect on airplane lift characteristics, except that maximum lift is slightly higher with dive brakes moved outboard.

DRAG CHARACTERISTICS

The effect of the brakes on airfoil drag is shown in Fig. 6. A substantial increase in drag is indicated for all dive-brake installations with little difference between the various types. The increment in drag coefficient varies from 0.295 for the flaps with small perforations to 0.305 for the nonperforated brakes. This amounts to a 3.4 per cent variation—certainly not enough to warrant making a selection on the basis of braking effect alone. Other considerations, pre-

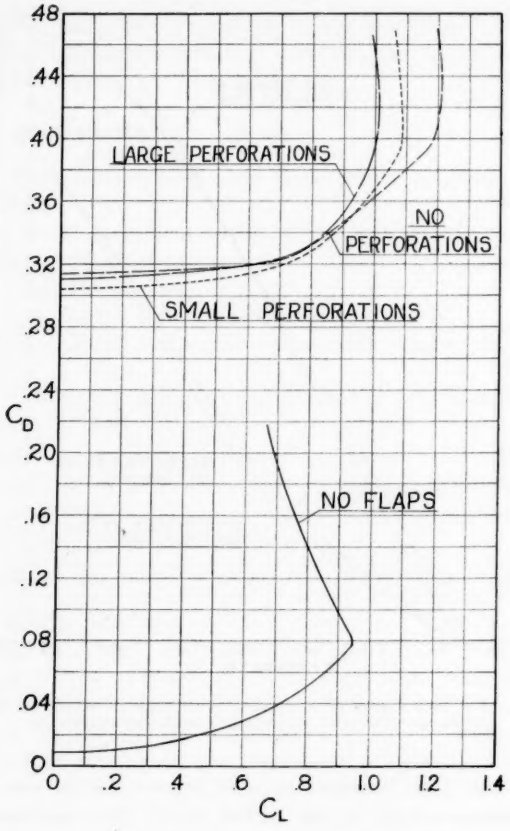

FIG. 6. Lift-drag polars for the airfoil with various dive-brake arrangements.

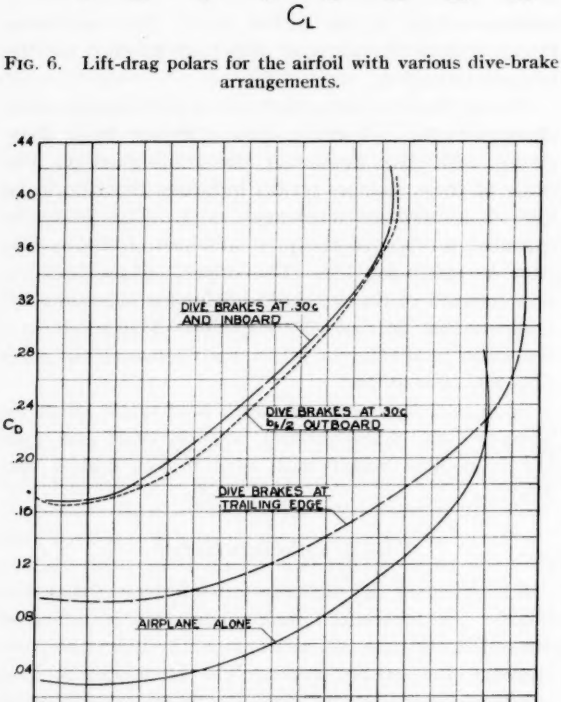

FIG. 7. Lift-drag polars for the airplane with various dive-brake arrangements.

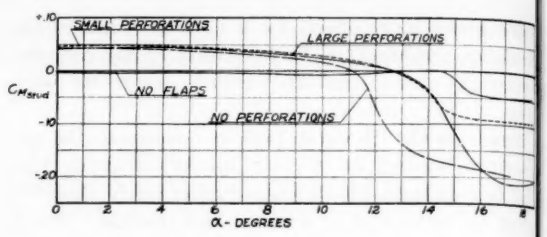

FIG. 8. Pitching moments about mounting stud point for the airfoil with various dive-brake arrangements.

viously and subsequently pointed out, are of equal or greater significance.

Fig. 7 shows the variation of airplane drag coefficient plotted against lift coefficient corrected for trim. Once again it will be noted that substantial increases in drag are indicated. In addition, appreciable differences in drag are shown between the trailing-edge position and the 0.30c position—the forward location yields over twice the increment. Spanwise position again plays a minor role.

The large difference in drag shown between the trailing-edge dive-brake position and the forward position can be attributed to the increased effective plate area produced by placing the flaps at the maximum thickness of the wing. If the increased drag coefficient at zero lift based on wing area be attributed to the increment of frontal area alone and a new coefficient based on this area is then computed, a value of 1.71 results. This corresponds to the drag of a flat plate having an aspect ratio of 50. It may be assumed that for the increased frontal area flow conditions approach two-dimensional characteristics and the previous approximation is in the right order. From the foregoing comparison it becomes evident that a forward position of the brakes is desirable if braking effect is the sole criterion. A smaller brake located forward can be expected to produce as much drag as a larger brake located at the trailing edge.

Pitching Moment Characteristics

The effect of the dive brakes on airfoil pitching moments is shown in Fig. 8. Once again the predominating effects of the upper surface flap make themselves apparent in the shift of the pitching moment curve from near zero values to some positive value. This fact serves to demonstrate the similarity of action between the upper surface flap and a reflex trailing edge. Both alter pressure distribution in such a way that diving moment is decreased. When, for the moment, pitch due to the tail is disregarded, the dive brakes affect wing pitching moments in such a way as to cause the airplane to trim at some higher positive angle of attack with but slight change in static longitudinal stability. This is apparent when it is observed that the pitching moment variation about the stud point for the airfoil over the low angle of attack range is

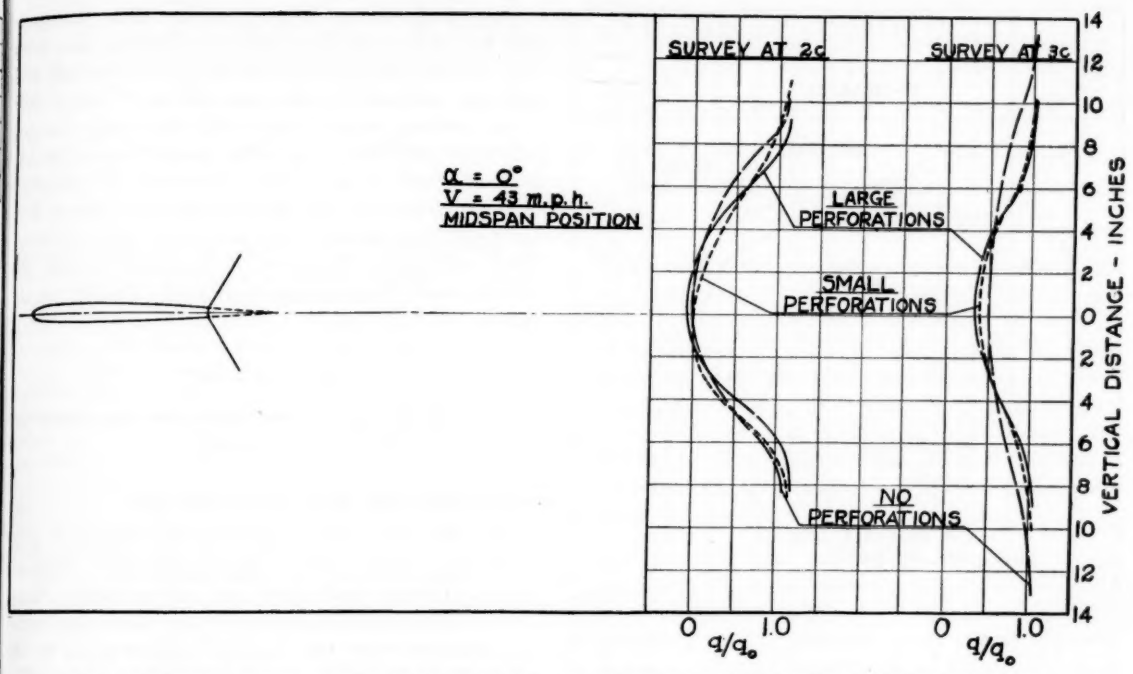

FIG. 9. Dynamic pressure surveys for the airfoil at points two and three chord lengths aft of the trailing edge.

small. Much the same characteristics would be shown if pitching moments were taken about any other point within the range used for center of gravity position. Static longitudinal stability as determined by the slope of the airplane pitching moments plotted against angle of attack becomes independent of that portion of pitching moment which remains constant with angle of attack.

Preliminary insight as to the effect of dive brakes on pitching moments due to the tail may be had from Fig. 9. Here are shown dynamic pressure surveys at two and three chord lengths aft of the trailing edge of the airfoil for all dive-brake installations. These surveys were made at zero angle of attack. The results of the surveys are plotted as the ratio of dynamic pressure in the wake to the free-stream value against the distance above and below the extension of the chord line. The tail position with respect to the wake is of definite importance. Not only do the surveys show considerable loss of dynamic pressure in the wake but also one may suspect that this region is one of highly turbulent flow. Probably it is characterized by the familiar Kármán vortex trail ordinarily associated with the wake region. Some indication of this is given by the fact that the q/q_0 values in the center of the wake at two chord lengths aft pass through zero and reach negative values. Such values would be given on a pitot static tube with flow reversed. Additional evidence of flow reversal is shown for the center-wake q/q_0 values at three chord lengths aft of the trailing edge. In this case the dynamic pressure in the wake has reached about 35 per cent of the free-stream value. There are then two reasons why the wake region should prove unsuitable environment for the horizontal tail.

(1) Energy losses in the wake would result in poor tail efficiency—detrimental to both static stability and longitudinal control.

(2) Eddies and vortices in the wake would cause severe tail buffeting.

In addition to the above effects, it is evident that the width of the wake increases with distance aft of the trailing edge. This is particularly true with the nonperforated dive brakes.

Effect of Dive-Brake Combinations on Stability

The effects of the various dive-brake combinations on airplane stability are shown in Fig. 10, where pitching moments about the center of gravity are plotted against angle of attack. In general, static longitudinal stability is positive for all cases, but considerable variation is shown between the various installations.

There appears to be little effect on stability with dive brakes mounted at the trailing edge. The pitching moment curve is preserved in its original regularity with but slight change in trim and slope. None of these changes are of sufficient magnitude as to be found objectionable. Further analysis of the pitching moment curve just cited may be made by considering the airfoil tests. In this case both the pitching moment curves and the wake surveys should be given thought. On the one hand, the pitching moment of the wing alone should become more positive, thus causing trim

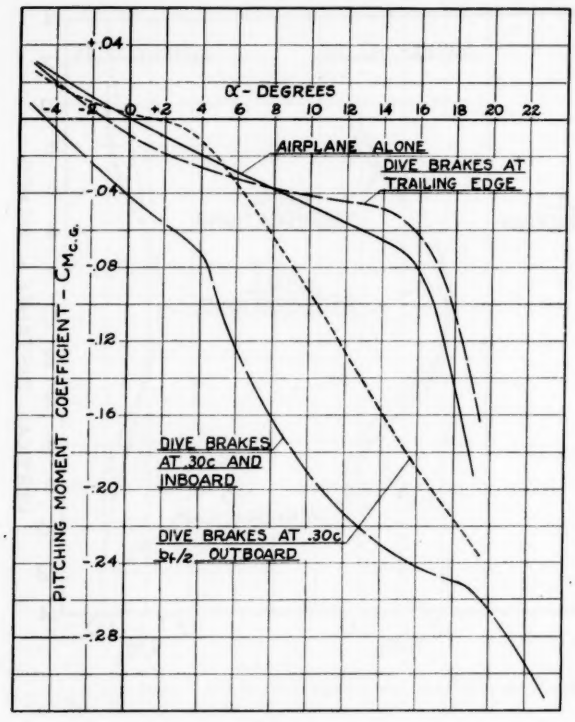

FIG. 10. Pitching moments about the center of gravity for the airplane model with various dive-brake installations.

at some higher angle of attack. On the other hand, the position of the horizontal tail with respect to the wake ought also to be considered. From Fig. 2 it is apparent that the horizontal tail lies somewhere above the wake centerline. That it lies entirely outside of the wake is doubtful. This is evidenced by a change in trim to a more negative angle rather than more positive as would be the case if the change in wing moment alone were considered. It may be concluded that the wing-alone moments are shifted positively, but the moments due to the tail are decreased so as to produce trim at a lower angle of attack.

The pitching moment curves with dive brakes at 0.30*c* indicate variables of considerable magnitude. Not only is there substantial change in trim but there is also shown a sudden change in slope, fortunately toward greater stability. There is undoubtedly a broadening of the wake region amounting to something near the maximum thickness of the wing—in this case about 1.25 in. This would then cause the tail to operate nearer to the center of the wake region. Likewise, the forward position of the brakes changes the pitching moments due to the wing alone. The variations can be attributed almost wholly to the change in flow conditions around the tail and to the change in wing-alone pitching moments. The proper apportioning of the total effect to each of the causes is a subject for additional research.

Only one more variable requires attention—the spanwise location of the dive brakes. It will be seen from Fig. 10 that movement of the brakes to one-half of a flap span outboard results generally in a vertical shift of the pitching moment curve with trim angle changed positively and with substantial parallelism in the low angle-of-attack range. This, in general, is indicative of some change in flow around the tail, though here again spanwise position may have some effect on wing-alone moments. However, it is doubtful that the change would be as large as is shown by the shift in the curves.

CONCLUSIONS

In review of the previous discussion and results the following conclusions can be made.

Airfoil Tests—Dive Brakes at Trailing Edge

(1) The dive brakes decrease the lift-curve slope in the low angle-of-attack range with little difference shown between perforated and nonperforated flaps.

(2) Increases in maximum lift for all brakes tested are indicated with the highest increase going to the nonperforated brake. Maximum lift occurs at a higher angle of attack with dive brakes extended.

(3) Considerable increase in drag for all types of flaps is shown. Slight variation may be found between perforated and nonperforated types.

(4) The pitching moments are shifted toward lower negative or higher positive values for all types of tests.

(5) The tail region is characterized by highly disturbed flow tending toward poor static longitudinal stability and severe tail buffeting.

Airplane Model Tests

(1) With dive brakes at the trailing edge the effects on lift are generally the same as for the airfoil tests. Moving dive brakes forward to 0.30*c* results in a lift curve of variable slope but never equal to the airplane-alone value. Maximum lift is reduced by the spoiler characteristics of the upper surface flap.

(2) Brakes placed forward on the wing are much more effective as a drag-producing device.

(3) The forward position of the dive brakes results in an expanded wake, thus making it more difficult to design for a tail position outside of this critical region.

REFERENCES

[1] Jacobs, Hans, and Wanner, Adolph, *DFS Dive-Control Brakes for Gliders and Airplanes;* Wanner, Adolph, *Analytical Study of the Drag of the DFS Dive-Control Brake*, N.A.C.A. T.M. No. 926, January, 1940.

[2] Fuchs, D., *Wind-Tunnel Investigations of Diving Brakes*, N.A.C.A. T.M. No. 1033, November, 1942.

[3] Landis, M. A., and Hermes, R. F., *Experimental Investigation of Air Brake Flaps*, University of Detroit Thesis No. 225, May, 1941.

Propeller Design Requirements*

H. M. McCOY†

Materiel Command, U.S.A.A.F.

SUMMARY

Functional requirements which have formed the basis for propeller development by the U.S. Army Air Forces in recent years are separately discussed in considerable detail.

The importance of feathering and reverse pitch with a maximum rate of pitch change of 45° per sec. is emphasized. Experiments show that reverse-pitch propellers are at least as effective in ground braking as the best wheel brakes. They are more effective than any known flap-type dive brakes in retarding aircraft in flight.

Air-line experience indicates an emergency feathering of the propeller to stop a damaged engine occurs every 3,000 engine-hours on the average. The full-feathering propeller is without doubt the most valuable single contribution in the past decade to safety in flight of multiengined aircraft.

Tracings are included of oscillograph records of propeller governing response to propeller and engine control changes for different types of governors and rates of pitch change. It is shown how improved governing to prevent overspeeding has permitted increasing engine ratings by 10 per cent during the past few years. Further developments in anticipatory governing promise to give an additional 10 per cent improvement.

It is pointed out that refinements in hollow steel blade design permit saving as much as 25 per cent in the weight of a given propeller. The effect of weight-savings of this magnitude on transports and military aircraft operation is illustrated by factual examples.

A survey is made of current experiments on propeller ice elimination, and attention is focused on the promise of pastes and thermal means to solve this difficult problem.

Numerous other items which must be included in a propeller design to make it successful are briefly discussed.

INTRODUCTION

THE BASIC FUNCTIONAL REQUIREMENTS for aircraft propellers which are the subject of this paper were compiled more than 5 years ago. These requirements were intended primarily for military applications, but experience has shown the desirability of adaptation of many of the features to private and commercial types of aircraft. The changes in the original specifications over the years have been mainly quantitative as shown by experience to be desirable or required. These requirements have formed the basis for propeller development sponsored by the Army Air Forces in recent years. Each major function will be treated separately in the following discussion. No attempt has been made to evaluate the relative importance of these items, so the arrangement is necessarily of little moment.

Presented at the Power Plants and Propellers Session, Twelfth Annual Meeting, I.A.S., New York, January 25-27, 1944.

* The views expressed in this report are those of the author and not necessarily those of the War Department.

† Colonel Chief, Propeller Laboratory, Engineering Division, Wright Field, Ohio.

COMPLIANCE WITH ESTABLISHED STANDARDS

There should be no changes necessary in any approved engine to accommodate a given type of propeller. Engine production is of such a nature that even a minor change takes many months to effect. The existing standards have stood the test of time and are adequate. The ideal propeller is entirely self-contained; it should not depend on an involved and often marginal engine lubrication system to furnish it operating or lubricating oil; preferably it should not require a separate governor drive.

It is fortunate that propeller shaft, governor drive, and engine nose end standards were firmly established in this country prior to this war. It has permitted the interchangeability of different types of propellers on the same or different airplanes as the production schedule demanded. The small weight penalty for interchangeability has been paid for many times over. This factor is considered absolutely essential to a production effort of the present magnitude.

It is not quite so important that the propellers for private and commercial aircraft meet military standards of interchangeability. The weight efficiency of the self-contained propulsive unit called the "power egg" must not be overlooked. There are many arguments in favor of this arrangement wherein the propeller shaft and pitch-change mechanism are integral parts of the engine or reduction gearing. An interesting modern example is found in the German BMW 800 series engines equipped with the VDM propeller and pitch-changing mechanism as used in the Focke-Wulf 190 pursuit and the Dornier Do 217 twin-engined medium bomber.[1] This engine also includes an integral gear-driven blower cooling fan. This compact arrangement may well form a farsighted example for postwar practice when aircraft are again built for a 5- to 7-year life and weight efficiency will pay more dividends than interchangeability. It is too inflexible for wartime use, however, because engine powers and critical altitudes are continually increasing every few months, requiring an extreme elasticity in propeller design which such an arrangement necessarily lacks.

Many promising propeller designs have failed to mature into production types because of dependence on a certain type of engine with special features to accommodate that particular propeller. It is sound judgment in designing a new propeller to make it fit the standards.

Feathering—Reverse Pitch

Any general propeller type that does not include full-feathering and reverse-pitch functions will soon be classed as obsolescent. The development of full-feathering propellers is without doubt the most valuable single contribution in the past decade to safety in flight of multiengined aircraft.[2, 3] The freedom from catastrophic vibration and performance increase over the windmilling propeller in partial-engined flight have been responsible for the safe return of military aircraft from many missions and have also saved many lives in transport operation. Large propellers capable of full feathering have been in general use in this country for more than 5 years. This feature will soon be available in several new types of propellers developed by the Air Forces for powers under 500 hp. Small multiengined private and feeder-line transport planes particularly need this feature because single engine performance is relatively poor because of the high power loading usually found in this class of airplane.

Emergency Feathering

A survey of feathering experiences of the airplanes in this country indicates that on the average an emergency feathering due to engine failure occurs approximately every 3,000 engine-hours. The major variables affecting this period between featherings include differences between types of airplanes and engines, length of overwater hops, distances between emergency landing fields, single-engined performance characteristics, and terrain features. Feathering periods vary from 2,000 engine-hours to 14,000 between air lines using the same equipment. Quality of maintenance, differences in operational procedure, and pilot experience evidently are additional factors that help to explain this wide variation. The period for precautionary featherings for indicated troubles such as high operating temperatures, low oil pressure, etc., is as low as 250 engine-hours for those airplanes where access may be had in flight to the rear engine compartment for minor repairs. It is significant that Pan American Airways' experience with the Boeing 314 flying boats shows that 85 per cent of engine troubles requiring feathering may be repaired during flight.

It is unfortunate that data cannot be presented at this time concerning the frequency of featherings on military aircraft. It will suffice, however, to point out that engine reliability would be expected to be reduced because of the higher normal and emergency engine ratings employed in military aircraft. Additional featherings can be expected from battle damage due to enemy action on both engines and propellers. The increased performance with feathered propellers over windmilling or braked propellers has saved many an airplane and crew by permitting flight at higher altitudes and sufficiently increased speed to maintain position in formation. At least one twin-engined military airplane is reported to operate most efficiently at extreme ranges by feathering the propeller on one engine.

It is imperative that full feathering be accomplished in a minimum of time. The worst flight condition requiring fast feathering occurs after engine failure during take-off. Feathering can be accomplished in 5 sec in some designs. New designs will feather in even less time. A windmilling propeller on a damaged engine occasionally causes such severe vibration of the instrument panel that it is difficult to determine quickly which propeller requires feathering. It is particularly difficult on four-engined airplanes. There is a current requirement for an automatic means to indicate the malfunctioning engine.

Braking

After a lapse of over 20 years, a need for reverse-pitch propellers has again arisen. The Air Forces experimented with this type of propeller as early as 1921 on a JN-4H airplane to obtain ground braking because airplane wheel brakes were not used at that time. Today's operation of fast-landing nose-wheel type aircraft from icy, wet, or muddy landing strips would be greatly improved with propellers capable of reverse-pitch operation. Large commercial aircraft and small "feeder-line" type transports will undoubtedly find braking propellers of great value. Recent Army Air Force experiments with reverse-pitch propellers on several classes of aircraft permit the following conclusions:

(a) Using full engine power for braking, reverse-pitch propellers with a fast rate of pitch change are just as effective overall as the best wheel brake installations in retarding the ground roll of aircraft. There is no danger of engine overheating for a full brake landing run lasts less than 20 sec.

(b) Reverse-pitch propellers are most effective at the higher speeds during the landing run.

(c) Wheel brakes will continue to be used to supplement reverse-pitch braking because they are most effective at low speeds and are needed for taxiing purposes. Substantial economies due to reduced tire and brake maintenance and replacement can be expected.

(d) Reverse-pitch propellers are more effective than any known flap-type dive brakes in retarding aircraft in flight.

(e) Propeller braking in flight by means of high-speed windmilling with closed throttle is not so effective as using engine power but is attractive because the geometrically higher blade settings used do not tend to windmill the propeller backward as is the case with the negative settings used in power braking.

Reverse-pitch propellers have been standard equipment for several years on some four-engined flying boat designs.[4]

The standard Swiss Escher Wyss propeller installed on a pursuit airplane is reported to be about twice as effective as wheel brakes alone in retarding the landing run.[5]

A short but excellent summary of the use of reverse-pitch propellers, with charts showing the various forces acting on the blade element for the two conditions commented on in conclusions (d) and (e) above, is found in a recent issue of *Flight*.[6] This reference contains an excellent bibliography to supplement references 4 and 5 above. Possible uses of reverse pitch include:

(a) Ground braking on all landplanes.
(b) Water taxiing for seaplanes.
(c) Air braking for use on dive bombers and night fighters.
(d) Offensive and defensive pursuit tactics.
(e) Defensive evasive tactics, particularly for lightly or unarmed observation and photographic type aircraft.

It is noted that full-feathering and reverse-pitch functions will require a total blade angle range of about 120°—from −30° to +90°. In this connection automatic pitch limit stops for both extreme positions and the normal constant speed range are a necessity.

Rate of Pitch Change

A maximum rate of pitch change of about 45° per sec. is desired for fast reversal of pitch and for fast feathering.

Experiments made in this country show that reverse pitch may be made at near full throttle conditions provided that a maximum rate of pitch change of about 45° per sec. is used. Engine overspeeding under these conditions is only momentary and does not exceed 10 per cent under static thrust conditions. German literature dated as early as 1939 also shows that a rate of pitch change of between 30° to 50° per sec. is required for reverse-pitch operation.[7] There is no evidence to date, however, to show that the Germans have achieved such a high rate in any production propeller. Their latest propeller has a maximum pitch-change rate of slightly less than 4° per sec. for full feathering and manual control.[1] The maximum rates of pitch change used for constant speed governing of available German propellers are quite low—averaging about 1° per sec. Judging from German production propellers, their development is several years behind that in this country from a functional standpoint.

The power required for changing pitch at such high rates as 45° per sec. for a four-bladed propeller for a 2000-hp. engine may vary from 10 to 20 hp., depending on the type of blade construction and mechanical efficiency of representative pitch-change mechanisms. Larger propellers that will be needed in the next few years will require 60 to 80 hp. for pitch change. Fortunately, pitch change at this high rate will endure for only a very few seconds. This leads to the conclusion that stored up energy in some form may be used to obtain the high rates or that recourse will be taken to using engine power directly by means of clutches or brakes.

The rate of pitch change possessed by a given propeller greatly affects its governing qualities. Governing is of increasing importance and is briefly discussed below.

Governing Problems

As much as 50 per cent of the total engineering effort in connection with the development of a given propeller design may be spent on governing and control problems. The importance of sensitive control is not generally understood outside of the propeller engineering fraternity. It is difficult to present many details of this problem in the short space allotted. It is hoped that the following general discussion will promote an appreciation of the detailed engineering involved in developing a sensitive control means to handle the tremendous forces dealt with in propeller operation.

Few laymen realize the magnitude of forces incident to the use of propellers. One production-type medium bomber is equipped with four-bladed propellers with each blade weighing 83 lbs. At take-off each blade tends to be thrown from the hub with a centrifugal force of about 70 tons, roughly equivalent to the combined weight of five fully loaded DC-3 transport airplanes. At this condition a net output of 65,000 lb.-in. of torque is required of the hub mechanism to increase the blade pitch. The wonder ever grows that such forces can be controlled so safely and so accurately.

Governor Control

It is desired for military use and necessary for air-line use that a propeller be capable of being governed approximately to one propeller r.p.m. This averages about one part in 1,500. It is necessary in order to accomplish this result to have, first, a governor capable of sensing this small deviation from a selected equilibrium speed and, second, a means to accomplish the extremely minute change in pitch necessary to bring the speed back to equilibrium. This fine control has been found necessary to avoid the "out-of-synchronism-beat" which is so objectionable from the vibration and physiological standpoint on multiengined aircraft. Present manually adjusted governors are capable of such sensitive performance.

This governing problem is at present being solved by the application of two relatively simple principles. Two American production propeller types that effect change of pitch by hydraulic means are governed by varying the *rate* of pitch change directly as a function of the offspeed variation in r.p.m. from a selected equilib-

rium value. Another type that changes pitch by electromechanical means governs by varying the *duration* of the pitch-changing impulse directly as a function of the offspeed variation. The rate of pitch change in this latter case may be considered constant if the transient periods before the pitch change motor gets up to rated speed are neglected. A minute pitch change is effected by closing the motor circuit switches for only a fraction of a second. The greater the offspeed variation, the longer the duration of the pitch change. The first may be called "rate proportionalizing" and the second "time proportionalizing." The two types of governing are equivalent providing the maximum rates of pitch change are equal.

Rate of Pitch Change

A one-degree change in blade angle on a small two-blade propeller for a direct-drive engine of about 200 hp. will cause a speed change of from 70 to 90 r.p.m. at full throttle. The same blade angle change on a large four-blade propeller for a geared supercharged engine will change the engine speed several hundred r.p.m. On a propeller load curve a small unsupercharged engine may accelerate 500 to 700 engine r.p.m. per sec. A large engine with gear-driven supercharger may accelerate 1,000 to 1,200 r.p.m. per sec. Although the average propeller has a large polar moment of inertia compared to the inertia of rotating and reciprocating engine parts, the acceleration on modern engines is so great that the prevention of overspeeding puts a demand on the governing system which is difficult to meet. To prevent serious overspeeding when emergency application of full power is made from a closed throttle position, as often occurs in military combat flying and during landing approaches, it has been determined that a 6° per sec. rate of pitch change is sufficient. Figs. 1 to 8 are partial traces of data taken from recording oscillograph records recently made at Wright Field. Newly developed equipment was used which for the first time has permitted the full evaluation of all factors affecting engine acceleration and propeller governing for all types of engines and propellers. These data are so unusual that it is worth while to discuss them briefly. Some of these tracings are from records obtained during flight and some are from test stand operations. Many pertinent records, such as torque meter pressures, "in" and "out" governor oil pressures, relay contact closing and opening times, blade angle, motor current, etc., have been deleted in order to simplify the drawings. Only data pertinent to this discussion are shown.

All of Figs. 1 to 8 inclusive are plots of engine speed, governor control, and throttle control positions against time. Only Figs. 7 and 8 have blade angle readings added. The time scale is as shown on each figure. Figs. 1 to 4 inclusive are concerned with the propeller on a medium bomber. Several thousand bombers of this

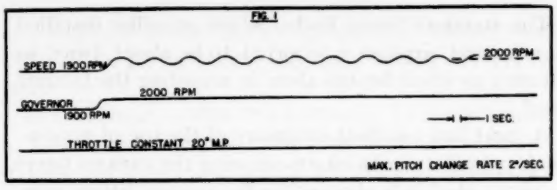

FIG. 1. *Undamped governing* {governor change / throttle constant

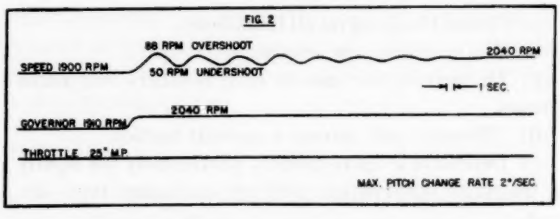

FIG. 2. *Underdamped governing* {governor change / throttle constant

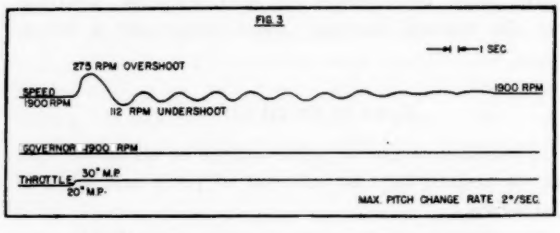

FIG. 3. *Underdamped governing* {governor constant / throttle change

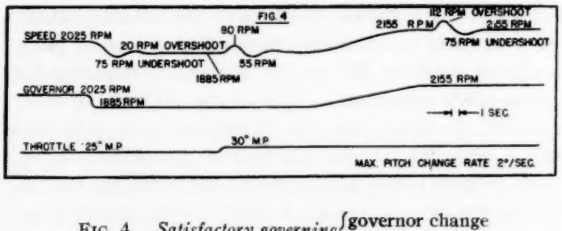

FIG. 4. *Satisfactory governing* {governor change / throttle change

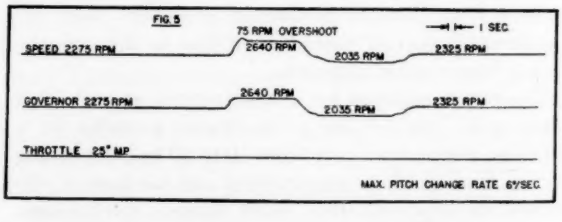

FIG. 5. *Excellent governing* {governor changes / throttle constant

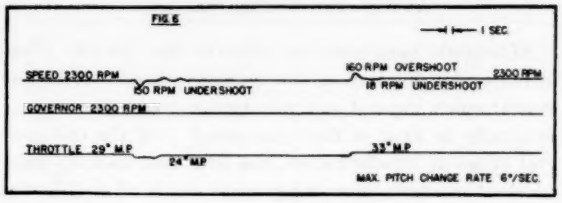

FIG. 6. *Excellent governing* {governor constant / throttle changes

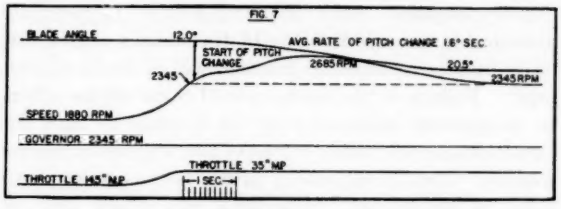

FIG. 7. *Unsatisfactory governing* (excessive overspeeding) {governor constant / throttle advanced from "idle"

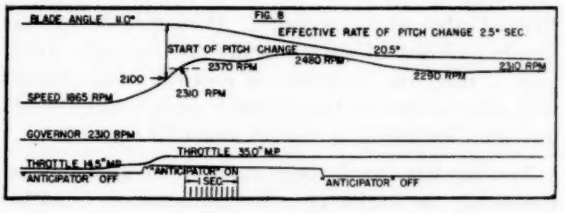

FIG. 8. *Anticipatory governing* (allowable overspeeding) {governor constant / throttle advanced from "idle"

design had been in service with satisfactory propeller operation when the engine rating was increased by nearly 10 per cent with no other change than increased manifold pressure. It was necessary to use the same propeller. On the first installation the propeller hunted badly whenever there was a governor change as shown in Fig. 1. Minute changes were made in the governor throttling valve clearances leading to the slightly improved governing as indicated in Figs. 2 and 3. However, oscillations induced by either a governor or throttle change still took over 30 sec. to dampen out. One more small change involving a simple milling cut in the control valve provided enough damping to give the barely satisfactory governing depicted in Fig. 4. Without precision recording oscillograph equipment this problem could only have been solved by extensive cut-and-try methods. Similar troubles had been experienced before, but an adequate explanation of the causes and cures had never been made. It was determined that the increase in engine power had provided more torque for acceleration of the engine. The marginal damping on the earlier installation was inadequate to compensate for this condition of higher acceleration due to the greater engine torque. Not until the damping factor was increased by the simple changes in the governor valve was satisfactory performance obtained. Note that the propeller of Figs. 1 to 4 had a maximum rate of pitch change of only 2° per sec. It will be shown later that rates of pitch change of this order are insufficient to prevent overspeeding with sudden throttle advances to full power. However, this rate of pitch change is adequate for all flight maneuvers and normal throttle applications.

Figs. 5 and 6 show excellent governing on a single-engined pursuit airplane. Here the maximum rate of pitch change is about 6° per sec., and overspeeding even with rapid throttle advance is of small value and of extremely short duration. The damping in the governor of this propeller has a high value. This governor is not so sensitive as those with a lower maximum rate of pitch change. It is extremely difficult to make governing with high rates of pitch change compatible with desired sensitivity. This problem is a challenge to the industry and will probably not be entirely satisfactorily solved until "anticipatory" controls are fully developed.

Anticipatory Governors

It was explained how the "proportionalizing" type governors simply vary the rate of pitch change or its equivalent as a function of the offspeed variation in r.p.m. from an arbitrary equilibrium setting. Those governors that additionally measure accelerations of the engine, regardless of whether the engine is under or over speed, are called "anticipatory." Examination of Figs. 1 to 7 will show that the blade angle does not change with the proportionalizing type governors until a fraction of a second after the engine speed has reached the equilibrium setting. Because of time lag in the pitch-change mechanism and the high acceleration of the engine, some overspeeding is thus bound to occur. This can be minimized by using an anticipatory governor. Fig. 7 shows records taken with a proportionalizing type governor on a large engine installed on a test stand. The governor was set for 2,345 r.p.m. With the throttle cut back, the engine was running at 1,880 r.p.m. with the blade angle at 12°. As the throttle was rapidly advanced to 35 in. manifold pressure, the engine overspeeded 340 r.p.m. to 2,685 r.p.m. Note that the pitch did not start to change until a fraction of a second after the engine speed had passed the equilibrium setting of 2,345 r.p.m. Also note that the average rate of pitch change is 1.6° per sec. Fig. 8 shows the results obtained under practically identical conditions to those of Fig. 7 except that an electronic anticipatory device was added. This device was developed at Wright Field. As the engine initially accelerated, the pitch was caused to change to slow down the engine momentarily, even though the engine was not yet up to equilibrium speed. This occurred at 2,100 r.p.m. and the equilibrium setting was 2,310 r.p.m. This early change of pitch gave an effective rate of pitch change of 2.5°

per sec., with overspeeding cut down to 170 r.p.m. or a maximum speed of 2,480 r.p.m. Contrast this to the rate of 1.6° per sec. and 340 r.p.m. overspeed for the conditions of Fig. 7. Several types of anticipatory governors have been under development for several years.

Prevention of Overspeeding

The prevention of overspeeding is a most valuable contribution of the propeller industry to increased engine performance. Because all engine designs are limited to a maximum permissible r.p.m., any device that reduces overspeeding is extremely valuable, for it permits increasing normal engine ratings until they approach the maximum permissible, often called the "dive ratings." A few years ago normal engine r.p.m. ratings were 30 per cent under the dive ratings. Because of improved constant speed governing, this differential is now only 20 per cent, and it is hoped that future improved governing methods will further reduce it to below 10 per cent.

It is apparent from examination of Figs. 1 to 8 that it is not necessary to have a pitch change rate of more than 6° per sec. for excellent governing; yet it is necessary to have a maximum rate of about 45° per sec. for reverse pitch and feathering operations. A simple proportionalizing governor, whether of the "rate" or "time" type, does not inherently possess sufficient damping qualities to permit satisfactory and sensitive governing much above 6° per sec. Those propellers with a 45° per sec. maximum rate of pitch change which are capable of continuously varying the rate from 0° to 45° per sec. must contain adequate "follow-up" or "compensating" mechanisms to provide the equivalent of damping for rates above 6° per sec. A suggested solution to this difficult governing problem would be to have two ranges of rate of pitch change with the lower range from 0° to 6° per sec. for constant speed governing purposes and the high rate of 45° per sec. for fast reverse pitch and feathering.

New governing problems, in addition to those discussed above, continually present themselves. Experiments with reverse-pitch propellers have shown the desirability of governing while in reverse pitch for both the flight and ground braking conditions. The pilot is already loaded with too many instruments to watch and duties to perform. The operation of an airplane under any condition with the propellers in reverse pitch requires that undivided attention be given to the airplane controls. It is desired to use full engine power for propeller braking. Without governing in reverse pitch, full power can only be used at one forward velocity. Reverse-pitch governing permits taking full advantage of optimum braking thrust at all velocities. It greatly simplifies the operation of going into and back out of reverse pitch without the special attention of the pilot to the engine instruments. The pilot demand for this feature is unanimous.

Automatic Synchronization

Automatic synchronizing relieves the already overworked pilot of a tedious but necessary task. With one synchronizer control any number of engines can automatically be kept at the same speed. Of the two general types of synchronizers, the one that uses an independent master source of r.p.m. to which all engines are matched has more advantages than the type that uses one engine as a "master." A more reliable and usually a lighter installation can be had with the former. When one engine is used as the master, the others are called "slave" engines. Such an arrangement is normally undesirable because hunting of the master engine due to ignition or carburetion troubles will make all engines hunt. Failure of the master would cause all the others to dangerously reduce r.p.m. It is usual to have the choice of selecting either of two of four engines as master sources. This is necessarily heavy because equipment must be duplicated. Experience has shown that an independent constant-speed master source can be made very reliable. It is usually placed in a central location remote from engine vibration where it can be directly controlled by the pilot. It may be placed in the supercharged cabin when necessary. Protective devices are simply included to automatically and instantly disengage it from the propellers it controls. Installations with direct control of the propeller pitch usually weigh less than individual governors manually controlled.

Mention has already been made of the need for synchronizing the engine-propeller combination to within one propeller r.p.m. On a bi-motored airplane out-of-synchronism is readily corrected by ear by changing the speed of either engine. Synchronizing by ear is impracticable with three or more engines. Automatic synchronizers for one type of four-engined airplane have been standard equipment for some time. Several satisfactory synchronizing methods have been developed which can be used to control the pitch of the propellers directly, or by the use of servo motors attached to the governors, to keep the latter in automatic adjustment. Automatic synchronization should come into more widespread use in the future when full realization of its advantages becomes more widely appreciated. A fairly complete bibliography of pertinent constant speed control references is cited for those individuals whose interest may have been aroused in the manifold problems met in propeller governing and synchronizing.[8–12]

Design Factors Affecting Weight

It is said that a pound of weight saved in a large airplane is worth its weight in gold. This can readily be proved statistically.[13] Weight is most readily saved in items of fixed equipment. Propeller weights between different designs probably vary more than any other major fixed item. The main source of weight-saving

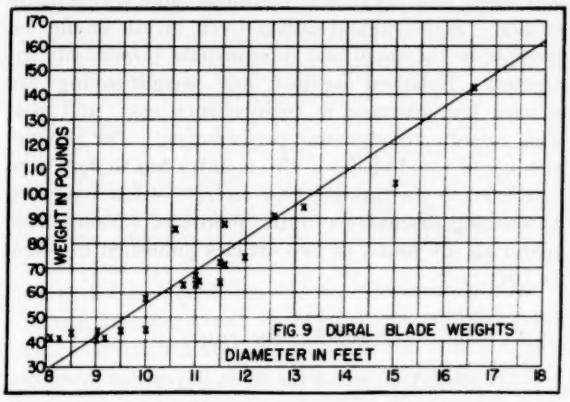

FIG. 9. Dural blade weights.

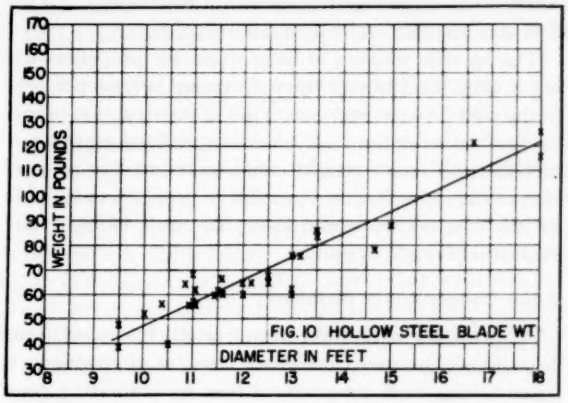

FIG. 10. Hollow steel blade weights.

in a propeller is in refinement of blade design. Fig. 9 shows a curve of dural blade weights versus diameter. Fig. 10 is a similar curve of hollow steel blade weights. The weight variation in either chart for a given diameter is mainly due to the difference in critical altitudes for which the blades are designed to operate. The higher the altitude, the wider the blade and, hence, the greater the weight. The curves are representative of propellers for medium altitudes and provide average values for preliminary weight estimates. In order to estimate, roughly, dry assembled propeller weights, less controls, take the chart blade weight, multiply by the number of blades, and then divide by the percentage factor given in Table 1 below for the selected type of propeller.

TABLE 1

Six-blade dual rotation (hollow steel)	0.50
Four-blade hollow steel	0.57
Four-blade dural	0.62
Three-blade hollow steel	0.54
Three-blade dural	0.56
Two-blade dural	0.52

Blade Material

Hollow steel blades are at least equivalent in every respect to dural. They generally weigh less in diameters above 10 ft. because of the nature of their construction. Being hollow, the metal is better distributed to withstand the complex loads imposed in flight. The percentage use of steel blades is steadily increasing.

Based on present knowledge it is unlikely that any construction other than hollow metal will be used in this country for the large diameters. The use of steel blades permits additional weight-savings in the hub because of reduced shank sizes. However, the pitching moments are generally higher so that the pitch-changing mechanism usually weighs slightly more than with dural blades.

Types of Blades

There are at present four production types of hollow steel blades in use in this country. They are all made by widely different methods. There is considerable variation in weight between hollow steel designs in large diameters. Everything else being equal, there is considerable economic and military advantage to be gained in the use of the lightest blades. It is believed the following factual example will be of interest. Two competitive propellers, A and B, having hollow steel blades, are suitable for use on a large four-engined transport. Propeller A (1,000 lbs.) weighs 200 lbs., or 25 per cent more than B (800 lbs.). The propellers are aerodynamically equivalent except that blade B is 1 per cent less efficient in cruising. The total weight-saving using B is 800 lbs. per airplane. At 75 per cent load capacity that saving would be expected to return about $90,000 in revenue yearly. The gasoline weight-saving due to difference in cruising efficiency is calculated to be 240 lbs. per 10-hour flight, or $27,000 in favor of A per year. The cost of the gasoline saved using A is $3,000 annually. The net revenue advantage of the lighter blade B is therefore $60,000. It is evident that the airline can afford to pay considerably more for propeller B than for A and still make a profit. By the same token the designers of blade B could afford to spend more engineering effort in refining the design.

Value of Weight-Saving

It is extremely difficult to evaluate the worth of large units of weight saved in military aircraft. With the extensive damage wrought by the U.S. Army Air Forces' precision daylight bombing, it must be many times that saved in air-line operation. Perhaps it may most readily be evaluated in terms of man-hours.[14] If the airplane in the example above was a bomber rather than a transport, the propeller weight saved would be 2 per cent of the average bomb load. That means 2 per cent fewer airplanes, crews, gasoline, etc.,

could be used for a given amount of destruction. This is of considerable and calculable value.

The specific weights of large diameter propellers using hollow steel blades have decreased several per cent in the past 5 years, and new types of construction promise further reduction. If all items of fixed equipment including air-frame weight could be reduced in proportion to the reduction now possible in propellers available in this country we would have the most efficient aircraft it is possible to build.

Pitch-Change Power Required

As propeller sizes and rates of pitch change continue to increase, the power necessary to effect pitch change is approaching such proportions that in evaluating competitive designs recognition must be given to the weight of fuel burned in generating this power. It is noted that all the power must originate in the engine regardless of the form in which it is applied to the propeller pitch-change mechanism. It is significant that contemporary propellers with "rate" type proportionalizing governing expend about four times as much energy as those types with "time" proportionalizing. The former are usually hydraulic types that maintain a continuous maximum operating pressure past a relief valve whether or not the propeller pitch is being changed. The latter operate only about 18 per cent of the time but have other losses while operating to make up the 4-to-1 difference. Future designs of the "rate" type using hydraulic pitch-change means should provide variable displacement pumps of the "demand" type or use unloading valves.[15]

The Aeroplane in July, 1941, published two interesting articles concerning specific propeller weights.[16, 17] In general, the British experience closely follows that in this country. Specific weights tend to decrease slightly with increase in engine power, other factors being equal. American experience shows that specific weights have decreased steadily during the past decade until the lightest designs today weigh in the order of 0.25 lb. per hp. for take-off powers. This trend should continue as new and improved methods of blade construction are developed.

Wooden Blades

The topic of wood materials for blades deserves some comment. Wood is used quite extensively in the British Isles where operating and climatic conditions are favorable. The high strength-weight ratio of wood materials is responsible for the continued consideration of their use under favorable operating and installation conditions. However, some mechanical and physical properties compare unfavorably with metals, particularly with regard to uniformity of material, moduli of elasticity, resistance to abrasion, and moisture absorption. The last two deficiencies make the use of wood undesirable in many localities throughout the world where there are extremes of temperature and humidity and where local operating conditions cause severe blade erosion. Some weight-saving over metal should be possible in the small and intermediate powers and diameters. Balanced against any weight-saving are shorter life, increase in maintenance cost, and possible inferior aerodynamic performance. The production use of wood blades in this country has to date been restricted to the training type aircraft of lower powers. Interesting discussions of the merits of various blade materials are found in two articles published in *Flight* in 1941.[18, 19]

Ice Elimination

This subject is one of the most important in connection with propeller operation. Without adequate anti-icing provisions on a propeller, safe flight through all weather conditions is not possible. The standard alcohol slinger ring method used the past several years with so much success has about reached the limit of usefulness as propeller diameters grow larger and propeller rotation speeds become slower. All ice elimination means depend heavily on centrifugal force to aid in removing the ice. It is increasingly difficult to get good blade coverage with alcohol on the larger, slow-turning propellers. The feed shoes and distribution system require continual maintenance. Alcohol cannot be used in combat areas because of the fire hazard.

Electrical Deicing

There has been considerable development in both Canada and this country during the past few years on electric hub generators. In this system conductive rubber heating elements are cemented to the blades somewhat in the manner and appearance of the old alcohol feed shoes. Current is supplied these elements from an armature attached to and rotating with the propeller hub. The stationary field bolted to the nose of the engine is energized from the airplane battery and can be controlled to provide any quantity of heat within its capacity. This is a fairly heavy system with weights comparable to the conventional complete alcohol system. Its use is unlimited in contrast to the alcohol system with its restricted tank capacity. This method of ice elimination is sufficiently effective, based on present knowledge. The heating elements are susceptible to cutting and erosion and create a maintenance problem not unlike the alcohol feed shoe. The adaptation to four-bladed propellers poses several problems. As propeller r.p.m.'s decrease, so will the weight efficiency of the generator, until finally a weight will be reached that is uneconomical. At this point electrical heating by means of slip rings may enter the picture. Energy will undoubtedly have to be furnished by an auxiliary engine. Large propellers will each require several thousand watts energy, which would be beyond the capacity of the normal aircraft electrical system to handle.

Pastes and Lacquers

Experiments and service trials with anti-icing pastes and lacquers readily applied and removed from the blades show considerable promise of eventually providing protection as good as any yet obtained by any other means. Their life and effectiveness have not yet been fully determined. It appears possible eventually to develop a preparation or applied finish that will have an effective service life of up to 50 hours. These means fall into two general classes. Those compounds that contain ingredients to lower the freezing point are named freezing point depressant compounds. Other types of finishes attempt to lower the adhesion shear values of the ice, permitting centrifugal force to clear the blade of ice periodically as soon as a sufficient thickness collects to be affected by centrifugal force.

Thermal Deicing

It is possible in the future that some thermal method other than the electric ones described may provide the most satisfactory and universally efficient solution to this vexing problem. Vast quantities of unused heat are continuously being dissipated from the engine exhaust. Preliminary experiments promise that it will some day be feasible to use engine exhaust energy through heat exchangers in connection with hollow steel blades for ice elimination purposes. This system would be available continuously throughout the entire flight period.

The successful solution of this general propeller ice elimination problem is of immediate importance. At the present time it does not look to be as close to solution as that for the wing and control surfaces. It is a much more difficult problem and more effort will have to be expended. Any new propeller design should be flexible enough to permit using whichever method of anti-icing proves to be the best.

Dual-Rotation and Hollow Hub Propellers

Several military airplanes require that the propeller installation permit firing a cannon through the hub. Any new design should provide for this feature. Of necessity the pitch-change mechanism for such an installation must be arranged around the hub in some workable manner, and this feature permits the adaptation of the pitch-change principle for dual-rotation by supplying intergearing or intercontrols between the inboard and outboard propellers. A discussion of dual-rotation (counterrotating) propellers with an extensive bibliography is found in the June, 1940, *Journal of The Royal Aeronautical Society*.[20] The use of dual-rotation propellers is restricted to date to experimental airplanes, but the manifold advantages of such a propeller arrangement should cause more widespread use in the future. In order to completely balance out all torque effects with dual-rotation propellers, a selective controllable-pitch differential should be provided between propellers. This is fully discussed in reference 20.

The dual-rotation arrangement wherein the propellers are each driven by a separate engine and the governing, feathering, and reverse-pitch controls are independent is occasionally referred to as "divorced dual-rotation." It is interesting that the first recorded flight of such an arrangement, but without controllable propellers, was that of Hirth in February, 1912, near Berlin, Germany, in a Loutzkoy monoplane with two 100-hp. Argus engines each separately driving a tractor propeller.[21] This reference contains a most interesting bibliography on the earliest tandem and counterrotating propellers to supplement that of reference 20.

Pitch Lock

It is desired in case of damage to the propeller pitch-change mechanism or failure of the governing system that the blades lock at the operating pitch at the instant of failure. This permits continuing flight at whatever condition the malfunctioning occurred and is a safety feature of considerable merit. In this connection auxiliary direct manual control of the blade pitch should be provided. This should include switching means for shifting from automatic constant-speed operation to manual selective pitch control at the option of the pilot. This permits periodic checking of engine operation and is particularly valuable during long flights. Carburetor icing can be readily detected when operating in locked pitch in those airplanes with engine induction systems susceptible to such icing. A pitch lock is often convenient for flight-test purposes, when the propeller design does not include a pitch indicator, because it permits measurement of the blade angle after landing.

Those familiar with the art know that rotating propeller blades if unrestrained and not counterbalanced will immediately lower against the low pitch stop. Some types of propellers have only a hydraulic pressure restraining the blades against this negative blade twisting moment. When for any reason the hydraulic pressure fails, the blades hit the low pitch stop, and with the throttle retarded the propeller overspeeds an amount that is a function of the airplane's velocity. Such propellers for safety reasons should automatically go to high pitch or seek some relatively high-pitch equilibrium setting to prevent overspeeding. Otherwise it is necessary to feather the propeller, losing the use of what might be an active engine.

Miscellaneous Requirements

There are several other operational demands that a given propeller design must meet. Most of them are important to insure successful operation under all operating conditions that may confront the propeller

Others are desirable and so obvious that they will be mentioned only with a minimum of discussion.

Lubricating and Actuating System

The propeller lubricating and actuating system should be self-contained. This permits operation of the propeller entirely independent of the engine and its oil system. It is mandatory that the propeller function properly to feather in case of engine failure. The propeller must control satisfactorily under all conditions of engine operation.

All bearings, gears and running parts should be 100 per cent enclosed and lubricated.

Great care must be taken to eliminate loss of lubricant from the propeller hub. Oil leakage with quantities as low as 1 oz. per hour have been known to cloud dangerously and fatally the windshield of single-engined aircraft. It is common test procedure at Wright Field with new designs to cover the entire hub and blade shanks with a dry whiting compound. Wetting is cause for rejection on experimental hubs until the sealing is satisfactory.

All pitch-change mechanism and running parts if exposed must be sealed against dust and sand. Dust-proof spinners have been found to pay for their weight in decreased maintenance in many instances.

Operation in feathering, unfeathering, and constant speed control is required over an ambient temperature range of $-65°$ to $+160°$ F.

Mounting and Dismounting Accessories

Ready dismounting of the propeller from the engine as a complete assembly is desirable. Quick disconnectors for both electrical and manual cockpit controls are helpful. A carefully engineered design should require no special tools for field dismounting and a minimum for shop disassembly,

The hub design must include means for attaching and supporting spinners and possibly cooling fans. Provision must be made where applicable to mount electrical hub generator parts for anti-icing. If other anti-icing means, such as alcohol slinger rings, are used, provision must be made for suitable attachment. Suitable means must also be provided for ice elimination from the spinner. The spinners should preferably be of the quick-detachable type, requiring no more than a screw driver for attachment and removal.

The blade design should provide for shank fairings or cuffs. These are required for radial engine cooling and for reduction of aerodynamic drag on in-line engine applications.

Propellers that derive their energy for pitch change as a result of rotation of the propeller must have auxiliary means to complete the feathering and unfeathering cycles. This also permits checking propeller operation on the ground with the engine stopped.

Slip rings should be avoided on propellers whenever possible. If it is desired to use an electric motor for pitch change, differential gearing can be used to permit placing the pitch-change motor on the stationary engine nose. All electric motors and controls must meet applicable specifications with regard to elimination of radio interference.

A reliable pitch indicator is strongly recommended. It is valuable for flight testing and, in normal operation, provides a constant reference for checking propeller and engine operation.

Test Requirements

A few words concerning test requirements seem pertinent here. After designing and building a propeller to perform the functions discussed above it must successfully pass substantially the following tests:

Electric Motor Whirl Rig	Miscellaneous calibrations		9 hrs.
	Endurance testing, 200% power		20 hrs.
	Overspeed test	100–200% power	
		132–143% overspeed	1 hr.
	Total		30 hrs.
Engine Test	Vibration analysis (miscellaneous)		5 hrs.
	Rated power and r.p.m.		50 hrs.
	Power and r.p.m. for greatest blade stress		50 hrs.
	Take-off power and r.p.m.		10 hrs.
	1,500–3,000 control cycles		10–20 hrs.
	Total		125–135 hrs.
Flight Test	Vibration analysis (miscellaneous)		5 hrs.
	Control Tests (miscellaneous)		5–10 hrs.
	Total		10–15 hrs.

If the propeller successfully passes these tests and if tear-down inspection shows no major faults, the propeller could be expected to be released for limited or service test production. In lieu of the specified tests a background of 1,500 hours of flight operation may be substituted.

To the uninitiated the many functions discussed above may seem impossible to attain. Propellers capable of meeting practically all of these rigid specifications are, however, in the last stages of development. It can be expected that as new requirements develop the propeller art will continue to meet their challenge.

Conclusions

An aircraft propeller should be capable of performing the functions and meeting the requirements listed below:

(1) Compliance with propeller and engine standards.

(2) Self-contained propeller assembly and oil system independent of engine.

(3) A maximum rate of pitch change of about 45° per sec. for reverse pitch and feathering.

(4) A pitch range from −30° to +90°.

(5) Adequate ice-elimination means for both blades and spinners.

(6) Proportional governing and automatic synchronization to one propeller r.p.m.

(7) Anticipatory governing control is desirable.

(8) Automatic constant speed governing in reverse pitch.

(9) Provision for hollow steel blades.

(10) Proper operation over an ambient temperature range from −65° to +160°F.

(11) Automatic blade pitch locking means.

(12) Auxiliary manual control when in fixed (locked) pitch.

(13) Hollow hubs on single-rotation propellers to permit cannon fire.

(14) Dual-rotation (counterrotating) hub and pitch-change mechanism incorporating selective differential pitch for torque balance.

(15) Auxiliary pitch-change means for unfeathering on those propellers deriving their pitch-change energy as a result of propeller rotation.

(16) Variable displacement "demand" pumps or unloading valves on hydraulic propellers.

(17) Slip rings should be avoided on electric propellers.

(18) Radio interference must be avoided with electric motors, controls, and auxiliary equipment.

(19) No external oil leakage.

(20) Attaching and supporting means for spinners, cooling fans, and ice-elimination equipment. Quick detachable spinners and controls.

(21) All bearings, gears, and running parts enclosed and lubricated.

(22) Automatic pitch limit stops.

(23) Pitch indicator.

(24) Provision for blade shank fairings or "cuffs."

(25) A maximum number of parts interchangeable between sizes and types of propellers, and special tools kept to an absolute minimum.

References

[1] *VDM Propeller Pitch Changing Mechanism*, Automotive and Aviation Industries, pp. 40 and 41, February 15, 1943.

[2] McCoy, H. M., *Full-Feathering Propellers*, Journal of the Aeronautical Sciences, Vol. 5, No. 7, pp. 253–259, May, 1938.

[3] Beard, M. G., and Fuller, E. W., *Feathering Propellers in Airline Transport Operation*, SAE Journal, Vol. 45, No. 3, pp. 372–384, September, 1939.

[4] Chillson, C. W., *Reversible Pitch Propellers as Applied to Water Handling of Multi-Engine Flying Boats*, Journal of the Aeronautical Sciences, Vol. 7, No. 7, pp. 269–275, May, 1940.

[5] Switzerland: Escher Wyss c.p. Airscrew, Excerpt from Inter Avia No. 848–849, December 21, 1942.

[6] Mullin, J., *Reversible-Pitch Airscrews*, Flight, pp. 284 and 285, September 9, 1943.

[7] Schmidt, K. A., *Fundamental Problems of Controllable Pitch Propeller Technique with Consideration of Principal German Designs*, Luftwissen, pp. 267–273, October, 1939.

[8] Hazen, H. L., *Theory of Servo-Mechanisms*, Journal of the Franklin Institute, Vol. 218, No. 3, September, 1934.

[9] Trinks, W., *Governors and the Governing of Prime Movers;* Constable & Company, Ltd., London, 1919.

[10] Weiss, Herbert K., *Constant Speed Control Theory*, Journal of the Aeronautical Sciences, Vol. 6, No. 4, pp. 147–152, February, 1939.

[11] Weiss, Herbert K., *Dynamics of Constant-Speed Propellers*, Journal of the Aeronautical Sciences, Vol. 10, No. 2, pp. 58–67, and 70, February, 1943.

[12] Oppelt, W., *Comparison of Automatic Control Systems*, N.A.C.A. T.M. No. 966, February, 1941, and Supplement, August, 1941.

[13] Ayers, John E., Sr., *The Value of a Pound Saved by Weight Control*, Part 1, Aero Digest, October, 1942; Part 2, Aero Digest, November, 1942.

[14] Masefield, Peter G., *London Survey*, Flying, September, 1943.

[15] Smith, G. Geoffrey, *Evolution of the Variable Pitch Airscrew*, Flight, August 14, 1941.

[16] Gillmore, K. B., and Cleaver, A. V., *Airscrew Weight—I*, The Aeroplane, pp. 70–72, July 18, 1941.

[17] Gillmore, K. B., and Cleaver, A. V., *Airscrew Weight—II*, The Aeroplane, pp. 105 and 106, July 25, 1941.

[18] Gillmore, K. B., *Airscrew Blade Materials*, Flight, pp. 167–172, September 18, 1941.

[19] Chown, W. R., *The Case for Wood*, Flight, pp. 365–367, November 20, 1941.

[20] McCoy, H. M., *Counter-Rotating Propellers*, The Journal of The Royal Aeronautical Society, Vol. XLIV, No. 354, pp. 481–498, June, 1940.

[21] Weyl, A. R., Letter, The Journal of The Royal Aeronautical Society, pp. 677 and 678, August, 1940.

A Theorem on the Shearing Stress in Beams with Applications to Multicellular Sections

J. N. GOODIER*
Cornell University

ABSTRACT

The methods in use for the calculation of the flexural shearing stress in wing beams of multicellular section are rigorously examined by means of the Saint-Venant theory of flexure and torsion. It is shown that the line integral of the shearing stress around a cell does not, in general, vanish as has been supposed. Its value is found in a simple form. The effect on the magnitude of the shearing stress is calculated for several examples and found small for certain one-, two-, and three-cell sections. Solutions of the flexural shear stress problem are given for rectangular cell sections of one, two, three, and any number of equal cells, with flange areas.

INTRODUCTION

THE SHEARING STRESSES in beams of multicellular section are at present calculated by means of equations of the form

$$\int \tau \, ds = 0 \tag{1}$$

for bending and

$$\int \tau \, ds = 2GA_c\theta \tag{2}$$

for torsion, or torsion combined with bending. Here $\int \tau \, ds$ represents the line integral of the shearing stress taken around a closed curve C in the cross section of the beam, A_c is the area enclosed by this curve, G the shear modulus of the material, and θ the twist per unit length.

Eq. (2) is undoubtedly true for pure torsion. It represents, in the Saint-Venant torsion theory, the condition that the axial displacement is a single-valued function of position in the cross section. It appears to have been incorporated into methods for calculating shearing stress in combined bending and torsion without proof that it holds beyond the conditions of pure torsion. It has been used for cases of pure bending,† and for the determination of the shear center, simply by putting $\theta = 0$, when it reduces, of course, to Eq. (1). Eq. (1), for pure bending of thin-walled hollow beams, was derived by Hatcher[1] from minimum energy considerations.

In the present paper it is shown that Eq. (1) is not true for pure bending, and an explanation is offered for the failure of Hatcher's proof. It follows at once that Eq. (2) is not true for combined bending and torsion. The correct forms of the equations are found to be

$$\int \tau \, ds = [\mu/(1 + \mu)]A_cL \tag{3}$$

for pure bending and

$$\int \tau \, ds = 2GA_c\theta + [\mu/(1 + \mu)]A_cL \tag{4}$$

for combined bending and torsion. Here μ is Poisson's ratio and L represents $(F_1\bar{y}_c/I_1) - (F_2\bar{x}_c/I_2)$, where F_1, F_2 are the components of the shear force on the section, in the directions of principal co-ordinate axes x, y (Fig. 1) through the centroid of the section; I_1, I_2 are the moments of inertia of the whole section about the y- and x-axes, respectively; and $\bar{x}_c$, $\bar{y}_c$ are the coordinates of the centroid of the area A_c within the curve C round which the line integral is taken. C may be any curve in the material cross section. A form of the result applicable to nonprincipal axes is given in a latter section.

The proof will be based on Saint-Venant's theory of flexure.

THE FLEXURE PROBLEM OF SAINT-VENANT

Consider a uniform cantilever beam (Fig. 1). The axis of z is the axis of centroids of cross sections, and Ox, Oy are taken along the principal axes of a section at the centroid, forming, with Oz, a right-handed set of axes. The origin of z, however, is not at O but at some fixed section to the left of the section containing O.

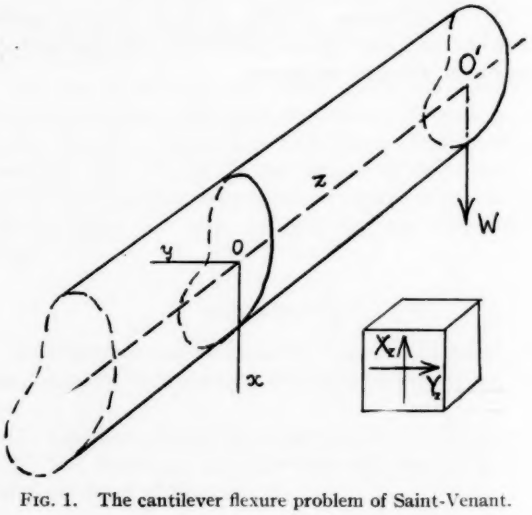

FIG. 1. The cantilever flexure problem of Saint-Venant.

Received September 8, 1943.

* Professor in Charge, Department of Mechanics of Engineering, Sibley School of Mechanical Engineering.

† "Pure bending" here means bending without torsion.

The cantilever is loaded by a force W parallel to Ox and passing through the centroid O' of the end section at $z = l$.

This is the flexure problem of Saint-Venant. Its solution yields expressions for the components of shear stress X_z, Y_z on the section in the forms[2]

$$X_z = \mu\tau\left(\frac{\partial\phi}{\partial x} - y\right) - \frac{W}{2(1+\sigma)I_1}\times \left[\frac{\partial\chi}{\partial x} + \frac{1}{2}\sigma x^2 + \left(1 - \frac{1}{2}\sigma\right)y^2\right] \quad (5)$$

$$Y_z = \mu\tau\left(\frac{\partial\phi}{\partial y} + x\right) - \frac{W}{2(1+\sigma)I_1}\times \left[\frac{\partial\chi}{\partial y} + (2+\sigma)xy\right] \quad (6)$$

The changed notation employed here is that of Love,[2] whose account of the Saint-Venant flexure theory is particularly appropriate for the purpose of this paper. Retention of his notation facilitates reference to the basic equations. Some of the results are translated into the customary American notation later.

In these formulas μ is the shear modulus, τ is a constant yet to be determined, $\tau\phi$ is the axial displacement when the beam is twisted (without bending) to a unit twist τ (right handed in the positive z-direction), σ is Poisson's ratio, and χ is the "flexure function." It is the solution of the equation

$$(\partial^2\chi/\partial x^2) + (\partial^2\chi/\partial y^2) = 0$$

whose normal derivative has a certain prescribed value at the boundary.[2] The shear stress components (Eqs. (5) and (6)) form not only the resultant shear force W, as they must, but also a couple about the z-axis (counterclockwise as a couple formed by the shear stress on the section of Fig. 1) of magnitude

$$\mu\tau\int\int\left(x^2 + y^2 + x\frac{\partial\phi}{\partial y} - y\frac{\partial\phi}{\partial x}\right)dx\,dy + \frac{W}{2(1+\sigma)I_1}\int\int\left\{y\frac{\partial\chi}{\partial x} - x\frac{\partial\chi}{\partial y} + \left(1 - \frac{1}{2}\sigma\right)y^3 - \left(2 + \frac{1}{2}\sigma\right)x^2y\right\}dx\,dy \quad (7)$$

To meet the conditions of the problem as stated above—where the applied load W passes through the z-axis—this couple must vanish. This requirement determines the constant τ.

The axial displacement is given by

$$w = \tau\phi - \frac{W}{EI_1}\left\{x\left(lz - \frac{1}{2}z^2\right) + \chi + xy^2\right\} - \beta x + \alpha y + \gamma \quad (8)$$

where E is Young's modulus and α, β, γ are constants.

A Definition of Pure Bending

The Saint-Venant theory of flexure and torsion as it is at present formulated does not define a center of twist, a state of pure bending, or a shear center. It is necessary for the present purpose to define the last two. Any appropriate definition should, of course, agree with the accepted meanings of these terms, meanings that arise from the well-known approximate theory of flexure. Bending free from torsion is there obtained by displacement of cross sections without relative rotation about the longitudinal axis of the beam. The shear center is the point through which the shear force on a section, the resultant of the shearing stresses, passes in such a state of deformation.

This definition of bending is inadequate because it regards the cross sections as displaced without relative movement of points in them, whereas the theory admits the existence of this relative movement. Consequently, it contemplates different rotations of different elements of area in the cross section. Such rotations occur even though one would say that there is no rotation of the section "as a whole." In an arbitrary cross section there is no reason to select any one element as more important than the others and say that we have pure bending when its rotation is zero.*

The "rotation," in the sense of the theory of elasticity, has a z-component at any point given by

$$\omega_z = [(\partial v/\partial x) - (\partial u/\partial y)]/2$$

where u, v are the x and y components of displacement. Differentiating with respect to z,

$$\partial\omega_z/\partial z = [(\partial e_{yz}/\partial x) - (\partial e_{xz}/\partial y)]/2$$

where e_{xz}, e_{yz} are the components of shearing strain corresponding to X_z, Y_z. The Saint-Venant theory yields a simple formula for the expression on the right in the form

$$\tau - (\sigma W/EI_1)y \quad (9)$$

(See reference 2, page 331.)

The relative rotation of similarly situated elements in two cross sections occurs at the rate (9) per unit axial length. It is impossible to have this zero for all elements of the cross section.

In accordance with the foregoing it is proposed here to define pure bending—that is, bending free from torsion—by the condition that the average value of Eq. (9) over the whole cross section vanishes. Then

$$\int [\tau - (\sigma W/EI_1)y]\,dA = 0 \quad (10)$$

Now $\int y\,dA$ vanishes since the origin is at the centroid of the section. Thus, τ (which is a constant for any given state of torsion and bending) is zero in pure bending.

The flexure problem as formulated above contemplates the force passing through the z-axis. But all the results quoted above from Love's account remain

* Such selections have been made, explicitly or implicitly, by several writers in locating a center of shear. These choices are discussed by W. R. Osgood, *The Center of Shear Again*, Journal of Applied Mechanics, June, 1943.

valid when W is placed in any parallel line in the plane of the end except that it is no longer necessary to make the couple (7) vanish. It must merely balance the moment of W about the z-axis.

The state of pure bending being characterized by $\tau = 0$ in accordance with the above definition, the couple (7) becomes completely determined and with it the y-coordinate of the shear center, y_s. For $-Wy_s$ must be identical with Eq. (7) when $\tau = 0$. Thus

$$y_s = -\frac{1}{2(1+\sigma)I_1}\int\int\left[y\frac{\partial\chi}{\partial x} - x\frac{\partial\chi}{\partial y} + \left(1-\frac{1}{2}\sigma\right)y^3 - \left(2+\frac{1}{2}\sigma\right)x^2y\right]dx\,dy \quad (11)$$

The other coordinate would be obtained by considering a force in the y-direction.

Proof of Eqs. (3) and (4)

Consider the integral $\int_c (X_z\,dx + Y_z\,dy)$ as a line integral taken around any curve C in the cross section lying wholly within the material. It is equivalent to $-\int_c T\,ds$ around the curve, where ds is an arc element, the arc being described in the counterclockwise sense on the section indicated in Fig. 1, and where T is the component of shearing stress along the curve in the same sense. For the elements of shear force being $X_z\,dA$ and $Y_z\,dA$ on an element of area dA, the work done by these forces in a displacement dx, dy would be $-(X_z\,dx + Y_z\,dy)\,dA$. The work done by the component T would be $T\,ds\,dA$. These are to be the same since T and the component normal to it are to represent the same force on the element dA.

For pure bending, Eqs. (5) and (6), with $\tau = 0$, give

$$-\int_c T_b\,ds = \int_c (X_z\,dx + Y_z\,dy) = -\frac{W}{2(1+\sigma)I_1}\left\{\int_c\left(\frac{\partial\chi}{\partial x}dx + \frac{\partial\chi}{\partial y}dy\right) + \int_c\left[\frac{1}{2}\sigma x^2\,dx + \left(1-\frac{1}{2}\sigma\right)y^2\,dx + (2+\sigma)\,xy\,dy\right]\right\} \quad (12)$$

where T_b has been written to indicate that only pure bending is considered. The χ-terms in the integrand form the total differential of χ. Their integral round the curve is therefore zero when χ is a continuous single-valued function on the curve.

That this must be so can be seen from Eq. (8). The displacement w is continuous and single-valued for physical reasons. All the functions other than χ on the right of Eq. (8) obviously have these properties and therefore χ also is continuous and single-valued.

Of the remaining integrals on the right of Eq. (12), $\int_c x^2\,dx$ is clearly zero. It is readily shown that

$$\int_c y^2\,dx = 2A_c\bar{y}_c, \qquad \int_c xy\,dy = -A_c\bar{y}_c$$

where A_c is the total area enclosed by C (not merely the area occupied by material) and $\bar{y}_c$ the y-coordinate of the centroid of this area. Eq. (12) now reduces to

$$\int_c T_b\,ds = -\sigma WA_c\bar{y}_c/(1+\sigma)I_1 \quad (13)$$

It may be seen that if W is in the direction of the y-axis instead of the x-axis, we shall have

$$\int_c T_b\,ds = \sigma WA_c\bar{x}_c/(1+\sigma)I_2 \quad (14)$$

where I_2 is the moment of inertia about the x-axis. Therefore, if we have a load P_1 in the direction of the x-axis, P_2 in the direction of the y-axis, we shall have, by addition of the forms corresponding to Eqs. (13) and (14),

$$\int_c T_b\,ds = -\frac{\sigma A_c}{1+\sigma}\left(\frac{P_1\bar{y}_c}{I_1} - \frac{P_2\bar{x}_c}{I_2}\right) \quad (15)$$

In pure torsion, the rotation increasing along the positive z-axis in the right-handed sense, we have the equation

$$\int_c T_t\,ds = 2\mu A_c\theta \quad (16)$$

where T_t is the torsional shearing stress component. This equation is usually established in the torsion theory for a boundary curve only,* but it can be equally well established for any curve in the section. Thus, for combined torsion and bending, we have, by addition of Eqs. (15) and (16),

$$\int_c T\,ds = 2\mu A_c\theta - \frac{\sigma A_c}{1+\sigma}\left(\frac{P_1\bar{y}_c}{I_1} - \frac{P_2\bar{x}_c}{I_2}\right) \quad (17)$$

where T is the actual shearing stress component, $T_b + T_t$. In deriving Eq. (15) it was implied that P_1, P_2 were applied so as to pass through the shear center and give rise to pure bending. If they are applied at another point, they are statically equivalent to P_1 and P_2 at the shear center responsible for T_b, together with a twisting couple responsible for T_t and θ. It follows that Eq. (17) may be used for any state of combined bending and twist.

Eq. (15), being applicable to any curve in any cross section, is, in particular, applicable to thin-walled sections where the shear stress is known to be sensibly uniform across the wall thickness. The argument by which Hatcher arrived at the incorrect Eq. (1) was limited to this case. Hatcher considered a variation of the shear stress which was consistent with the maintenance of equilibrium and imposed the condition that the strain energy must be a minimum. But the proposition that the variation of the strain energy vanishes for such stress variations is true only when certain further conditions are imposed. If U is the strain energy; u, v, w, the displacements; and X, Y, Z, the components of boundary force per unit area, it may be shown that variations of the stress consistent with equilibrium, involving the variations δX, δY, δZ of

* See, for instance, Timoshenko, *Theory of Elasticity*, page 268. The theorem is attributed by T. J. Higgins (*American Journal of Physics*, Vol. 10, p. 248, 1942) to Boussinesq

the boundary forces, produce a variation of the strain energy given by[3]

$$\delta U = \int\int (u\delta X + v\delta Y + w\delta Z)\, dS$$

where the surface integral covers the boundary. The energy is only stationary when this integral vanishes—as it does for instance for a fixed boundary—or when the variations of the stress are such that δX, δY, δZ vanish. In Hatcher's analysis the satisfaction of this condition was not ensured, and the failure of his method to yield a result equivalent to Eq. (15) indicates that the condition was violated.

To see how this may have occurred, consider a beam under a bending load. There is a change of shape of cross sections corresponding to nonzero values of u and v. The variations considered in Hatcher's method are equivalent to the imposition of uniform shear stress, or shear flow, around each independent circuit. This variation of the shear stress, which applies to the ends as part of the surface of the body, constitutes the δX, δY, δZ of the above integral. There is no obvious reason why the integral so formed should vanish. It may be argued that u and v are, in the main, merely rigid body displacements, the part corresponding to deformation of the section being small, and that the work of the shear variation on the former would vanish and the work on the latter would be small. But the energy being varied is the shear energy, and this also is small in comparison with the energy of bending.

Form of the Result Applicable When the x-y Axes Are Not Principal Axes

Since the stress analysis of wing structures as beams is frequently based on x-y axes passing through the centroid which are not principal axes, it will be convenient to have the corresponding forms of Eqs. (15) and (17).

Such forms may be obtained by observing that the equations of the Saint-Venant flexure theory as given by Love remain valid for nonprincipal x-y axes. The fiber stress given by him as (reference 2, page 330, Eq. 1)

$$Z_z = -W(l - z)x/I_1$$

(where I_1 has been written for I) still forms a moment $W(l - z)$ about the y-axis balancing that of the load W. But since the axes are no longer principal, the product of inertia of the section, I_{12}, is no longer zero, and these same stresses form a moment about the x-axis given by

$$W(l - z)I_{12}/I_1$$

in the counterclockwise sense looking along the positive x-axis toward the origin. It follows that the load giving rise to these stresses consists not only of the component W but also of a component WI_{12}/I_1 in the direction of the positive y-axis.

Thus, when the load consists of these two components, the shearing stress on the section will satisfy Eq. (13). Correspondingly, Eq. (14) will be satisfied when the load consists of W in the direction of the positive y-axis, accompanied by WI_{12}/I_2 in the direction of the *negative* x-axis or $-WI_{12}/I_2$ in the direction of the positive x-axis.

Now let the actual load consist of P_1' in the direction of the positive x-axis and P_2' in the direction of the positive y-axis. Then the P_1 and P_2 of Eq. (15) must be replaced according to

$$P_1' = P_1 - \frac{P_2 I_{12}}{I_2}, \qquad P_2' = P_2 + \frac{P_1 I_{12}}{I_1}$$

whence

$$P_1 = \frac{1}{k}\left(P_1' + \frac{I_{12}}{I_2}P_2'\right), \qquad P_2 = \frac{1}{k}\left(P_2' - \frac{I_{12}}{I_1}P_1'\right)$$

where $k = 1 + (I_{12}^2/I_1 I_2)$.

Thus, dropping the primes, the form of the theorem valid, when P_1, P_2 are actual load components parallel to nonprincipal x-y axes to which I_1, I_2, I_{12} are referred, is

$$\int_c T\, ds = 2\mu A_c\theta - \frac{\sigma}{1+\sigma}\frac{A_c}{k}\times \left[\frac{\bar{y}_c}{I_1}\left(P_1 + \frac{I_{12}}{I_2}P_2\right) - \frac{\bar{x}_c}{I_2}\left(P_2 - \frac{I_{12}}{I_1}P_1\right)\right]$$

for combined bending and torsion.

In the customary American notation, with τ for the shearing stress component along the curve C, G for the shear modulus, μ for Poisson's ratio, the equation is

$$\int_c \tau\, ds = 2GA_c\theta - \frac{\mu}{1+\mu}\frac{A_c}{k}\times \left[\frac{\bar{y}_c}{I_1}\left(P_1 + \frac{I_{12}}{I_2}P_2\right) - \frac{\bar{x}_c}{I_2}\left(P_2 - \frac{I_{12}}{I_1}P_1\right)\right] \quad (18)$$

To express the results in terms of shearing force components F_1, F_2 formed by the stress on the section of Fig. 1, as was done in the "Introduction," P_1 is replaced by $-F_1$, P_2 by $-F_2$.

Analysis of the Shear Stress in Certain Beam Sections with Rectangular Cells

Fig. 2 indicates a section considered by Hatcher. It is symmetric about the horizontal bisector but not about the vertical one, the flange areas A_1, A_2 and the web thicknesses t_1, t_2 being unequal. The problem is to determine the shear stress distribution for bending and the shear center. Let τ_1 denote the (upward) shear stress in the web A_1A_1 just above the lower flange A_1, and, by symmetry, also just below the upper flange A_1. Let τ_2 refer similarly to the other web A_2A_2. Let τ_3 be the shear stress at the midpoint of the upper sheet A_1A_2 and by antisymmetry, also, with direction reversed, at the midpoint of the lower sheet A_1A_2. The shear stress in the upper or lower sheets varies linearly in

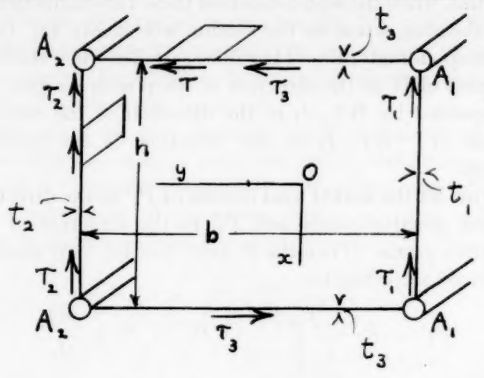

FIG. 2. Single cell section.

accordance with the equilibrium conditions. If s is the horizontal coordinate measured to the left from the midpoint of the upper sheet and τ is the shear stress there from right to left as indicated in Fig. 2, one equation of equilibrium of the element sketched is

$$(\partial\tau/\partial s)\, ds\, dz\, t_3 = (dM\, h/2I_1)\, ds\, t_3$$

or $\partial\tau/\partial s = (h/2I_1)(dM/dz)$, M being the bending moment causing tension in the upper sheet. Since, also, $W = -dM/dz$,

$$\frac{\partial\tau}{\partial s} = -\frac{hW}{2I_1} \text{ and } \tau = -\frac{hWs}{2I_1} + \tau_3 \tag{20}$$

The line integral of this τ from A_1 to A_2 is simply $\tau_3 b$ and, similarly, the line integral from A_2 to A_1 in the lower sheet is also $\tau_3 b$.

The value of τ at the left end of the upper sheet is

$$\tau_4 = \tau_3 - (Whb/4I_1) \tag{21}$$

The relation between this and τ_2, required for the equilibrium of the element indicated in Fig. 3, is

$$\tau_4 t_3\, dz + \tau_2 t_2\, dz + (dM\, h/2I_1)A_2 = 0$$

or

$$\tau_4 t_3 + \tau_2 t_2 = (hA_2/2I_1)W \tag{22}$$

Similarly, if τ_5 denotes the value of τ at the other end, $s = -b/2$,

$$\tau_5 = \tau_3 + Whb/4I_1 \tag{23}$$

and

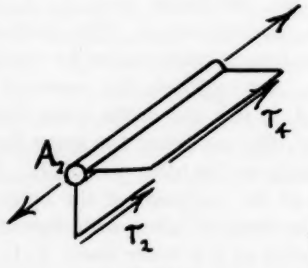

FIG. 3.

$$-\tau_3 t_3 + \tau_1 t_1 = (hA_1/2I_1)W \tag{24}$$

Starting with τ_2 at the top, the shear stress in the right-hand web varies in a parabolic manner down the web. Let s now be the coordinate measured upward from the midpoint of the web and τ be the upward shear stress as a function of s. Then

$$(\partial\tau/\partial s)\, ds\, t_2\, dz = (dM\, s/I_1)\, ds\, t_2$$

or

$$\partial\tau/\partial s = -Ws/I_1$$

and

$$\tau = (W/I_1)[(h^2/8) - (s^2/2)] + \tau_2 \tag{25}$$

The term $(W/I_1)[(h^2/8) - (s^2/2)]$ is independent of the thickness t_2. Its line integral (over the height h) is thus also independent of the thickness.

The expression for the upward shear stress on the right-hand web will evidently be

$$\tau = (W/I_1)[(h^2/8) - (s^2/2)] + \tau_1$$

The line integral for the whole circuit $A_1A_1A_2A_2A_1$ taken counterclockwise will contain a contribution from the term $(W/I_1)[(h^2/8) - (s^2/4)]$, but this will be canceled by the contribution from the similar term in the other web. The two webs together then yield simply $(\tau_1 - \tau_2)h$. The contributions from the upper and lower sheets have already been found to amount to $2\tau_3 b$, and the complete line integral $\int_c \tau\, ds$ is therefore $(\tau_1 - \tau_2)h + 2\tau_3 b$. Eq. (13) now becomes

$$(\tau_1 - \tau_2)h + 2\tau_3 b = -[\mu/(1+\mu)](WA_c\bar{y}_c/I_1) \tag{26}$$

(using μ for Poisson's ratio) and

$$A_c = bh, \quad \bar{y}_c = \frac{2(A_1 - A_2)b + (t_1 - t_2)bh}{4(A_1 + A_2) + 4bt_3 + 2h(t_1 + t_2)}$$

In Eqs. (21), (22), (23), (24), and (26) we have a set sufficient for the determination of τ_1, τ_2, τ_3, τ_4, τ_5 and knowledge of these establishes the shear stress distribution in each part of the section, and the shear center can be found. Substitution for τ_4 in Eq. (21) and τ_5 in Eq. (23) yields

$$\left.\begin{aligned} \tau_3 t_3 + \tau_2 t_2 &= \frac{Wh}{4I_1}(2A_2 + bt_3) \\ -\tau_3 t_3 + \tau_1 t_1 &= \frac{Wh}{4I_1}(2A_1 + bt_3) \end{aligned}\right\} \tag{27}$$

These with Eq. (26) may be solved for τ_1, τ_2, τ_3.

As a numerical example (one considered by Hatcher) we take, in inch units,

$$t_1 = 0.06, \quad t_2 = 0.04, \quad t_3 = 0.04$$
$$A_1 = 2, \quad A_2 = 1, \quad h = 10, \quad b = 30$$

The results for τ_1, τ_2, τ_3 are shown in the following table, and with them the values that are obtained when the expression on the right in Eq. (26) is replaced by zero, as it would be if Hatcher's equations were used:

	Equations of This Paper	Hatcher's Equations
τ_1	$0.994W$	$0.983W$
τ_2	$0.908W$	$0.924W$
τ_3	$0.0062W$	$-0.010W$

all in pounds per square inch when W is in pounds. It will be observed that the differences in the two sets of values are small.

Several Cells

The problem to be solved here is that of a section consisting of a row of any number of equal rectangular cells, with equal concentrated flanges of area a at all junctions, with all web and flange sheets effective in bending. A typical group of three cells somewhere in the row and the end cell on the left are indicated in Fig. 4. A vertical downward load W is applied through the centroid of the loaded end, as in Fig. 1. One of the questions to be answered is how much does the shear stress on the vertical webs depart from an even sharing of total shear force by each.

It is convenient to use the products of shear stress and sheet thickness—the "shear flows" rather than the shear stresses themselves.

The distribution of shear on the section can be specified as follows. Let the shear flow at the midpoint of the top flange sheet of the rth cell be g_r, from right to left. Let a uniform shear flow of this magnitude exist all around the rth cell, and correspondingly for the other cells so that in the web between the rth and $(r-1)$th cells they combine to form an upward shear flow $g_r - g_{r-1}$. The actual shear flow in the top sheet of any cell varies linearly, as shown in the preceding section, the varying term being $-Whbt_3s/2I_1$ with s and t_3 as in that section. The end magnitudes of this part are $Whbt_3/4I_1$, and this is the δ_1 shown on Fig. 4.

The shear flow in the internal web between the rth and $(r-1)$th cells consists of a uniform part δ_2 and the parabolic part of the type discussed in the preceding section, as well as the uniform part $g_r - g_{r-1}$, all reckoned upward.

The magnitude of δ_2 is determined by the equilibrium of the flange (Fig. 5), of area a. This requires satisfaction of the equation

$$\delta_2 = 2\delta_1 + (Wha/2I_1) \tag{28}$$

which shows that δ_2 is the same for all internal webs. The shear flows, etc., do not appear in this equation, since a shear flow passing into and out of the junction contributes to its forces which have zero resultant. This is the chief convenience in the use of the shear flow rather than the shear stress.

The last web on the left of the section is shown with δ_3 in place of δ_2 and, by similar considerations,

$$\delta_3 = \delta_1 + (Wha/2I_1) \tag{29}$$

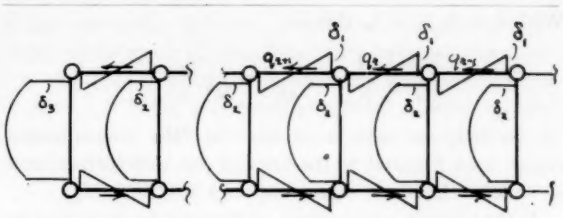

Fig. 4. Shear flow specification in rectangular cells.

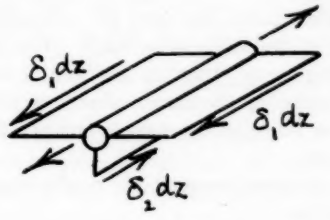

Fig. 5.

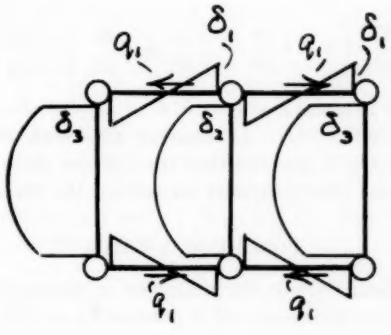

Fig. 6.

Two Equal Cells

The shear flow at the midpoint of the upper flange sheet in the left-hand cell is denoted by q_1, from right to left. The shear flow in the various parts of the cell is then specified just as before. That in the right-hand cell follows from symmetry, as indicated in Fig. 6.

Eqs. (28) and (29) remain valid. Eq. (13) becomes

$$q_1\left(3\frac{h}{t_1} + 2\frac{b}{t_3}\right) + \delta_2\frac{h}{t_1} - \delta_3\frac{h}{t_1} = -\frac{\mu}{1+\mu}\frac{Wb^2h}{2I_1}$$

Solving these three equations for q_1 we find

$$q_1 = -\frac{Wbht_3}{4I_1}\frac{1+2\xi\eta}{3+2\eta} \tag{30}$$

where ξ denotes $\mu/1+\mu$, and η denotes bt_1/ht_3. The upward shear *stress* at mid-height in the middle web is

$$(1/t_1)[2q_1 + \delta_2 + (Wh^2t_1/8I_1)]$$

which, by Eqs. (30) and (28), may be written

$$\frac{Wh^2}{8I_1}\left(1 + 4\frac{a}{ht_1} + 4\frac{bt_3}{ht_1} - 4\frac{bt_3}{ht_1}\frac{1+2\xi\eta}{3+2\eta}\right)$$

With $b = h$, $t_1 = t_3$, this is

$$\frac{Wh^2}{8I_1}\left[\frac{21}{5} + 4\frac{a}{ht_1} - \frac{8\mu}{5(1+\mu)}\right]$$

If, further, we take $a = ht_1$—i.e., the concentrated flange area is equal to the area of one web-section, and $\mu = 0.3$—the shear stress becomes $7.83Wh^2/8I_1$.

If the term in μ is omitted, as it would be according to Hatcher's equations, the result is increased, but by less than 5 per cent.

On the other hand, the term in μ contributes about 46 per cent of the value of q_1 itself. The shear stress corresponding to q_1—that is, the actual shear stress at the midpoint of the flange sheet—is $0.58Wh^2/8I_1$, and the shear stress at the outside end of a flange sheet is $2.58Wh^2/8I_1$.

The upward shear stress at mid-height in either of the outside webs is

$$(1/t_1)[-q_1 + \delta_3 + (Wh^2t_1/8I_1)]$$

which is

$$\frac{Wh^2}{8I_1}\left(1 + 4\frac{a}{ht_1} + 2\frac{bt_3}{ht_1} + 2\frac{bt_3}{ht_1}\frac{1+2\xi\eta}{3+2\eta}\right)$$

With the assumptions $b = h$, $t_1 = t_3$, $a = ht_1$, this becomes $7.58Wh^2/8I_1$. Comparing this with the value $7.83Wh^2/8I_1$, it appears that the vertical shear force is in this case nearly equally shared by the three webs.

Three Equal Cells

The shear flow at the midpoint of the upper flange sheet of the left-hand cell is denoted by q_1 (Fig. 7). By

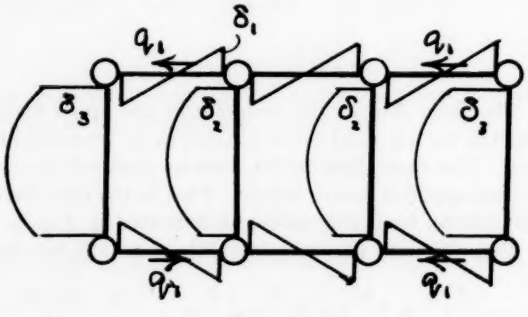

Fig. 7.

symmetry the shear flow at the middle of the flange sheet of the central cell is zero. As before we have Eqs. (28) and (29), and Eq. (13) yields

$$q_1\left(2\frac{h}{t_1} + 2\frac{b}{t_3}\right) + \delta_2\frac{h}{t_1} - \delta_3\frac{h}{t_1} = -\frac{\mu}{1+\mu}\frac{Wb^2h}{I_1}$$

whence

$$q_1 = -(Wbht_3/8I_1)[(1+\xi\eta)/(1+\eta)]$$

The shear stresses are now obtainable as before. We find for the upward shear stress at the midpoint of an outside web $7.61Wh^2/8I_1$ with $b = h$, $t_1 = t_3$, $a = ht_1$, $\mu = 0.3$ and, for the corresponding stress in an inside web, $8.38Wh^2/8I_1$. The contributions of the terms in μ to these values is only about $1^1/_2$ per cent. This percentage is approximately doubled when a is taken as zero. The terms in μ in q_1 itself, however, contribute 23 per cent of its value.

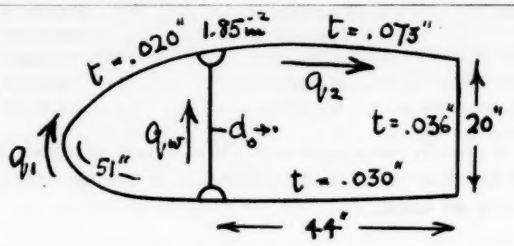

Fig. 8. Two-cell wing section.

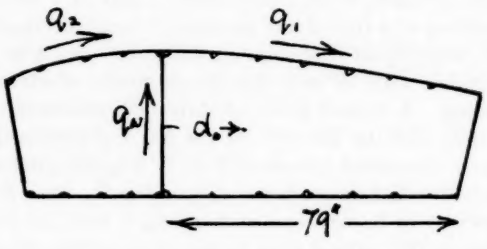

Fig. 9. Three-web section.

Calculations for Wing Sections*

Calculations based on the theorem expressed by Eq. (13) were made for three wing sections, the shear stresses of which had already been found according to Hatcher's method, in order to gain some idea of the error made in using the latter.

Section I is from an example worked out by Kuhn.[4] The values of the shear flows q_w, q_1, q_2, defined as indicated in Fig. 8 and due to a 5,000-lb. vertical load, are given in Table 1, in pounds per inch.

Table 1

	q_w	q_1	q_2
Hatcher's method	110	13.8	111
Present method	105	9.5	112

There is a considerable proportional error in q_1, but this is in a shear flow that is itself small. The error in the other q's is less than 5 per cent.

The distance d_0 of the shear center from the main web is 6.44 in. by Hatcher's method and 12.3 in. by the present method, a shift of 9 per cent of the chord.

* These calculations were carried out by the structural division of the Curtiss-Wright Research Laboratory at Buffalo, N. Y., under the direction of E. S. Jenkins.

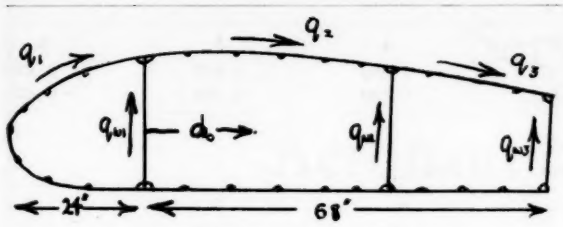

FIG. 10. Three-cell section.

Comparative results for the three-web Section II (Fig. 9) are given in Table 2,

TABLE 2

	q_1	q_2	q_w	d_0 (in.)
Hatcher's method	35.5	17.5	81.3	13.0
Present method	33.6	18.6	78.3	15.6

and the differences are again small. They correspond in magnitude to those found in the preceding two- and three-rectangular cell sections.

Section III (Fig. 10) yielded the comparative results shown in Table 3, and again the differences are small.

SOLUTION FOR $2n + 1$ EQUAL RECTANGULAR CELLS

We may apply the theorem of Eq. (13) to the circuit round the rth cell (Fig. 4) for a section containing a middle cell ($r = 0$), n cells on the left, and n on the right.* The cells $r = 1$ to $r = n$ (positive) are on the left. The centroid of the whole cross section is at the center of the middle cell. The centroid of the area within the rth cell has the y-coordinate (in the sense of Fig. 1), rb.

It will be evident from the manner in which the shear stress has been specified that the line integral for the circuit round the rth cell involves q_r, q_{r-1}, and q_{r+1} only, the contributions from the other parts of the shear flow vanishing. Eq. (13) thus yields

$$q_r\left(2\frac{h}{t_1}+2\frac{b}{t_3}\right)-q_{r-1}\frac{h}{t_1}-q_{r+1}\frac{h}{t_1}=-\frac{\mu}{1+\mu}\frac{Wbhrb}{I_1}$$

or

$$q_{r+1}-2\alpha q_r+q_{r-1}=\left(\frac{\mu}{1+\mu}\right)\left(\frac{Wb^2t_1}{I_1}\right)r \qquad (31)$$

where α is written for $1 + (bt_1/ht_3)$. The general solution of this equation of finite differences† in q_r consists of the particular solution $-[\mu/(1 + \mu)](Wbht_3/2I_1)r$ added to the general complementary solution, the solution of Eq. (31) when the term on the right is replaced by zero. If there is a complementary solution of the form $q_r = Ce^{\lambda r}$ with C and λ constants, we must have, by substitution,

$$e^{\lambda(r+1)}-2\alpha e^{\lambda r}+e^{\lambda(r-1)}=0$$

or $\cosh \lambda = \alpha$. Since α is necessarily greater than 1, λ is real and there are two roots, $\pm\lambda$. The complementary solution can thus be taken as

$$q_r = A \sinh \lambda r + B \cosh \lambda r \qquad (32)$$

where A and B are arbitrary constants.

In the present problem, q_r must be an *odd* function of r, because of the symmetry of the section (the numbering of the sections is continued to the right of the middle by negative numbers). The particular integral is already odd in r. Combining it with the odd part of Eq. (32) (i.e., putting $B = 0$),

$$q_n = -\left(\frac{\mu}{1+\mu}\right)\left(\frac{Wbht_3}{2I_1}\right)r + A \sinh \lambda r \qquad (33)$$

But Eq. (31) and, consequently, also Eq. (33) are only true for a cell which is not an end cell, since cells to both right and left of it were assumed. It is necessary to write a special form of Eq. (13) for the end cell $r = n$ (on the left). This is:

$$q_r\left(2\frac{h}{t_1}+2\frac{b}{t_3}\right)-q_{n-1}\frac{h}{t_1}+\delta_2\frac{h}{t_1}-\delta_3\frac{h}{t_1}=-\left(\frac{\mu}{1+\mu}\right)\left(\frac{Wbh}{I_1}\right)nb \qquad (34)$$

But from Eqs. (28) and (29),

$$\delta_2-\delta_3=\delta_1=\frac{Wbht_3}{4I_1}$$

Then Eq. (34) may be written

$$-\frac{Wbht_3}{4I_1}-2\alpha q_n+q_{n-1}=\left(\frac{\mu}{1+\mu}\right)\left(\frac{Wb^2t_1}{I_1}\right)n$$

But this is the form which Eq. (31) would assume if there were an $(n + 1)$th cell with $q_{n+1} = -Wbht_3/4I_1$. It is therefore satisfied if we determine A in Eq. (33) so as to satisfy this condition. Then

$$-\frac{Wbht_3}{4I_1}=-\frac{\mu}{1+\mu}\frac{Wbht_3}{2I_1}(n+1)+A \sinh \lambda(n+1)$$

The final form of the solution valid for $r = 0$ to $r = n + 1$ is

* A similar analysis can be made when the number of cells is even.

† See, for instance, Kármán and Biot, *Mathematical Methods in Engineering*, chap. XI.

TABLE 3

	q_1	q_2	q_3	q_4	q_5	q_{w_1}	q_{w_2}	q_{w_3}	d_0
Hatcher's method	3.26	−4.7	−5.4	0.1	1.4	17.6	14.5	12.6	3.16
Present method	4.84	−3.2	−6.8	−1.3	2.8	17.5	13.1	14.0	30.2

TABLE 4

r	1	2	3	4	5	6
$-f(r)$	0.229	0.456	0.673	0.862	0.916	0.495
$-f(r) + f(r-1)$	0.229	0.217	0.217	0.189	0.054	−0.421

TABLE 5

r	1	2	3	4	5	6
$\{\ \}$	1.021	1.033	1.033	1.061	1.196	1.671

TABLE 6

r	1	2	3	4	5
$1 - 2f(r)$	1.458	1.912	2.346	2.724	2.832

$$q_r = \frac{Wbht_3}{2I_1}\left\{-\left(\frac{\mu}{1+\mu}\right)r + \left[\frac{\mu}{1+\mu}(n+1) - \frac{1}{2}\right]\frac{\sinh \lambda r}{\sinh \lambda(n+1)}\right\} = (Wbht_3/2I_1)f(r) \tag{35}$$

where $f(r)$ is merely an abbreviation for the expression in braces. It is remarkable that q_r is independent of the concentrated flange areas at the junctions.

NUMERICAL EVALUATION FOR $n = 5$

When $n = 5$ the section has eleven cells. For simplicity we take square cells ($b = h$), no concentrated flange area at the junctions ($a = 0$), and suppose that the flange and web sheets are of equal thickness ($t_1 = t_3$). Poisson's ratio μ is taken as 0.3. Then $\alpha = 2$ and $\lambda = 1.32$.

The values of the function $f(r)$ of Eq. (35) are shown in Table 4, and these show the considerable variation of the flange sheet shear stress from cell to cell.

Consider the upward shear flow in the web between the $(r-1)$th and the rth cell. The value at mid-height is

$$(Wh^2t_1/8I_1) + \delta_2 + q_r - q_{r-1}$$

or, using Eqs. (28) and (35),

$$\frac{Wh^2t_1}{8I_1}\left\{1 + 4\frac{bt_3}{ht_1} + 4\frac{a}{ht_1} + 4\frac{bt_3}{ht_1}[f(r) - f(r-1)]\right\} \tag{36}$$

the factor $Wh^2t_1/8I_1$ being the maximum of the parabolic part. With the assumed values this becomes

$$(Wh^2t_1/8I_1)4\{(5/4) + [f(r) - f(r-1)]\}$$

The values of the quantity in braces are shown in Table 5, from which it appears that the vertical shear in the webs tends to fall considerably more heavily on the outside webs.

The horizontal shear flow in the flange sheets has its largest value, in a given cell, at one end of the cell—the left-hand end in Fig. 4, since $f(r)$ is negative. It is $-\delta_1 + q_r$ or

$$-(Wbht_3/4I_1)[1 - 2f(r)]$$

The values of $1 - 2f(r)$ are shown in Table 6. The greatest magnitude of the horizontal shear *stress* is $2.832Wbh/4I_1$ at the end of the section. The greatest magnitude of the vertical (web) shear stress is $1.671 \times 4Wh^2/8I_1$. Since we have taken $b = h$, these are in the ratio (horizontal/vertical) = 0.85.

REFERENCES

[1] Hatcher, R. S., *Rational Shear Analysis of Box Girders*, Journal of the Aeronautical Sciences, Vol. 4, No. 6, p. 233, April, 1937.

[2] Love, A. E. H., *Treatise on the Mathematical Theory of Elasticity*, 4th Edition, Chapter XV; The Macmillan Company, New York, 1927.

[3] See, for instance, the *Handbuch der Physik*, Vol. VI, Art. 17, p. 68. The two-dimensional form is given in Timoshenko's *Theory of Elasticity*, p. 148.

[4] Kuhn, P., *Some Elementary Principles of Shell Stress Analysis with Notes on the Use of the Shear Center*, N.A.C.A. T.N. No. 691, 1939.

Services of the Aeronautical Archives of the Institute of the Aeronautical Sciences

The services of the Aeronautical Archives are available to all members of the Institute, to Corporate Members, to advertisers in the Aeronautical Engineering Review and, under usual library limitations, to the public. Four specialized services are available.

The Paul Kollsman Library

This lending library service makes available, *without charge*, the latest and more important aeronautical books.

As far as the facilities permit, any person in the United States over 18 years of age who can furnish references which certify to his or her responsibility may become a member of the library.

Members may request the loan of any aeronautical or technical book they wish to borrow. Through an exchange agreement with the Engineering Societies Library, any book on general engineering may be borrowed from its great collection of over 160,000 volumes.

A photostating service is available at usual library rates.

Applications for membership in the library and further information will be sent on request.

The Burden Reference Library

This reference library contains over 14,000 aeronautical books, magazines, pamphlets, photographs, reports, and clippings gathered from world-wide sources and is one of the most complete aeronautical libraries in the world. Material from this library is not available for loan but may be used for reference purposes at the Aeronautical Archives.

The Pacific Aeronautical Library
6715 Hollywood Boulevard
Hollywood, California

Established in cooperation with the aircraft companies the library serves. The leading aircraft companies in or near Los Angeles participate in its support and operation.

This service library for aeronautical research is available to the public for reading privileges. Source material includes aerodynamic and structural research reports, as well as books on drafting, production methods, history, and allied sciences. It furnishes books, periodicals, and pamphlet material to the participating aircraft companies to supplement their engineering libraries.

The Aeronautical Archives Technical Information Service

This service has experienced personnel under the supervision of trained aeronautical engineers to compile any information desired. The services range from listing specialized reference books to the preparation of exhaustive bibliographies, digesting of reports, and general surveys of any aeronautical subject. Some of the available services are:

Bibliographies on any aeronautical subject.
Reports on any aeronautical subject.
Digests of aeronautical books, papers, periodicals, and references.
Translations.
Engineering investigations of special aeronautical subjects.
Biographies of individuals engaged in aeronautics.
Photostats of any aeronautical or general engineering material.
Microfilms made on special order.
Photographs made from the Institute's photographic collection.
Drawings and tracings made.

In addition to the services mentioned any commission which comes within the scope of the Service will be accepted. Special arrangements may be made for work requiring several weeks or months.

Translators are available for accurate transcriptions of all foreign language data. Translations are carefully edited by trained engineers.

Reproductions of any material in the Aeronautical Archives of the Institute may be ordered at standard photostat rates.

INSTITUTE OF THE AERONAUTICAL SCIENCES
1505 RCA BUILDING WEST
30 ROCKEFELLER PLAZA, NEW YORK 20, N. Y.

SUGGESTIONS FOR CONTRIBUTORS TO THE PUBLICATIONS *of the* INSTITUTE *of the* AERONAUTICAL SCIENCES

The Institute of the Aeronautical Sciences invites both members and nonmembers from any country to submit papers for publication in the JOURNAL OF THE AERONAUTICAL SCIENCES and the AERONAUTICAL ENGINEERING REVIEW. The Institute, following the practice of other societies, does not pay for contributions.

The following directions for the preparation of papers, if followed by authors, will save correspondence, avoid the return of papers for changes, minimize the work of preparation for the printer, and save the expense due to the charges made for "author's corrections."

MANUSCRIPTS: Papers must be written in English, in original typewriting on one side only of white paper sheets, consecutively numbered and be double or triple spaced with wide margins. Manuscripts should be prepared with great care so that they will be typographically accurate. Paragraphing should be given special attention. Papers should be written in the third person, reference to the writer being made as "the author." Avoid the use of the words "I," "we," and "you." Blueprint copies of papers are unacceptable as it is impossible to mark directions to the printer on them. Correcting, changing, or adding to papers after they are in type is costly. It is, therefore, imperative that papers submitted be in final form. Typographical errors may be corrected on proofs, but if authors wish to add material, they may do so at their own expense. In mailing, drawings may be rolled, but manuscripts should be sent flat. Send by first class mail (register if you wish for your own protection) to the Editorial Office, Institute of the Aeronautical Sciences, 1505 RCA Bldg. West, 30 Rockefeller Plaza, New York 20, N. Y. All manuscripts will be examined by the Editorial Committee and by the Editor. Authors will be advised as promptly as possible whether the paper is acceptable for publication.

TITLES: The title of the paper should be brief. The name and initials of the author should be written as he prefers. The use of the full name of an author is advocated because of the frequent duplication of initials and surnames which sometimes makes it difficult to establish the identity of the author. This is particularly important for large annual indexing and abstracting services. All titles and degrees or honors are omitted. The name of the organization with which the author is associated should be placed after his name on a separate line. The date on which the paper is received will be inserted by the Editor.

SUMMARIES OR ABSTRACTS: An abstract to be printed at the beginning should accompany each article. It should be adequate as an *index* and as a *summary*. It should contain a statement of major conclusions reached, since summaries in many cases constitute the only source of information used in compiling scientific reference indexes. Abstracts printed in other journals, especially foreign, in most cases, consist of summaries from printed papers. The summary should explain as adequately as possible the major conclusions to a nonspecialist in the subject. The summary should contain from 100 to 300 words, depending on the length of the paper.

SUBHEADINGS: Subheadings should be inserted by the author at frequent intervals. The work of editorial preparation will be simplified by the author providing many subheadings. Owing to the breaking of columns and the insertion of illustrations, some of the subheadings may have to be omitted.

SHORTENING OF PAPERS: Some papers, at the end, fill in only a portion of a page. This leaves much wasted blank space as succeeding articles are started at the top of a page. Authors should indicate by notation on the left-hand side of the page what matter may be omitted when "runovers" occur. This request is important as the Journal cannot afford in the future, as it has in its earlier issues, to have blank half pages or more at the end of papers.

MATTER USUALLY DELETED: Acknowledgments of assistance in preparation of paper, except by collaborators. Photographs or illustrations of little technical interest and not showing advances in general practice. Too detailed tabular matter (general results of such tables may be included in the text). Lengthy descriptions of materials or processes or of preliminary experiments or theories that preceded final results; salient features only are of interest.

REFERENCES AND FOOTNOTES: References should appear as footnotes only, numbered consecutively, grouped together at the end of the manuscript. The arrangement should be as follows: (for books)—[1] Durand, W. F., *Aerodynamic Theory*, 1st Edition, Vol. 1, p. 23; Julius Springer, Berlin, 1934. (For magazines)—[1]Englund, C. R., Crawford, A. B., and Mumford, W. W., *Some Results of a Study of Ultra-Short-Wave Transmission Phenomenon*, Proc. I. R. E., Vol. 20, No. 12, pp. 481 and 482, March, 1933. Please give author, title, edition, volume, page, publisher and date of publication as indicated. Omission of one required fact causes much extra editorial work and possible inaccuracies. All references are grouped at the end of the article.

ILLUSTRATIONS: Illustrations should accompany manuscripts and each should always be referred to in the text, preferably by number. Drawings or graphs should not be larger than 12 × 16 inches, and must be made with jet black India Ink on white paper or tracing cloth, the latter being preferred. *Do not use typewriter for lettering.* The smallest lettering on 8 × 10 inch figures should be no less than 1/4 inch high. Cross-section paper (white with black lines) may be used, but should not have more than 4 lines per inch. If finer ruled paper is used, the major division lines should be drawn in with black ink, omitting the finer divisions. In the case of finely ruled paper, only blue-lined paper can be accepted. *Tracing paper and blueprints* are not acceptable. Lettering and all markings must be large enough to be readable after reduction. Mail rolled or flat, never fold. Drawings that cannot be reproduced (including pencil drawings) will be returned to the author for redrawing, thus delaying publication of the paper. Photographs should be very distinct and show clear black and white contrasts. They must be on glossy white paper. Avoid round and oval photographs.

CAPTIONS AND LEGENDS: Legends or captions must accompany each drawing or photograph submitted. If written on the drawing or photograph, they should be placed below and well outside the part to be reproduced. It is better to place them on separate sheets of paper pasted to the back of the drawings or photographs. Each table should have a caption such as Table 1, Table 2, Table 3, etc. Captions should be complete in themselves so as to make the data intelligible to the reader without reference to the text. A duplicate list of captions for figures should be included as the last page of the manuscript. Use "Fig. 1" (not Figure 1), Figs. 3 and 4, etc., in both the text and the numbering of illustrations. In the text, "Eq. (1)," or "Eqs. (1) and (2)" are preferable to "Equation (1)." In captions and legends, except for "Fig." and "Eq." and table headings, write all words in full; do not abbreviate. Avoid placing explanatory written matter in the drawings; it should be in the text.

MATHEMATICAL WORK: Only the simplest formulas should be typewritten; all others should be carefully written in pen and ink, the writing to be large enough so that ample room is provided to mark mathematical matter for the printer. A considerable space for marking should be allowed above and below all equations. All complicated equations should be repeated on separate sheets with plenty of space left for marking. The solidus should be used for simple fractions appearing within the text. Make all expressions clear to the typesetter. Greek letters used in formulas should be clearly designated by name on the margin of the manuscript. All symbols should be clearly written and carefully checked. The difference between capital and lower-case letters should be clearly distinguished and care taken to avoid confusion between zero (0) and the letter (o), between the numeral (one) and the letter (ell) and the prime ('), between alpha and a, kappa and k, u and mu, v and nu, n and eta. All subscripts and exponents should be clearly marked and dots and bars over letters or mathematical expressions should be avoided. Avoid complicated exponents and subscripts. When it is necessary to repeat a complicated expression, it should be represented by some convenient symbol.

NOMENCLATURE AND ABBREVIATIONS: The National Advisory Committee for Aeronautics Nomenclature should be used in preference to any others. Standard abbreviations should be used and it should be noted that most abbreviations are lower case such as m.p.h., b.m.e.p., i.hp., b.hp., hp., . . . etc.